



**Novel heterocyclic ligands for the lipid
kinase PI4KIII β : a chemical biology
approach**

by

Brett Cosgrove

January 2020

University of Strathclyde and GlaxoSmithKline

Thesis submitted to the University of Strathclyde in
fulfilment of the requirements for the degree of Doctor
of Philosophy

DECLARATION

This thesis is the result of the author's original research. It has been composed by the author and has not been previously submitted for examination which has led to the award of a degree.

The copyright of this thesis belongs to GSK in accordance with the author's contract of engagement with GSK under the terms of the United Kingdom Copyright Acts. Due acknowledgement must always be made of the use of any material contained in, or derived from, this thesis.

Brett Cosgrove

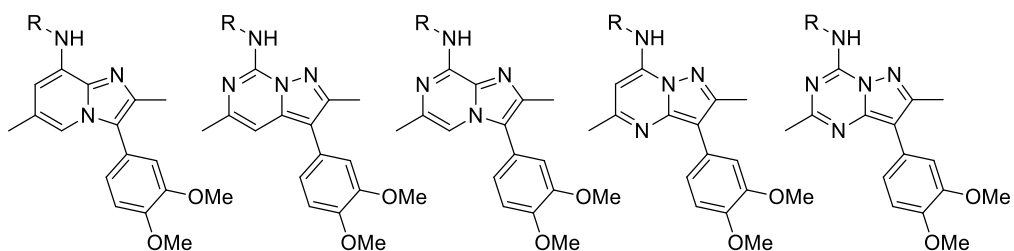
Signed: Brett Cosgrove

Date: 17.03.20

ABSTRACT

This thesis is divided into two parts. Part One investigates the physicochemical properties, in particular the thermodynamic solubility, of 6,5-bicyclic heterocycles. The heterocycle with the best balance of properties was taken forward as a scaffold for Part Two of the research, where lipid kinase PI4KIII β was targeted with an electrophilic, covalent warhead.

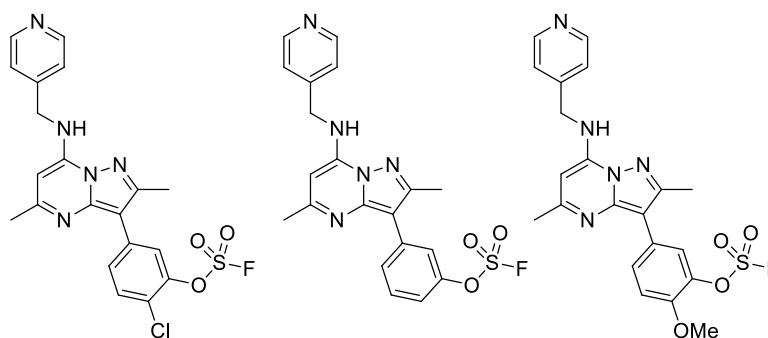
Part One of this thesis details the synthesis of a range of nitrogen containing 6,5-bicyclic heterocyclic cores shown below which are common scaffolds in medicinal chemistry. The physicochemical properties of these compounds were measured, and a comparison of the data was carried out. Crystalline solids were obtained where possible to give a more robust comparison of the thermodynamic solubility. Various parameters such as pKa, melting point and solubility, were investigated.



The biological target for the compounds prepared was lipid kinase PI4KIII β which is responsible for the synthesis of PI4P (phosphatidylinositol 4-phosphate), the most abundant phosphoinositide in eukaryotic cells, that plays a critical role in a number of pathological processes, one being a key mediator for viral replication. There is significant interest in targeting PI4KIII β because viruses are able to hijack the cell's machinery for replication. This has led to an interest in PI4KIII β as being a potential target to treat diseases such as hepatitis C, human rhinovirus infection and also cancer cell proliferation.¹

Part Two of the thesis builds upon the results of Part One, where the core with the best balance of activity against PI4KIII β and physicochemical properties was taken forwards. This was appended with different electrophilic warheads to initially target covalent modification of the conserved lysine in the active site of PI4KIII β .

A range of novel fluorosulfate based inhibitors were synthesised and their stability to buffers and reactivity to amino acids were investigated. In addition to measuring enzymatic potency a long incubation cellular assay was also carried out, and the enhanced potency indicated the possibility of a non-reversible binding event. To determine the potential for covalent modification, the compounds were profiled by protein mass spectrometry to identify adducts. The onset of inhibition was measured and the rate constants for the reversible and irreversible binding events were determined.



The success of the fluorosulfate covalent inhibitors targeting PI4KIII β led to the exploration of the first in-house non-cysteine targeted covalent fragment library. Data on the solubility from Part One of the thesis was used to aid the design of PI4KIII β fragment fluorosulfate molecules to selectively target PI4KIII β and validate the concept of a fluorosulfate fragment library. Finally, a robust and high throughput synthetic procedure for synthesising a first generation of a fluorosulfate fragment library was established and the fragment set was screened against several protein targets.

ACKNOWLEDGMENTS

I would like to acknowledge:

My two supervisors:

Mike Barker (GSK) and **Prof. Nick Tomkinson** (Strathclyde).

Ken Down, Sophie Bertrand, Emma Grant, Don Somers and John Evans.

Contents

Declaration	ii
Abstract	iii
Acknowledgments	v
Contents	vi
Abbreviations	viii
1 Part 1	1
1.1 Physicochemical properties in drug discovery	1
1.2 Strategies for improving solubility	6
1.3 Project aims	12
1.4 Synthesis of Cores 1-5	15
1.5 Physicochemical properties of the synthesised heterocycles	26
1.6 Summary.....	36
Experimental	37
1.7 General methods and assays.....	37
1.8 Synthesis.....	42
References	70
2 Part 2	74
2.1 Kinases	74
2.2 Lipid kinases: PI4KIII β	77
2.3 Covalent inhibition in drug discovery.....	80
2.4 Mechanism of covalent inhibition.....	83
2.5 Beyond cysteine	84
2.6 Targeting a lipid kinome conserved lysine	87
2.7 Sulfur Fluoride Exchange (SuFEx): Emerging technology in drug discovery	89
2.8 Fragment library technology	92
2.9 Project aims	94
2.10 Synthesis of activated esters	98
2.11 Synthesis and characterisation of a sulfonyl fluoride inhibitor	111
2.12 Fluorosulfate inhibitor design and characterisation	114
2.13 Lipid kinase selectivity of lead compound 2.45	124

2.14	Stability screen of fluorosulfates.....	125
2.15	Amino acid screen	129
2.16	HPLC reactivity assay	130
2.17	Mass spectrometry characterisation of lysine targeted inhibition.....	137
2.18	PI4KIII β kinetic binding assay and characterisation of lysine inhibition ...	144
2.19	Targeting tyrosine.....	148
2.20	Characterisation of tyrosine targeted covalent inhibition	154
2.21	Dual covalent inhibitor	157
2.22	Fragment library design.....	162
2.23	Conclusions.....	182
	Experimental	187
2.24	General methods and assays.....	187
2.25	Synthesis.....	194
	References	258
3	Appendices.....	267
3.1	XRPD analysis.....	267
3.2	Lipid kinase screen of 2.45	268
3.3	HPLC reference control plots.....	269
3.4	Crystallography data.....	271
3.5	Fragment mass spectrometry control compound 2.98	277

ABBREVIATIONS

Ac	Acetyl
AcOH	Acetic acid
ADP	Adenosine Diphosphate
AISF	(Acetylamino)phenyl]ImidodiSulfuryldiFluoride
AMP	Artificial membrane permeability
ATP	Adenosine Triphosphate
Aq	Aqueous
BRD4	Bromodomain-containing protein 4
BrettPhos	Dicyclohexyl(2',4',6'-triisopropyl-3,6-dimethoxy-[1,1'-biphenyl]-2-yl)phosphine
Bu	Butyl
Boc	<i>tert</i> -butyloxycarbonyl
BTK	Bruton's Tyrosine Kinase
CAD	Charged Aerosol Detection
CDK	Cyclin Dependent Kinase
ChromLogD _{7.4}	Chromatographic distribution coefficient at a particular pH, usually physiological; 7.4
Cl	Clearance
CLND	Chemiluminescence Nitrogen Detector
clogP	Calculated partition coefficient
CML	Chronic Myeloid Leukaemia
COPD	Chronic Obstructive Pulmonary Disease
COX	Cyclooxygenase
CPE	Cytopathic effect
Cys	Cysteine
DABSO	1,4-Diazabicyclo[2.2.2]octane bis(sulfur dioxide) adduct
DBU	1,8-Diazabicyclo[5.4.0]undec-7-ene
Db	Dibenzylideneacetone

DIPEA	<i>N,N</i> -Diisopropylethylamine
DMAP	<i>N,N</i> -Dimethylpyridin-4-amine
DMF	<i>N,N</i> -Dimethylformamide
DMSO	Dimethyl sulfoxide
Dppf	1,1-Bis(diphenylphosphino)ferrocene
DTT	Dithiothreitol (Cleland's reagent)
E ₁ cB	Elimination Unimolecular conjugate Base
EDC	<i>N</i> ¹ -((ethylimino)methylene)- <i>N</i> ³ , <i>N</i> ³ -dimethylpropane-1,3-diamine
Et	Ethyl
EGFR	Epidermal Growth Factor Receptor
ESI	Electrospray Ionisation
Eq.	Equivalent(s)
FaSSIF	Fasted state simulated intestinal fluid (biorelevant solubility test)
For	Formic acid
g	Grams
GSE	General Solubility Equation
GSH	Glutathione
GSK	GlaxoSmithKline
h	Hour(s)
HATU	1-[Bis(dimethylamino)methylene]-1 <i>H</i> -1,2,3-triazolo[4,5- <i>b</i>]pyridinium 3-oxid hexafluorophosphate
HEPES	4-(2-Hydroxyethyl)-1-piperazine ethanesulfonic acid
hERG	Human ether à-go-go related gene
HpH	High pH
HPLC	High performance liquid chromatography
HRMS	High resolution mass spectrometry
HRV	Human Rhinovirus

IC ₅₀	Concentration of inhibitor required to inhibit activity by 50 %
IPA	Isopropanol
IR	Infra-red (spectroscopy)
JAK	Janus Kinase
KJ	Kilojoule
LCMS	Liquid chromatography mass spectrometry
LE	Ligand Efficiency
LLE	Lipophilic Ligand Efficiency
Lys	Lysine
m	Metre
M	Concentration in moles/L
MDAP	Mass directed auto preparative chromatography
MDCK	Madin Darby Canine Kidney cells
min	Minutes
Me	Methyl
mL	Millilitres
mM	Millimolar
mmol	Millimoles
mp	Melting point
mRNA	Messenger RNA
MW	Molecular Weight
NBS	<i>N</i> -Bromosuccinimide
NFSI	<i>N</i> -Fluoro- <i>N</i> -(phenylsulfonyl)benzenesulfonamide
NIS	<i>N</i> -Iodosuccinimide
nm	Nanometre
NMR	Nuclear Magnetic Resonance
NSCLC	Non-Small Cell Lung Carcinoma
PBS	Phosphate Buffered Saline
Perm	Permeability

Ph	Phenyl
PI	Phosphoinositide
PIP	Phosphatidylinositol phosphate
PI3K	Phosphatidylinositol 3-Kinases
PI4K	Phosphatidylinositol 4-Kinases
pKa	$-\log K_a$ (pH at which 50% of the molecule is ionised)
pH	$-\log [H^+]$
pIC ₅₀	$-\log IC_{50}$
PMB	<i>Para</i> -MethoxyBenzyl
PSA	Polar Surface Area
PtdIns	Phosphatidylinositol
RBF	Round-Bottomed Flask
RCC	Renal Cell Carcinoma
R _f	Retardation factor
RNA	Ribonucleic acid
RT	Room Temperature
SDI	Sulfonyldiimidazole
Ser	Serine
SuFEx	Sulfur Fluoride Exchange
Sol.	Solubility
SLF	Simulated Lung Fluid
S _N Ar	Nucleophilic aromatic substitution
TCEP	Tris-(2-carboxyethyl)phosphine
TGN	Trans-Golgi Network
TFA	Trifluoroacetic acid
TFE	Trifluoroethanol
THF	Tetrahydrofuran
TLC	Thin-layer chromatography
TMS	Trimethylsilane

T3P	2,4,6-Tripropyl-1,3,5,2,4,6-trioxatriphosphinane 2,4,6-trioxide
t_{ret}	Retention time
Tyr	Tyrosine
Val	Valine
VEGFR	Vascular Endothelial Growth Factor Receptor
XRPD	X-ray Powder Diffraction
μL	Microliters
μM	Micromolar
μm	Micrometres

1 PART 1

1.1 Physicochemical properties in drug discovery

Physicochemical and molecular properties such as solubility, permeability and lipophilicity are important parameters in drug discovery. They can influence the pharmacokinetic, pharmacodynamic and safety profile of a potential drug.² There is often a balancing act between these various parameters to find candidates with sufficient solubility, permeability and metabolic stability for the desired target.^{3,4}

Solubility is a critical parameter in drug discovery, particularly for orally dosed compounds.⁵ Poorly soluble compounds can have reduced gut absorption and variability in drug plasma concentration which can lead to attrition during development.⁶ It is important to measure solubility during lead optimisation, and to be able to have strategies for improving it.^{3,7}

Solubility is reported as either thermodynamic or kinetic; these refer to two different aspects of behaviour that a molecule possesses when undergoing dissolution.⁸ Kinetic solubility refers to any solubility that is associated with a metastable form of a compound.⁹ Thermodynamic solubility is the maximum amount of the most stable form of the compound (preferably crystalline) that can remain in solution under equilibrium conditions.¹⁰ In the literature, kinetic solubility is widely reported and accepted as it can be automated more easily.⁵

Obtaining permeable compounds is crucial as it is important for the drug to reach the desired site of action. Permeability is often reported as artificial membrane permeability (AMP) and is a measure of the passive diffusion of molecules across an artificial phospholipid membrane.¹¹ There are other permeability assays e.g. the MDCK cell line, where active transporters are present which will affect the permeability.¹² Permeability assays with active transporters present are desirable as

they can establish an *in vitro* model to screen for orally absorbed compounds, which can provide an indication of the mechanism of transport i.e. is the compound likely to be actively transported into or out of the cell? Often, increasing lipophilicity helps increase the passive permeability of the compounds.¹³

Lipophilicity is measured experimentally as a partition coefficient and is reported as logP or logD. Log P describes the partition equilibrium of un-ionized solutes between water and *n*-octanol.¹⁴ Whereas, log D describes the ratio of the sum of the concentration of all forms of the compound in the aqueous phase and is measured at a specific pH.^{15,16} Under physiological conditions the pH of blood is 7.4 and is the standard pH quoted for logD. However, it can also be informative to measure the lipophilicity under more basic (pH 10) and acidic (pH 4) systems. Our laboratories have developed a high-throughput chromatographic measure of lipophilicity using a reversed phase HPLC column which is referred to as chromlogD_{7.4}.¹⁷ The value of the chromatographic measurement of the lipophilicity has been demonstrated by Young *et al*, where it could be correlated with the distribution of all species present at a given pH.¹⁸

These three parameters combined make up part of the physicochemical profile of a compound and being able to optimise these is key to the drug development process, where these types of issues are often encountered in lead optimisation. For example, Pfizer have published work around the lead optimisation of the physicochemical properties of a series of molecules **1.1**.¹⁹ As the lipophilicity of the compound was decreased (lowered logD), the permeability was reduced but the thermodynamic solubility increased. The optimisation of the physicochemical profile led to the development of a candidate selected compound **1.2 (Figure 1.1)**.¹⁹

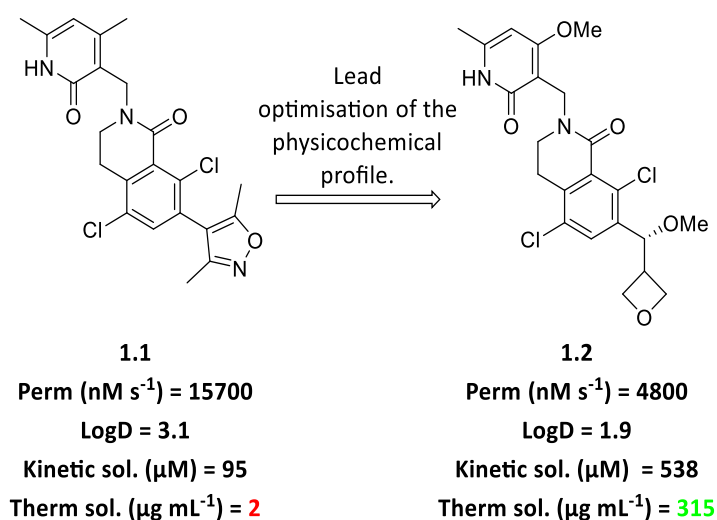


Figure 1.1: Optimisation of the physicochemical profile.

To aid the medicinal chemist, in 1997, Lipinski introduced the rule of five which is the most cited rule to evaluate the likelihood of a compound being orally bioavailable.^{20,21} The rule of five was based on the observation that phase II candidates fall within a certain size, lipophilicity and polarity range regardless of the pharmacological class. Lipinski's rules state that, in general, an orally bioavailable drug has no more than one violation of the following:

1. Lipophilicity should be less than 5 (clogP).
2. Number of H-bond donor groups should be less than 5 (HBD).
3. Number of H-bond acceptor groups should be less than 10 (HBA).
4. A molecular mass less than 500 Da (MW).

It has been well established that over 90% of marketed drugs obey these guidelines, exhibiting a good pharmacokinetic profile.²² More recently, the literature has reported modifications to Lipinski's rule of five in the design of molecules with a good physicochemical space for orally dosed drugs.²³ Pfizer developed the golden triangle which has been used as a visualisation tool to help medicinal chemists achieve metabolically stable, permeable and potent drug candidates.^{24,25} The golden triangle can be used as a tool to impact the design of new targets with desirable drug-like properties (**Figure 1.2**).

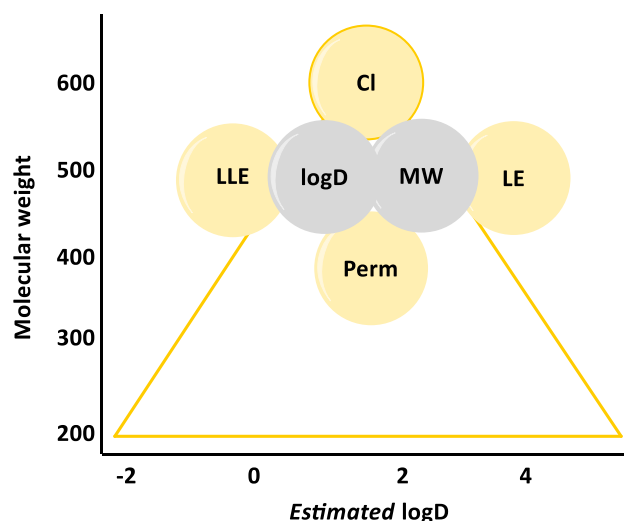


Figure 1.2: The golden triangle; visualisation tool to aid compound design (Graphical image adapted from pfizer, see reference 24).²⁴

Additionally, building upon Lipinski's rule of five, subsequent reports have identified both polar surface area (PSA), i.e., surface belonging to polar atoms, and rotatable bonds as factors which impact the likelihood of drug developability.^{7,26,27} Veber and co-workers measured the oral bioavailability in rats for over 1100 drug candidates which allowed them to delineate the effects of the number of rotatable bonds and polar surface area on the oral bioavailability of the compounds.^{28,29} This revealed the benefits of reducing the polar surface area (≤ 140) and keeping the number of rotatable bond less than or equal to 10 on the oral bioavailability of the compounds.

Despite the success of chemists obeying the 'rule of five' there are recent reports regarding the development of new therapeutic agents that surpass the rule of five.³⁰ AbbVie stressed the observation that approximately 6% of oral drugs are outside of Lipinski's guidelines which suggests that there are opportunities to exploit. Lipinski later published his views on Navitoclax **1.3** (**Figure 1.3**) an orally bioavailable drug which does not comply with the rule of five.⁹ Compound **1.3** has a clogP greater than 5, 14 hydrogen bond acceptors and a molecular weight greater than 500 Da, breaking three of Lipinski's rules. Generally, recent marketed drugs appear to be increasing in molecular weight and lipophilicity which suggests more drug discovery efforts are

1.2 Strategies for improving solubility

In drug-discovery, phenyl and heteroaromatic rings are ubiquitous, with benzene **1.4** and pyridine **1.5** being the two most commonly found aromatic systems in marketed drugs.³⁷ Varying the aromatic and heteroaromatic groups can confer different physicochemical properties to the molecule which can have potential impact on the progression of drug discovery projects.^{38,39} The introduction of a basic centre and polarity to the compound have been shown to influence the properties of the compound (**Figure 1.4**).^{40,41} The presence of the nitrogen atom in the pyridine ring alters the electron distribution, inducing a dipole and introducing polarity into the ring which can influence the properties of the compound. Thus, understanding how these types of modifications impact the physicochemical profile of the compounds is crucial. As a result, different approaches in the pharmaceutical industry have been employed for improving the physicochemical properties.^{38,42,43} For example, replacing a phenyl ring with a pyridyl ring is frequently used by medicinal chemists to improve the profile of a molecule.⁴⁴

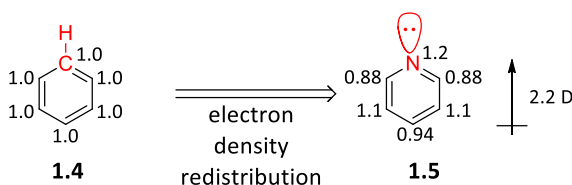


Figure 1.4: Substitution of CH with an N atom is a small structural modification with potential implications on the physicochemical and pharmacological profile.

It has been shown that too many carboaromatic rings lead to poorer overall developability of a compound by increasing the lipophilicity and decreasing the solubility.⁴⁵ A widely used strategy to overcome this problem is to increase the solubility of a drug candidate by increasing its polarity through replacement of carboaromatic rings with heteroaromatic rings; the use of this approach is reflected in the increasing prominence of heteroaromatics in drug discovery (**Figure 1.5**).^{36,46} The increase in carboaromatic character represents a significant decrease in the

average solubility.⁴⁵ Introducing heteroatoms improves the average solubility and decreasing the aromatic ring count by replacing with heteroaliphatic rings increases the average solubility further.³⁸

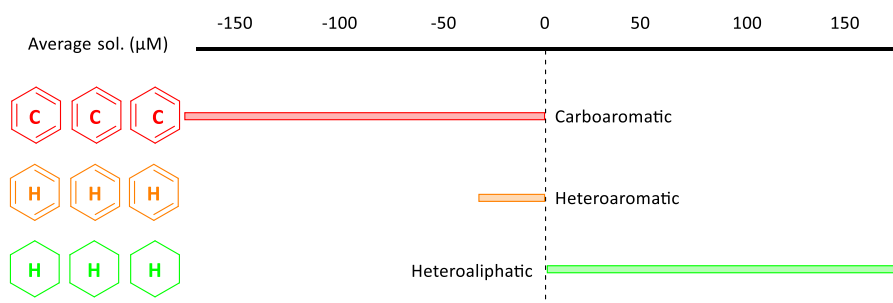


Figure 1.5: Change in average solubility for 3 classes of rings (set of 19196 compounds). Red = carboaromatic; Yellow = heteroaromatic; Green = heteroaliphatic.⁴⁵ Adapted from reference 45.

Humblet and co-workers hypothesised that increasing saturation was an approach to improving clinical success.⁴⁷ They demonstrated that both fraction of sp^3 character and the presence of chiral centres correlated with the success as compounds transitioned from discovery, through to drug molecules (**Figure 1.6**).⁴⁸ This could be further correlated to the solubility and melting point temperature.³² The increased saturation disrupts the crystal lattice energy, decreasing the melting point and thereby increasing compound solubility.⁴⁹

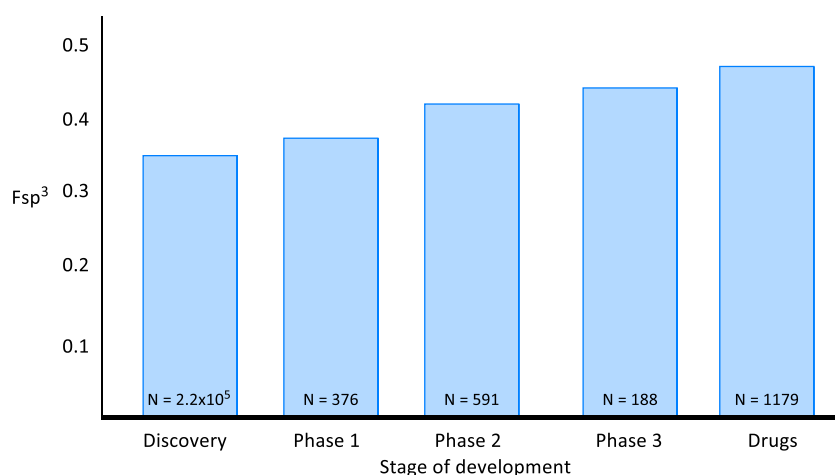


Figure 1.6 The average Fsp³ character at the different stages of drug development (adapted from reference 47).

This hypothesis was explored by Wang *et al* where significant gains in thermodynamic aqueous solubility were obtained for their clinical candidate **1.7** as shown in **Figure 1.7**.⁵⁰ Their strategy was to increase the sp³ character of **1.6** to reduce structural planarity thereby disrupting the crystal-stacking capability of the molecule.⁵¹ These changes meant that the thermodynamic solubility was increased and this was reflected in the decreased melting point temperature of **1.7** (**Figure 1.7**). However, the lipophilicity of **1.7** was reduced and so this was also likely to have contributed to the thermodynamic solubility gains, thus highlighting the difficulties associated with correlating solubility gains with a single molecular property.

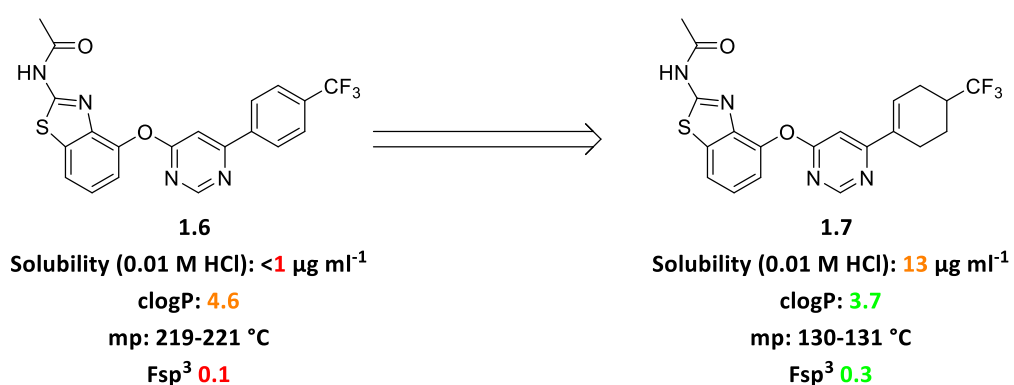


Figure 1.7: The effect of increasing carbon sp³ character on the thermodynamic solubility.

Nitrogen atoms are ubiquitous in drug discovery programs and contribute to the molecular properties of the compound.⁴¹ Whether or not basic nitrogen atoms are protonated under physiological conditions may not only be critical for binding potency, but also affects the physicochemical properties. Protonation of a nitrogen leads to an increase in aqueous solubility but can also be linked with introducing other liabilities.⁵² It has been established that basic nitrogen atoms increase the volume of distribution leading to wider tissue distribution, thus in some cases increasing off target effects.^{53,54} Bristol Myers Squibb have correlated the effects of introducing basic groups with the probability of increasing hERG inhibition.⁵⁵ hERG encodes a voltage-gated potassium channel which is key for the function of the cardiac action potential. Pharmacological blockage of this channel can cause sudden death.⁵⁶ There are reported strategies for controlling the pKa of basic nitrogens which could potentially overcome the risks associated with the introduction of a basic centre e.g. fluorination. Therefore, basic nitrogens are common structural modifications for improving the physicochemical profile of a candidate drug molecule.⁵⁷

A carboxylic acid group is ionised under physiological conditions which significantly improves the aqueous solubility of the compound. However, a carboxylate group is known to be detrimental to the permeability of a molecule, leading to poor cell activity and reduced oral exposure.^{21,58} This has led to the work of Christel and co-workers, where the physicochemical properties of ciprofloxacin (**1.8**) derivatives were investigated through synthesising flexible lipophilic esters of the acid as shown in **Figure 1.8**.⁵⁹ It was hypothesised lipophilic fragments (**1.9**) could disrupt the crystal lattice energy by increasing the molecular flexibility, resulting in improved solubility and permeability. In this study, the introduction of lipophilic ester groups improved the permeability of **1.8**, but did not always improve the solubility of the compound which highlighted the importance of striking a balance between polarity and flexibility when considering compound solubility.

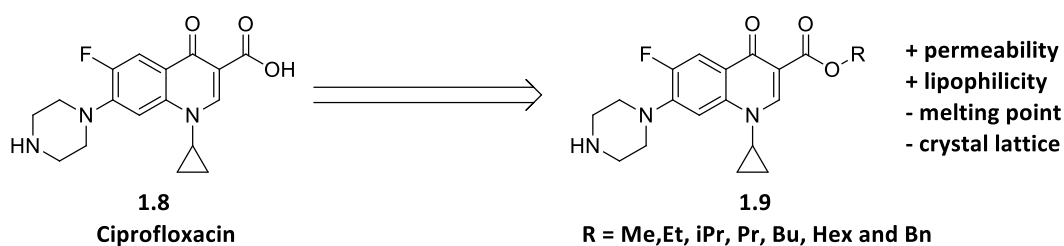


Figure 1.8: Ciprofloxacin and analogues appended with different groups.

AstraZeneca have proposed a strategy for improving the properties of compounds through ‘building bridges’ (**Figure 1.9**).⁶⁰ The properties of common medicinal chemistry containing groups (e.g. morpholine, piperazine and piperidine) were explored and it was demonstrated how building a one carbon- sp^3 bridge actually decreased the lipophilicity of the resulting bicyclic structure.⁵³ As shown in **Figure 1.9**, compound **1.10** showed an increase in basicity and a decrease in lipophilicity in comparison to compound **1.11**. Quantum mechanical calculations showed that the 3-dimensional shape of the compound was significantly altered, and this led to an increased solvent exposed polar surface area, increasing the basicity. This has potential implications on the crystal lattice packing which can influence the solubility through decreasing the melting point (see **Equation 1.1**).

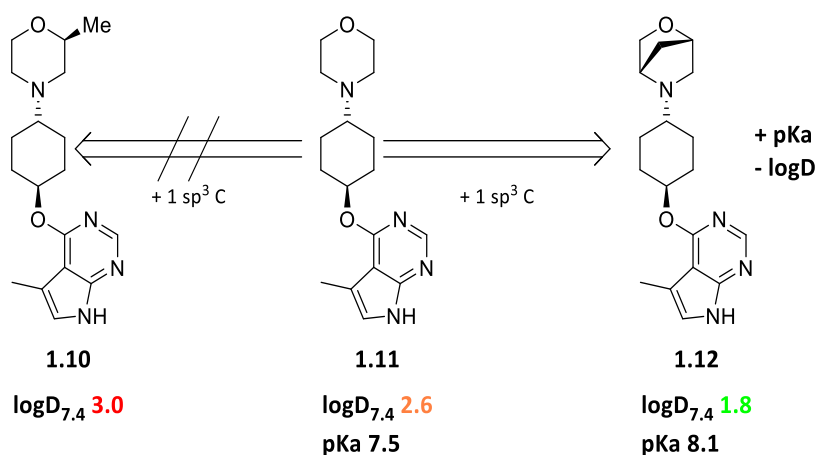


Figure 1.9: The positional influence of introducing a single sp^3 carbon on the physicochemical properties.

Ferrins *et al* explored the work carried out by AstraZeneca.⁶¹ Their lead compound **1.13** was potent towards the desired target but lacked appropriate physicochemical properties. Multiparameter optimisation was carried out through increasing the carbon sp³ character and significant changes to the profile of the compound were observed through this approach. The appended piperazine group (**1.13**) was changed to a bridged piperazine, **1.14**, and this gave significant gains in the aqueous solubility, potency, lipophilic ligand efficiency (LLE) and metabolic stability (**Figure 1.10**).⁶²

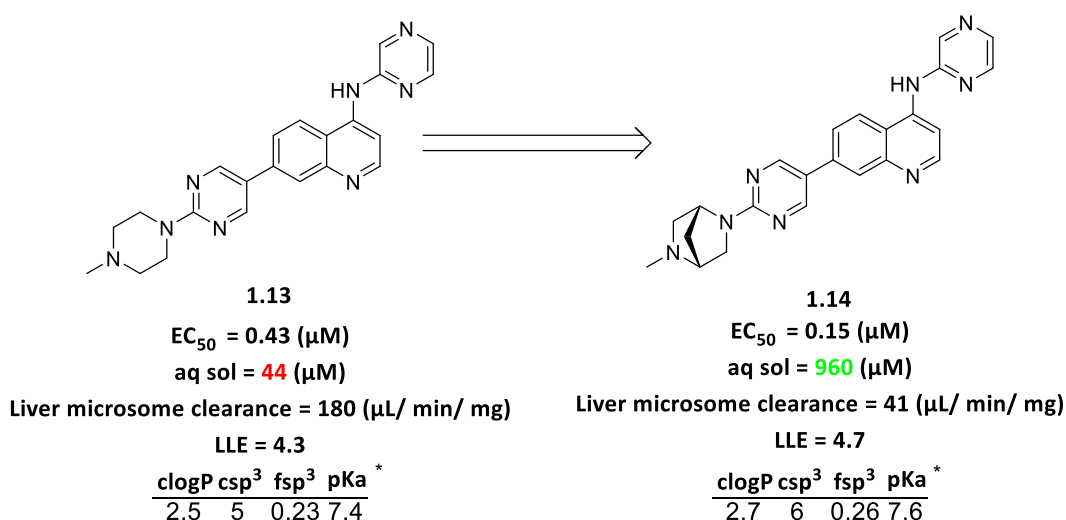


Figure 1.10: Multiparameter optimisation of a quinoline series through building a carbon bridge. * Properties calculated using GSK predictive algorithms.

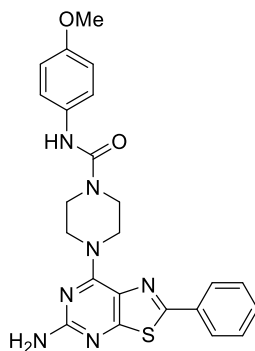
Significant improvements to the profile of the compound was achieved through increasing the fraction of carbon sp³ character (0.23 vs 0.26). Additionally, the pKa of the most basic centre was calculated using GSK predictive tools and a 0.2 log difference is estimated (7.4 vs 7.6). This correlated to approximately a 1.5-fold difference in protonation of the bridged piperazine ring and there is a 20-fold difference in the aqueous solubility. In addition, the paper should have reported the chromlogD and pKa values of the molecule which could be further correlated with the increased basicity of the bridged piperazine ring. As a result, the increased solubility could have been due to several parameters. From the limited data, the authors concluded that the solubility increase was due to the increased fsp³ character

(0.23 vs 0.26). Despite the improved profile, hERG inhibition was identified (linked with increased basicity) and the authors were sceptical about further development of this compound series.⁶³ This work highlights the difficulties associated with multiparameter optimisation and how improvement of one parameter can often introduce other liabilities and affect compound progression in drug development.⁶⁴

In summary, current literature methods for improving the physicochemical profile of a compound include decreasing the lipophilicity of molecule, through replacement of aromatic rings with heteroaromatic rings. Increasing the saturation of the compound by increasing the sp³ character has been shown to disrupt the crystal lattice packing, resulting in a solubility improvement. Current strategies for improving the overall profile of lead candidates have highlighted the associated issues encountered. Liabilities are often introduced which prevents further progression of the lead compound series, therefore, other strategies for improving the physicochemical profile require exploration.

1.3 Project aims

PI4KIII β has recently generated attention in drug discovery projects within our laboratories and elsewhere. A key focus within optimising has been on the potency of the compounds.⁶⁵ The current literature shows the design of some highly potent molecules with a 6,5-bicyclic cores, however, many of these compounds demonstrate suboptimal physicochemical properties for further progression (**Figure 1.11**).⁶⁶ Lead compound **1.15** shows desirable activity towards PI4KIII β but has a poor overall physicochemical profile e.g. low solubility. Due to the tendency to focus on selectivity and potency during series optimisation within kinase drug discovery programmes, there is limited literature available with a specific focus on the physicochemical properties of the compounds and how this effects the progression of compounds.



1.15
PI4KIIIβ IC₅₀ (nM) 11
logD (pH_{7.4}) not determined
Kinetic solubility (μM) 6
clogP 3.8, Fsp³ 0.2 *

Figure 1.11: Literature example of a potent PI4KIIIβ inhibitor with poor physicochemical properties.¹ * Properties calculated using GSK predictive algorithms.

Due to the ubiquitous nature of heteroaromatic ring systems in drug discovery, investigation of the properties of these ring systems is important. The initial aim of this work was to investigate the systematic effects of different nitrogen atom configurations of 6,5 bicyclic heterocycles on the physicochemical properties of a compound, such as thermodynamic solubility (**Figure 1.12**). Analysis of the physicochemical properties was carried out on crystalline batches (supported by XRPD analysis) to give a robust comparison of the thermodynamic solubility data. Additional properties such as pKa, melting point and lipophilicity were measured to understand how subtle core changes can influence physicochemical properties. The rationale behind this was that there could potentially be a drug scaffold with better physicochemical properties to build the molecule around and therefore provide a greater chance of the molecule meeting the GSK candidate quality criteria.³⁹

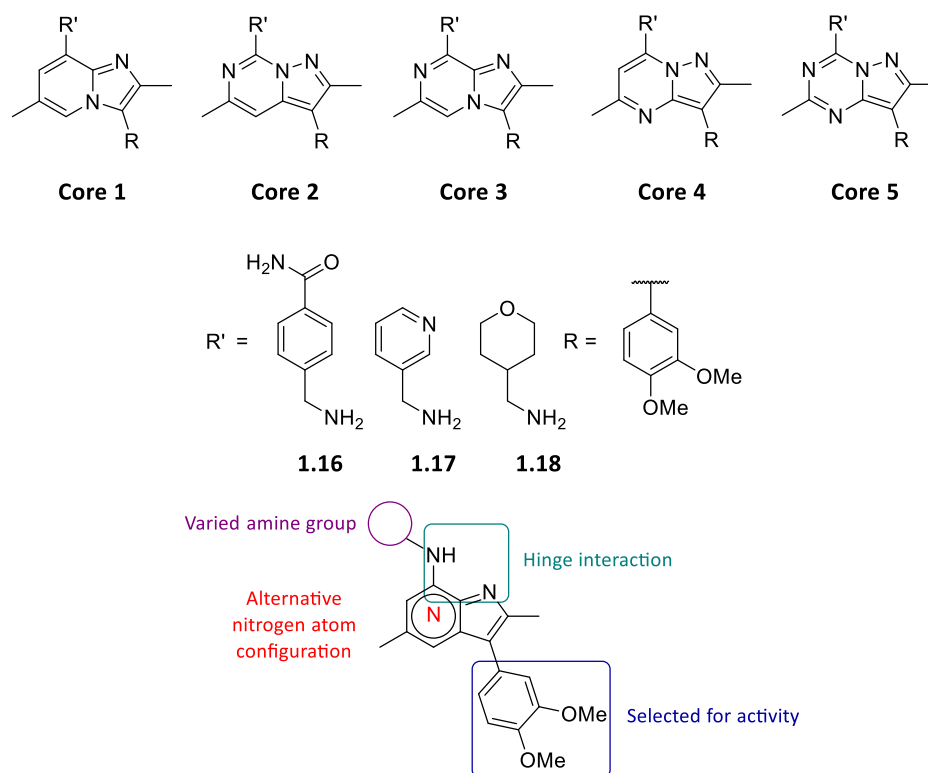


Figure 1.12: 6,5-Bicyclic heterocycles investigated, each core was appended with three different rings (**1.16-1.18**).

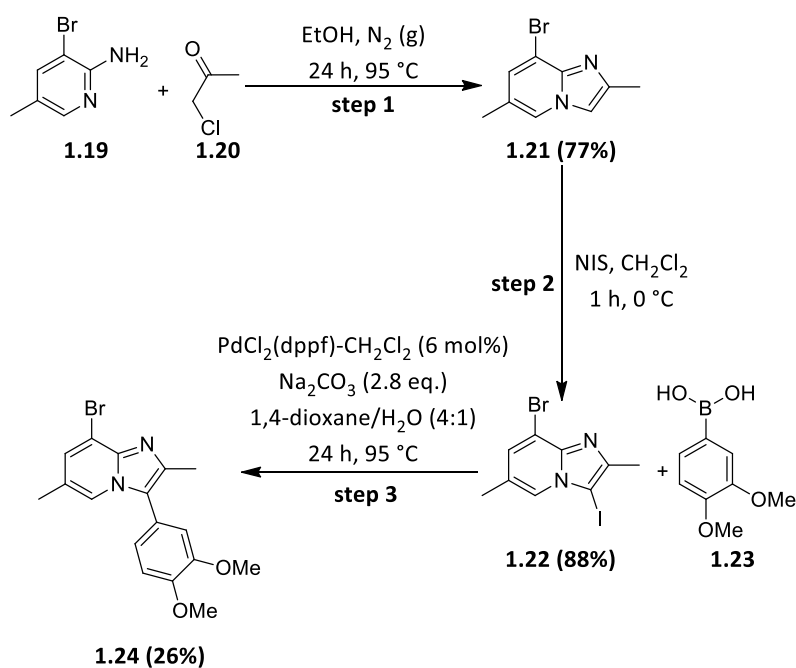
To enable the direct comparison of the effect of altering the core on the physicochemical profile of the molecule, the pendant groups were kept constant. Based upon project knowledge, 3,4-dimethoxy benzene was selected for all final compounds to provide a level of solubility and potency in the final molecule. The methoxy substituents of the phenyl ring made key hydrogen bonding interactions inside the active site of the lipid kinase PI4KIII β . The pendant amine R' group (**1.16-1.18**) consists of typical medicinal chemistry functional groups: an aromatic ring, a heteroaromatic ring and a fully saturated ring which provided a broader range of functionality on each of the cores to determine how the properties were affected.

Part Two of the thesis builds upon this work, where the core with the best balance of potency and physicochemical properties was taken forward to investigate whether a covalent warhead could be appended to the scaffold to target the conserved lysine in the active site of PI4KIII β .

1.4 Synthesis of Cores 1-5

The synthetic procedures to prepare the 5 cores are described below. Crystalline batches of the final compounds were obtained, excluding Core 3 where multiple crystallisation techniques were performed but the set of compounds remained as amorphous solids. The crystallinity of the molecules was supported by plane polarised light microscopy and X-ray powder diffraction analysis (**Appendices 3.1**).

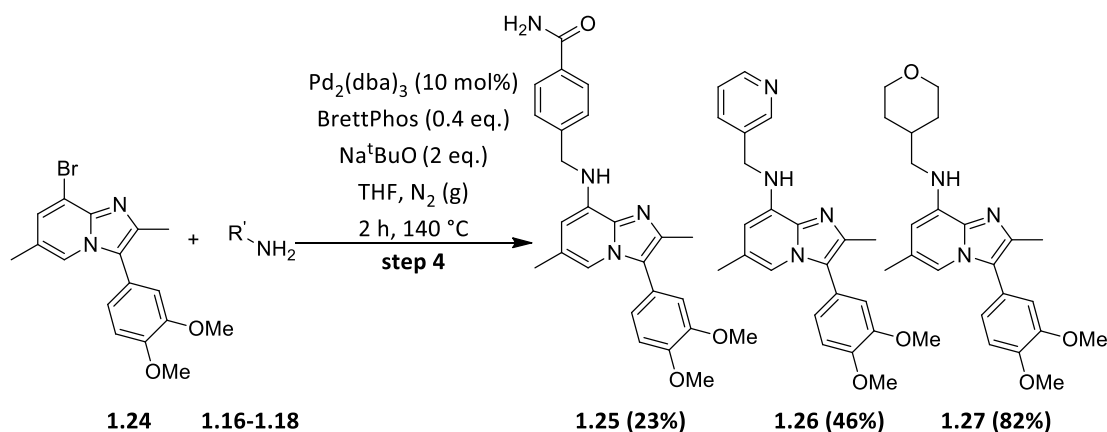
Core 1 was the only core to contain 2 nitrogen atoms and the first three steps of the synthesis are shown in **Scheme 1.1**.



Scheme 1.1: Synthesis of intermediate **1.24**.

Compound **1.19** underwent cyclisation with chloroacetone **1.20** under an inert nitrogen atmosphere and forcing reaction conditions to afford 8-bromo-2,6-dimethylimidazo[1,2-*a*]pyridine (**1.21**) in 77% yield (**Scheme 1.1**). Compound **1.21** was purified by an aqueous wash and characterised by ¹H NMR, ¹³C NMR and LCMS. 8-Bromo-2,6-dimethylimidazo[1,2-*a*]pyridine (**1.21**) was iodinated with NIS in CH₂Cl₂ at 0 °C to form the bis-halogenated compound (**1.22**) in 88% yield. The reaction

progressed smoothly, and an aqueous work up was adequate for purification purposes. 8-Bromo-3-(3,4-dimethoxyphenyl)-2,6-dimethylimidazo[1,2-*a*]pyridine (**1.24**) was formed by a Suzuki-cross coupling reaction. The boronic acid (**1.23**) was coupled with the bis-halogenated reactant (**1.22**) to form the desired product in poor yield (26%), after purification by column chromatography. The poor yield was due to selectivity issues during the reaction of the bis-halogenated intermediate (**1.22**) which was supported by LCMS. To overcome this, the subsequent Buchwald-Hartwig cross coupling reaction could have been performed before the iodination. However, the presence of the amino group may have been problematic for the Suzuki-cross coupling reaction.⁶⁷ At this stage sufficient amounts of **1.24** had been prepared for subsequent investigations.



Scheme 1.2: Synthesis of target compounds of Core 1.

Finally, a series of Buchwald-Hartwig cross coupling reactions were carried out under inert reaction conditions on compound (**1.24**) to form the new carbon nitrogen bond as shown in **Scheme 1.2**. Forcing reaction conditions were required to bring about the transformation which led to the formation of side-products which introduced challenges to the purification. The reactions gave poor to good yields of the products (23-82%) and were purified by column chromatography or by mass directed auto preparative chromatography (MDAP). The basicity associated with the imidazo-pyridine core led to target products eluting in a higher proportion of EtOAc (**1.25**,

1.26 & 1.27) from the silica column. The final compounds were isolated as solids and were fully characterised by ^1H NMR, ^{13}C NMR, LCMS, IR, Mp and HRMS.

Core 2 contained an additional nitrogen atom in the 6,5-bicyclic system. This was selected as it could identify whether an additional nitrogen atom would be necessary to improve the overall physicochemical profile. A general overview for the synthesis of Core 2 is shown below in **Figure 1.13**.

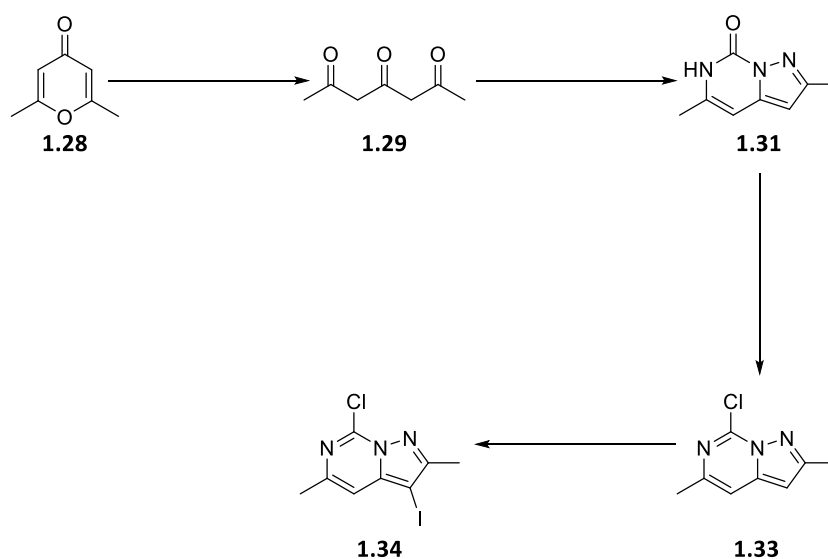
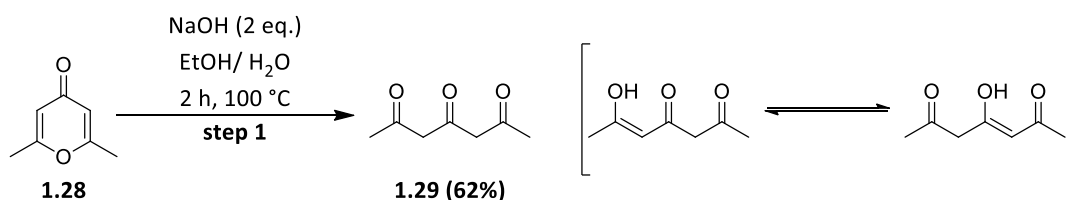


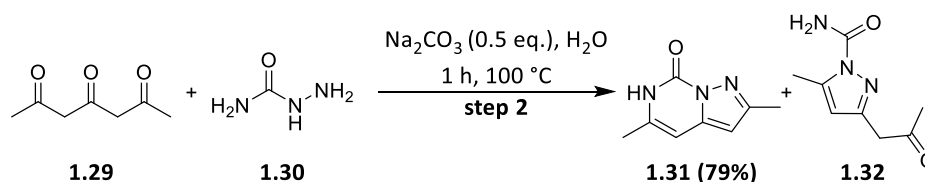
Figure 1.13: General synthetic procedure for key intermediate (**1.34**).

The additional nitrogen atom was introduced into the 6,5-bicyclic system to investigate the effects this could potentially have on the physicochemical profile of the final compounds.



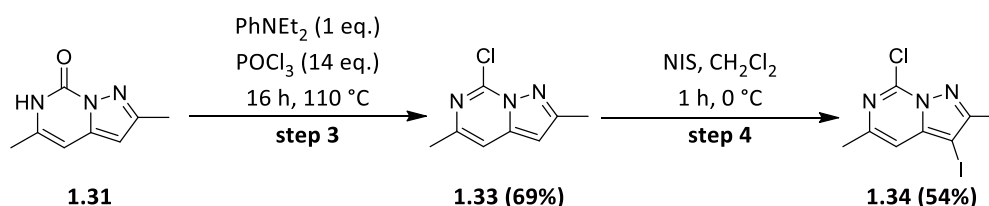
Scheme 1.3: Synthesis of tricarbonyl intermediate (**1.29**).

To begin with, 2,6-dimethyl-pyran-4-one (**1.28**) and aqueous NaOH (16 M) were refluxed together in ethanol for 2 hours. The product was purified by precipitation from solution, and was collected by vacuum filtration, washed with diethyl ether and isolated in good yield (62%). Compound (**1.29**) exhibits tautomerism with different enol forms being present in solution as shown in **Scheme 1.3** which gave rise to complex ^1H and ^{13}C NMR data, consistent with the literature.⁶⁸



Scheme 1.4: Synthesis of 2,5-dimethylpyrazolo-pyrimidin-7-one (**1.31**).

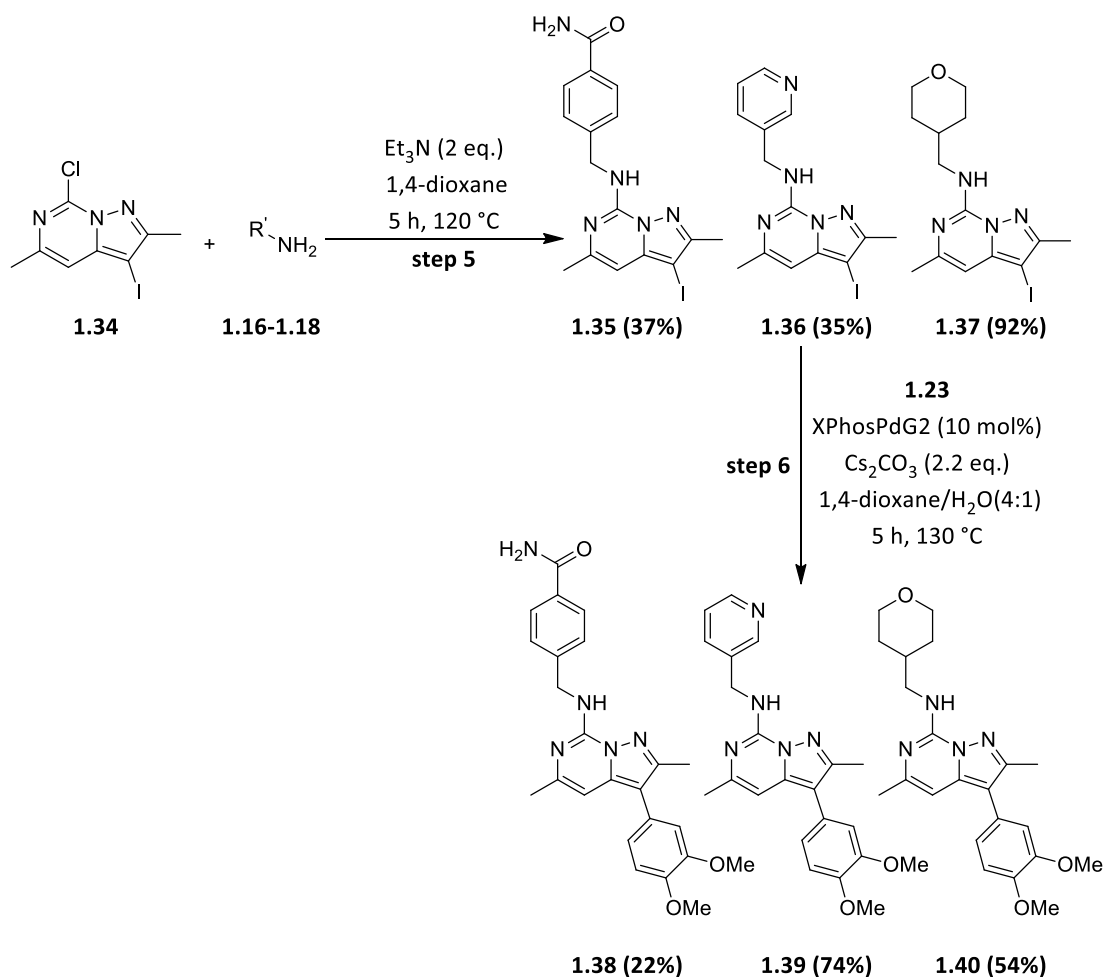
The tricarbonyl reactant (**1.29**) and hydrazinecarboxamide (**1.30**) were heated together under aqueous basic conditions to form the bicyclic heterocycle **1.31** in a single step. A co-product **1.32** was also observed in the crude ^1H NMR spectrum of the reaction. Nucleophilic attack of compound (**1.30**) could occur at the central carbonyl group of **1.29** instead of the terminal carbonyl group leading to **1.32**. This produced a pyrazole species which was not detectable by LCMS (**1.32**). Column chromatography was used to remove this unwanted product.



Scheme 1.5: Synthesis of compound (**1.34**).

The pyrimidone species (**1.31**) was refluxed in POCl_3 in the presence of *N,N*-diethylaniline for 16 hours to give the chlorinated compound (**1.33**). The solvent was removed *in vacuo* and the crude material was purified by an aqueous work-up to afford the product in good yield (69%). Compound (**1.33**) was iodinated with NIS in

CH₂Cl₂ at 0 °C to form the bis-halogenated compound (**1.34**) as shown in **Scheme 1.5**. Aqueous sodium thiosulfate was used to remove excess iodine residues. The crude product was purified by column chromatography to give the desired product (**1.34**) in moderate yield (54%).

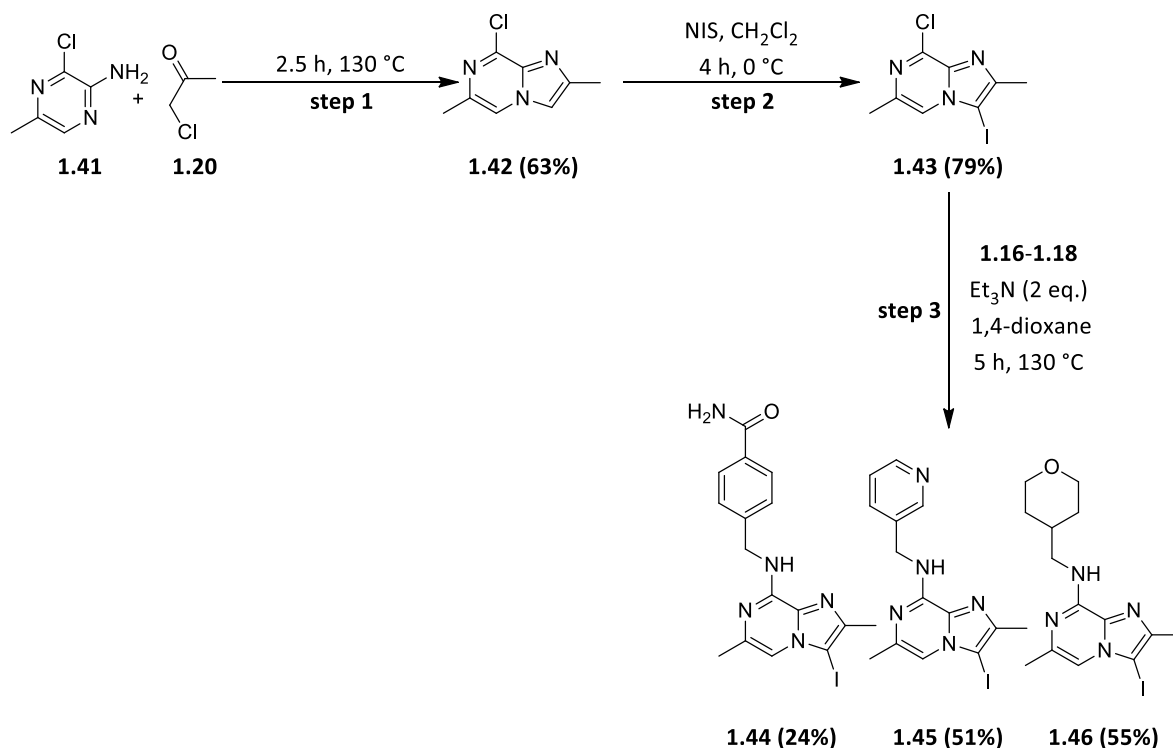


Scheme 1.6: Synthesis of compounds **1.38**, **1.39** and **1.40**.

The bis-halogenated intermediate (**1.34**) was heated to 120 °C for 5 hours in the presence of triethylamine and a primary amine (as shown in **Scheme 1.6**) to give the products of a nucleophilic aromatic substitution (S_NAr) reaction. After the reaction went to completion, an aqueous work-up was performed and the crude product was purified by MDAP (high pH method). The final step of the synthesis involved a series of Suzuki cross-coupling reactions under forcing reaction conditions, whereby the

aryl iodide was reacted with the boronic acid (**1.23**). All of the reactions required column chromatography to obtain analytically pure material.

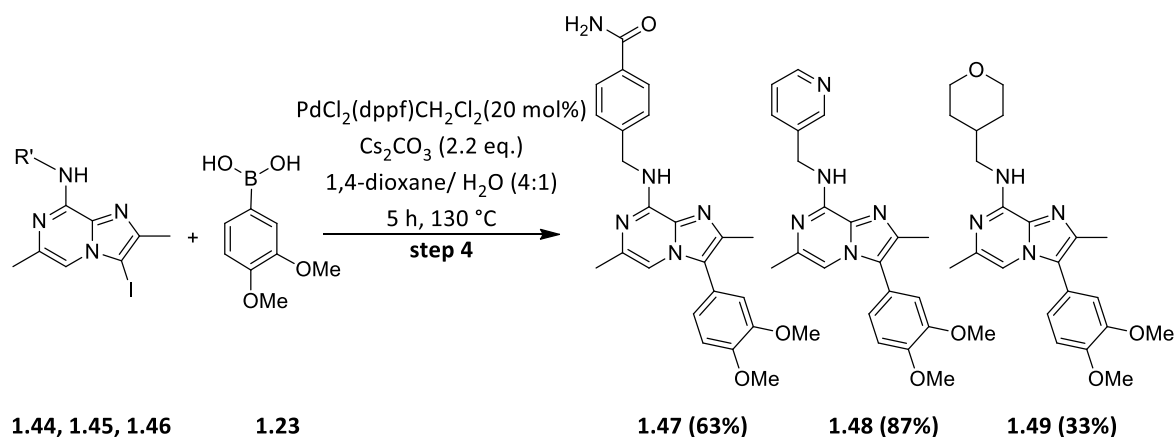
The synthesis for Core 3 is shown below in **Scheme 1.7**, where the position of the central bridged nitrogen was shifted one position.



Scheme 1.7: Synthesis of bis-halogenated intermediate (**1.43**) and subsequent S_NAr reactions.

Compounds **1.41** and **1.20** were heated together at 130 °C for 2.5 hours to form the cyclised product (**1.42**) in good yield (**Scheme 1.7**). It was important to carry out the reaction under solvent free conditions to prevent the formation of multiple alkylation side-products. An aqueous work up was carried out and the product was characterised by ¹H NMR, ¹³C NMR and LCMS. Compound **1.42** was halogenated with NIS at 0 °C to give compound **1.43** in 79% yield (**Scheme 1.7**). The penultimate step of the synthesis involved a series of S_NAr reactions where compound **1.43** was treated

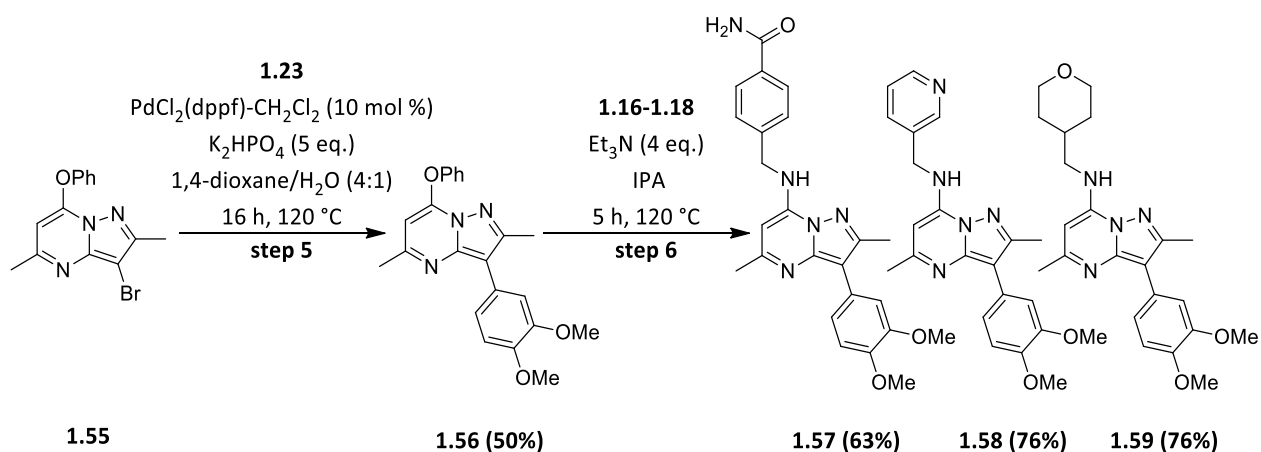
with amines (**1.16-1.18**) under forcing reaction conditions to give compounds **1.44**, **1.45** and **1.46** in low to moderate yield (24-55%).



Scheme 1.8: Synthesis of final compounds **1.47**, **1.48** and **1.49**.

Intermediates **1.44**, **1.45** and **1.46** were coupled with 3,4-dimethoxyphenyl boronic acid (**1.23**) under forcing reaction conditions to give the final compounds (**1.47**, **1.48** & **1.49**) as gums in moderate to high yields (33-87%), after column chromatography and MDAP purification (**Scheme 1.8**). Multiple crystallisation techniques were carried out on these final compounds, however, amorphous solids could only be obtained, and this was supported by plane polarised light microscopy and XRPD analysis. This could potentially influence the thermodynamic solubility data because the most stable form of the compounds (crystalline) were not obtained which could therefore lead to an over estimation of the compound's true thermodynamic solubility.

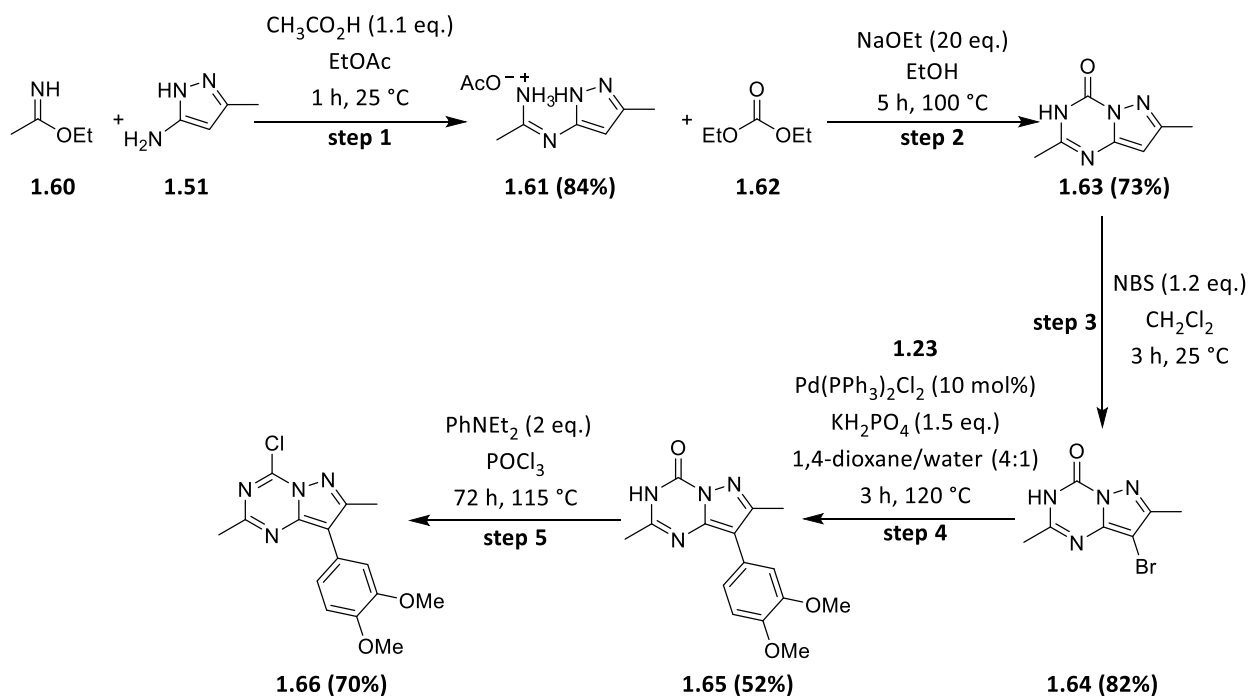
A four-step sequence to prepare Core 4 is shown below in **Scheme 1.9**.



Scheme 1.10: Final compounds of Core 4.

3-(3,4-Dimethoxyphenyl)-2,5-dimethyl-7-phenoxy-pyrazolopyrimidine (**1.56**) was synthesised according to **Scheme 1.10** by carrying out a Suzuki-coupling reaction of compound (**1.55**) with boronic acid (**1.23**). The reaction was purified by column chromatography to give the product (**1.56**) in moderate yield (50%). A significant by-product of this reaction was the *des*-bromo species. Subsequently, a series of $\text{S}_{\text{N}}\text{Ar}$ reactions were performed on compound (**1.56**) as shown in **Scheme 1.10**. The phenoxy group was displaced by heating in the presence of a primary amine (**1.16-1.18**), and triethylamine in IPA at 120 °C for 5 hours. The products were purified by MDAP (high pH method) to give solid products in good yields (63-76%).

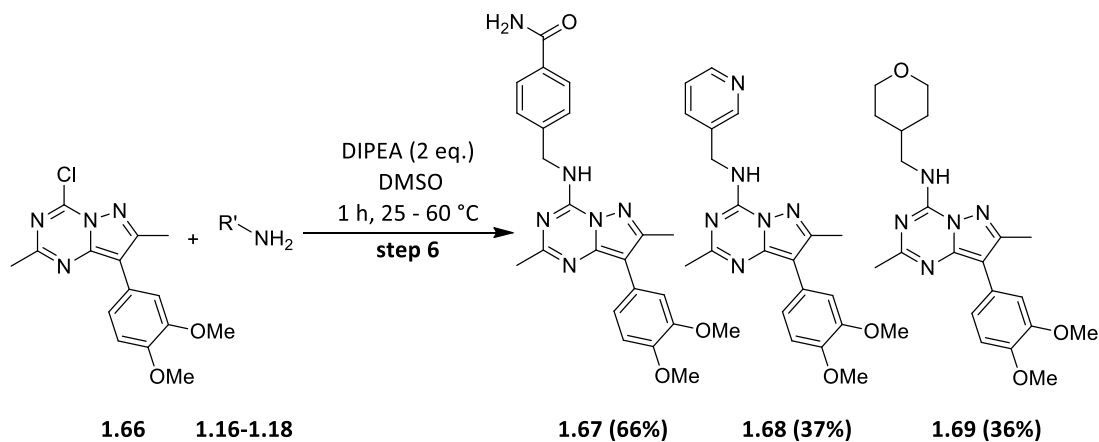
The final target was to synthesise Core 5. An additional fourth nitrogen atom was introduced into the ring system.



Scheme 1.11: Synthetic route to key intermediate (**1.66**).

3-Methyl-1*H*-pyrazol-5-amine (**1.51**) was stirred with ethyl acetimidate (**1.60**) at room temperature for 1 hour. Subsequently, acetic acid was added to the reaction, stirred for 30 min and the desired product was collected by vacuum filtration affording **1.61** in 84% yield. Amidine derivative **1.61** does not ionise under LCMS conditions but the parent compound (minus the acetate) was detected by HRMS. To form the cyclised intermediate (**1.63**), excess diethyl carbonate (**1.62**) was used, in the presence of sodium ethoxide. Foaming of the reaction mixture was initially observed and it was important to use a new bottle of sodium ethoxide to ensure the progression of the reaction. Compound **1.63** was treated with *N*-bromosuccinimide to incorporate and the reaction progressed smoothly, with the desired product (**1.64**) precipitating out of solution as a white solid without the need for further purification. A Suzuki-cross coupling reaction was then carried out and this gave the desired product (**1.65**) in 52% yield. A problematic step of the synthesis was the formation of the chlorinated compound (**1.66**). The desired reaction gradually progressed over three days, however, there was an instability associated with **1.66** which led to difficulties with the isolation of this compound. A quick aqueous work up was

performed, and column chromatography was carried out efficiently to prevent the hydrolysis of the chloride product.



Scheme 1.12: Final compounds of Core 5 synthesis.

Primary amines (**1.16-1.18**) were pre-mixed with DIPEA in DMSO before the addition of the chlorinated substrate (**1.66**). The desired compounds were obtained in moderate yields (36-66%), the unstable nature of compound (**1.66**) may have contributed to the poorer yields of the final compounds. The reaction conditions were varied through controlling the reaction temperature. Initially the S_NAr reaction was carried out at 60 °C and this led to poorer overall yields for compounds (**1.68** & **1.69**). Potentially the rate of hydrolysis was faster than the rate of the desired reaction. The reaction was then carried out at RT and this led to an improved yield for **1.67** (66%). Crystalline batches of the final compounds were obtained, and the compounds were fully characterised.

The 6,5-bicyclic heterocycles (shown in **Figure 1.14**) were successfully synthesised and characterised. The next step was to investigate the properties of all fifteen compounds to determine which pendant group and core molecule displayed the most promising physicochemical properties. In combination with the potency data, one of the cores would be taken forwards to the next part of the project.

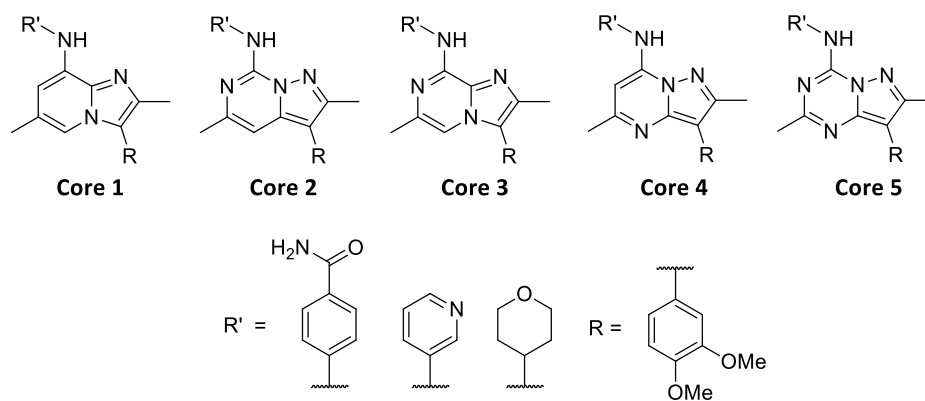


Figure 1.14: Final 6,5-bicyclic heterocycles.

1.5 Physicochemical properties of the synthesised heterocycles

The subsequent part of this work was to measure the kinetic and thermodynamic solubilities of the synthesised nitrogen containing heterocycles in order to determine if there was a difference between the cores. The protocols for the solubility assays are discussed in **Section 1.7**. The kinetic solubility was determined by the precipitation of the sample out of solution, whereas, the thermodynamic solubility was measured through the solid sample undergoing dissolution.

The kinetic and thermodynamic solubility were measured for each final compound. The kinetic solubility was detected by CAD (charged aerosol detection) which is a method used to accurately determine the absolute concentration of stock and sample solution. This can be important for the kinetic assay as overestimation of the compound's solubility is often observed due to the hygroscopic nature of DMSO.

The thermodynamic solubility was measured using two different biorelevant media, FaSSIF (Fasted State Intestinal Fluid, pH 6.5) and SLF (Simulated Lung Fluid, pH 6.9). Additional properties such as permeability, lipophilicity, pKa and potency were measured for each final compound. The permeability was measured as it would give an indication for how well the compound enters through the cell membrane. The pKa was experimentally measured as the basicity of the core was altered through the

changes in the nitrogen atom configuration. The physicochemical data of the compounds is summarised in **Table 1.1**.

For the thermodynamic solubility assay, the physical form of the compound was important as the solubility is a measure of dissolution from the solid state and less energy would be required to break up a less ordered arrangement of atoms. Consequently, the form of compounds (**1.25-1.69**) were analysed. Plane polarised light microscopy was used initially to observe the birefringence displayed by crystalline material as shown in **Figure 1.15**. Whereas, amorphous compounds do not show colour and absorb all of the plane polarised light, thus appear black. The compounds (**1.25-1.69**) were then analysed by X-Ray Powder Diffraction (XRPD) to determine their crystallinity (see **Appendices 3.1** for details). XRPD was crucial as it could determine whether the compound was crystalline or not and it is important when measuring thermodynamic solubility to know whether the compound is crystalline. The spectrum generated can act as a fingerprint for the compound's polymorph, which can help with comparing crystal forms of different batches of the same compound. Often, different crystallisation techniques can lead to different polymorphs which can have differing thermodynamic solubilities.

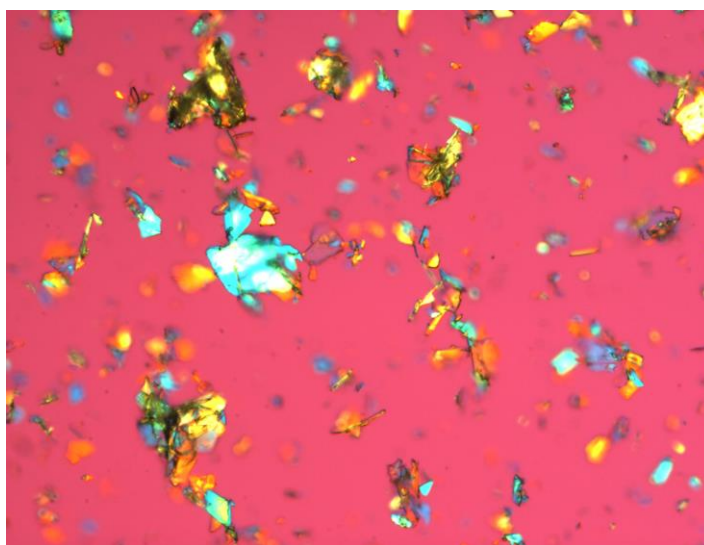
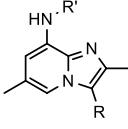
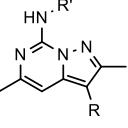
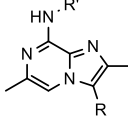
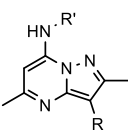
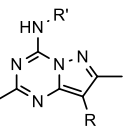


Figure 1.15: Birefringence was observed by plane polarised light microscopy of compound **1.58**.

Table 1.1: Physicochemical profile of compounds (**1.25-1.69**).

The solubility experiments were performed in duplicate (or more) and on crystalline material unless otherwise noted. ^a n = 1, ^b = amorphous material, ^c = pKa of pyridine measured. Melting point (Mp, °C), Permeability (Perm, nm/s), Kinetic solubility_{7.4} (µg/mL), FaSSiF solubility_{6.5} (µg/mL), SLF solubility_{6.9} (µg/mL), and ChromlogD_{7.4}. clogP and PSA (Å) were calculated using GSK algorithm tools.

	Cpd	Kinetic	FaSSiF	SLF	pKa	ChromlogD _{7.4}	Mp	Perm	clogP	PSA
	1.25	29	6	2	6.6	4.3	203-205	300	3.9	90.9
	1.26	86	109	33	6.5/4.7 ^c	4.9	85-88	280	3.9	60.7
	1.27	64	233	29	6.7	6	90-94	290	4.2	57.0
	1.38	19	5	<6	3.8	4.8	194-198	345	3.0	103.8
	1.39	35	31	6	2.8/4.9 ^c	5.5	101-103	430	3.0	73.6
	1.40	44	13	3	4.4	6.4	104-107	340	3.3	69.9
	1.47	53	32 ^b	9 ^b	5	3.9	191-193 ^b	370	3.3	103.8
	1.48	67	335 ^b	58 ^b	5.3/4.0 ^c	4.5	128-131 ^b	480	3.3	73.6
	1.49	99	7 ^b	10 ^b	5.6	5.2	93-95 ^b	410	3.6	69.9
	1.57	79	15 ^a	1 ^a	5.4	3.7	238-240	523	3.0	104
	1.58	>107	141 ^a	39 ^a	5.4/4.1 ^c	4.3	149-151	625	3.0	73.6
	1.59	>180	25 ^a	18 ^a	5.7	5.2	157-159	585	3.3	69.9
	1.67	19	32	10	2.9	3.9	167-169	420	2.3	116.7
	1.68	>150	36	36	2.5/4.7 ^c	4.5	149-152	600	2.3	86.5
	1.69	>165	29	18	3.1	5.1	143-145	620	2.6	82.8

The individual compound solubility shown in **Table 1.1** was averaged for each core (**1-5**) and plotted in **Figure 1.16**. The effects of each different nitrogen atom configuration was best represented in this format (**Figure 1.16**). The effects of the different amine monomers is shown in **Figure 1.17**. The permeability for the final compounds (**1.25-1.69**) was high across all five cores.

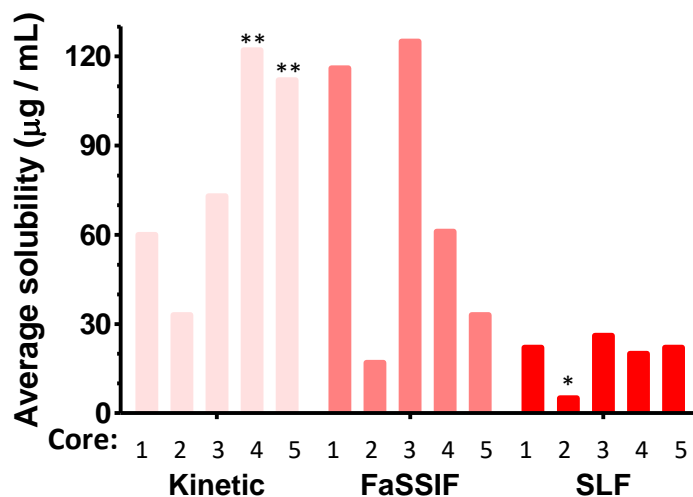


Figure 1.16: Compounds (**1.25-1.69**) measured kinetic solubility (pH = 7.4) and thermodynamic (**FaSSIF**, pH = 6.5 & **SLF**, pH = 6.9) solubility. Data is displayed as an average for each Core 1-5, in numerical order. ** **1.58**, **1.59**, **1.68** and **1.69** contain a greater than (>) modifier in the kinetic solubility measurement. * **1.38** contains a less than (<) modifier in the SLF solubility measurement.

The thermodynamic solubility differs depending on the media in which it is measured. The two standard assays used at GSK during lead optimisation are FaSSIF and SLF. They have different buffer compositions, FaSSIF is buffered to pH 6.5 and contains 0.75 mM lecithin which comprises fatty lipids (see **Section 1.7**). Whereas, SLF is at pH 6.9 and contains both 0.75 mM lecithin and bovine serum albumin (BSA) which is a protein. Therefore, the presence of the fatty lipids and protein in the buffer will influence the solubility of the compounds. The lipids could potentially form micelles in the buffer and the BSA could also interact with the compounds through non-covalent interactions.

An additional point to consider is the pKa of the compounds, which were experimentally determined. Two units above the measured pKa, the compound is expected to be fully ionised and two units below the pKa, the compound is expected to be neutral. As shown in **Table 1.1**, the pKa values were experimentally determined to help aid the understanding of the solubility of the compounds. However, it is

important to consider the buffer composition and the effects it could have on the basicity of the compound. The presence of the fatty lipids and BSA, is likely to reduce the pKa of the compound and in turn reduce the solubility. Therefore, the measured pKa values could possibly be overestimated in the biorelevant buffers for measuring the thermodynamic solubility.

There are some interesting trends in the data. Core 2 demonstrates the lowest average solubility of all five cores, across all three solubility assays. This can potentially be correlated with its inherent lipophilicity, whereby it has the highest measured ChromLogD values at pH=7.4. As previously discussed, lipophilicity is linked to poorer solubility (see **Section 1.2**).

All of the five cores had an average FaSSIF solubility that was greater than the average SLF solubility. The 0.4 log unit difference in the pH of the two media equates to a 2.5-*fold* difference. In the more acidic FaSSIF media, the equilibrium will be shifted towards the protonated state if it contains a basic centre. Obviously, the increased ionisation state will increase solubility of a compound. The pKa of each compound was measured to help investigate this.

Core 1, containing an imidazopyridine bicycle, was the most basic core of the five examined. This had the greatest average FaSSIF solubility of the four crystalline cores. Interestingly, the pKa of around 6.6 falls between the 2 pH values of the FaSSIF and SLF media and so its ionisation state will be susceptible to small changes in pH. Going from FaSSIF to SLF the solubility drops, probably due to decreasing ionised compound in the SLF assay medium.

Another trend observed is that the average kinetic solubility (measured at pH = 7.4) is higher than the SLF solubility (measured at pH = 6.9) for all of the cores, and also individually for all fifteen compounds. Often, medicinal chemists will use kinetic solubility to drive SAR as this is a higher throughput assay. However, there is often a

drop off observed when measuring thermodynamic solubility e.g. kinetic solubility vs SLF. The data supports the need for measuring thermodynamic solubility early in the optimisation of a series, and also ensuring that this is done on a crystalline form. Core 3 was amorphous, and although this was more soluble in the kinetic assay than the SLF, it was more soluble in the FaSSIF assay than the kinetic solubility assay. As a consequence of this, it is important to try to find a stable crystalline polymorph of a compound as early as possible to get a realistic measurement of the thermodynamic solubility.

Each core was appended with an aromatic, heteroaromatic and saturated group. This provided a broader range of functionality to understand how each of the groups affected the solubility. The effect of each monomer (benzamide (**1.16**), *meta*-pyridine (**1.17**) and tetrahydropyran (**1.18**)) on the average solubility was plotted (**Figure 1.17**).

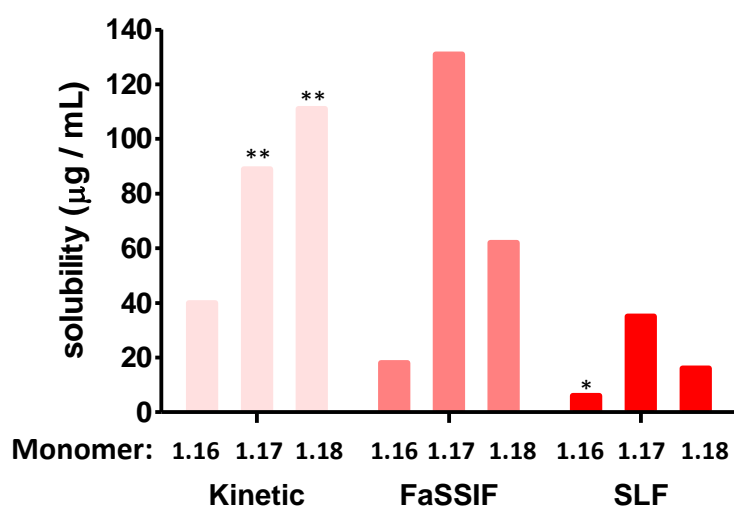


Figure 1.17: The average solubility for cores containing each monomer (**1.16-1.18** attached to the core of the molecule). ** **1.58**, **1.59**, **1.68** and **1.69** contain a greater than (>) modifier in the kinetic solubility measurement. * **1.38** contains a less than (<) modifier in the SLF solubility measurement.

The cores containing the pyridine monomer (**1.17**) show the highest thermodynamic solubility in both FaSSIF and SLF. This is probably due to the additional basic centre

resulting in a higher proportion of protonated species. A higher proportion of compound could be protonated in the lower pH system (FaSSIF) which was reflected in the improved solubility.

Compounds appended with the benzamide monomer (**1.16**) display the poorest solubility across all three solubility assays. This was likely due to the presence of an additional carboaromatic ring which can support π - π stacking, with the amide group co-planar to the aromatic ring. It is also able to interact with other molecules *via* intermolecular hydrogen bonding. This led to an enhanced crystal lattice energy, and compounds appended with the benzamide monomer showed the highest melting point which reflected in the poorest solubility. Furthermore, as represented in the General Solubility Equation (GSE), a high melting point is associated with a low solubility, consistent with the data represented in **Table 1.2**.

The GSE, also known as the Yalkowsky equation, is shown below **Equation 1.1**. It is used to predict the solubility of a given compound if the melting point and clogP of the compound are known. The equation is a predictive tool which serves as platform to analyse large data sets. It is important to be aware of the form of the compound as the melting point can influence the accuracy of the GSE, and so a stable crystalline solid would be more informative. An interesting observation of using the equation is that it predicts that an increase of 100 °C in melting point would reduce the intrinsic solubility by a factor of 10 (logarithmic scale) which equates to a unit lower in logS.^{8,35,36}

$$\log S = 0.5 - \text{clog}P - 0.01(tm - 25)$$

Equation 1.1: Yalkowsky (GSE) equation.

The equation utilises clogP, but it should be noted that clogP does not take into consideration the ionisation of the molecule and it was treated as a neutral species in solution. A compound would display some ionisation character and the extent of the ionisation depends on both the pH of the buffered environment and the pKa of

the most basic centre of the compound as represented in **Figure 1.16** and **Figure 1.17**. For example, the pH of the buffered solution used in the FaSSIF thermodynamic solubility assay is 6.5 and for example, if a compound of interest contained a carboxylic acid group ($pK_a \sim 4.5$, dependant on adjacent functional groups), the ratio between charged and uncharged molecules would be roughly 99:1 and this would significantly alter the dissolution of the compound of interest. The equation neglects this important observation and so it must be carefully considered upon interpretation.

Moreover, the physical state of the compound is important to know. For example, an amorphous solid can display multiple melting points which reduces the reliability of interpreting the GSE equation. On the other hand, a crystalline solid will only show one single sharp melt. Therefore, predicting the solubility of a crystalline solid would provide a more reliable comparison instead of an amorphous solid.

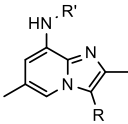
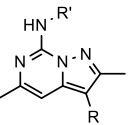
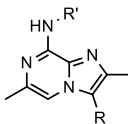
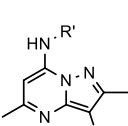
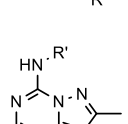
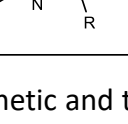
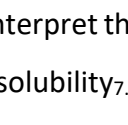
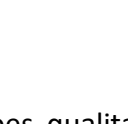
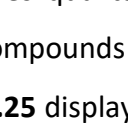
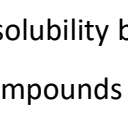
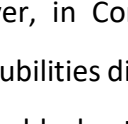
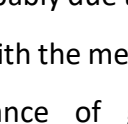
Cpd	Kinetic	FaSSIF	SLF	logS	clogP	Mp	
	1.25	29	6	2	-5.2	3.9	203-205
	1.26	86	109	33	-4.0	3.9	85-88
	1.27	64	233	29	-4.4	4.2	90-94
	1.38	19	5	6<	-4.2	3.0	194-198
	1.39	35	31	6	-3.3	3.0	101-103
	1.40	44	13	3	-3.6	3.3	104-107
	1.47	53	32 ^b	9 ^b	-4.5	3.3	191-193 ^b
	1.48	67	335 ^b	58 ^b	-3.8	3.3	128-131 ^b
	1.49	99	7 ^b	10 ^b	-3.8	3.6	93-95 ^b
	1.57	79	15 ^a	1 ^a	-4.6	3.0	238-240
	1.58	>107	141 ^a	39 ^a	-3.8	3.0	149-151
	1.59	>180	25 ^a	18 ^a	-4.1	3.3	157-159
	1.67	19	32	10	-3.2	2.3	167-169
	1.68	>150	36	36	-3.1	2.3	149-152
	1.69	>165	29	18	-3.3	2.6	143-145

Table 1.2: Kinetic and thermodynamic solubility of all compounds and GSE variables required to interpret the equation. ^an = 1, ^b= amorphous material, Melting point (Mp, °C), Kinetic solubility_{7.4} (µg/mL), FaSSIF solubility_{6.5} (µg/mL) and SLF solubility_{6.9} (µg/mL).

Table 1.2 does qualitatively show a correlation between the FaSSIF solubility of crystalline compounds and their predicted solubility values. As shown in **Table 1.2**, compound **1.25** displays the lowest solubility in Core 1 and it was predicted to have the poorest solubility by the GSE equation. This trend was consistent with all of the crystalline compounds where the logS value was reflective of the compounds in each core. However, in Core 3, where the set of compounds were amorphous, the predicted solubilities did not follow the measured FaSSIF thermodynamic solubilities. This was probably due to the amorphous form of the compounds and the uncertainty associated with the measured melting points of the compounds. This again highlights the importance of gathering thermodynamic solubility data on crystalline compounds.

6,5-Bicyclic heterocycles are prominent in the field of lipid kinase drug design.⁷⁰⁻⁷² It was not only important to investigate the physicochemical properties of the compounds, but also the activity in the enzyme assay when taking any of these cores forwards. Therefore, due to the high interest, the pIC₅₀ values of compounds (**1.25-1.69**) were generated (shown in **Figure 1.18**). The physicochemical properties could be combined with an activity profile against the targeted lipid kinase and could provide a more optimal starting point for carrying out lead optimisation.

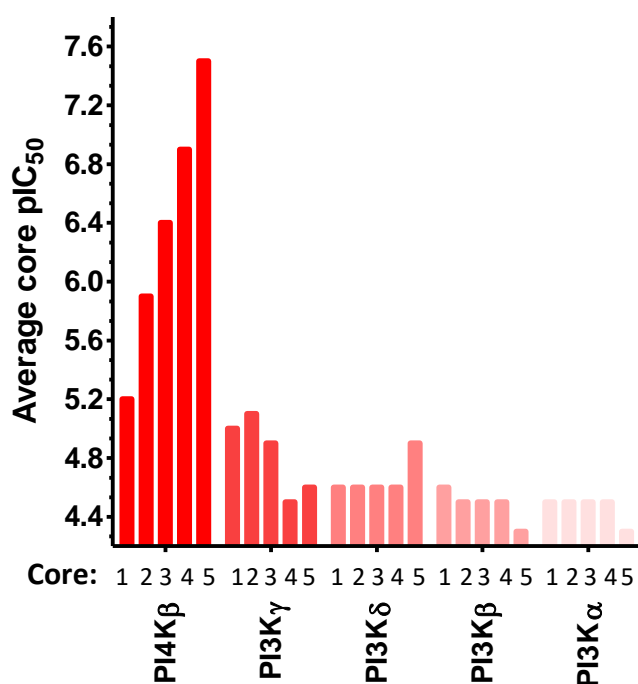


Figure 1.18: The averaged measured pIC₅₀s for each core (**1.25-1.69**).

The synthesised 6,5-bicyclic heterocycles displayed a general selectivity preference for PI4KIII β over all isoforms of closely related PI3K (**Figure 1.18**). Where Core 1, the most thermodynamically soluble template (**Figure 1.16**), was the least active and Core 5, a template with lower solubility, displayed the greatest activity towards PI4KIII β .

1.6 Summary

Five 6,5-bicyclic nitrogen containing heterocycles were synthesised and crystalline batches were obtained for 4 of the 5 cores in order to gather thermodynamic solubility data for a more robust comparison between the cores. Overall, promising physicochemical data was obtained for the final compounds. The intrinsic properties of the nitrogen atom configuration was shown to influence the solubility considerably through modifications to lipophilicity and basicity. The effect of varying the amine monomer was investigated and it was established that the carboaromatic group gave the poorest solubility.

The data also showed that the kinetic solubility was consistently higher when compared with the thermodynamic solubility. In addition, the solubility in SLF was, in all cases, lower than in FaSSIF. This was most likely due to the pH difference of these media (pH 6.9 for SLF compared to pH 6.5 for FaSSIF). The effect of the core variation on solubility showed that Core 1 was the most soluble, potentially driven by its increased basicity (pKa) and that Core 2 was the least soluble, probably due to its high lipophilicity.

The subsequent part of this research was to select the core with the best balance of physicochemical properties and potency to target lipid kinase PI4KIII β and to synthesise potential covalent inhibitors. As a result, Core 4, appended with the *meta*-pyridyl group (**1.58**) was selected for this reason.

EXPERIMENTAL

1.7 General methods and assays

Solvents and reagents – Solvents and reagents were purchased from commercial suppliers and used as received unless otherwise noted.

Reaction monitoring – Reactions were monitored by either liquid chromatography-mass spectroscopy (LCMS) or thin-layer chromatography (TLC).

Thin-layer chromatography (TLC) – TLC was carried out using polyester-backed precoated silica plates (0.2 mm particle size). Spots were visualised under ultraviolet (UV) light of $\lambda_{\text{max}} = 254$ nm or 365 nm. Where spots were difficult to see, they were stained with either vanillin or phosphomolybdic acid before gentle drying.

Liquid chromatography mass spectrometry – LCMS analysis was completed on a Waters® Acquity UPLC instrument equipped with a BEH column (50 mm x 2.1 mm with 1.7 μm packing diameter) and a Waters® Micromass ZQ MS using alternate-scan positive and negative electrospray ionisation. Analytes were then detected as a summed UV wavelength spectrum between 210-350 nm.

Two methods were used:

Formic: 40 °C, 1 mL/min flow rate, using a gradient with mobile phases of water containing 0.1% volume (v/v) of formic acid and MeCN with 0.1% formic acid (v/v). Gradient conditions were initially 1% of the MeCN mixture, increasing linearly to 97 % over 1.5 min, and remaining at 97% for 0.4 min, before increasing to 100% over 0.1 min.

High pH: 40 °C, 1 mL/min flow rate, using a gradient of mobile phases of 10.0 mM aqueous ammonium bicarbonate solution, adjusted to pH 10.0 with 0.880 M aqueous ammonia and MeCN. Gradient conditions began at 1% MeCN, and increased linearly to 97% MeCN over 1.5 min, before remaining at this concentration for 0.40 min, and rising to 100% over 0.1 min.

Silica gel column chromatography – Column chromatography was carried out using the Teledyne ISCO CombiFlash® *R_f+* apparatus with RediSep® silica cartridges.

Infa-red (IR) spectroscopy – spectra were recorded using an RT-IR Perkin Elmer® Spectrum 1 machine directly from a solid sample. Absorption maxima (ν_{\max}) are reported in wavenumbers (cm^{-1}) and are described as strong (s), medium (m), weak (w) and broad (br.).

Nuclear magnetic resonance (NMR) spectroscopy – Proton (^1H) and carbon (^{13}C) spectra were recorded in deuterated solvents at ambient temperatures (unless otherwise stated) using the standardised pulse methods on the Bruker AV-400 (^1H = 400 MHz, ^{13}C = 101 MHz) spectrometer. Chemical shifts are reported in ppm and referenced to tetramethylsilane (TMS) or the following solvent peaks: CDCl_3 (^1H = 7.27 ppm, ^{13}C = 77.0 ppm), d_4 -Methanol (^1H = 3.31, ^{13}C = 49.0) or d_6 -DMSO (^1H = 2.50 ppm, ^{13}C = 39.5 ppm). Peak assignments were chosen based on chemical shifts, integrations, and coupling constants, considering 2D analyses where necessary. Coupling constants are quoted to the nearest 0.1 Hz and multiplicities described as singlet (s), doublet (d), triplet (t), quartet (q), quintet (quin), sextet (sxt), septet (sept), broad (br.) or multiplet (m).

High-resolution mass spectrometry – High-resolution mass spectra were recorded on a micromass Q-ToF Ultima® time-of-flight mass spectrometer, and analytes were separated on an Agilent® 1100 Liquid Chromatograph equipped with a Phenomenex® Luna C18 (2) reversed phase column (100 mm x 2.1 mm, 3 μm packing diameter). Conditions used were 0.5 mL/min flow rate at 35 °C, and an injection volume of 2-5 μL , using a gradient elution made up of water with 0.1 % volume formic acid (v/v) and 0.1 % formic acid (v/v) in MeCN. Elution conditions began with 5 % MeCN mixture, and increased linearly to 100 % over 6 min, before remaining at 100 % for 2.5 min, decreasing back to 5 % MeCN mixture for 1 min and equilibrating for 2.5 min prior to the next injection in the machine. Mass to charge (m/z) ratios are shown in Daltons.

Mass directed auto preparation (MDAP) – Mass directed auto preparation was carried out on a Waters® ZQ MS using alternate scan positive and negative electrospray ionisation and a summed UV wavelength of 210–350 nm.

Two methods were used:

Formic: Sunfire® C18 column (100 mm x 19.0 mm, 5.00 µm packing diameter, 20.0 mL/min flow rate) using a gradient elution at ambient temperature with the mobile phases of water with 0.100 % formic acid by volume (v/v) and MeCN containing 0.1 % formic acid by volume (v/v).

High pH: Xbridge C18 column (100 mm x 19.0 mm, 5.00 µm packing diameter, 20.0 mL/min flow rate) using a gradient elution at ambient temperature using mobile phases as 10.0 mM aqueous ammonium bicarbonate solution, adjusted to pH 10.0 with 0.880 M aqueous ammonia, and MeCN.

Microwave – Reactions were carried out in a Biotage Initiator microwave, model: INITIATOR ROBOT SIXTY 355381,20233-14T.

X-ray Powder Diffraction – Carried out using a pan analytical diffractometer, using method M0000757,v1. The samples were applied to slightly greased silicon wafer for a 10 min scan 0-40 ° 2θ.

Simulated Lung Fluid – SLF buffer pH 6.9 contains 0.75 mM Lecithin Disperse 59 mg Lecithin (Lipoid grade) and 100 mg bovine serum albumin (Sigma A7906) in 100 mL of phosphate buffer pH 6.9. Phosphate buffer solution pH 6.9 contains sodium dihydrogen orthophosphate and sodium chloride. The final solution has an expiry date of one month. The injection sequence: DMSO and SLF. Standard injection volume (unless otherwise stated), 1 µL Injection sequence, three DMSO blank injections from vial position 1 (0.2 µL Injection volume) to settle system. Samples are then run (0.2 µL injection volume). The assay is carried out on an Agilent 1290 µHPLC with an HDR-DAD cluster. 2 x 1 mg of solid, one for the internal standard in DMSO

and the other incubated for 4 hours then filtered and analysed. The method uses a fast 2min generic gradient on a water CSH C18 column 2 mm x 50 mm using water and MeCN with 0.1% TFA.

Fasted State Simulated Intestine Fluid – FaSSIF, pH 6.5 contains 0.75 mM Lecithin and 3.0 mM Taurocholate. Phosphate buffered solution pH 6.5: NaCl (6.19 g), Sodium phosphate monobasic monohydrate (3.95 g), 1 M Sodium hydroxide Solution (10 mL). Dissolve all components in deionised water (900 mL) and titrate to pH 6.5, then make up to volume (1 L). Standard injection volume (unless otherwise stated): 3 μ L. Injection sequence: 3 DMSO blanks run initially to allow the system to settle followed by a 1 μ L DMSO blank injection. All of the standards are then run in sequence with two injections for each standard (1 x 3 μ L, 1 x 1 μ L) followed by two DMSO blanks once all of the standards have been run. This is then followed by 2 FaSSIF blanks (2 x 10 μ L) and an additional 2 FaSSIF blanks (2 x 1 μ L). All of the samples are then run in sequence with two injections (1 x 10 μ L, 1 x 1 μ L) for each sample followed by two DMSO blank runs once all of the samples have run. The assay is carried out on an Agilent 1290 μ HPLC with an HDR-DAD cluster. 2 x 1 mg of solid. One for the internal standard in DMSO and the other incubated for 4 hours then filtered and analysed. The method uses a fast 2min generic gradient on a water CSH C18 column 2mm x 50mm using water and MeCN with 0.1% TFA.

Kinetic solubility – The kinetic aqueous solubility at pH 7.4 was determined by measuring the concentration of solute in solution after precipitation from DMSO stock solution. The DMSO stock solution was diluted 20-fold with PBS pH 7.4 and the solubility of the compound is measured after 1-hour equilibration at room temperature. In this procedure quantification is done using a Charged Aerosol Detector (CAD). The actual DMSO concentration of the stock solution was also determined using this technique. Calibration parameters generated for CAD response of two calibrants (Primidone and Ketoconazole) are used to calculate the solubility of solutes considering the density of the compound and ion-pairing effects.

pKa measurements – Carried out using a Sirius T3 (T304037 or FB5012) instrument. 0.5-1 mg of solid was accurately weighed into a vial and this is blown to dryness prior to starting assay. From the T3 software the appropriate experiment (pKa) was picked from the drop-down menu. The data was fitted within T3 software (Refinement Pro) by Target Factor Analysis. The no. of ionised species was determined and when combined with Yasuda-Shedlovsky extrapolation also the acid or basic character could be assigned.

Permeability (AMP nm s^{-1}) – Lipid preparation: 1.8% phosphatidylcholine in 1% Cholesterol Decane solution. Weigh out 600 mg of cholesterol and dissolve it in 60 mL of decane (sonicate if needed). 1.8% phosphatidylcholine in 1% cholesterol decane solution. Weigh out 1 g of phosphatidylcholine and dissolve in 56 mL of 1% cholesterol decane solution. Sonicate (the solution should keep at the room temperature when sonicating). Transfer the lipid solution to 4 mL vials and seal the vials with parafilm, then store at $-20\text{ }^{\circ}\text{C}$ freezer. The assay is run by the Biomek FX and Biomek software. The assay procedure is written under the Biomek software. For one batch assay, it can test two 96-well sample plates with at least one standard on each sample plate. The total assay time is about 4 hours. Add $3.5\text{ }\mu\text{L}$ of lipid solution to the filter plate, shake the plate for 12 seconds, and then add $250\text{ }\mu\text{L}$ of buffer to donor side and $100\text{ }\mu\text{L}$ to the receiver side. The assay plate is shaking for 45 min before adding the compounds. Add the compounds. The test compounds ($2.5\text{ }\mu\text{L}$) are added to the donor side. The assay is run as replicates. Assay plate 1 and 2 test the sample plate 1; assay plate 3 and 4 test the sample plate 2. The assay plates are then incubated at room temperature on the shaker for 3 hours. Transfer the assay samples to the HPLC analysis plates Aspirate $100\text{ }\mu\text{L}$ of receiver solution and transfer them to the receiver analysis plate, then transfer $100\text{ }\mu\text{L}$ donor solution to the donor analysis plate.

Melting points – Melting points were recorded on a Stuart SMP40 melting point apparatus.

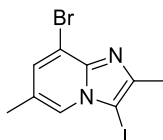
1.8 Synthesis

8-Bromo-2,6-dimethylimidazo[1,2-*a*]pyridine (1.21)⁶⁵



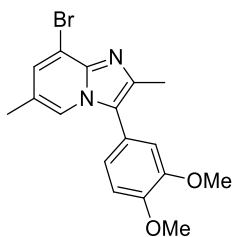
3-Bromo-5-methylpyridin-2-amine (3.54 g, 18.94 mmol) was added to an RBF (100 mL) and the reaction vessel was degassed and placed under a nitrogen atmosphere. Anhydrous ethanol (25 mL) and 1-chloropropan-2-one (3.17 mL, 39.8 mmol) were added and the reaction mixture was heated at 95 °C for 24 h. After cooling, the reaction mixture was concentrated *in vacuo* and the residue was diluted with CH₂Cl₂ (20 mL) and washed with aqueous sodium bicarbonate (20 mL). The organic layer was passed through a hydrophobic frit and concentrated *in vacuo* to give 8-bromo-2,6-dimethylimidazo[1,2-*a*]pyridine (3.28 g, 14.58 mmol, 77% yield). ¹H NMR (400 MHz, CDCl₃) δ = 7.86 (s, 1H), 7.39 (s, 1H), 7.28 (s, 1H), 2.49 (s, 3H), 2.31 (d, *J* = 0.8 Hz, 3H). ¹³C NMR (101 MHz, CDCl₃) δ = 143.4, 141.7, 129.8, 124.3, 122.4, 111.2, 109.7, 17.8, 14.1. LCMS (HpH) 92% desired product; *t*_{ret} = 0.81 min, MH⁺ 227.05.

8-Bromo-3-iodo-2,6-dimethylimidazo[1,2-*a*]pyridine (1.22)



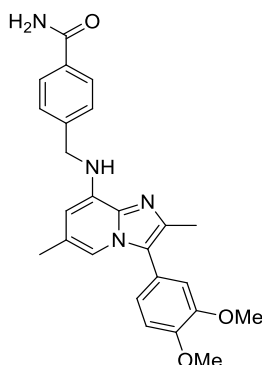
8-Bromo-2,6-dimethylimidazo[1,2-*a*]pyridine (3.96 g, 17.59 mmol) was dissolved in CH₂Cl₂ (40 mL) at 0 °C. Cold 1-iodopyrrolidine-2,5-dione (4.35 g, 19.35 mmol) was added and the reaction mixture was left to stir for 1 h. The reaction mixture was partitioned between water (40 mL) and CH₂Cl₂ (40 mL). The organic layer was passed through a hydrophobic frit and concentrated *in vacuo* to give 8-bromo-3-iodo-2,6-dimethylimidazo[1,2-*a*]pyridine (5.45 g, 15.48 mmol, 88% yield). ¹H NMR (400 MHz, DMSO-*d*₆) δ = 8.14 (s, 1H), 7.64 (s, 1H), 2.39 (s, 3H), 2.37 (s, 3H). ¹³C NMR (101 MHz, DMSO-*d*₆) δ = 146.2, 143.2, 131.6, 124.7, 124.0, 108.6, 30.0, 17.7, 14.7. LCMS (HpH) 93% desired product; *t*_{ret} = 1.08 min, MH⁺ 352.3.

8-Bromo-3-(3,4-dimethoxyphenyl)-2,6-dimethylimidazo[1,2-*a*]pyridine (1.24)



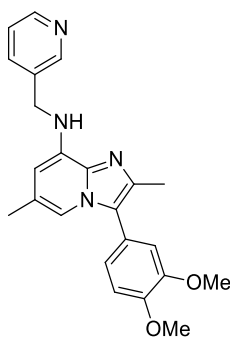
8-Bromo-3-iodo-2,6-dimethylimidazo[1,2-*a*]pyridine (4.44 g, 12.66 mmol), PdCl₂(dppf)-CH₂Cl₂ adduct (60 mg, 0.07 mmol), (3,4-dimethoxyphenyl)boronic acid (2.32 g, 12.74 mmol) and sodium carbonate (3.76 g, 35.5 mmol) were added to an RBF (500 mL). The reaction vessel was degassed and placed under a nitrogen atmosphere. 1,4-Dioxane (88 mL) and water (12 mL) were added and nitrogen was bubbled through the solution for 5 minutes. The reaction was heated at 95 °C for 24 h and, after cooling, the reaction mixture was concentrated *in vacuo*. The residue was diluted with EtOAc (40 mL) and washed with brine (40 mL). The organic layer was evaporated *in vacuo*, re-dissolved in a minimum amount of CH₂Cl₂ and filtered through Celite™. The crude product was purified by column chromatography eluting with EtOAc in cyclohexane (0-100% gradient). The appropriate fractions were combined and concentrated *in vacuo* to give 8-bromo-3-(3,4-dimethoxyphenyl)-2,6-dimethylimidazo[1,2-*a*]pyridine (1.18 g, 3.29 mmol, 26% yield). ¹H NMR (400 MHz, DMSO-*d*₆) δ = 8.05 - 8.02 (m, 1H), 7.46 (d, *J* = 1.0 Hz, 1H), 7.15 (d, *J* = 8.1 Hz, 1H), 7.09 - 7.01 (m, 2H), 3.85 (s, 3H), 3.81 (s, 3H), 2.35 (s, 3H), 2.25 (d, *J* = 1.0 Hz, 3H). ¹³C NMR (101 MHz, DMSO-*d*₆) δ = 179.4, 149.6, 149.4, 140.8, 129.5, 123.2, 122.6, 122.2, 121.4, 119.6, 113.5, 112.8, 109.8, 56.2, 56.1, 17.7, 14.3. LCMS (HpH) 90% desired product; *t*_{ret} = 1.08 min, MH⁺ 363.1.

4-(((3-(3,4-Dimethoxyphenyl)-2,6-dimethylimidazo[1,2-*a*]pyridin-8-yl)amino)methyl)benzamide (1.25)



8-Bromo-3-(3,4-dimethoxyphenyl)-2,6-dimethylimidazo[1,2-*a*]pyridine (300 mg, 0.83 mmol) in a microwave vial (20 mL) was dissolved in THF (8 mL). 4-(Aminomethyl)benzamide (162 mg, 1.08 mmol), sodium *tert*-butoxide (144 mg, 1.50 mmol), Pd₂(dba)₃ (76 mg, 0.08 mmol) and BrettPhos™ (131 mg, 0.33 mmol) were added and nitrogen was bubbled into the solution for 5 minutes. The reaction vessel was sealed and heated in a microwave at 135 °C for 2 h. After cooling, the reaction mixture was passed through Celite™, diluted with EtOAc (20 mL) and washed with brine (20 mL). The organic layer was passed through a hydrophobic frit and concentrated *in vacuo*. The orange solid was purified by MDAP (high pH method). The appropriate fractions were combined and evaporated *in vacuo* to give 4-(((3-(3,4-dimethoxyphenyl)-2,6-dimethylimidazo[1,2-*a*]pyridin-8-yl)amino)methyl)benzamide (81 mg, 0.19 mmol, 23% yield). **¹H NMR** (400 MHz, DMSO-*d*₆) δ = 7.91 - 7.87 (m, 1H), 7.84 - 7.81 (m, 2H), 7.46 - 7.43 (m, 2H), 7.29 - 7.27 (m, 2H), 7.14 - 7.11 (m, 1H), 7.02 - 7.00 (m, 2H), 6.72 - 6.68 (m, 1H), 5.82 (d, *J* = 1.0 Hz, 1H), 4.52 (d, *J* = 6.0 Hz, 2H), 3.83 (s, 3H), 3.80 (s, 3H), 2.34 (s, 3H), 2.06 (s, 3H). **¹³C NMR** (101 MHz, DMSO-*d*₆) δ = 168.2, 149.5, 149.0, 143.8, 137.7, 136.7, 136.1, 133.2, 128.0, 127.1, 122.6, 122.4, 122.3, 122.0, 113.5, 112.8, 109.8, 100.3, 56.1, 56.0, 45.9, 18.9, 14.2. **LCMS** (HpH) 97% desired product; *t*_{ret} = 1.01 min, MH⁺ 431.4. **HRMS** (C₂₅H₂₆N₄O₃) [M+H⁺] requires 431.2083, found [M+H⁺] 431.2079. **v**_{max} (neat) / cm⁻¹ 3489, 3261, 2955, 1675, 1565, 1510, 1456, 1414, 1373, 1269, 1253, 1216, 1144, 1025, 829, 774, 765. **Mp** 203-205 °C.

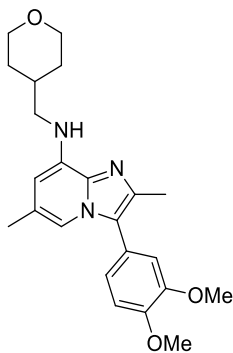
3-(3,4-Dimethoxyphenyl)-2,6-dimethyl-N-(pyridin-3-ylmethyl)imidazo[1,2-*a*]pyridin-8-amine (1.26)



8-Bromo-3-(3,4-dimethoxyphenyl)-2,6-dimethylimidazo[1,2-*a*]pyridine (300 mg, 0.83 mmol) in a microwave vial (20 mL) was dissolved in THF (8 mL). Pyridin-3-ylmethanamine (0.110 mL, 1.08 mmol), sodium *tert*-butoxide (144 mg, 1.50 mmol), Pd₂(dba)₃ (76 mg, 0.08 mmol) and BrettPhos™ (178 mg, 0.33 mmol) were added and nitrogen was bubbled into the solution for 5 minutes. The reaction vessel was sealed and heated in the microwave at 140 °C for 2 h. After cooling, the reaction mixture was passed through Celite™, diluted with EtOAc (20 mL) and washed with brine (40 mL). The organic layer was concentrated *in vacuo* and crude product was purified by column chromatography eluting with EtOAc in cyclohexane (gradient 0-100%) and then flushed with ethanol in EtOAc (1:3) to retrieve the product. The appropriate fractions were concentrated *in vacuo* to give an orange oil which was further purified by MDAP (high pH method). The solvent was evaporated *in vacuo* to give 3-(3,4-dimethoxyphenyl)-2,6-dimethyl-*N*-(pyridin-3-ylmethyl)imidazo[1,2-*a*]pyridin-8-amine (146 mg, 0.38 mmol, 46% yield). ¹H NMR (400 MHz, DMSO-*d*₆) δ = 8.65 - 8.61 (m, 1H), 8.46 - 8.42 (m, 1H), 7.82 - 7.76 (m, 1H), 7.37 - 7.31 (m, 1H), 7.30 - 7.28 (m, 1H), 7.12 (d, *J* = 8.1 Hz, 1H), 7.03 - 6.96 (m, 2H), 6.74 - 6.68 (m, 1H), 5.93 - 5.90 (m, 1H), 4.51 (d, *J* = 6.5 Hz, 2H), 3.83 (s, 3H), 3.80 (s, 3H), 2.33 (s, 3H), 2.08 (d, *J* = 1.0 Hz, 3H). ¹³C NMR (101 MHz, DMSO-*d*₆) δ = 149.5, 149.2, 148.9, 148.4, 137.7, 136.7, 135.9, 135.7, 135.2, 123.9, 122.6, 122.4, 122.3, 122.0, 113.4, 112.8, 110.0, 100.4, 56.1, 56.0, 43.7, 18.9, 14.2. LCMS (HpH) 100% desired product; *t*_{ret} = 1.05 min, MH⁺ 389.3. HRMS (C₂₃H₂₄N₄O₂) [M+H⁺] requires 389.1978, found [M+H⁺] 389.1973. *v*_{max} (neat) / cm⁻¹

3331, 2930, 1564, 1506, 1455, 1415, 1250, 1213, 1172, 1138, 1024, 875, 812, 766, 751, 712, 690. **Mp** 85-88 °C.

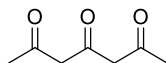
3-(3,4-Dimethoxyphenyl)-2,6-dimethyl-N-((tetrahydro-2H-pyran-4-yl)methyl)imidazo[1,2-*a*]pyridin-8-amine (1.27)



8-Bromo-3-(3,4-dimethoxyphenyl)-2,6-dimethylimidazo[1,2-*a*]pyridine (307 mg, 0.85 mmol) in a microwave vial (20 mL) was dissolved in THF (8 mL). (Tetrahydro-2H-pyran-4-yl)methanamine (0.135 mL, 1.11 mmol), sodium *tert*-butoxide (147 mg, 1.53 mmol), Pd₂(dba)₃ (78 mg, 0.09 mmol) and BrettPhos™ (182 mg, 0.34 mmol) were added and nitrogen was bubbled into the solution for 5 minutes. The reaction vessel was sealed and heated in a microwave at 140 °C for 2 h. After cooling, the reaction mixture was passed through Celite™, diluted with EtOAc (20 mL) and washed with brine (40 mL). The organic layer was concentrated *in vacuo* and the crude product was purified by column chromatography eluting with EtOAc in cyclohexane (gradient 0-100%). The column was flushed with ethanol in EtOAc (1:3) to retrieve the product. The appropriate fractions were combined and concentrated *in vacuo* to give 3-(3,4-dimethoxyphenyl)-2,6-dimethyl-N-((tetrahydro-2H-pyran-4-yl)methyl)imidazo[1,2-*a*]pyridin-8-amine (277 mg, 0.70 mmol, 82% yield). **¹H NMR** (400 MHz, DMSO-*d*₆) δ = 7.30 - 7.26 (m, 1H), 7.13 (d, *J* = 8.1 Hz, 1H), 7.03 - 6.97 (m, 2H), 6.00 - 5.97 (m, 1H), 5.88 - 5.83 (m, 1H), 3.84 - 3.83 (m, 3H), 3.81 - 3.80 (m, 3H), 3.30 - 3.24 (m, 2H), 3.19 - 3.17 (m, 2H), 3.14 - 3.10 (m, 2H), 2.31 (s, 3H), 2.18 - 2.16 (m, 3H), 2.00 - 1.90 (m, 1H), 1.66 (br dd, *J* = 2.0, 12.6 Hz, 2H), 1.31 - 1.19 (m, 2H). **¹³C NMR** (101 MHz, DMSO-*d*₆) δ = 149.5, 148.9, 137.5, 136.7, 136.6, 122.9, 122.4, 122.0, 113.5, 112.8, 109.3, 99.5, 67.3, 56.1, 56.0, 49.1, 48.7, 34.3, 31.1, 19.0, 14.1. **LCMS** (HpH) 99% desired product;

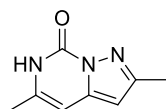
$t_{\text{ret}} = 1.18$ min, MH^+ 396.4. **HRMS** ($\text{C}_{23}\text{H}_{29}\text{N}_3\text{O}_3$) [$\text{M}+\text{H}^+$] requires 396.2287, found [$\text{M}+\text{H}^+$] 396.2286. ν_{max} (neat) / cm^{-1} 2935, 1568, 1509, 1464, 1441, 1415, 1254, 1216, 1174, 1139, 1093, 1026 985, 812, 765, 751. **Mp** 91-94 °C.

Heptane-2,4,6-trione (1.29)



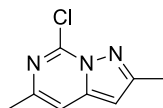
Sodium hydroxide pellets (3.22g) were stirred in water (5 mL) to form sodium hydroxide (16 M) solution. To the RBF (100 mL), ethanol (25 mL) and 2,6-dimethyl-4*H*-pyran-4-one (5.0 g, 40.3 mmol) were added and the reaction mixture was heated at 100 °C for 2 h, after which time, precipitation occurred. The solid was collected by filtration and washed with diethyl ether (20 mL). The solid was re-dissolved in water (20 mL) and acidified with aqueous HCl (2M, 75 mL). The product was extracted out of the aqueous layer with diethyl ether (40 mL) and the organic layer was passed through a hydrophobic frit and concentrated *in vacuo* to give heptan-2,4,6-trione (3.5 g, 25 mmol, 62% yield). Characterisation data was consistent with literature.⁷³

2,5-Dimethylpyrazolo[1,5-*c*]pyrimidin-7(6*H*)-one (1.31)



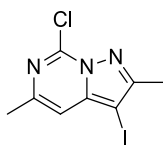
Hydrazinecarboxamide, hydrochloride (3.02 g, 27.0 mmol) and water (40 mL) were added to an RBF (250 mL) containing heptane-2,4,6-trione (3.49 g, 24.58 mmol). The reaction mixture was stirred at RT followed by the addition of saturated aqueous sodium carbonate (40 mL, 12.55 mmol). The reaction mixture was heated at 100 °C for 1 h. After cooling, the product was extracted out of the aqueous with CH_2Cl_2 (4 x 15 mL). The combined organics were passed through a hydrophobic frit and concentrated *in vacuo* to give 2,5-dimethylpyrazolo[1,5-*c*]pyrimidin-7(6*H*)-one (2.51 g, 7.8 mmol, 79% yield). **¹H NMR** (600 MHz, CDCl_3) $\delta = 11.12$ (br s, 1H), 6.18 (s, 1H), 6.09 (s, 1H), 2.43 (s, 3H), 2.33 (d, $J = 0.9$ Hz, 3H). **¹³C NMR** (151 MHz, CDCl_3) $\delta = 155.6$, 147.8, 143.1, 137.0, 99.8, 95.9, 18.7, 14.1. **LCMS** (HpH) 96% desired product; $t_{\text{ret}} = 0.58$ min, MH^+ 163.9.

7-Chloro-2,5-dimethylpyrazolo[1,5-c]pyrimidine (1.33)



2,5-Dimethylpyrazolo[1,5-c]pyrimidin-7(6H)-one (2.434 g, 14.95 mmol) and POCl₃ (20 mL, 215 mmol) were stirred in an RBF (500 mL). *N,N*-Diethylaniline (2.38 mL, 14.96 mmol) was added dropwise and the reaction mixture was heated at 110 °C for 16 h. After cooling, the reaction mixture was concentrated *in vacuo*, diluted with CH₂Cl₂ (30 mL) and washed with aqueous ammonium chloride (30 mL). The organic layer was passed through a hydrophobic frit and concentrated *in vacuo* to give 7-chloro-2,5-dimethylpyrazolo[1,5-c]pyrimidine (1.85 g, 10.3 mmol, 69% yield). ¹H NMR (400 MHz, CDCl₃) δ = 7.10 (s, 1H), 6.32 (s, 1H), 2.54 (s, 3H), 2.48 (s, 3H). ¹³C NMR (101 MHz, CDCl₃) δ = 155.7, 147.3, 144.0, 108.4, 98.1, 53.7, 23.0, 14.2. LCMS (HpH) 98% desired product; t_{ret} = 0.81 min, MH⁺ 181.9.

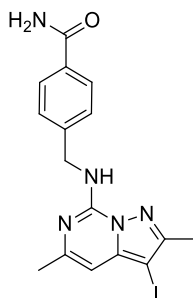
7-Chloro-3-iodo-2,5-dimethylpyrazolo[1,5-c]pyrimidine (1.34)



7-Chloro-2,5-dimethylpyrazolo[1,5-c]pyrimidine (1.85 g, 10.19 mmol) was dissolved in CH₂Cl₂ (50 mL) at 0 °C. 1-Iodopyrrolidine-2,5-dione (2.30 g, 10.20 mmol) was added and the reaction mixture was stirred at RT for 0.5 h. The organic layer was washed with aqueous sodium thiosulfate (20 mL), passed through a hydrophobic frit and concentrated *in vacuo*. The crude material was purified by column chromatography eluting with EtOAc in cyclohexane (0-100% gradient). The appropriate fractions were combined and concentrated *in vacuo* to give 7-chloro-3-iodo-2,5-dimethylpyrazolo[1,5-c]pyrimidine (1.67 g, 5.5 mmol, 54% yield). ¹H NMR (600 MHz, CDCl₃) δ = 7.05 (d, *J* = 0.9 Hz, 1H), 2.53 (s, 3H), 2.51 (d, *J* = 0.9 Hz, 3H). ¹³C NMR (151 MHz, CDCl₃) δ = 157.1, 149.0, 144.8, 138.1, 108.7, 53.0, 23.2, 14.4. LCMS (For) 94% desired product; t_{ret} = 1.11 min, MH⁺ 307.9.

4-(((3-iodo-2,5-dimethylpyrazolo[1,5-c]pyrimidin-7-yl)amino)methyl)benzamide

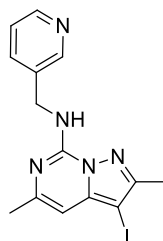
(1.35)



7-Chloro-3-iodo-2,5-dimethylpyrazolo[1,5-c]pyrimidine (271 mg, 0.88 mmol) was dissolved in 1,4-dioxane (2 mL) and added to a microwave vial (5 mL). Triethylamine (0.267 mL, 1.92 mmol) and 4-(aminomethyl)benzamide (0.246 mL, 1.92 mmol) were added and the reaction vessel was sealed and heated at 120 °C for 5 h. After cooling, the reaction mixture was concentrated *in vacuo* and purified by MDAP (high pH method). The appropriate fractions were combined and concentrated *in vacuo* to give 4-(((3-iodo-2,5-dimethylpyrazolo[1,5-c]pyrimidin-7-yl)amino)methyl)benzamide (146 mg, 0.35 mmol, 37% yield). ¹H NMR (400 MHz, DMSO-*d*₆) δ ppm 2.27 (s, 3 H) 2.38 (s, 3 H) 4.72 (d, *J* = 6.0 Hz, 2 H) 6.45 (s, 1 H) 7.27 (br s, 1 H) 7.42 (d, *J* = 8.6 Hz, 2 H) 7.80 (d, *J* = 8.1 Hz, 2 H) 7.88 (br s, 1 H) 8.41 - 8.48 (m, 1 H). ¹³C NMR (101 MHz, DMSO-*d*₆) δ = 168.2, 154.2, 150.4, 145.4, 144.2, 143.3, 133.3, 127.9, 127.4, 98.2, 51.7, 43.8, 24.1, 14.4. LCMS (HpH) 100% desired product; *t*_{ret} = 1.14 min, MH⁺ 422.2.

3-iodo-2,5-dimethyl-*N*-(pyridin-3-ylmethyl)pyrazolo[1,5-c]pyrimidin-7-amine

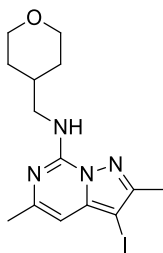
(1.36)



7-Chloro-3-iodo-2,5-dimethylpyrazolo[1,5-c]pyrimidine (287 mg, 0.93 mmol) was dissolved in 1,4-dioxane (2 mL) and added to a microwave vial (5 mL). Triethylamine

(0.267 mL, 1.92 mmol) and pyridin-3-ylmethanamine (0.195 mL, 1.92 mmol) were added. The reaction vessel was sealed and heated at 120 °C for 5 h. After cooling, the reaction mixture was concentrated *in vacuo*. The residue was dissolved in CH₂Cl₂ (20 mL) and washed with sodium bicarbonate solution (20 mL). The organic layer was passed through a hydrophobic frit and concentrated *in vacuo* to give 3-iodo-2,5-dimethyl-*N*-(pyridin-3-ylmethyl)pyrazolo[1,5-*c*]pyrimidin-7-amine (124 mg, 0.33 mmol, 35% yield). ¹H NMR (400 MHz, CDCl₃) δ = 8.73 - 8.68 (m, 1H), 8.58 - 8.54 (m, 1H), 7.79 - 7.74 (m, 1H), 7.31 - 7.26 (m, 1H), 6.54 (br t, *J* = 5.5 Hz, 1H), 6.51 (d, *J* = 1.0 Hz, 1H), 4.85 (d, *J* = 6.5 Hz, 2H), 2.42 (s, 3H), 2.41 (d, *J* = 1.0 Hz, 3H). ¹³C NMR (101 MHz, CDCl₃) δ = 179.3, 154.6, 150.2, 149.3, 144.6, 144.0, 135.6, 133.9, 123.5, 99.5, 50.3, 42.4, 24.0, 14.1. LCMS (For) 98% desired product; *t*_{ret} = 0.81 min, MH⁺ 379.9.

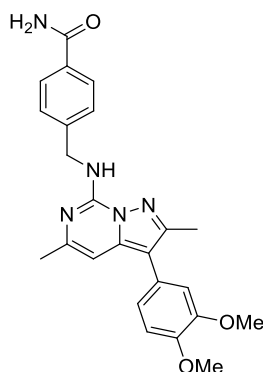
3-Iodo-2,5-dimethyl-*N*-((tetrahydro-2*H*-pyran-4-yl)methyl)pyrazolo[1,5-*c*]pyrimidin-7-amine (1.37)



7-Chloro-3-iodo-2,5-dimethylpyrazolo[1,5-*c*]pyrimidine (295 mg, 0.96 mmol) was dissolved in 1,4-dioxane (2 mL) and added to a microwave vial (5 mL). Triethylamine (0.534 mL, 3.84 mmol) and (tetrahydro-2*H*-pyran-4-yl)methanamine (0.470 mL, 3.84 mmol) were added and the reaction vessel was sealed and heated at 120 °C for 5 h. After cooling, the reaction mixture was concentrated *in vacuo* and the residue was dissolved in CH₂Cl₂ (20 mL) and washed with aqueous ammonium chloride (20 mL). The organic layer was passed through a hydrophobic frit and concentrated *in vacuo*. The crude product was purified by MDAP (high pH method). The appropriate fractions were combined and concentrated *in vacuo* to give 3-iodo-2,5-dimethyl-*N*-((tetrahydro-2*H*-pyran-4-yl)methyl)pyrazolo[1,5-*c*]pyrimidin-7-amine (342 mg, 0.88 mmol, 92% yield). ¹H NMR (400 MHz, CDCl₃) δ = 6.45 (d, *J* = 1.0 Hz, 1H), 6.29 - 6.20 (m, 1H), 4.05 - 4.00 (m, 2H), 3.57 - 3.53 (m, 2H), 3.45 - 3.39 (m, 2H), 2.43 (s, 3H), 2.40

(d, $J = 1.0$ Hz, 3H), 2.04 - 1.92 (m, 1H), 1.78 - 1.72 (m, 2H), 1.51 - 1.40 (m, 2H). ^{13}C NMR (101 MHz, CDCl_3) $\delta = 154.3, 150.3, 145.1, 143.9, 98.7, 67.6, 50.0, 46.5, 35.3, 30.7, 24.1, 14.2$. LCMS (For) 100% desired product; $t_{\text{ret}} = 1.26$ min, $\text{MH}^+ 386.9$.

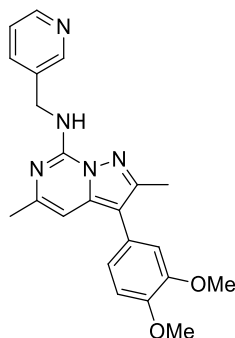
4-(((3-(3,4-Dimethoxyphenyl)-2,5-dimethylpyrazolo[1,5-c]pyrimidin-7-yl)amino)methyl)benzamide (1.38)



4-(((3-Iodo-2,5-dimethylpyrazolo[1,5-c]pyrimidin-7-yl)amino)methyl)benzamide (305 mg, 0.72 mmol) in a microwave vial (20 mL) was dissolved in 1,4-dioxane (8 mL). Cesium carbonate (519 mg, 1.59 mmol) dissolved in water (2 mL), (3,4-dimethoxyphenyl)boronic acid (264 mg, 1.45 mmol) and XPhosPdG2TM (5.70 mg, 7.24 μmol) were added. The reaction vessel was sealed and heated at 130 °C for 5 h. After cooling, the reaction mixture was passed through CeliteTM and diluted with EtOAc (20 mL). The organic layer was washed with brine (20 mL), passed through a hydrophobic frit and concentrated *in vacuo*. The crude product was purified by column chromatography eluting with EtOAc in cyclohexane (+ 2% NEt_3) (0-40% gradient). The appropriate fractions were combined and concentrated *in vacuo* to give 4-(((3-(3,4-dimethoxyphenyl)-2,5-dimethylpyrazolo[1,5-c]pyrimidin-7-yl)amino)methyl)benzamide (68 mg, 0.16 mmol, 22% yield). ^1H NMR (400 MHz, DMSO-d_6) $\delta = 8.36 - 8.31$ (m, 1H), 7.92 - 7.87 (m, 1H), 7.85 - 7.79 (m, 2H), 7.47 - 7.41 (m, 2H), 7.30 - 7.26 (m, 1H), 7.08 - 7.03 (m, 1H), 7.00 - 6.93 (m, 2H), 6.69 - 6.66 (m, 1H), 4.78 - 4.73 (m, 2H), 3.81 (s, 3H), 3.80 (s, 3H), 2.47 (s, 3H), 2.25 - 2.24 (m, 3H). ^{13}C NMR (101 MHz, DMSO-d_6) $\delta = 168.2, 150.6, 149.4, 149.0, 147.9, 145.2, 143.5, 139.9, 133.3, 127.9, 127.4, 125.6, 121.2, 112.9, 112.9, 110.0, 97.8, 56.1, 56.1, 43.7, 24.2, 13.5$. LCMS (HpH) 98% desired product; $t_{\text{ret}} = 1.06$ min, $\text{MH}^+ 432.4$. HRMS

(C₂₄H₂₅N₅O₃) [M+H⁺] requires 432.2036, found [M+H⁺] 432.2028. ν_{\max} (neat) / cm⁻¹ 3410, 3326, 2901, 1634, 1603, 1570, 1537, 1512, 1439, 1328, 1254, 1234, 1218, 1141, 1017, 824, 778, 765. **Mp** 194-197 °C.

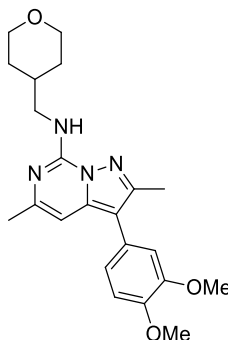
3-(3,4-Dimethoxyphenyl)-2,5-dimethyl-N-(pyridin-3-ylmethyl)pyrazolo[1,5-c]pyrimidin-7-amine (1.39)



3-Iodo-2,5-dimethyl-N-(pyridin-3-ylmethyl)pyrazolo[1,5-c]pyrimidin-7-amine (468 mg, 1.23 mmol) in a microwave vial (20 mL) was dissolved in 1,4-dioxane (8 mL). Cesium carbonate (885 mg, 2.72 mmol) dissolved in water (2 mL), (3,4-dimethoxyphenyl)boronic acid (449 mg, 2.47 mmol) and XPhosPdG2TM (9.71 mg, 0.01 mmol) were added. The reaction vessel was sealed and heated at 130 °C for 5 h. After cooling, the reaction mixture was passed through CeliteTM and diluted with EtOAc (20 mL). The organic layer was washed with brine (20 mL), passed through a hydrophobic frit and concentrated *in vacuo*. The crude product was purified by column chromatography eluting with EtOAc in cyclohexane (+ 2% NEt₃) (0-100% gradient). The appropriate fractions were combined and concentrated *in vacuo* to give 3-(3,4-dimethoxyphenyl)-2,5-dimethyl-N-(pyridin-3-ylmethyl)pyrazolo[1,5-c]pyrimidin-7-amine (355 mg, 0.95 mmol, 74% yield). ¹H NMR (400 MHz, CDCl₃) δ = 8.75 - 8.72 (m, 1H), 8.58 - 8.55 (m, 1H), 7.83 - 7.78 (m, 1H), 7.32 - 7.29 (m, 1H), 6.99 - 6.97 (m, 2H), 6.94 - 6.93 (m, 1H), 6.68 - 6.67 (m, 1H), 6.62 - 6.58 (m, 1H), 4.88 (d, *J* = 6.0 Hz, 2H), 3.95 (s, 3H), 3.94 (s, 3H), 2.49 (s, 3H), 2.38 (d, *J* = 1.0 Hz, 3H). ¹³C NMR (101 MHz, CDCl₃) δ = 150.9, 149.5, 149.1, 148.9, 148.9, 147.8, 144.5, 140.1, 135.7, 134.2, 125.7, 123.5, 121.3, 112.4, 111.7, 110.5, 98.8, 56.0, 56.0, 42.3, 24.8, 13.0. **LCMS** (HpH) 96% desired product; *t*_{ret} = 1.14 min, MH⁺ 390.0. **HRMS** (C₂₂H₂₃N₅O₂) [M+H⁺] requires

390.1930, found $[M+H^+]$ 390.1927. ν_{\max} (neat) / cm^{-1} 2995, 1588, 1577, 1537, 1461, 1453, 1440, 1423, 1247, 1228, 1214, 1174, 1135, 1024, 791, 711. **Mp** 101-103 °C.

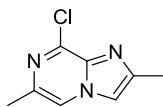
3-(3,4-Dimethoxyphenyl)-2,5-dimethyl-*N*-((tetrahydro-2*H*-pyran-4-yl)methyl)pyrazolo[1,5-*c*]pyrimidin-7-amine (1.40)



3-Iodo-2,5-dimethyl-*N*-((tetrahydro-2*H*-pyran-4-yl)methyl)pyrazolo[1,5-*c*]pyrimidin-7-amine (69 mg, 0.18 mmol) in a microwave vial (20 mL) was dissolved in 1,4-dioxane (8 mL). Cesium carbonate (128 mg, 0.39 mmol) dissolved in water (2 mL), (3,4-dimethoxyphenyl)boronic acid (65 mg, 0.36 mmol) and XPhosPdG2™ (15 mg, 0.02 mmol) were added. The reaction vessel was sealed and heated at 130 °C for 5 h. After cooling, the reaction mixture was passed through Celite™ and diluted with EtOAc (20 mL). The organic layer was washed with brine (20 mL), passed through a hydrophobic frit and concentrated *in vacuo*. The crude product was purified by column chromatography eluting with EtOAc in cyclohexane (0-100% gradient). The appropriate fractions were combined and concentrated *in vacuo* to give 3-(3,4-dimethoxyphenyl)-2,5-dimethyl-*N*-((tetrahydro-2*H*-pyran-4-yl)methyl)pyrazolo[1,5-*c*]pyrimidin-7-amine (38 mg, 0.10 mmol, 54% yield). **¹H NMR** (400 MHz, CDCl₃) δ = 6.98 - 6.94 (m, 3H), 6.63 - 6.62 (m, 1H), 6.32 - 6.28 (m, 1H), 4.06 - 4.01 (m, 2H), 3.95 (s, 3H), 3.94 - 3.94 (m, 3H), 3.60 - 3.56 (m, 2H), 3.47 - 3.40 (m, 2H), 2.51 (s, 3H), 2.38 (s, 3H), 2.06 - 1.95 (m, 1H), 1.82 - 1.75 (m, 2H), 1.53 - 1.42 (m, 2H). **¹³C NMR** (101 MHz, CDCl₃) δ = 150.6, 149.1, 149.1, 147.7, 145.0, 140.0, 125.9, 121.3, 112.3, 111.6, 110.3, 98.0, 67.7, 56.0, 56.0, 46.5, 35.4, 30.7, 24.1, 13.0. **LCMS** (HpH) 100% desired product; t_{ret} = 1.22 min, MH^+ 397.1. **HRMS** (C₂₂H₂₈N₄O₃) $[M+H^+]$ requires 397.2240, found

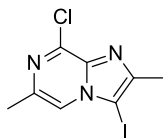
[M+H⁺] 397.2235. ν_{\max} (neat) / cm⁻¹ 3321, 2935, 1604, 1579, 1536, 1451, 1328, 1254, 1217, 1092, 1016, 979, 823, 801, 702. **Mp** 104-107 °C.

8-Chloro-2,6-dimethylimidazo[1,2-*a*]pyrazine (1.42)



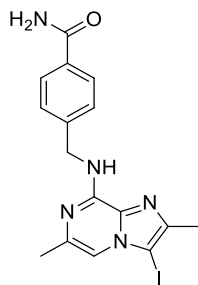
3-Chloro-5-methylpyrazin-2-amine (219 mg, 1.53 mmol) and 1-chloropropan-2-one (486 μ L, 6.10 mmol) were added to a microwave vial (5 mL). The reaction vessel was sealed and heated in a microwave at 130 °C for 2.5 h. After cooling, the reaction mixture was diluted with CH₂Cl₂ (20 mL) and washed with aqueous sodium bicarbonate (20 mL). The organic layer was passed through a hydrophobic frit and concentrated *in vacuo* to give 8-chloro-2,6-dimethylimidazo[1,2-*a*]pyrazine (173 mg, 0.96 mmol, 63% yield). **¹H NMR** (400 MHz, DMSO-*d*₆) δ = 8.39 (d, *J* = 1.0 Hz, 1H), 7.93 (d, *J* = 1.0 Hz, 1H), 2.40 (s, 3H), 2.37 (d, *J* = 1.0 Hz, 3H). **¹³C NMR** (101 MHz, DMSO-*d*₆) δ = 145.6, 139.5, 136.2, 135.8, 117.2, 114.4, 20.3, 14.7. **LCMS** (HpH) 94% desired product; t_{ret} = 0.63 min, MH⁺ 182.1.

8-Chloro-3-iodo-2,6-dimethylimidazo[1,2-*a*]pyrazine (1.43)



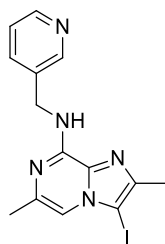
8-Chloro-2,6-dimethylimidazo[1,2-*a*]pyrazine (173 mg, 0.95 mmol) was dissolved in CH₂Cl₂ (10 mL) at 0 °C. *N*-iodosuccinimide (386 mg, 1.72 mmol) was added and the reaction was stirred for 4 h. The reaction mixture was diluted with CH₂Cl₂ (20 mL) and washed with aqueous sodium thiosulfate (30 mL). The organic layer was passed through a hydrophobic frit and concentrated *in vacuo* to give 8-chloro-3-iodo-2,6-dimethylimidazo[1,2-*a*]pyrazine (230 mg, 0.75 mmol, 79% yield). **¹H NMR** (400 MHz, DMSO-*d*₆) δ = 8.20 (d, *J* = 1.0 Hz, 1H), 2.46 (d, *J* = 1.0 Hz, 3H), 2.43 (s, 3H). **¹³C NMR** (101 MHz, DMSO-*d*₆) δ = 149.6, 139.5, 138.9, 137.8, 117.3, 71.5, 20.3, 15.2. **LCMS** (HpH) 98% desired product; t_{ret} = 0.89 min, MH⁺ 308.0.

4-(2-(3-Iodo-2,6-dimethylimidazo[1,2-*a*]pyrazin-8-yl)ethyl)benzamide (1.44)



8-Chloro-3-iodo-2,6-dimethylimidazo[1,2-*a*]pyrazine (474 mg, 1.54 mmol), 4-(aminomethyl)benzamide (463 mg, 3.08 mmol), triethylamine (0.86 mL, 6.17 mmol) and 1,4-dioxane (8 mL) were added to a microwave vial (20 mL). The reaction vessel was sealed and heated at 130 °C for 5 h. After cooling, the reaction mixture was diluted with EtOAc (30 mL) and washed with aqueous sodium bicarbonate (30 mL). The organic layer was passed through a hydrophobic frit and concentrated *in vacuo*. The crude product was purified by MDAP (high pH method). The appropriate fractions were combined and concentrated *in vacuo* to give 4-(2-(3-iodo-2,6-dimethylimidazo[1,2-*a*]pyrazin-8-yl)ethyl)benzamide (150 mg, 0.37 mmol, 24% yield). ¹H NMR (400 MHz, DMSO-*d*₆) δ = 8.03 (t, *J* = 6.4 Hz, 1H), 7.89 - 7.85 (m, 1H), 7.80 (d, *J* = 8.5 Hz, 2H), 7.41 (d, *J* = 8.5 Hz, 2H), 7.31 (d, *J* = 1.0 Hz, 1H), 7.28 - 7.23 (m, 1H), 4.71 (d, *J* = 6.3 Hz, 2H), 2.36 (s, 3H), 2.23 (d, *J* = 1.0 Hz, 3H). ¹³C NMR (101 MHz, DMSO-*d*₆) δ = 147.4, 145.1, 144.0, 137.6, 134.3, 133.1, 127.8, 127.4, 115.0, 107.0, 67.9, 43.4, 21.4, 14.7. LCMS (HpH) 100% desired product; *t*_{ret} = 0.97 min, MH⁺ 422.2.

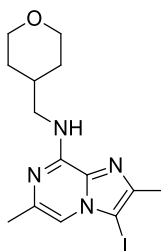
3-Iodo-2,6-dimethyl-*N*-(pyridin-3-ylmethyl)imidazo[1,2-*a*]pyrazin-8-amine (1.45)



8-Chloro-3-iodo-2,6-dimethylimidazo[1,2-*a*]pyrazine (517 mg, 1.68 mmol) was dissolved in 1,4-dioxane (8 mL) and transferred to a microwave vial (20 mL). Triethylamine (0.47 mL, 3.36 mmol) and pyridin-3-ylmethanamine (0.342 mL, 3.36 mmol) were added, the reaction vessel was sealed and heated at 130 °C for 5 h. After

cooling, the reaction mixture was diluted with EtOAc (20 mL) and washed with aqueous sodium bicarbonate (20 mL). The organic layer was passed through a hydrophobic frit and concentrated *in vacuo*. The crude product was purified by column chromatography eluting with EtOAc in cyclohexane (0-100% gradient) and then flushed with ethanol in EtOAc (1:3) to retrieve the product. The appropriate fractions were combined and concentrated *in vacuo* to give 3-iodo-2,6-dimethyl-*N*-(pyridin-3-ylmethyl)imidazo[1,2-*a*]pyrazin-8-amine (321 mg, 0.86 mmol, 51% yield). ¹H NMR (400 MHz, DMSO-*d*₆) δ = 8.61 - 8.57 (m, 1H), 8.44 - 8.40 (m, 1H), 8.11 - 8.07 (m, 1H), 7.79 - 7.73 (m, 1H), 7.34 - 7.28 (m, 2H), 4.65 (d, *J* = 6.5 Hz, 2H), 2.34 (s, 3H), 2.23 (d, *J* = 1.0 Hz, 3H). ¹³C NMR (101 MHz, DMSO-*d*₆) δ = 149.6, 148.3, 147.2, 145.1, 137.5, 136.0, 135.7, 134.2, 123.8, 107.1, 68.0, 41.4, 21.4, 14.7. LCMS (HpH) 98% desired product; *t*_{ret} = 1.03 min, MH⁺ 380.15.

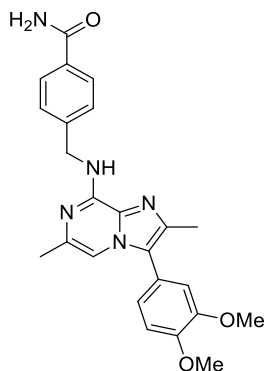
3-Iodo-2,6-dimethyl-*N*-((tetrahydro-2*H*-pyran-4-yl)methyl)imidazo[1,2-*a*]pyrazin-8-amine (1.46)



8-Chloro-3-iodo-2,6-dimethylimidazo[1,2-*a*]pyrazine (217 mg, 0.71 mmol), (tetrahydro-2*H*-pyran-4-yl)methanamine (0.173 mL, 1.41 mmol), triethylamine (0.4 mL, 2.87 mmol) and 1,4-dioxane (8 mL) were added to a microwave vial (20 mL). The reaction vessel was sealed and heated at 130 °C for 5 h. After cooling, the reaction mixture was diluted with EtOAc (20 mL) and washed with aqueous sodium bicarbonate (20 mL). The organic layer was passed through a hydrophobic frit and concentrated *in vacuo*. The crude product was purified by column chromatography eluting with EtOAc in cyclohexane (0-100% gradient). The appropriate fractions were combined and concentrated *in vacuo* to give 3-iodo-2,6-dimethyl-*N*-((tetrahydro-2*H*-pyran-4-yl)methyl)imidazo[1,2-*a*]pyrazin-8-amine (150 mg, 0.39 mmol, 55% yield). ¹H NMR (400 MHz, DMSO-*d*₆) δ = 7.41 - 7.35 (m, 1H), 7.27 - 7.24 (m, 1H), 3.87 - 3.80 (m,

2H), 3.37 - 3.34 (m, 2H), 3.28 - 3.22 (m, 2H), 2.33 (s, 3H), 2.24 (s, 3H), 2.00 - 1.87 (m, 1H), 1.63 - 1.55 (m, 2H), 1.27 - 1.15 (m, 2H). ¹³C NMR (101 MHz, DMSO-d₆) δ = 147.9, 144.8, 137.7, 134.3, 106.4, 67.7, 67.2, 46.0, 34.8, 31.1, 21.5, 14.7. LCMS (HpH) 100% desired product; t_{ret} = 1.11 min, MH⁺ 387.2.

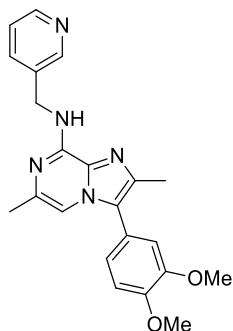
4-(((3-(3,4-Dimethoxyphenyl)-2,6-dimethylimidazo[1,2-*a*]pyrazin-8-yl)amino)methyl)benzamide (1.47)



4-(((3-Iodo-2,6-dimethylimidazo[1,2-*a*]pyrazin-8-yl)amino)methyl)benzamide (160 mg, 0.38 mmol), (3,4-dimethoxyphenyl)boronic acid (104 mg, 0.57 mmol), cesium carbonate (272 mg, 0.84 mmol), PdCl₂(dppf)-CH₂Cl₂ adduct (31.0 mg, 0.04 mmol), 1,4-dioxane (8 mL) and water (2 mL) were added to a microwave vial (20 mL). The reaction vessel was sealed and heated at 130 °C for 5 h. After cooling, the reaction mixture was passed through Celite™, diluted with EtOAc (30 mL) and washed with brine (30 mL). The organic layer was passed through a hydrophobic frit and concentrated *in vacuo*. The crude product was purified by MDAP (high pH method). The solvent was evaporated *in vacuo* to give 4-(((3-(3,4-dimethoxyphenyl)-2,6-dimethylimidazo[1,2-*a*]pyrazin-8-yl)amino)methyl)benzamide (102 mg, 0.24 mmol, 63% yield). ¹H NMR (400 MHz, DMSO-d₆) δ = 7.95 (s, 1H), 7.92 - 7.85 (m, 1H), 7.82 (d, *J* = 8.5 Hz, 2H), 7.43 (d, *J* = 8.3 Hz, 2H), 7.31 (d, *J* = 1.0 Hz, 1H), 7.28 - 7.23 (m, 1H), 7.15 (d, *J* = 8.3 Hz, 1H), 7.06 - 7.01 (m, 2H), 4.73 (d, *J* = 6.3 Hz, 2H), 3.87 - 3.83 (m, 3H), 3.82 (s, 3H), 2.37 (s, 3H), 2.15 (d, *J* = 1.0 Hz, 3H). ¹³C NMR (101 MHz, DMSO-d₆) δ =, 149.6, 149.3, 147.7, 144.3, 138.7, 136.7, 133.1, 130.3, 127.8, 127.4, 123.6, 122.4, 121.4, 113.3, 112.8, 104.6, 56.2, 56.1, 49.1, 43.3, 21.5, 14.1. LCMS (HpH) 100% desired product; t_{ret} = 0.96 min, MH⁺ 432.4. HRMS (C₂₄H₂₅N₅O₃) [M+H⁺] requires 432.2036,

found $[M+H]^+$ 432.2035. ν_{\max} (neat) / cm^{-1} 3353, 2913, 1652, 1615, 1567, 1533, 1505, 1456, 1414, 1244, 1219, 1174, 1139, 1024, 756, 694. **Mp** 191-193 °C.

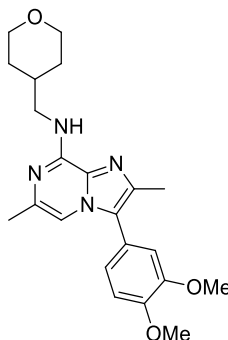
3-(3,4-Dimethoxyphenyl)-2,6-dimethyl-*N*-(pyridin-3-ylmethyl)imidazo[1,2- α]pyrazin-8-amine (1.48)



A microwave vial (5 mL) was charged with $\text{PdCl}_2(\text{dppf})\text{-CH}_2\text{Cl}_2$ adduct (14 mg, 0.02 mmol), (3,4-dimethoxyphenyl)boronic acid (47 mg, 0.26 mmol), cesium carbonate (580 mg, 1.78 mmol), 3-iodo-2,6-dimethyl-*N*-(pyridin-3-ylmethyl)imidazo[1,2- α]pyrazin-8-amine (307 mg, 0.81 mmol), 1,4-dioxane (7 mL) and water (1 mL). The reaction vessel was sealed and heated at 130 °C for 5 h. After cooling, the reaction mixture was passed through Celite™, diluted with EtOAc (20 mL) and washed with brine (20 mL). The organic layer was passed through a hydrophobic frit and concentrated *in vacuo*. The crude product was purified by column chromatography eluting with EtOAc in cyclohexane (0-100% gradient). The appropriate fractions were combined and concentrated *in vacuo* to give 3-(3,4-dimethoxyphenyl)-2,6-dimethyl-*N*-(pyridin-3-ylmethyl)imidazo[1,2- α]pyrazin-8-amine (274 mg, 0.70 mmol, 87% yield). $^1\text{H NMR}$ (400 MHz, DMSO-d_6) δ = 8.63 - 8.61 (m, 1H), 8.43 (dd, J = 1.8, 4.8 Hz, 1H), 8.05 - 7.98 (m, 1H), 7.82 - 7.77 (m, 1H), 7.35 - 7.31 (m, 2H), 7.16 - 7.13 (m, 1H), 7.06 - 7.00 (m, 2H), 4.69 (d, J = 6.3 Hz, 2H), 3.85 (s, 3H), 3.82 (s, 3H), 2.36 (s, 3H), 2.17 (d, J = 1.0 Hz, 3H). $^{13}\text{C NMR}$ (101 MHz, DMSO-d_6) δ = 149.6, 149.6, 149.3, 148.3, 147.5, 138.7, 136.6, 136.2, 135.7, 130.3, 123.8, 123.6, 122.4, 121.3, 113.3, 112.8, 104.7, 56.2, 56.1, 41.3, 21.5, 14.1. **LCMS** (HpH) 100% desired product; t_{ret} = 1.01 min, MH^+ 390.3. **HRMS** ($\text{C}_{22}\text{H}_{23}\text{N}_5\text{O}_2$) $[M+H]^+$ requires 390.1930, found $[M+H]^+$ 390.1926. ν_{\max}

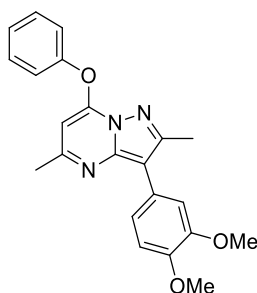
(neat) / cm^{-1} 3251, 2917, 1537, 1505, 1478, 1463, 1417, 1260, 1247, 1219, 1175, 1136, 1023, 812, 763, 712, 696. **Mp** 128-131 °C.

3-(3,4-Dimethoxyphenyl)-2,6-dimethyl-*N*-((tetrahydro-2*H*-pyran-4-yl)methyl)imidazo[1,2-*a*]pyrazin-8-amine (1.49)



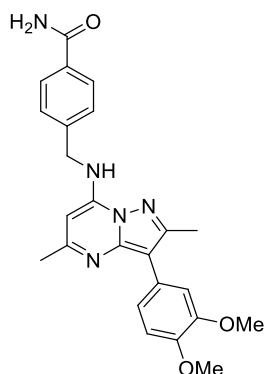
3-Iodo-2,6-dimethyl-*N*-((tetrahydro-2*H*-pyran-4-yl)methyl)imidazo[1,2-*a*]pyrazin-8-amine (150 mg, 0.39 mmol), (3,4-dimethoxyphenyl)boronic acid (106 mg, 0.58 mmol), cesium carbonate (278 mg, 0.85 mmol), $\text{PdCl}_2(\text{dppf})\text{-CH}_2\text{Cl}_2$ adduct (31.7 mg, 0.04 mmol), 1,4-dioxane (8 mL) and water (2 mL) were added to a microwave vial (20 mL). The reaction vessel was sealed and heated at 130 °C for 5 h. After cooling, the reaction mixture was passed through Celite™, diluted with EtOAc (20 mL) and washed with brine (20 mL). The organic layer was passed through a hydrophobic frit and purified by MDAP (high pH method). The appropriate fractions were combined and concentrated *in vacuo* to give 3-(3,4-dimethoxyphenyl)-2,6-dimethyl-*N*-((tetrahydro-2*H*-pyran-4-yl)methyl)imidazo[1,2-*a*]pyrazin-8-amine (50 mg, 0.13 mmol, 33% yield). **$^1\text{H NMR}$** (400 MHz, DMSO-d_6) δ = 7.31 - 7.24 (m, 2H), 7.17 - 7.11 (m, 1H), 7.05 - 6.99 (m, 2H), 3.85 (s, 3H), 3.82 (s, 3H), 3.39 (t, J = 6.5 Hz, 2H), 3.28 (dt, J = 2.0, 11.5 Hz, 2H), 2.35 (s, 3H), 2.18 (d, J = 0.8 Hz, 3H), 1.98 (tdd, J = 3.7, 7.4, 14.8 Hz, 1H), 1.62 (br dd, J = 2.0, 12.8 Hz, 2H), 1.31 - 1.18 (m, 2H). **$^{13}\text{C NMR}$** (101 MHz, DMSO-d_6) δ = 149.5, 149.3, 148.2, 138.5, 136.8, 130.3, 123.5, 122.4, 121.4, 113.3, 112.8, 104.0, 67.3, 56.2, 56.1, 45.9, 34.9, 31.1, 21.6, 14.0. **LCMS** (HpH) 97% desired product; t_{ret} = 1.07 min, MH^+ 397.4. **HRMS** ($\text{C}_{22}\text{H}_{28}\text{N}_4\text{O}_3$) [$\text{M}+\text{H}^+$] requires 397.2240, found [$\text{M}+\text{H}^+$] 397.2239. ν_{max} (neat) / cm^{-1} 3343, 2918, 1544, 1510, 1466, 1422, 1262, 1249, 1220, 1176, 1146, 1089, 1024, 985, 853, 823, 762. **Mp** 93-95 °C.

3-(3,4-Dimethoxyphenyl)-2,5-dimethyl-7-phenoxy-pyrazolo[1,5-*a*]pyrimidine (1.56)



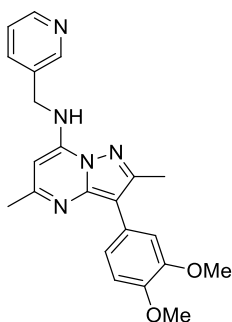
An RBF (100 mL) was charged with (3,4-dimethoxyphenyl)boronic acid (287 mg, 1.58 mmol), 3-bromo-2,5-dimethyl-7-phenoxy-pyrazolo[1,5-*a*]pyrimidine (641 mg, 2.01 mmol), PdCl₂(dppf)-CH₂Cl₂ adduct (136 mg, 0.17 mmol), potassium phosphate, dibasic (1.371 g, 7.87 mmol), water (5 mL) and 1,4 dioxane (20 mL). The reaction mixture was heated under nitrogen at 120 °C for 16 h. After cooling, the reaction mixture was diluted with EtOAc (40 mL) and washed with brine (40 mL). The combined organics were dried over magnesium sulfate, filtered through Celite™ and concentrated *in vacuo*. The crude product was purified by column chromatography eluting with EtOAc in cyclohexane (gradient 0-40%). The appropriate fractions were concentrated *in vacuo* to yield 3-(3,4-dimethoxyphenyl)-2,5-dimethyl-7-phenoxy-pyrazolo[1,5-*a*]pyrimidine (290 mg, 0.77 mmol, 50% yield). **¹H NMR** (400 MHz, DMSO-*d*₆) δ = 7.62 - 7.56 (m, 2H), 7.47 - 7.41 (m, 3H), 7.39 (d, *J* = 2.0 Hz, 1H), 7.25 (dd, *J* = 2.0, 8.1 Hz, 1H), 7.06 (d, *J* = 8.1 Hz, 1H), 5.94 (s, 1H), 3.82 (s, 3H), 3.81 (s, 3H), 2.57 (s, 3H), 2.41 (s, 3H). **¹³C NMR** (101 MHz, DMSO-*d*₆) δ = 179.2, 160.8, 154.2, 152.3, 152.1, 149.0, 147.8, 147.6, 131.2, 127.4, 125.5, 121.3, 113.1, 112.6, 107.5, 90.6, 56.1, 56.0, 25.3, 14.9. **LCMS** (HpH) 100% desired product; *t*_{ret} = 1.18 min, MH⁺ 376.1.

4-(((3-(3,4-Dimethoxyphenyl)-2,5-dimethylpyrazolo[1,5-*a*]pyrimidin-7-yl)amino)methyl)benzamide (1.57)



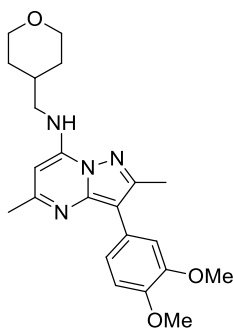
3-(3,4-Dimethoxyphenyl)-2,5-dimethyl-7-phenoxy pyrazolo[1,5-*a*]pyrimidine (95 mg, 0.25 mmol), triethylamine (0.141 mL, 1.01 mmol), 4-(aminomethyl)benzamide (111 mg, 0.74 mmol), isopropanol (2 mL) and DMSO (2 mL) were added to a microwave vial (5 mL). The reaction vessel was sealed and heated at 130 °C for 5 h. After cooling, the reaction mixture was purified by MDAP (high pH method). The appropriate fractions were combined and concentrated *in vacuo* to give 4-(((3-(3,4-dimethoxyphenyl)-2,5-dimethylpyrazolo[1,5-*a*]pyrimidin-7-yl)amino)methyl)benzamide (83 mg, 0.19 mmol, 76% yield). **¹H NMR** (400 MHz, CDCl₃) δ = 7.87 - 7.83 (m, 2H), 7.51 - 7.47 (m, 2H), 7.43 - 7.41 (m, 1H), 7.25 (dd, *J* = 2.0, 8.1 Hz, 1H), 6.99 (d, *J* = 8.1 Hz, 1H), 6.70 (t, *J* = 6.0 Hz, 1H), 5.76 (s, 1H), 4.69 (d, *J* = 6.0 Hz, 2H), 3.96 (s, 3H), 3.94 (s, 3H), 2.61 (s, 3H), 2.48 (s, 3H). **¹³C NMR** (101 MHz, CDCl₃) δ = 168.5, 159.5, 151.1, 148.9, 147.4, 146.1, 145.6, 140.8, 133.1, 128.0, 127.2, 125.9, 121.0, 119.6, 112.6, 111.6, 85.6, 56.0, 55.9, 45.7, 25.4, 14.4. **LCMS** (For) 100% desired product; *t*_{ret} = 0.6 min, MH⁺ 431.2. **HRMS** (C₂₄H₂₅N₅O₃) [M+H⁺] requires 432.2036, found [M+H⁺] 432.2030. **v**_{max} (neat) / cm⁻¹ 3474, 3326, 3143, 1667, 1616, 1580, 1563, 1406, 1394, 1357, 1249, 1172, 1146, 1021, 800, 782, 764, 750. **Mp** 238-240 °C.

3-(3,4-Dimethoxyphenyl)-2,5-dimethyl-*N*-(pyridin-3-ylmethyl)pyrazolo[1,5-*a*]pyrimidin-7-amine (1.58)



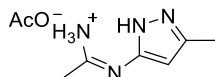
3-(3,4-Dimethoxyphenyl)-2,5-dimethyl-7-phenoxy-pyrazolo[1,5-*a*]pyrimidine (95 mg, 0.25 mmol), triethylamine (0.141 mL, 1.01 mmol), isopropanol (2 mL), DMSO (2 mL) and pyridin-3-ylmethanamine (0.078 mL, 0.83 mmol) were added to a microwave vial (5 mL). The reaction vessel was sealed and heated at 130 °C for 4 h. After cooling, the reaction mixture was concentrated *in vacuo* and purified by MDAP (high pH method). The appropriate fractions were combined and concentrated *in vacuo* to give 3-(3,4-dimethoxyphenyl)-2,5-dimethyl-*N*-(pyridin-3-ylmethyl)pyrazolo[1,5-*a*]pyrimidin-7-amine (75 mg, 0.19 mmol, 77% yield). **¹H NMR** (400 MHz, CDCl₃) δ = 8.70 - 8.65 (m, 1H), 8.60 (dd, *J* = 1.5, 5.0 Hz, 1H), 7.74 (td, *J* = 1.5, 7.9 Hz, 1H), 7.39 - 7.27 (m, 2H), 7.21 (dd, *J* = 2.0, 8.1 Hz, 1H), 6.96 (d, *J* = 8.6 Hz, 1H), 6.87 (br s, 1H), 5.78 (s, 1H), 4.63 (br s, 2H), 3.94 (s, 3H), 3.91 (s, 3H), 2.57 (s, 3H), 2.47 (s, 3H). **¹³C NMR** (101 MHz, CDCl₃) δ = 163.8, 159.6, 151.2, 148.9, 148.2, 147.5, 146.1, 145.5, 135.3, 132.6, 125.7, 124.0, 121.2, 112.7, 111.6, 107.6, 85.7, 56.0, 55.9, 43.5, 25.3, 14.2. **LCMS** (HpH) 100% desired product; *t*_{ret} = 0.98 min, MH⁺ 390.3. **HRMS** (C₂₂H₂₃N₅O₂) [M+H⁺] requires 390.1930, found [M+H⁺] 390.1926. **v**_{max} (neat) / cm⁻¹ 2954, 1617, 1590, 1579, 1538, 1514, 1445, 1434, 1410, 1250, 1216, 1152, 1024, 821, 747, 710. **Mp** 149-151 °C.

3-(3,4-Dimethoxyphenyl)-2,5-dimethyl-N-((tetrahydro-2H-pyran-4-yl)methyl)pyrazolo[1,5-*a*]pyrimidin-7-amine (1.59)



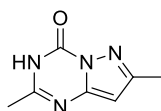
3-(3,4-Dimethoxyphenyl)-2,5-dimethyl-7-phenoxy pyrazolo[1,5-*a*]pyrimidine (74 mg, 0.20 mmol), triethylamine (0.110 mL, 0.79 mmol), isopropanol (2 mL) and (tetrahydro-2*H*-pyran-4-yl)methanamine (0.072 mL, 0.41 mmol) were added to a microwave vial (5 mL). The reaction vessel was sealed and heated at 130 °C for 5 h. After cooling, the reaction mixture was diluted with EtOAc (20 mL) and washed with aqueous ammonium chloride (20 mL). The aqueous was re-extracted twice with EtOAc (30 mL). The combined organics were washed with aqueous sodium bicarbonate (20 mL), passed through a hydrophobic frit and concentrated *in vacuo*. The crude product was purified by MDAP (high pH method). The appropriate fractions were combined and evaporated *in vacuo* to give 3-(3,4-dimethoxyphenyl)-2,5-dimethyl-N-((tetrahydro-2*H*-pyran-4-yl)methyl)pyrazolo[1,5-*a*]pyrimidin-7-amine (49 mg, 0.20 mmol, 63% yield). **¹H NMR** (400 MHz, CDCl₃) δ = 7.44 - 7.41 (m, 1H), 7.24 (dd, *J* = 2.0, 8.1 Hz, 1H), 6.98 (d, *J* = 8.1 Hz, 1H), 6.32 - 6.25 (m, 1H), 5.82 (s, 1H), 4.08 - 4.02 (m, 2H), 3.96 (s, 3H), 3.93 (s, 3H), 3.48 - 3.40 (m, 2H), 3.34 - 3.29 (m, 2H), 2.59 (s, 3H), 2.53 (s, 3H), 2.08 - 1.95 (m, 1H), 1.83 - 1.76 (m, 2H), 1.54 - 1.40 (m, 2H). **¹³C NMR** (101 MHz, CDCl₃) δ = 179.2, 159.4, 150.9, 148.9, 147.3, 146.2, 145.8, 126.1, 121.0, 112.6, 111.6, 85.1, 67.5, 56.0, 55.9, 47.9, 35.1, 30.8, 25.5, 14.3. **LCMS** (HpH) 99% desired product; *t*_{ret} = 1.08 min, MH⁺ 397.4. **HRMS** (C₂₂H₂₈N₄O₃) [M+H⁺] requires 397.2240, found [M+H⁺] 397.2237. **v**_{max} (neat) / cm⁻¹ 3385, 2906, 1615, 1583, 1551, 1513, 1459, 1330, 1265, 1242, 1144, 1090, 1027, 805, 766, 749. **Mp** 157-159 °C.

(E)-N'-(3-Methyl-1H-pyrazol-5-yl)acetimidamide acetate (1.61)



1-Ethoxyethan-1-amine (3.63 g, 28.9 mmol) and EtOAc (30 mL) were added to an aqueous solution of potassium carbonate (6.39 g, 46.2 mmol). The reaction mixture was stirred for 10 minutes. The organic layer was dried over anhydrous MgSO₄, filtered and transferred to an RBF (150 mL) containing 3-methyl-1H-pyrazol-5-amine (3.6 g, 37.1 mmol). The reaction was stirred for 1 h at RT followed by the addition of acetic acid (1.82 mL, 31.8 mmol). The reaction was stirred for a further 30 minutes and the precipitate was filtered and washed with EtOAc (30 mL) to give (E)-N'-(3-methyl-1H-pyrazol-5-yl)acetimidamide acetate (4.83 g, 24.4 mmol, 84% yield). ¹H NMR (400 MHz, METHANOL-d₄) δ = 5.92 (s, 1H), 2.40 (s, 3H), 2.33 (s, 3H), 1.92 (s, 3H). ¹³C NMR (101 MHz, METHANOL-d₄) δ = 178.5, 162.2, 147.7, 140.7, 94.5, 22.6, 17.6, 9.1. Compound does not ionise under LCMS conditions. HRMS Parent ion (C₆H₁₀N₄) [M+H⁺] requires 139.0984, found [M+H⁺] 139.0984. Characterising data consistent with the literature.⁶⁸

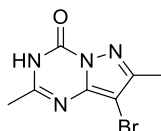
2,7-Dimethylpyrazolo[1,5-a][1,3,5]triazin-4(3H)-one (1.63)



An RBF (500 mL) under a nitrogen atmosphere was charged with (E)-N'-(3-methyl-1H-pyrazol-5-yl)acetimidamide acetate (7.05 g, 35.6 mmol) and diethyl carbonate (64.6 ml, 533 mmol). Sodium ethoxide in ethanol (21%, 55.8 mL, 711 mmol) was added to the reaction and heated at 100 °C for 5 h. After cooling, the reaction mixture was concentrated *in vacuo*. Aqueous HCl (50 mL, 2 M) was added and the mixture was reduced under vacuum. The residue was diluted with chloroform (50 mL) and the organic layer was passed through a hydrophobic frit and concentrated *in vacuo*. The crude product was purified by column chromatography eluting with EtOAc in cyclohexane (0-100% gradient). The appropriate fractions were combined and concentrated *in vacuo* to give 2,7-dimethylpyrazolo[1,5-a][1,3,5]triazin-4(3H)-one

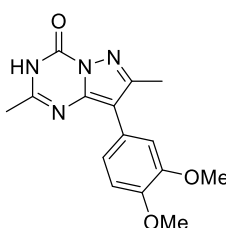
(4.23 g, 25.8 mmol, 73% yield). $^1\text{H NMR}$ (400 MHz, DMSO- d_6) δ = 12.38 - 12.18 (m, 1H), 6.19 (s, 1H), 2.30 (s, 3H), 2.30 (s, 3H). $^{13}\text{C NMR}$ (101 MHz, DMSO- d_6) δ = 155.2, 154.4, 149.9, 144.2, 98.1, 21.2, 14.7. **LCMS** (Formic) 92% desired product; t_{ret} = 0.41 min, MH^+ 165.1. **HRMS** ($\text{C}_7\text{H}_8\text{N}_4\text{O}$) [$\text{M}+\text{H}^+$] requires 165.080, found [$\text{M}+\text{H}^+$] 165.078.

8-Bromo-2,7-dimethylpyrazolo[1,5-*a*][1,3,5]triazin-4(3*H*)-one (1.64)



2,7-Dimethylpyrazolo[1,5-*a*][1,3,5]triazin-4(3*H*)-one (616 mg, 3.75 mmol) was added to CH_2Cl_2 (25 mL) at 0 °C. Cold *N*-bromosuccinimide (801 mg, 4.50 mmol) was added and the reaction mixture was stirred at 0 °C for 10 minutes. The reaction mixture was gradually brought to RT and further stirred for 3 h. White solid precipitated out of solution and the compound was collected *via* vacuum filtration to give 8-bromo-2,7-dimethylpyrazolo[1,5-*a*][1,3,5]triazin-4(3*H*)-one (744 mg, 3.1 mmol, 82% yield). $^1\text{H NMR}$ (400 MHz, DMSO- d_6) δ = 12.53 (br s, 1H), 2.34 (s, 3H), 2.30 (s, 3H). $^{13}\text{C NMR}$ (101 MHz, DMSO- d_6) δ = 156.2, 153.4, 146.9, 143.8, 85.9, 21.3, 13.3. **LCMS** (Formic) 93% desired product; t_{ret} = 0.60 min, MH^+ 243.0.

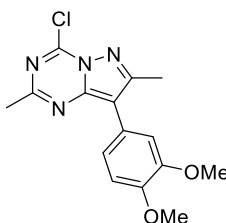
8-(3,4-Dimethoxyphenyl)-2,7-dimethylpyrazolo[1,5-*a*][1,3,5]triazin-4(3*H*)-one (1.65)



8-Bromo-2,7-dimethylpyrazolo[1,5-*a*][1,3,5]triazin-4(3*H*)-one (1.3 g, 5.35 mmol), (3,4-dimethoxyphenyl)boronic acid (1.95 g, 10.70 mmol), potassium phosphate, tribasic (1.73 g, 8.02 mmol), bis(triphenylphosphine)palladium(II) chloride (56 mg, 0.08 mmol), 1,4-dioxane (10 mL) and water (2 mL) were added to a microwave vial (20 mL). The reaction vessel was sealed and heated at 120 °C for 3 h. After cooling, the reaction mixture was passed through CeliteTM, diluted with EtOAc (30 mL) and

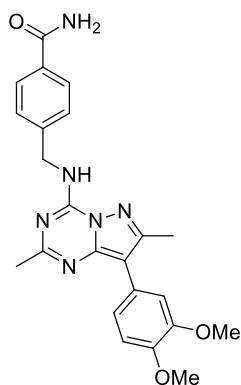
washed with brine (30 mL). The crude product was purified by column chromatography eluting with EtOAc in cyclohexane (0-70% gradient). The appropriate fractions were combined and concentrated *in vacuo* to yield 8-(3,4-dimethoxyphenyl)-2,7-dimethylpyrazolo[1,5-*a*][1,3,5]triazin-4(3*H*)-one (830 mg, 4.3 mmol, 52% yield). ¹H NMR (400 MHz, DMSO-*d*₆) δ = 7.25 (d, *J* = 2.0 Hz, 1H), 7.16 - 7.10 (m, 1H), 7.05 - 7.01 (m, 1H), 3.79 (s, 6H), 2.43 (s, 3H), 2.32 (s, 3H). ¹³C NMR (101 MHz, DMSO-*d*₆) δ = 170.8, 149.0, 148.0, 124.7, 121.4, 118.5, 113.1, 112.5, 60.2, 56.1, 31.1, 21.8, 21.2, 14.5, 1.6. LCMS (HpH) 100% desired product; *t*_{ret} = 0.57 min, MH⁺ 301.1.

4-Chloro-8-(3,4-dimethoxyphenyl)-2,7-dimethylpyrazolo[1,5-*a*][1,3,5]triazine (1.66)



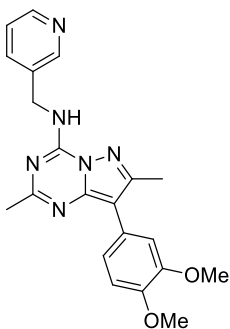
8-(3,4-Dimethoxyphenyl)-2,7-dimethylpyrazolo[1,5-*a*][1,3,5]triazin-4(3*H*)-one (0.508 g, 1.69 mmol) and POCl₃ (11.82 ml, 127 mmol) were stirred in an RBF (100 mL), followed by the slow addition of *N,N*-diethylaniline (0.592 ml, 3.72 mmol). The reaction mixture was heated at 115 °C for 72 h. After cooling, the reaction mixture was concentrated *in vacuo* and azeotroped with toluene. The residue was diluted with CH₂Cl₂ (40 mL) and washed with aqueous brine/ sodium bicarbonate solution (40 mL). The organic layer was passed through a hydrophobic frit and concentrated *in vacuo*. The crude product was purified by column chromatography eluting with EtOAc in cyclohexane (0-50% gradient). The appropriate fractions were combined and concentrated *in vacuo* to give 4-chloro-8-(3,4-dimethoxyphenyl)-2,7-dimethylpyrazolo[1,5-*a*][1,3,5]triazine (375 mg, 1.2 mmol, 71% yield). No characterising data available due to poor stability.

4-(((8-(3,4-Dimethoxyphenyl)-2,7-dimethylpyrazolo[1,5-*a*][1,3,5]triazin-4-yl)amino)methyl)benzamide (1.67)



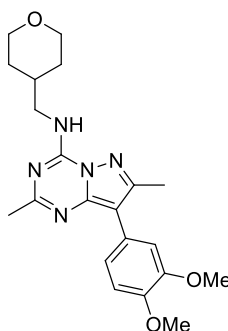
4-Chloro-8-(3,4-dimethoxyphenyl)-2,7-dimethylpyrazolo[1,5-*a*][1,3,5]triazine (90 mg, 0.28 mmol) was dissolved in DMSO (3 mL) and transferred to a microwave vial (5 mL). 4-(Aminomethyl)benzamide (63.6 mg, 0.42 mmol) and DIPEA (0.064 mL, 0.37 mmol) were added and the reaction mixture was stirred at RT for 1 h. The reaction mixture was diluted with EtOAc (20 mL) and washed with brine (20 mL). The organic layer was passed through a hydrophobic frit and concentrated *in vacuo*. The crude product was purified by column chromatography, eluting with EtOAc in cyclohexane (0-100% gradient). The appropriate fractions were combined and concentrated *in vacuo* to give 4-(((8-(3,4-dimethoxyphenyl)-2,7-dimethylpyrazolo[1,5-*a*][1,3,5]triazin-4-yl)amino)methyl)benzamide (80 mg, 0.19 mmol, 66% yield). **¹H NMR** (400 MHz, DMSO-*d*₆) δ = 9.26 - 9.15 (m, 1H), 7.95 - 7.90 (m, 1H), 7.86 - 7.82 (m, 2H), 7.47 - 7.42 (m, 2H), 7.33 - 7.31 (m, 1H), 7.31 - 7.27 (m, 1H), 7.22 - 7.17 (m, 1H), 7.08 - 7.01 (m, 1H), 4.82 - 4.69 (m, 2H), 3.81 (s, 3H), 3.80 (s, 3H), 2.54 (s, 3H), 2.38 (s, 3H). **¹³C NMR** (151 MHz, DMSO-*d*₆) δ = 168.1, 163.2, 152.6, 149.0, 148.6, 147.8, 146.4, 142.4, 133.6, 128.0, 127.5, 125.1, 121.2, 113.1, 112.6, 107.3, 56.1, 55.5, 43.4, 26.3, 14.7. **LCMS** (Formic) 99% desired product; t_{ret} = 0.89 min, MH^+ 433.3. **HRMS** ($\text{C}_{23}\text{H}_{24}\text{N}_6\text{O}_3$) $[\text{M}+\text{H}^+]$ requires 433.1988, found $[\text{M}+\text{H}^+]$ 433.1984. ν_{max} (neat) / cm^{-1} 3356, 2930, 1655, 1586, 1310, 1219, 1137, 1025, 760, 623. **Mp** 167-169 °C.

8-(3,4-Dimethoxyphenyl)-2,7-dimethyl-N-(pyridin-3-ylmethyl)pyrazolo[1,5-*a*][1,3,5]triazin-4-amine (1.68)



4-Chloro-8-(3,4-dimethoxyphenyl)-2,7-dimethylpyrazolo[1,5-*a*][1,3,5]triazine (219 mg, 0.69 mmol) was dissolved in DMSO (2.5 mL) and transferred to a microwave vial (5 mL). Pyridin-3-ylmethanamine (0.091 mL, 0.89 mmol) and DIPEA (0.240 mL, 1.37 mmol) were added and the reaction vessel was sealed and stirred at 60 °C for 1 h. After cooling, the reaction mixture was diluted with EtOAc (20 mL), washed with brine (20 mL) and the organic layer was passed through a hydrophobic frit. The crude product was purified by column chromatography eluting with EtOAc in cyclohexane (0-100% gradient). The appropriate fractions were combined and concentrated *in vacuo* to give 8-(3,4-dimethoxyphenyl)-2,7-dimethyl-N-(pyridin-3-ylmethyl)pyrazolo[1,5-*a*][1,3,5]triazin-4-amine (98 mg, 0.25 mmol, 37% yield). **¹H NMR** (600 MHz, DMSO-*d*₆) δ = 9.26 - 9.21 (m, 1H), 8.63 (d, *J* = 1.8 Hz, 1H), 8.48 (dd, *J* = 1.5, 4.8 Hz, 1H), 7.81 (td, *J* = 1.8, 8.1 Hz, 1H), 7.36 (dd, *J* = 5.0, 7.5 Hz, 1H), 7.31 (d, *J* = 2.2 Hz, 1H), 7.18 (dd, *J* = 1.8, 8.4 Hz, 1H), 7.04 (d, *J* = 8.4 Hz, 1H), 4.73 (d, *J* = 5.9 Hz, 2H), 3.80 (s, 3H), 3.79 (s, 3H), 2.53 (s, 3H), 2.40 (s, 3H). **¹³C NMR** (151 MHz, DMSO-*d*₆) δ = 163.2, 152.6, 149.5, 149.0, 148.8, 148.5, 147.8, 146.4, 135.8, 134.6, 125.1, 124.0, 121.2, 113.1, 112.6, 107.3, 56.1, 56.1, 41.4, 26.3, 14.7. **LCMS** (Formic) 96% desired product; *t*_{ret} = 0.66 min, *M*H⁺ 391.2. **HRMS** (C₂₁H₂₂N₆O₂) [*M*+*H*⁺] requires 391.1882, found [*M*+*H*⁺] 391.1887. ***v*_{max}** (neat) / cm⁻¹ 2936, 1587, 1546, 1426 1309, 1248, 1136, 1021, 710, 624. **Mp** 149-152 °C.

8-(3,4-Dimethoxyphenyl)-2,7-dimethyl-*N*-((tetrahydro-2*H*-pyran-4-yl)methyl)pyrazolo[1,5-*a*][1,3,5]triazin-4-amine (1.69)



4-Chloro-8-(3,4-dimethoxyphenyl)-2,7-dimethylpyrazolo[1,5-*a*][1,3,5]triazine (219 mg, 0.69 mmol) was dissolved in DMSO (2.5 mL) and transferred to a microwave vial (5 mL). Tetrahydro-2*H*-pyran-4-yl)methanamine (0.106 mL, 0.89 mmol) and DIPEA (0.240 mL, 1.37 mmol) were added. The reaction vessel was sealed and stirred at 60 °C for 1 h. After cooling, the reaction mixture was diluted with EtOAc (20 mL) and washed with brine (20 mL). The crude product was purified by column chromatography eluting with EtOAc in cyclohexane (0-100% gradient). The appropriate fractions were combined and concentrated *in vacuo* to give 8-(3,4-dimethoxyphenyl)-2,7-dimethyl-*N*-((tetrahydro-2*H*-pyran-4-yl)methyl)pyrazolo[1,5-*a*][1,3,5]triazin-4-amine (98 mg, 0.25 mmol, 36% yield). **¹H NMR** (600 MHz, DMSO-*d*₆) δ = 8.62 (t, *J* = 6.1 Hz, 1H), 7.31 (d, *J* = 2.2 Hz, 1H), 7.18 (dd, *J* = 2.0, 8.3 Hz, 1H), 7.03 (d, *J* = 8.4 Hz, 1H), 3.85 (br dd, *J* = 2.2, 11.4 Hz, 2H), 3.80 (s, 3H), 3.79 (s, 3H), 3.42 (t, *J* = 6.6 Hz, 2H), 3.27 (dt, *J* = 1.8, 11.4 Hz, 2H), 2.52 (s, 3H), 2.40 (s, 3H), 1.98 (tdd, *J* = 3.8, 7.6, 14.9 Hz, 1H), 1.59 (br dd, *J* = 1.7, 13.0 Hz, 2H), 1.28 - 1.20 (m, 2H). **¹³C NMR** (151 MHz, DMSO-*d*₆) δ = 163.2, 152.3, 149.0, 148.7, 147.7, 146.3, 125.2, 121.2, 113.1, 112.6, 107.1, 67.1, 56.1, 56.1, 45.8, 34.9, 30.7, 26.4, 14.7. **LCMS** (Formic) 100% desired product; *t*_{ret} = 1.00 min, *M*H⁺ 398.3. **HRMS** (C₂₁H₂₇N₅O₃) [*M*+*H*⁺] requires 398.2192, found [*M*+*H*⁺] 398.2196. ***v*_{max}** (neat) / cm⁻¹ 3357, 2929, 2837, 1587, 1447, 1220, 1078, 760, 626. **Mp** 143-145°C.

REFERENCES

- (1) Reuberson, J.; Horsley, H.; Franklin, R. J.; Ford, D.; Neuss, J.; Brookings, D.; Huang, Q.; Vanderhoydonck, B.; Gao, L. J.; Jang, M. Y.; Herdewijn, P.; Ghawalkar, A.; Fallah-Arani, F.; Khan, A. R.; Henshall, J.; Jairaj, M.; Malcolm, S.; Ward, E.; Shuttleworth, L.; Lin, Y.; Li, S.; Louat, T.; Waer, M.; Herman, J.; Payne, A.; Ceska, T.; Doyle, C.; Pitt, W.; Calmiano, M.; Augustin, M.; Steinbacher, S.; Lammens, A.; Allen, R. *J Med Chem* **2018**, *61*, 6705.
- (2) Vallianatou, T.; Giaginis, C.; Tsantili-Kakoulidou, A. *Springer International Publishing*, **2015**, 187-194.
- (3) Nakashima, S.; Yamamoto, K.; Arai, Y.; Ikeda, Y. *Chem Pharm Bull (Tokyo)* **2013**, *61*, 1228.
- (4) Morgan, P.; Van Der Graaf, P. H.; Arrowsmith, J.; Feltner, D. E.; Drummond, K. S.; Wegner, C. D.; Street, S. D. *Drug Discov Today* **2012**, *17*, 419.
- (5) Saal, C.; Peterleit, A. C. *Eur J Pharm Sci* **2012**, *47*, 589.
- (6) Schneider, N.; Lowe, D. M.; Sayle, R. A.; Tarselli, M. A.; Landrum, G. A. *J Med Chem* **2016**, *59*, 4385.
- (7) Wenlock, M. C.; Austin, R. P.; Barton, P.; Davis, A. M.; Leeson, P. D. *J Med Chem* **2003**, *46*, 1250.
- (8) Valko, K. *Physicochemical and Biomimetic Properties in Drug Discovery*; John Wiley & Sons, Inc., 2014.
- (9) Ahmad, N. M. *Bioorg Med Chem Lett* **2016**, *26*, 2975.
- (10) Bard, B.; Martel, S.; Carrupt, P. A. *Eur J Pharm Sci* **2008**, *33*, 230.
- (11) Hernandez-Covarrubias, C.; Vilchis-Reyes, M. A.; Yepez-Mulia, L.; Sanchez-Diaz, R.; Navarrete-Vazquez, G.; Hernandez-Campos, A.; Castillo, R.; Hernandez-Luis, F. *Eur J Med Chem* **2012**, *52*, 193.
- (12) Volpe, D. A. *Future Med Chem* **2011**, *3*, 2063.
- (13) Sugano, K. *Int J Pharm* **2011**, *405*, 79.
- (14) Bannan, C. C.; Calabro, G.; Kyu, D. Y.; Mobley, D. L. *J Chem Theory Comput* **2016**, *12*, 4015.
- (15) Arnott, J. A.; Planey, S. L. *Expert Opinion on Drug Discovery* **2012**, *7*, 863.
- (16) Lapins, M.; Arvidsson, S.; Lampa, S.; Berg, A.; Schaal, W.; Alvarsson, J.; Spjuth, O. *J Cheminform* **2018**, *10*, 17.
- (17) Young, R. J.; Green, D. V.; Luscombe, C. N.; Hill, A. P. *Drug Discov Today* **2011**, *16*, 822.
- (18) Pallicer, J. M.; Calvet, C.; Port, A.; Roses, M.; Rafols, C.; Bosch, E. *J Chromatogr A* **2012**, *1240*, 113.
- (19) Kung, P. P.; Bingham, P.; Brooun, A.; Collins, M.; Deng, Y. L.; Dinh, D.; Fan, C.; Gajiwala, K. S.; Grantner, R.; Gukasyan, H. J.; Hu, W.; Huang, B.; Kania, R.; Kephart, S. E.; Krivacic, C.; Kumpf, R. A.; Khamphavong, P.; Kraus, M.; Liu, W.; Maegley, K. A.; Nguyen, L.; Ren, S.; Richter, D.; Rollins, R. A.; Sach, N.; Sharma, S.; Sherrill, J.; Spangler, J.; Stewart, A. E.; Sutton, S.; Uryu, S.; Verhelle, D.; Wang, H.;

- Wang, S.; Wythes, M.; Xin, S.; Yamazaki, S.; Zhu, H.; Zhu, J.; Zehnder, L.; Edwards, M. *J Med Chem* **2018**, *61*, 650.
- (20) Lipinski, C. A.; Lombardo, F.; Dominy, B. W.; Feeney, P. J. *Adv Drug Deliv Rev* **1997**, *23*, 3.
- (21) Lipinski, C. A. *J Pharmacol Toxicol Methods* **2000**, *44*, 235.
- (22) Lipinski, C. A.; Lombardo, F.; Dominy, B. W.; Feeney, P. J. *Adv Drug Deliv Rev* **2001**, *46*, 3.
- (23) Benet, L. Z.; Hosey, C. M.; Ursu, O.; Oprea, T. I. *Adv Drug Deliv Rev* **2016**, *101*, 89.
- (24) Johnson, T. W.; Dress, K. R.; Edwards, M. *Bioorg Med Chem Lett* **2009**, *19*, 5560.
- (25) Hughes, J. D.; Blagg, J.; Price, D. A.; Bailey, S.; Decrescenzo, G. A.; Devraj, R. V.; Ellsworth, E.; Fobian, Y. M.; Gibbs, M. E.; Gilles, R. W.; Greene, N.; Huang, E.; Krieger-Burke, T.; Loesel, J.; Wager, T.; Whiteley, L.; Zhang, Y. *Bioorg Med Chem Lett* **2008**, *18*, 4872.
- (26) Valko, K.; Butler, J.; Eddershaw, P. *Expert Opin Drug Discov* **2013**, *8*, 1225.
- (27) Ertl, P.; Rohde, B.; Selzer, P. *J Med Chem* **2000**, *43*, 3714.
- (28) Veber, D. F.; Johnson, S. R.; Cheng, H. Y.; Smith, B. R.; Ward, K. W.; Kopple, K. D. *J Med Chem* **2002**, *45*, 2615.
- (29) Leeson, P. D.; Springthorpe, B. *Nature Reviews Drug Discovery* **2007**, *6*, 881.
- (30) DeGoey, D. A.; Chen, H. J.; Cox, P. B.; Wendt, M. D. *J Med Chem* **2018**, *61*, 2636.
- (31) Shultz, M. D. *J Med Chem* **2019**, *62*, 1701.
- (32) Ran, Y.; He, Y.; Yang, G.; Johnson, J. L. H.; Yalkowsky, S. H. *Chemosphere* **2002**, *48*, 487.
- (33) Sanghvi, T.; Jain, N.; Yang, G.; Yalkowsky, S. H. *QSAR Coml Sci* **2003**, *22*, 258.
- (34) Jain, N.; Yalkowsky, S. H. *J Pharm Sci* **2001**, *90*, 234.
- (35) Jorgensen, W. L.; Duffy, E. M. *Adv Drug Deliv Rev* **2002**, *54*, 355.
- (36) Cisneros, J. A.; Robertson, M. J.; Mercado, B. Q.; Jorgensen, W. L. *ACS Med Chem Lett* **2017**, *8*, 124.
- (37) Taylor, R. D.; MacCoss, M.; Lawson, A. D. *J Med Chem* **2014**, *57*, 5845.
- (38) Ritchie, T. J.; Macdonald, S. J. *Drug Discov Today* **2009**, *14*, 1011.
- (39) Hill, A. P.; Young, R. J. *Drug Discov Today* **2010**, *15*, 648.
- (40) Li, K. *J Phys Chem* **1957**, *61*, 782.
- (41) Charifson, P. S.; Walters, W. P. *J Med Chem* **2014**, *57*, 9701.
- (42) Bostrom, J.; Hogner, A.; Llinas, A.; Wellner, E.; Plowright, A. T. *J Med Chem* **2012**, *55*, 1817.
- (43) Young, R. J.; Leeson, P. D. *J Med Chem* **2018**, *61*, 6421.
- (44) Meanwell, N. A. *Chem Res Toxicol* **2016**, *29*, 564.
- (45) Ritchie, T. J.; Macdonald, S. J. F.; Peace, S.; Pickett, S. D.; Luscombe, C. N. *MedChemComm* **2012**, *3*, 1062.
- (46) Ritchie, T. J.; Macdonald, S. J. F. *Eur J Med Chem* **2016**, *124*, 1057.

- (47) Lovering, F.; Bikker, J.; Humblet, C. *J Med Chem* **2009**, *52*, 6752.
- (48) Yang, Y.; Engkvist, O.; Llinas, A.; Chen, H. *J Med Chem* **2012**, *55*, 3667.
- (49) Lee, M. C.; Chian, E. S. K.; Griffin, R. A. *Water Research* **1979**, *13*, 1249.
- (50) Ishikawa, M.; Hashimoto, Y. *J Med Chem* **2011**, *54*, 1539.
- (51) Wang, H. L.; Katon, J.; Balan, C.; Bannon, A. W.; Bernard, C.; Doherty, E. M.; Dominguez, C.; Gavva, N. R.; Gore, V.; Ma, V.; Nishimura, N.; Surapaneni, S.; Tang, P.; Tamir, R.; Thiel, O.; Treanor, J. J.; Norman, M. H. *J Med Chem* **2007**, *50*, 3528.
- (52) Morgenthaler, M.; Schweizer, E.; Hoffmann-Roder, A.; Benini, F.; Martin, R. E.; Jaeschke, G.; Wagner, B.; Fischer, H.; Bendels, S.; Zimmerli, D.; Schneider, J.; Diederich, F.; Kansy, M.; Muller, K. *ChemMedChem* **2007**, *2*, 1100.
- (53) Smith, D. A.; Beaumont, K.; Maurer, T. S.; Di, L. *J Med Chem* **2015**, *58*, 5691.
- (54) Park, B. K.; Boobis, A.; Clarke, S.; Goldring, C. E.; Jones, D.; Kenna, J. G.; Lambert, C.; Laverty, H. G.; Naisbitt, D. J.; Nelson, S.; Nicoll-Griffith, D. A.; Obach, R. S.; Routledge, P.; Smith, D. A.; Tweedie, D. J.; Vermeulen, N.; Williams, D. P.; Wilson, I. D.; Baillie, T. A. *Nat Rev Drug Discov* **2011**, *10*, 292.
- (55) Meanwell, N. A. *Chem Res Toxicol* **2011**, *24*, 1420.
- (56) Jing, Y.; Easter, A.; Peters, D.; Kim, N.; Enyedy, I. J. *Future Med Chem* **2015**, *7*, 571.
- (57) Wuitschik, G.; Carreira, E. M.; Wagner, B.; Fischer, H.; Parrilla, I.; Schuler, F.; Rogers-Evans, M.; Muller, K. *J Med Chem* **2010**, *53*, 3227.
- (58) Lassalas, P.; Gay, B.; Lasfargeas, C.; James, M. J.; Tran, V.; Vijayendran, K. G.; Brunden, K. R.; Kozlowski, M. C.; Thomas, C. J.; Smith, A. B., 3rd; Huryn, D. M.; Ballatore, C. *J Med Chem* **2016**, *59*, 3183.
- (59) Tehler, U.; Fagerberg, J. H.; Svensson, R.; Larhed, M.; Artursson, P.; Bergstrom, C. A. *J Med Chem* **2013**, *56*, 2690.
- (60) Degorce, S. L.; Bodnarchuk, M. S.; Cumming, I. A.; Scott, J. S. *J Med Chem* **2018**, *61*, 8934.
- (61) Bachovchin, K. A.; Sharma, A.; Bag, S.; Klug, D. M.; Schneider, K. M.; Singh, B.; Jalani, H. B.; Buskes, M. J.; Mehta, N.; Tanghe, S.; Momper, J. D.; Sciotti, R. J.; Rodriguez, A.; Mensa-Wilmot, K.; Pollastri, M. P.; Ferrins, L. *J Med Chem* **2019**, *62*, 665.
- (62) Johnson, T. W.; Gallego, R. A.; Edwards, M. P. *J Med Chem* **2018**, *61*, 6401.
- (63) Jamieson, C.; Moir, E. M.; Rankovic, Z.; Wishart, G. *J Med Chem* **2006**, *49*, 5029.
- (64) Waring, M. J. *Expert Opin Drug Discov* **2010**, *5*, 235.
- (65) Mejdrova, I.; Chalupska, D.; Kogler, M.; Sala, M.; Plackova, P.; Baumlova, A.; Hrebabecky, H.; Prochazkova, E.; Dejmek, M.; Guillon, R.; Strunin, D.; Weber, J.; Lee, G.; Birkus, G.; Mertlikova-Kaiserova, H.; Boura, E.; Nencka, R. *J Med Chem* **2015**, *58*, 3767.
- (66) Evzen Boura, R. N. a.; et al. *J. Med. Chem* **2015**, *58*, 3767.
- (67) Martin, R.; Buchwald, S. L. *Acc Chem Res* **2008**, *41*, 1461.
- (68) Long, J.; Lee, W. S.; Chough, C.; Bae, I. H.; Kim, B. M. *J Org Chem* **2015**, *80*, 4716.

- (69) Catalano, J. G.; Gaitonde, V.; Beesu, M.; Leivers, A. L.; Shotwell, J. B. *Tet Lett* **2015**, *56*, 6077.
- (70) Down, K.; Amour, A.; Baldwin, I. R.; Cooper, A. W.; Deakin, A. M.; Felton, L. M.; Guntrip, S. B.; Hardy, C.; Harrison, Z. A.; Jones, K. L.; Jones, P.; Keeling, S. E.; Le, J.; Livia, S.; Lucas, F.; Lunniss, C. J.; Parr, N. J.; Robinson, E.; Rowland, P.; Smith, S.; Thomas, D. A.; Vitulli, G.; Washio, Y.; Hamblin, J. N. *J Med Chem* **2015**, *58*, 7381.
- (71) Amour, A.; Barton, N.; Cooper, A. W.; Inglis, G.; Jamieson, C.; Luscombe, C. N.; Morrell, J.; Peace, S.; Perez, D.; Rowland, P.; Tame, C. J.; Uddin, S.; Vitulli, G.; Wellaway, N. *J Med Chem* **2016**, *59*, 7239.
- (72) Knight, S. D.; Adams, N. D.; Burgess, J. L.; Chaudhari, A. M.; Darcy, M. G.; Donatelli, C. A.; Luengo, J. I.; Newlander, K. A.; Parrish, C. A.; Ridgers, L. H.; Sarpong, M. A.; Schmidt, S. J.; Van Aller, G. S.; Carson, J. D.; Diamond, M. A.; Elkins, P. A.; Gardiner, C. M.; Garver, E.; Gilbert, S. A.; Gontarek, R. R.; Jackson, J. R.; Kershner, K. L.; Luo, L.; Raha, K.; Sherk, C. S.; Sung, C. M.; Sutton, D.; Tummino, P. J.; Wegrzyn, R. J.; Auger, K. R.; Dhanak, D. *ACS Med Chem Lett* **2010**, *1*, 39.
- (73) Schwolow, S.; Kunz, H.; Rheinheimer, J.; Opatz, T. *Eur J Org Chem* **2013**, 6519.

2 PART 2

2.1 Kinases

Kinases play a key role in cellular activation and signalling processes, and comprise 1.7% of the human genome.⁷⁴ They are a class of enzyme that catalyse the phosphorylation of hydroxyl groups using adenosine triphosphate (ATP) (**Figure 2.1**).⁷⁵ Kinases catalyse the transfer of a gamma phosphoryl group to a variety of different substrates including lipids, sugars and amino acids and are classified based upon the substrate they activate.⁷⁶ The most common class of kinases are protein kinases (518), and approximately 20 lipid kinases have been identified.⁷⁷

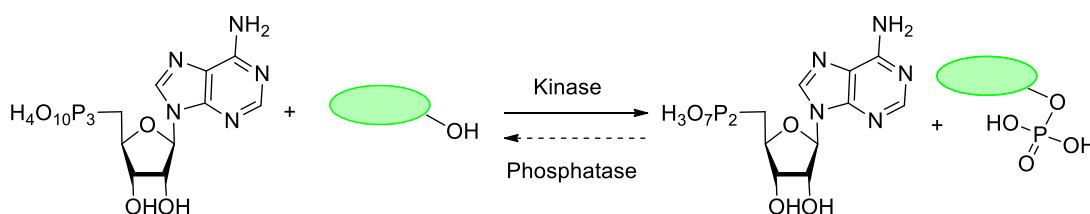


Figure 2.1: Generic phosphorylation reaction catalysed by kinases and reversed by a phosphatase.

The aim of kinase drug design is to find molecules which interrupt kinase signalling.⁷⁸ This has predominantly focused on finding inhibitors of the ATP binding site.^{79,80} The ATP site is conserved throughout the kinome and is not optimised for ATP binding, thus allowing small molecules to exploit the unique features of the ATP site to achieve high potency and selectivity.⁸¹ **Figure 2.2** shows the binding mode of an ATP molecule in a generic kinase active site. A key feature of the binding interaction is represented by the hinge binding region where there are hydrogen bond donor and acceptor atoms built into the aminopurine structure.⁸² In kinase drug discovery, the ATP binding site can be manipulated in a variety of ways to inhibit the phosphorylation. A common strategy is to develop a small molecule that acts as an ATP mimetic, therefore out-competing the natural substrate, ATP, for the active site of the

kinase.^{83,84} This can be achieved through reversible or irreversible binding of the small molecule kinase inhibitor.⁸⁵

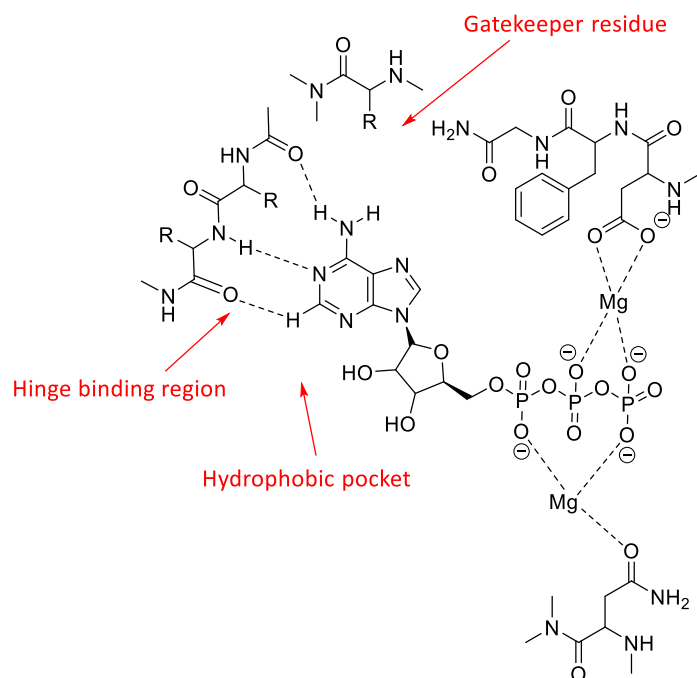


Figure 2.2: Generic ATP binding site.⁸⁶

However, the human genome encodes over five hundred different kinases. In addition, many other ATP binding proteins exist such as ATPases, motor proteins and ATP-gated ion channels.⁸⁷ Due to ATP being a widely used cofactor for many human processes, obtaining selectivity for a single kinase is extremely challenging.⁸⁸⁻⁹⁰ Because of this, chemically diverse kinase inhibitors must be synthesised in order to achieve high selectivity.⁹¹

The strategy for kinase drug design was established during late 1980s where inhibitors for epidermal growth factor receptor (EGFR) were first reported.⁹² Since then, significant efforts have been devoted to the investigation of small molecule inhibitors for the human protein kinase family (SMKIs). In 2001, Imatinib was the first protein kinase inhibitor approved by the FDA. It was marketed by Novartis as Gleevec, for the treatment of chronic myelogenous leukemia.^{75,93} This scientific breakthrough

led to a surge in interest in protein kinase drug design and in 2005, it was estimated that around one in three early drug discovery efforts targeted protein kinases.^{94,95} A few years on, it has translated into the regulatory approval of many small-molecule kinase inhibitor drugs as can be seen in **Figure 2.3**. Since the field of kinase drug design was established, 37 kinase inhibitors have received FDA approval for the treatment of different cancers and it is believed that 150 kinase targeted drugs are in clinical phase trials.^{96,97} The development of kinase inhibitors continues to grow, which has led to exploration of many other therapeutic indications.^{81,98}

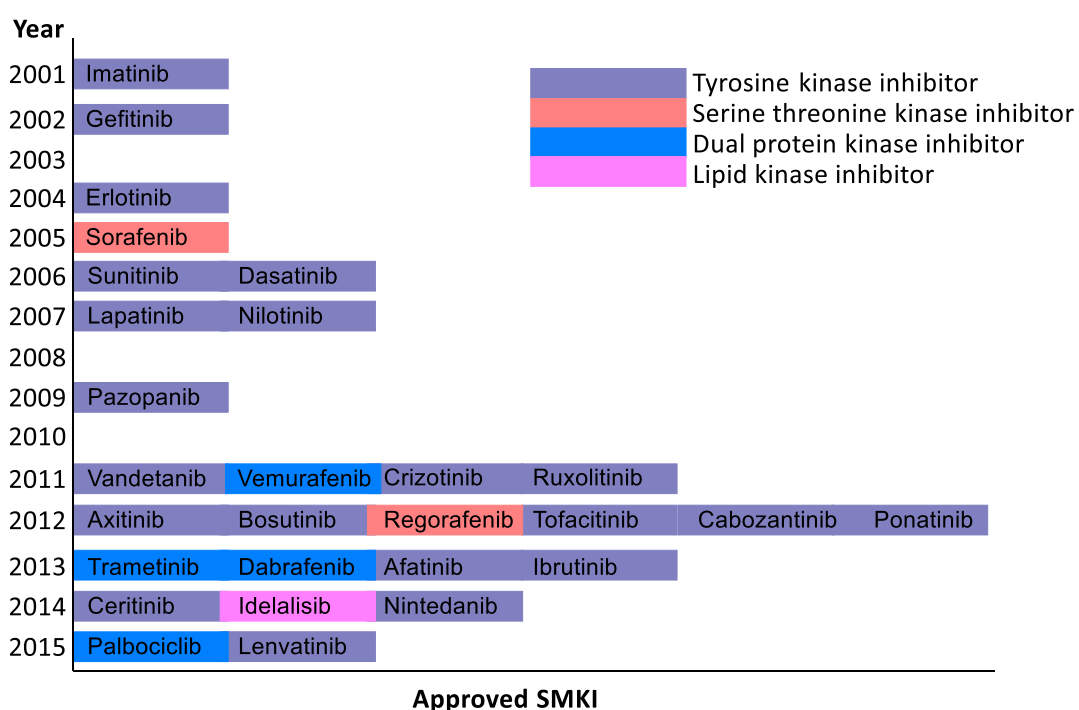


Figure 2.3: Approved small molecule kinase inhibitors from 2001 to 2015, figure adapted from reference 95.⁹⁵

As a result, kinase inhibitor drug discovery has progressed significantly over the past 20 years and has become an attractive target class for medicinal chemists to exploit.⁹⁵ Fragment library screening and crystallography have increased the understanding of the field and therefore, have been integrated into this work to further advance the field of kinase drug discovery.⁹⁶

2.2 Lipid kinases: PI4KIII β

It has been shown that current approaches for treating chronic diseases are not efficacious in treating all patients.⁹⁹ In regards to this therapeutic area, lipid kinases have gathered much attention. The lipid kinase sub-family is shown in **Figure 2.4**, where each branch represents a distinctive family of enzyme. They have been found to interact with many diverse receptors that can prevent cell proliferation.¹⁰⁰ As a result, lipid kinases have been investigated as they could provide an alternative approach for treating chronic diseases, for example, Idelalisib has been approved for treating chronic lymphocytic leukaemia through targeting PI3K δ .^{101,102}

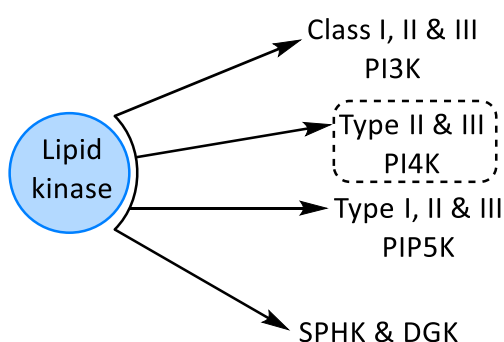


Figure 2.4: The generalised lipid kinome. The figure is adapted from DiscoverX (<https://www.discoverx.com/tools-resources/document-resource-library/documents/the-human-kinome>) Accessed 25.07.19.

To date, the majority of lipid kinase drug design has been focused on PI3K and its isoforms α , β , γ and δ .^{103,104} This has led to the FDA approval of Idelalisib, a PI3K δ inhibitor for the treatment of some B cell malignancies.¹⁰⁵ Achieving isoform selectivity of PI3K has proven to be challenging, however, it has been established that targeting multiple isoforms of PI3K could be beneficial due the potential of multiple combination therapy of different cancer types.¹⁰⁶⁻¹⁰⁸

More recently, strong evidence has implicated lipid kinase PI4K (see **Figure 2.5**) for the treatment of viruses such as human rhinovirus (HRV) due to its signalling

pathway.¹⁰⁹ The PI4K family of lipid kinases phosphorylate lipids in the cell, both on the plasma membrane as well as on the membranes of organelles.^{110,111} They are responsible for catalysing the addition of a phosphoryl group at the D-4 position of the phosphoinositide (PI) family of lipids.^{112,113} PI can be reversibly phosphorylated at positions 3, 4 and 5 of the inositol ring to allow for a variety of phosphatidylinositol phosphates (PIPs) as shown in **Figure 2.5**.⁶⁶

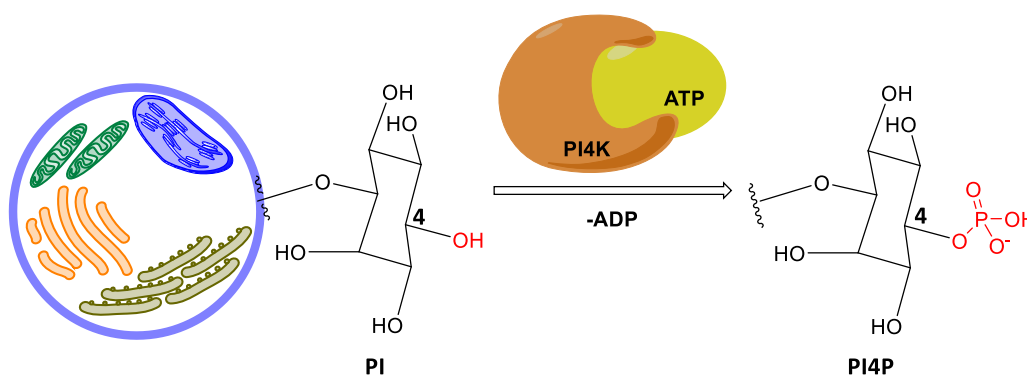


Figure 2.5: Phosphorylation reactions of the inositol ring of PI to form PIP. PI4K catalyses the phosphorylation reaction at the 4-position to form PI4P. Positions 3 & 5 can also be phosphorylated by the appropriate kinase.¹¹³

There are four PI4K isoforms in mammalian cells which are categorised based on their size and catalytic properties (Class II and Class III).¹¹⁴⁻¹¹⁶ Class II PI4K kinases are 45-55 kDa cellular membrane associated proteins and have important roles for cell maintenance and can be inhibited by adenosine and Ca^{2+} .^{117,118} Class III PI4K kinases, which are found on both organelle and cellular membranes, are 100-200 kDa proteins and are insensitive to adenosine and Ca^{2+} . Class II and Class III are subdivided further (α / β) based on their domain structure, i.e. Class III PI4K α and PI4K β . The signalling pathway and cell role of PI4K Class III render them an attractive target class. However, obtaining isoform selectivity of PI4KIII α and PI4KIII β is crucial to the treatment of inflammatory diseases.¹¹¹ Current *in vivo* studies have shown that inhibition of PI4KIII α was poorly tolerated a mouse toxicity study.¹¹⁹ As a result, lipid kinase PI4KIII β remains an appealing target and unpublished work has determined a long resynthesis rate of PI4KIII β in human T-cells. This suggests that small molecule

inhibitors with long residency time in the active site of PI4KIII β could be a viable approach for this therapeutic area.

The product catalysed by PI4KIII β , PI4P is the most abundant monophosphoinositide in eukaryotic cells and is crucial for lipid signalling, cell communication and membrane trafficking.^{65,115,120} It is understood that when viral pathogens enter the cell, they have been shown to take over PI4KIII β .^{121,122} The host membranes are hijacked and use PI4KIII β to generate PI4P, which can be used as a replication platform (**Figure 2.6**).¹²³ Viral replication machinery is assembled on these platforms as a supramolecular complex which triggers viral RNA synthesis, ultimately leading to human rhinovirus.^{111,124} These HRV infections can trigger severe asthma attacks and chronic obstructive pulmonary disease (COPD) exacerbations.¹²⁵

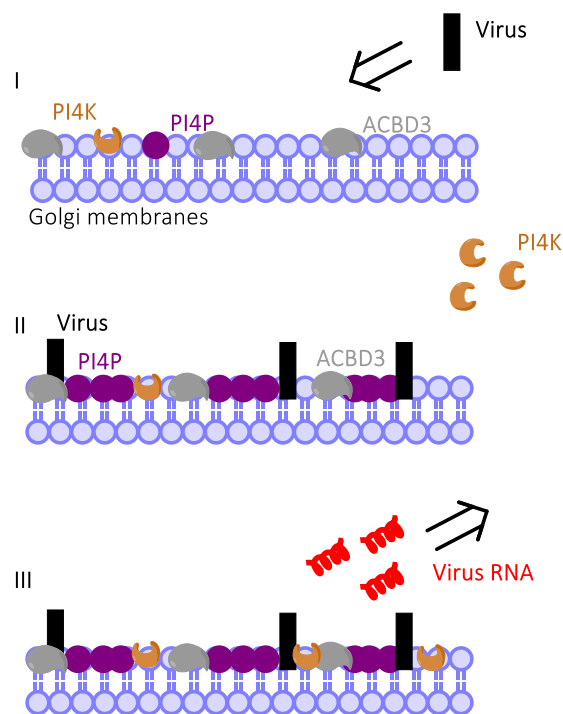


Figure 2.6: i) Virus recruits PI4KIII β through the Golgi protein ACBD3, ii) Virus concentration increases, influx of PI4P, iii) organelles are organised to help form the supramolecular complex, viral RNA synthesis takes place.¹²⁴

The World Health Organization has predicted that COPD will become the third leading cause of death worldwide by 2030.¹²⁶ An exacerbation of COPD causes an acute deterioration of the gas exchange in the lungs, due to airway inflammation and reduced expiratory air flow.¹²⁷ The severity of COPD becomes more dangerous as the exacerbation frequency increases, ultimately decreasing the quality of life for patients.¹²⁸

The therapeutic concept of PI4KIII β inhibition is to design a molecule which will inhibit the function of the protein when it is hijacked by the virus. This would prevent the formation of PI4P and the formation of the supramolecular complex, thus stopping viral RNA synthesis and reducing the likelihood of COPD exacerbations.¹²⁰

Inhaled treatment is desirable for this therapeutic area as the small molecule inhibitor is being delivered directly to the lungs where COPD is manifested. This has the potential to minimise off-target effects. To support low dose treatment, it is desirable to design a molecule which has a long residence time in the active site of PI4KIII β . The combination of low dose and long residence time would help protect the patient from possible non-desirable systemic effects. Ultimately this could provide a convenient treatment plan for the patient and therefore increase patient compliance.

2.3 Covalent inhibition in drug discovery

Covalent inhibition of proteins is not a novel concept and has proved to be very successful for many years.^{129,130} For example, aspirin **2.1** and penicillin **2.2**, have both been used, whereby they covalently inhibit a serine residue in the active site of the target *via* different mechanisms.¹³¹ Aspirin selectively acetylates the hydroxyl group of Ser 530 in cyclooxygenase-2 (COX-2).¹²⁹ The acetylation leads to irreversible COX-2 inhibition, as shown in **Figure 2.7**.¹³² Penicillin contains a highly strained 4-membered β -lactam ring which is susceptible to nucleophilic attack by the catalytic

serine residue of transpeptidases. Both disrupt the active site and prevent the natural substrate from binding, hence deactivating the protein. Aspirin **2.1** and penicillin **2.2** represent two different modes of covalent modification. Aspirin acetylates the enzyme through a serine residue, behaving as an irreversible covalent inhibitor.¹³³ On the other hand, the penicillin ring opened product is susceptible to slow hydrolysis and after time gives the inactive form of the compound and the active enzyme. The hydrolysed β -lactam can be readily metabolised and excreted whilst the free enzyme regains activity. These two examples demonstrate irreversible covalent inhibition and reversible covalent inhibition, both of which have been widely used in drug discovery projects.¹³⁴

A former blockbuster drug, Omeprazole **2.3**, is used to reduce acid secretion in the stomach, but before it can act as a covalent inhibitor, activation is required.^{135,136} The acidity associated with the stomach helps promote the conversion of Omeprazole **2.3** into its activated intermediate which can then interact with a cysteine residue.^{137,138} Importantly, these first three covalent inhibitors (**2.1**, **2.2** and **2.3**) were not designed to be covalent inhibitors, their mechanism of action was elucidated years after their discovery.^{129,139,140}

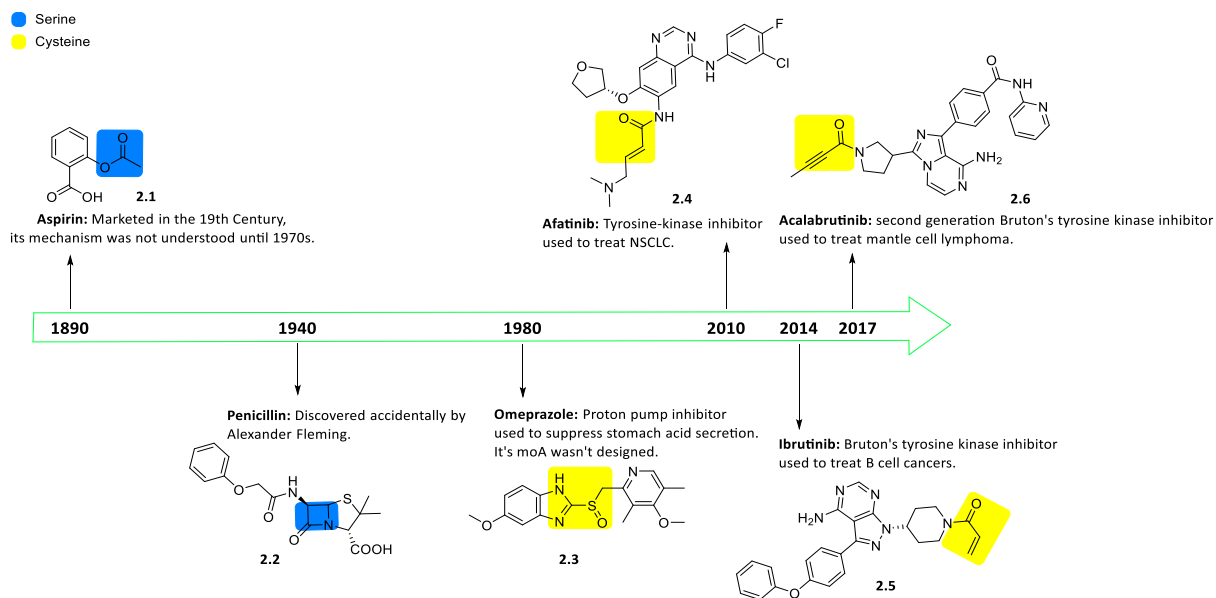


Figure 2.7: Timeline of approved covalent drugs.

Since the early examples of covalent inhibition, as shown in **Figure 2.7**, there has been a lack of activity in this field of drug design until more recently.¹⁴¹ This is predominantly due to the safety concerns of introducing an electrophilic moiety into the human body in the presence of multiple nucleophilic residues.^{54,142-146}

There are clear advantages to covalent inhibition:

- Gives increased potency due to irreversible nature of the inhibition;
- Gives prolonged duration of action due to the slow-off rate kinetics;
- Less frequent and smaller doses required due to high biochemical efficiency, which reduces potential side-effects;^{144,147}

However, there are also risks associated with covalent inhibition:

- Possible side-effects due to potential promiscuous reactivity;
- Reactive warheads could lead to other drug-induced toxicity;^{142,148,149}

Despite the safety concerns, more recent efforts have been focused on targeting cysteine residues which have proven to be successful (**Figure 2.8**).¹⁵⁰⁻¹⁵² It is believed that targeting the thiol of cysteine, which is nucleophilic and polarizable, would permit the use of lower reactivity warheads which should minimise the potential for off target reactivity.^{153,154} Subsequently, this has led to the breakthrough discovery of Afatinib **2.4** and Ibrutinib **2.5**, covalent tyrosine kinase inhibitors operating *via* a Michael addition (shown in **Figure 2.8**).^{140,155-157} Afatinib targets Cys797 in the epidermal growth factor receptor (EGFR) which has been linked with the prevention of cancer growth.^{158,159} Ibrutinib is a Bruton-tyrosine kinase (BTK) inhibitor, a member of the Tec family of kinases, which is key in the B-cell receptor signal pathway and is used to treat chronic lymphocytic leukaemia.^{156,160}

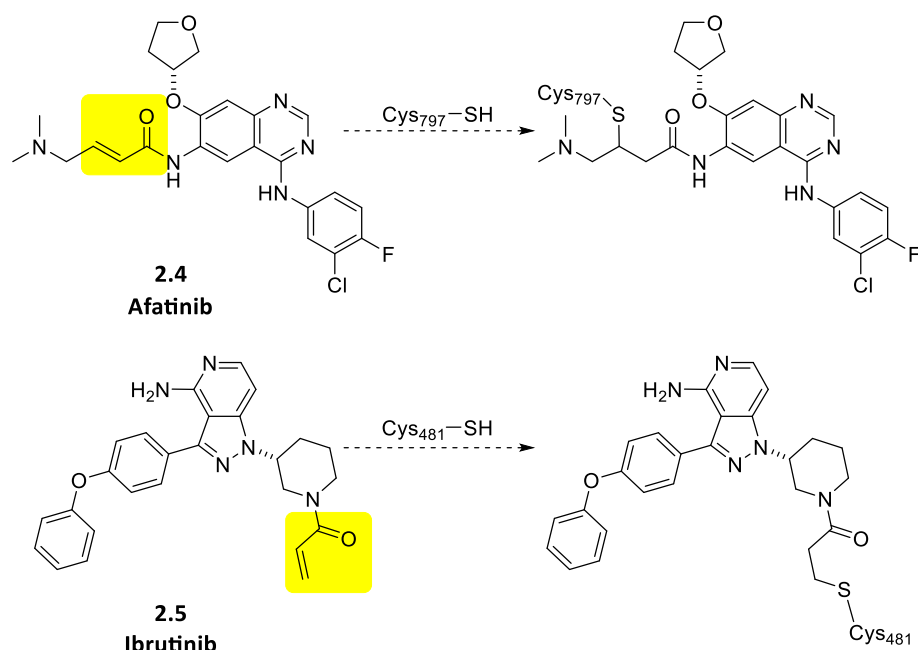
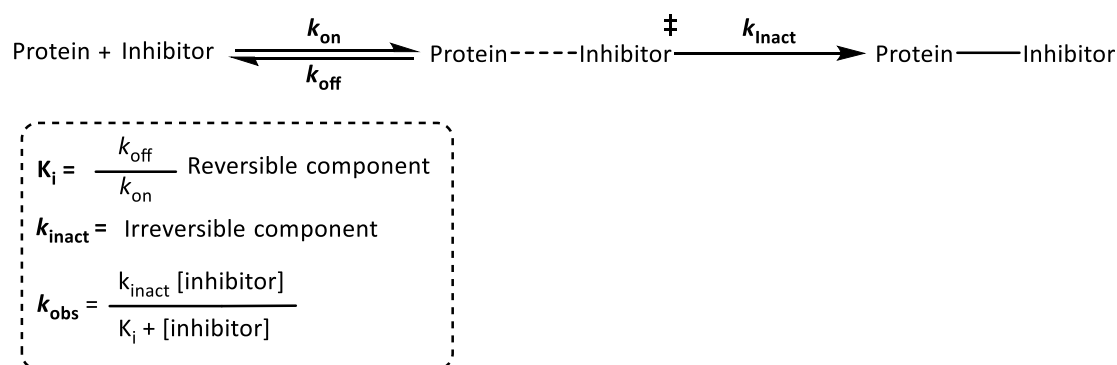


Figure 2.8: Free cysteine thiol adds across the α,β -unsaturated system to give the corresponding covalent adduct.

2.4 Mechanism of covalent inhibition

The biochemical mechanism of a target-specific covalent inhibitor is described by a general two-step mechanism, as shown in **Equation 2.1**.¹⁶¹ The first step is the rate-limiting step (rls) and it involves the non-covalent interactions between the target receptor and the inhibitor.¹⁴⁴ For example, van der Waals, ionic, π -stacking, lipophilic and hydrogen bonding interactions which give the inhibitor a chance to orientate itself in a way such that the electrophilic moiety is in close proximity to the target nucleophilic site.^{162,163,161,164} The second step (fast step) is the conversion of the bound intermediate to its irreversible covalent adduct and this is governed by both the electrophilicity of the covalent warhead and the nucleophilicity of the amino acid.^{129,165-167}



Equation 2.1: The general mechanism of the covalent modification of a protein.

The k_{inact} is a first-order rate constant describing the maximum potential rate of covalent bond formation. Whereas, K_i describes the affinity of the inhibitor required to form the initial protein-inhibitor complex. Put together, the overall rate of covalent bond formation from free protein to the covalent adduct is defined by the k_{obs} .¹⁶⁵

2.5 Beyond cysteine

Due to the recent successes of cysteine covalent inhibition, there has been a surge of interest in drug discovery efforts around cysteine targeted covalent inhibitors.¹⁶⁸ The unique reactivity of cysteine allows weakly electrophilic warheads to be targeted, reducing the risk of off-target effects and non-specific binding.¹⁶⁹ However, experts in the field of covalent inhibition have identified limitations associated with cysteine targeted covalent drug design.^{170,171}

Two major limitations identified are:

1. The natural abundance of cysteine is low.
2. Resistance has developed.

Approximately, ~20,000 human proteins have been identified and of these human proteins, ~260,000 cysteines residues have been estimated.^{170,172} In addition to this, many of these cysteine residues are engaged in disulfide bonds and are therefore

non-nucleophilic. In addition, patients who administered drugs which acted *via* a covalent mechanism of action were developing resistance, where the nucleophilic cysteine residues underwent single point mutations to methionine or serine residues, preventing the formation of the covalent adduct when dosed with the drug.^{146,158,173} In conclusion, cysteine targeted covalent drug design is well established and has proven successful. However, associated limitations have been identified such that other potential nucleophilic residues require exploration, along with the identification of alternative novel covalent warheads.

An attractive nucleophilic site to target is lysine as it is one of the most prevalent amino acids, with an estimated ~650,000 in the human proteome.^{54,170,174}

However, targeting lysine presents two significant challenges:

1. Highly abundant non-functional lysines.¹⁷⁵
2. The pKa of the ϵ -amino group of a typical lysine residue on the surface of a protein is ~10.4, hence 99.9% protonated at physiological pH (7.4) and thus unreactive towards electrophiles.^{163,176,177}

Cheeseman and co-workers have demonstrated the influence of the local protein environment of lysine residues in Snase 192K mutant protein.¹⁷⁶ As shown in **Figure 2.9**, Lys134 is solvent exposed and has a measured pKa of 10.4, under physiological conditions this lysine residue is protonated and therefore unable to act as nucleophile. Whereas, Lys92 is deeply buried in a protein pocket and has a measured pKa of 5.3, under physiological conditions this lysine residue is nucleophilic and can react with electrophilic groups.

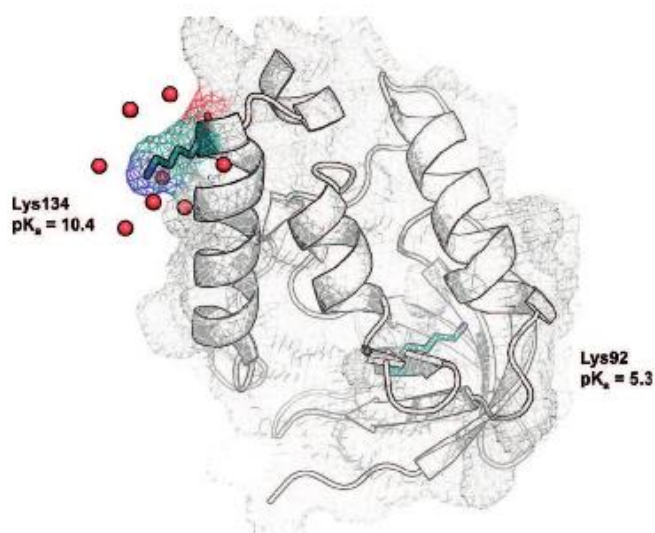


Figure 2.9: Perturbation of internal lysine pKa compared to solvent exposed lysine in Snase 192K mutant.¹⁷⁶ Permission granted by the author.

The 5-orders-of-magnitude decrease in basicity of active free lysine residues can be viewed as an advantage in lysine-targeted covalent inhibitor drug design. This highly abundant nucleophile is unable to readily react with electrophilic warheads in a non-specific manner, as many lysine residues are protonated under physiological conditions and therefore unreactive. Consequently, to target a lysine residue, their apparent pKa value must be perturbed rendering it hyper-reactive.^{177,178} Pioneering work of Cravatt and co-workers have identified several hundred lysine residues with heightened reactivity, rendering them hyper-reactive.¹⁷⁹ These lysine residues could, in principle, be targeted by electrophilic small molecules.

Despite the increasing interest of targeted covalent kinase inhibitor design, the protein microenvironment must be first considered.¹⁸⁰ Proteins can utilise nearby amino acids to perturb the pKa of the lysine. The surrounding charged residues/ basic centres can modulate the pKa of the targeted residue i.e. the catalytic triad for heightening the reactivity of serine.^{181,182} Additionally, proteins are able to exclude water from certain pockets in the active site, thus, perturbing the pKa of the amino acid through its solvent microenvironment.¹⁸³⁻¹⁸⁵ These changes to the microenvironment can result in large shifts in pKa. For example, the pKa of the lysine

decreases 5 orders of magnitude (**Figure 2.9**), thus validating the approach of lysine targeted drug design.¹⁷⁶

Consequently, computational and docking methods of predicting reactive residues in kinases are currently being developed.^{180,186-188} The computational simulations consider the protein microenvironment regarding the targeted amino acid, thus providing a prediction of the pKa which could in turn be correlated with its relative reactivity. This approach could play a significant role in the development of covalent drug design. However, currently, this technique is limited as it failed to predict the nucleophilicity of known lysine targeted covalent inhibition.¹⁸⁹ Presently, the simulations struggle to predict the effect of binding-induced solvent exclusion and as previously mentioned, exclusion of solvent can significantly impact the reactivity of the targeted amino acid. As a result, these techniques require further investigation but could be envisioned to be applicable for future targeted covalent drug design.

2.6 Targeting a lipid kinome conserved lysine

As previously mentioned, lipid kinase PI3K has been probed for its therapeutic benefits and more recently for the treatment of inflammatory conditions such as COPD.^{70,72,190} In 1957, the natural product, Wortmannin **2.6** was first isolated and was later shown to irreversibly inhibit the family of PI3K.¹⁹¹⁻¹⁹³ The covalent modification occurs at the catalytic lysine, which is shown in **Figure 2.10**. The nucleophilic lysine can attack into the C-2 position of the furan ring leading to the opening of the furan and this covalent modification leads to inhibition of all isoforms of PI3K, preventing ATP from binding in the active site.¹⁹⁴ Due to both its toxicity in biological systems and its promiscuous covalent nature, Wortmannin was not further developed in terms of drug discovery but was used as a tool compound to aid the understanding of inhibitor binding in PI3K.¹⁹⁵⁻¹⁹⁷

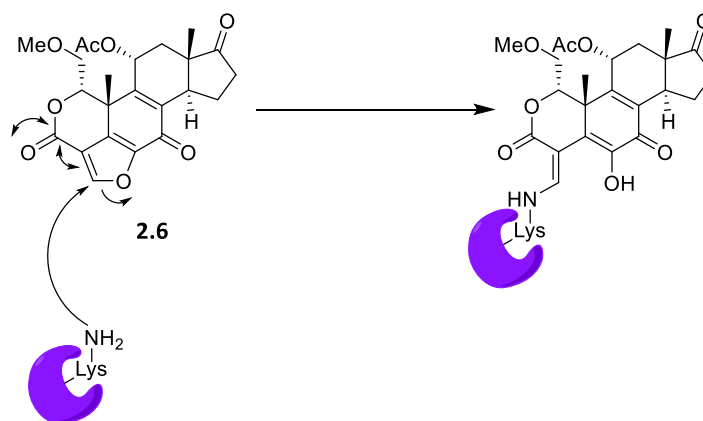


Figure 2.10: Covalent Pan-PI3K inhibition with Wortmannin.

More recently, Campos *et al* have built upon the Wortmannin findings and have reported selective engagement with Lys779 in PI3K δ .¹⁸⁹ They designed their compound **2.7** based on the potency profile of a clinical candidate using *in silico* modelling (**Figure 2.11**).^{198,199} They were able to synthesise a range of phenolic esters, varying the electronics to demonstrate that the *para*-fluoro phenolic ester **2.7** was the most selective from the series and the second most potent behind a *para*-nitro phenolic ester.¹⁸⁹ It was believed that the local microenvironment around Lys779 may have increased its reactivity, rendering it hyper-reactive. The covalent modification was detected by time-dependant mass spectrometry which revealed the formation of the covalent adduct after 5 minutes at 2-fold inhibitor excess.^{179,190,191}

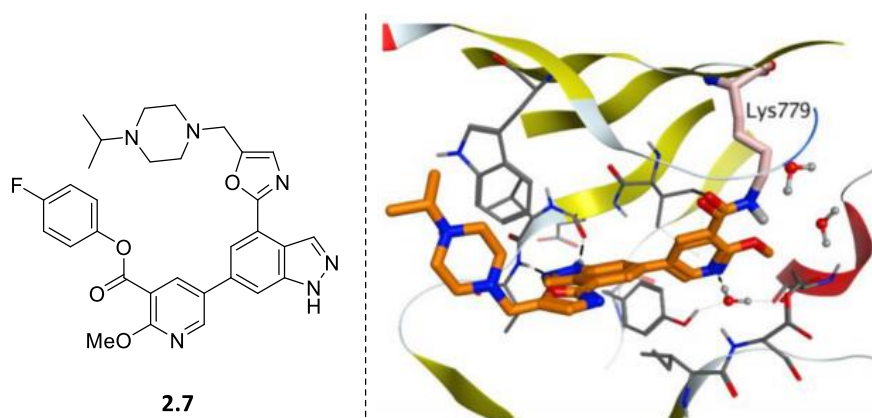


Figure 2.11: Selective covalent inhibition of PI3K δ .

More recently, lipid kinase PI4KIII β has generated much attention for treating COPD, a disease of high concern.^{66,122,127,200} Nencka and co-workers from Gilead Sciences have published a range of PI4KIII β inhibitors and have performed docking studies.⁶⁵ Their most potent PI4KIII β inhibitor **2.8**, is over 1000-*fold* selective over PI4KIII α and is shown in **Figure 2.12**. Their docking study suggested that the sulfonamide moiety interacted with the kinome conserved lysine through a hydrogen-bonding interaction. The nitrogen atom configuration of **2.8** is slightly different, despite this, the hinge binding interaction is identical to the compounds synthesised in Part One and therefore this type of scaffold is suitable for appending a covalent warhead to target Lys549.

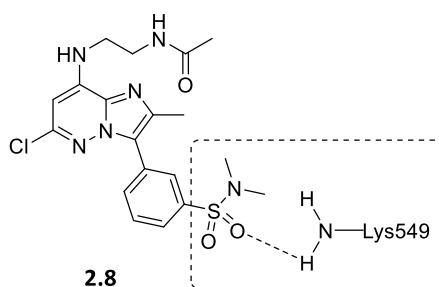


Figure 2.12: Docking study of literature PI4KIII β inhibitor showing proposed hydrogen bonding interaction of the sulfonamide with a lysine residue.

2.7 Sulfur Fluoride Exchange (SuFEx): Emerging technology in drug discovery

The success of cysteine targeted covalent inhibition has led to a range of Michael acceptors being explored.^{162,201} However, other nucleophilic residues in proteins remain underexplored and therefore offer an opportunity to discover alternative electrophiles to target these residues.

Lysine reactive warheads at present are limited but, new approaches are starting to emerge.¹⁹⁸ The sulfonyl fluoride warhead was first reported to behave as an

irreversible inhibitor in 1969 by Baker but this work seemingly went unnoticed.²⁰² Due to the recent surge of interest in covalent inhibition, this work has since been revived.²⁰³ Sulfonyl fluorides can react with a variety of different amino acids e.g. tyrosine, lysine and serine.^{202,204} However, there are limitations associated with these types of warheads which will be further discussed in **Section 2.11**. To overcome the associated challenges, Sharpless made recent advances in the chemical biology field using Sulfur Fluoride Exchange reactions (SuFEx, **Figure 2.13**).^{203,205} It is believed that SuFEx can assist with both target identification/validation and with covalent enzyme modification *via* a sulfur fluoride exchange reaction.^{204,206,207}

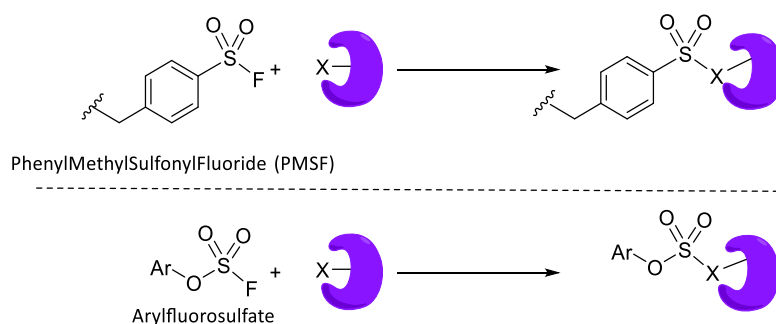


Figure 2.13: Sulfur(VI) fluoride based covalent warheads (X = OH or NH₂).

A recent example of the success of SuFEx chemistry was reported by Taunton and co-workers.²⁰⁸ A chemoselective reaction between a sulfonyl fluoride and a lysine residue in the ATP binding site of kinases within the intracellular kinome was observed.²⁰⁸ The probe **2.9** in **Figure 2.14** was shown to covalently modify 133 endogenous kinases, efficiently competing with the high intracellular concentrations of ATP when applied to a single cell line. This work highlights the potential of sulfonyl fluoride probes in chemoproteomic applications. This type of approach has also been successful in targeting specific tyrosine residues in the active site of mRNA-decapping scavenger enzyme DcpS.²⁰⁹

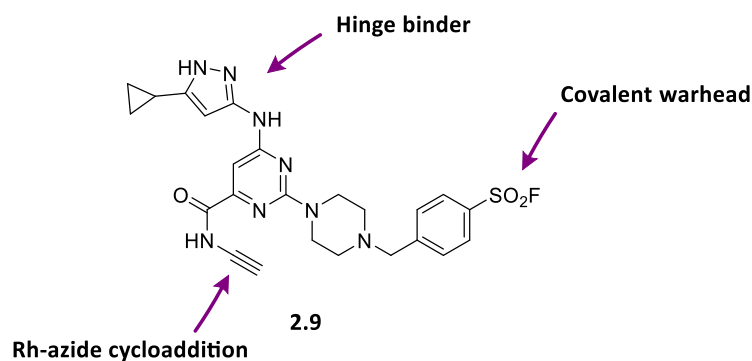


Figure 2.14: Sulfonyl fluoride probe used for kinase identification.

The current literature has highlighted the reactive and relatively unstable nature of sulfonyl fluoride warheads.^{204,210} There are numerous successful applications of sulfonyl fluorides as covalent probes.^{209,211} Grimster and co-workers decided to explore the reactivity of arylsulfonyl fluorides with tyrosine through adjusting the electronic properties around the aromatic ring as shown in **Figure 2.15**.²¹² It was demonstrated that as the electronic withdrawing capability was increased through changing the substituent R in **2.10-2.12**, the rate of reaction increased, but importantly, the rate of hydrolysis also increased significantly. This work highlights how balancing the reactivity of the sulfonyl fluoride warhead against its inherent stability is important. It should be noted that the substrate scope was biased in terms of the substitution pattern around the phenyl ring to the *para* position **2.10**.²¹² This could be due to the ease of the synthesis or the instability associated with the *meta* **2.11** and *ortho* **2.12** isomers.

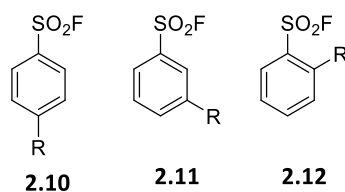


Figure 2.15: Varied electronics of phenyl sulfonyl fluoride.

To overcome the potential promiscuous reactivity and instability of sulfonyl fluoride warheads, Sharpless reinvented fluorosulfates.²⁰³ Coffman originally discovered

arylfuorosulfates in 1961, reacting phenol with sulfur oxytetrafluoride.²¹³ Perhaps due to the hazards associated with this synthetic transformation, this work went unnoticed.²¹³ Sharpless altered the synthesis by treating phenol **2.13** in the presence of base, with sulfuryl fluoride gas to give the fuorosulfate **2.14** as shown in **Figure 2.16**. More recently, other synthetic procedures for preparing fuorosulfates have emerged and will be discussed in **Section 2.12**.²¹⁴

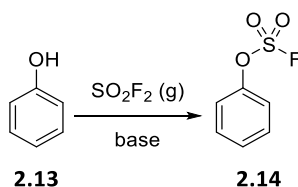


Figure 2.16: Conversion of phenol to fuorosulfates.

It has been reported that aryl fuorosulfates are surprisingly stable, across a range of pH and temperatures in comparison to their deoxy relatives, sulfonyl fluorides.²⁰⁵ The oxygen linker provides stabilisation at the sulfur centre, increasing its resistance to hydrolysis but also lowering its intrinsic reactivity.²⁰³ These features make the fuorosulfate an appealing covalent modifier as this minimises the potential for off-target reactivity.²¹⁵ The covalent modification operates *via* a two-step mechanism. This allows the labelling to be driven by the reversible interactions of the inhibitor and protein, leading to more selective protein labelling.^{216,217} Additionally, the increased stability is advantageous from a storage perspective and it also allows for more interesting experiments to be carried out, for example, studies within cells and cell lysates.^{218,219}

2.8 Fragment library technology

In drug discovery research, finding a suitable starting point is challenging.²²⁰ Ideally, a small molecule that binds to the target can serve as an appropriate starting point for chemistry exploration and optimisation.^{221,222} Small molecules (MW <300),

commonly referred to as fragments, have proven to be an effective approach for identifying 'hit' compounds which has led to a number of clinical candidates.²²³ This has led to the development of companies like Astex who specialise in fragment library synthesis and collaborate with external partners to aid the fragment screening process.²²⁴

There are four main considerations when assembling a covalent fragment library:

1. Suitable diversity (MW < 300).
2. Stability of the molecules over a period.
3. Sufficient solubility to allow screening at higher concentrations.
4. No known protein reactive groups other than the warhead electrophile.²²⁵⁻²²⁷

Recently, fragment photoaffinity labelling has been a developing area of research.²²⁸⁻²³¹ The concept is to add fragments appended with a photoreactive group to interact with proteins (**Figure 2.17**). After inducing covalent cross linking of the fragment to the protein with UV light, new fragment hits can be identified for the protein of interest. However, there are disadvantages associated with this approach. The reactive intermediate is a highly reactive species and can lead to unexpected side products. For example, photo-crosslinking with water molecules. This leads to poorer crosslinking yields with the protein target.²³² As a result, identifying the covalently modified amino acid residue can be challenging.

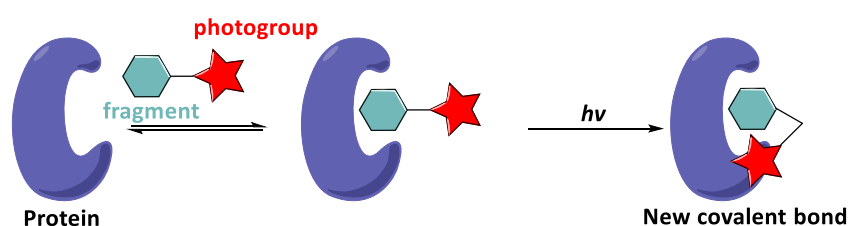


Figure 2.17: General concept of photoaffinity labelling (reproduced from reference 259).

Covalent fragment libraries have also gathered interest, mass spectrometry of the intact protein can be used to identify protein targets which have been covalently modified by the fragment. The advantage of this technique is that the fragments can be screened as mixtures rather than separate entities.²³³ Screening fragments as mixtures increases the throughput capability and reduces the number of false positives. However, a concern with this approach is the danger of selecting the most reactive fragment rather than the fragment with the most specific binding affinity to the protein target.²³⁴ Recently, cysteine reactive covalent fragment libraries have begun to emerge.²³⁵

Sharpless has also been involved in developing a protocol of SuFEx click chemistry for the late stage functionalisation of phenol containing drugs or drug candidates and converting them into their respective arylfluorosulfate derivatives.²³⁶ The *in situ* generated arylfluorosulfates could then be tested for their biological activity. Inspired by this work, and based on current project results, the validation and optimisation of the first generation of a fluorosulfate fragment library was carried out and is discussed in **Section 2.22**.

2.9 Project aims

The current literature shows the design of some highly selective and potent PI4KIII β inhibitors, indicating an interaction between the lysine of the protein and the inhibitor.⁶⁵ Recent work from Campos and co-workers has shown that they were able to covalently modify the lysine of a closely related lipid kinase, PI3K δ .¹⁸⁹ The rationale behind this was to directly target the infected area, keeping the drug in the lungs. This could potentially treat the patient with smaller doses and minimise systemic circulation.

As a result, the concept of covalently modifying the conserved lysine in PI4KIII β was appealing. This approach would both satisfy the approach of long residence time for

inhaled drugs and validate the current literature of targeting the kinome conserved lysine as a general approach for lipid kinase drug design. If the covalent modification proved to be successful, then it could be explored further to covalently modify lysine in a wider range of proteins. The initial strategy was to synthesise a range of activated esters (**2.15**) as shown in **Figure 2.18**.

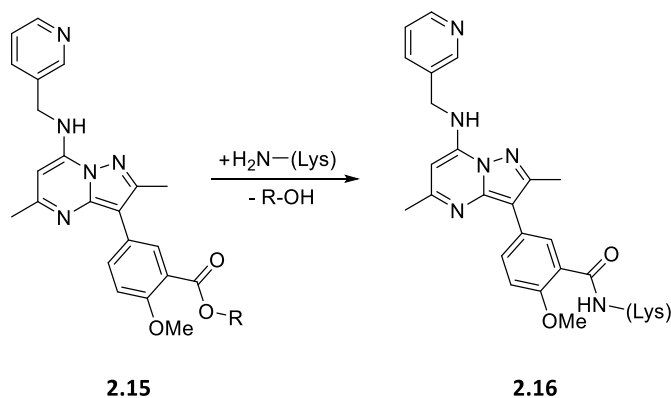


Figure 2.18: Initial design of activated esters.

Fluorosulfates are considered an emerging covalent technology in drug discovery. To date, the literature is limited in terms of targeting a lysine with a fluorosulfate covalent warhead, as they generally react with tyrosine residues.²¹⁵ Their properties such as increased hydrolytic stability and reduced reactivity, compared to sulfonyl fluorides, make them an attractive class of covalent modifiers to explore. We therefore targeted the preparation of both sulfonyl fluorides **2.17** and fluorosulfates **2.18** as potential warheads to interact with the lysine residue of PI4KIII β (**Figure 2.19**). After the initial *in vitro* screening in the project assays, the potential covalent inhibitors would be characterised by mass spectrometry to investigate the potential covalent interaction with the protein. Compounds of interest would then be progressed to kinetic studies and submitted for X-ray crystallography to see if this could provide evidence for a covalent interaction.

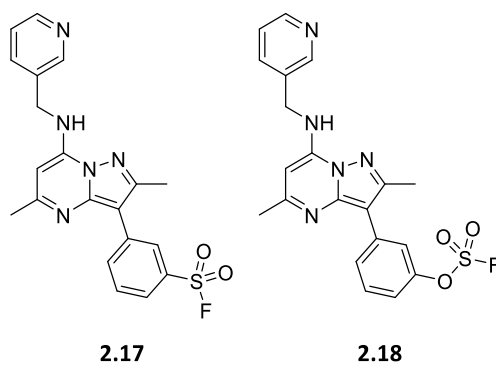


Figure 2.19: Initial series of sulfur fluoride based covalent warheads.

Promising results were gathered through the investigation of covalently modifying PI4KIII β with fluorosulfate inhibitors. Unique reactivity and stability profiles were obtained through different substitution patterns of the inhibitors. Subsequently, this led to the validation of the first fluorosulfate fragment library using PI4KIII β . The fluorosulfate warhead was appended to an unsubstituted phenyl ring in the *meta* and *para* positions (**Figure 2.20**). The rationale and design behind these types of scaffolds will be discussed further in **Section 2.22**.

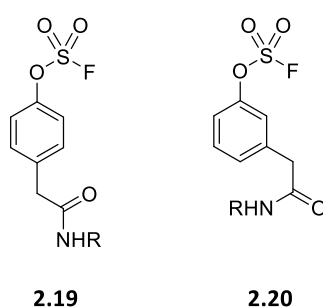
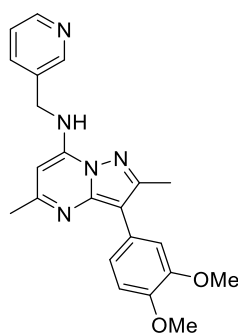


Figure 2.20: The design of a *meta* and *para* fluorosulfate fragment library.

This Chapter explores the discovery of the first selective covalent PI4KIII β inhibitors targeting the kinase conserved lysine and how it translated into alternative PI4KIII β covalent inhibitors. Interesting reactivity and stability properties of these sulfur fluoride-based compounds were investigated. Finally, I will discuss how this work transitioned into the development of the first fluorosulfate fragment library.

The aim of the work was to identify whether the conserved lysine in PI4KIII β could be covalently modified, thus validating the approach of lysine-targeted covalent lipid kinase drug design. As demonstrated in the previous Chapter, Core 4, appended with the *meta*-pyridyl head group, was the optimal molecule (**1.58**) in terms of PI4KIII β selectivity, activity and physicochemical properties (**Figure 2.21**). As a result, compound **1.58** was selected as the initial molecule for covalent drug design. Recent literature surrounding PI4KIII β has highlighted an electrostatic interaction between a sulfonamide moiety in the *meta* position of the structure and the lysine.⁶⁵ Therefore, a hypothesised starting point for this work is shown in **Figure 2.22**.



1.58
PI4KIII β pIC₅₀ **7.2**
PI4K α pIC₅₀ **5.8**
ChromlogD_{7.4} **4.3**
Kinetic sol. ($\mu\text{g mL}^{-1}$) **107**>
FaSSIF ($\mu\text{g mL}^{-1}$) **141**
SLF ($\mu\text{g mL}^{-1}$) **39**

Figure 2.21: Optimal scaffold for appending a covalent warhead to target PI4KIII β .

As previously discussed, Campos and co-workers targeted lipid kinase PI3K δ using activated phenolic esters to covalently modify the lysine,¹⁸⁹ and so this was selected as the initial electrophile for targeting the lysine in PI4KIII β . The nucleophilic residue would attack into the electrophilic centre and release the phenolate leaving group as the by-product of the covalent modification. The electronics regarding the aromatic ring and substituents *ortho* to the warhead position were investigated, and it was anticipated that increased electrophilicity would correlate with its potential covalent reactivity.

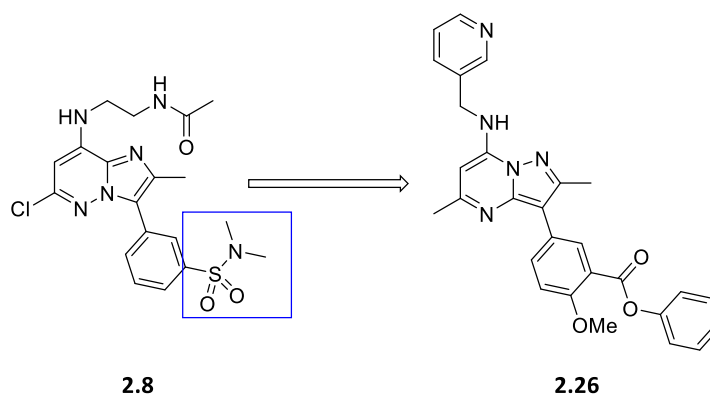
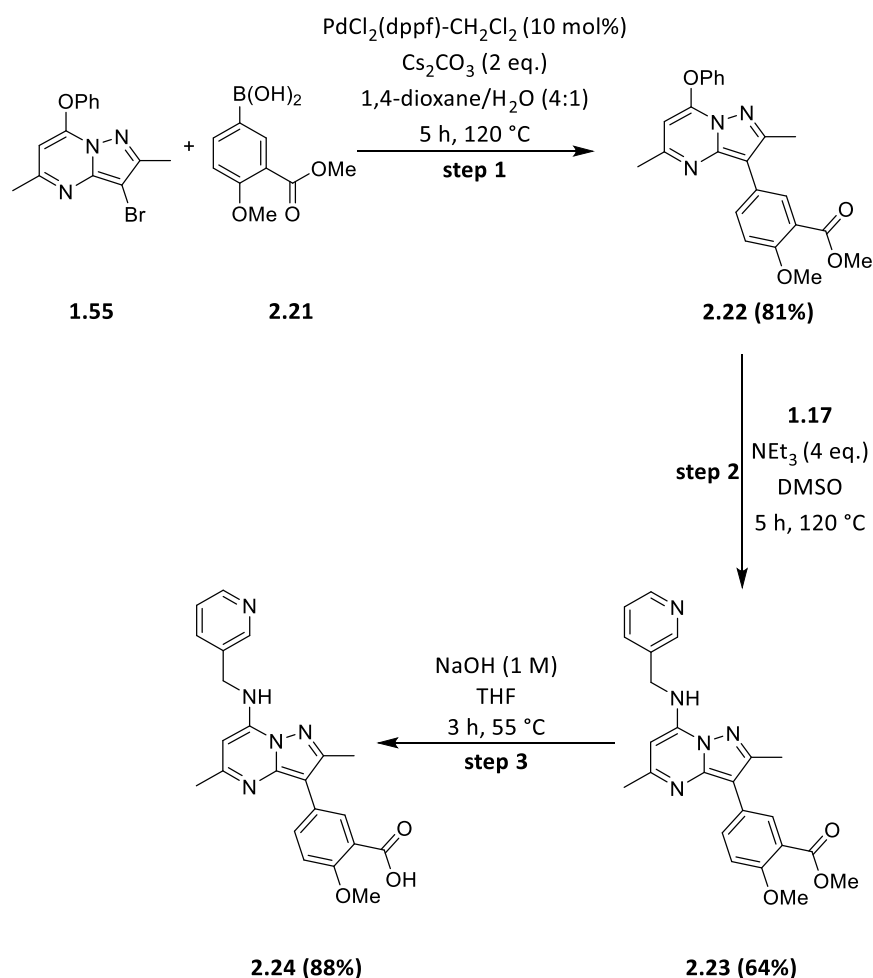


Figure 2.22: Initial hypothesis for covalently targeting the conserved lysine (Lys549).

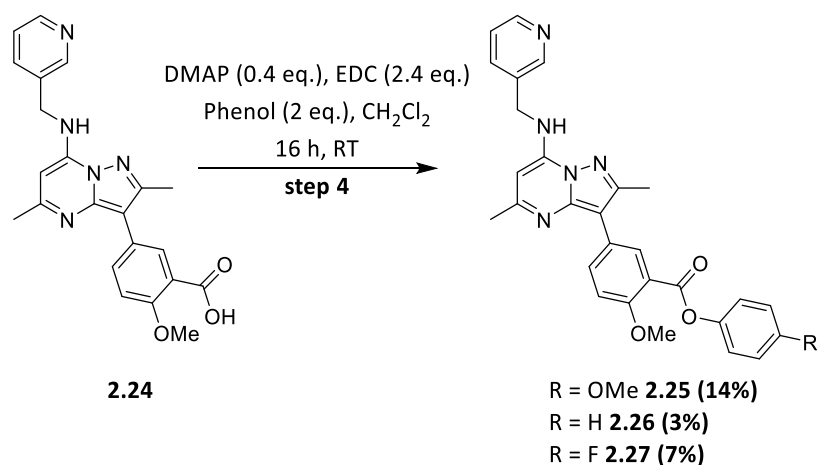
2.10 Synthesis of activated esters

Compound **1.55** was synthesised as previously discussed in **Section 1.4**. This key intermediate was taken forward for the subsequent part of this work in the design of lysine targeted covalent inhibitors.



Scheme 2.1: Synthetic route to key intermediate compound **2.24**.

3-Bromo-2,5-dimethyl-7-phenoxy-pyrazolo[1,5-*a*]pyrimidine **1.55** was subjected to a Suzuki cross coupling reaction. Boronic acid **2.21** was coupled with the aryl bromide **1.55** under forcing reaction conditions. The product **2.22** was purified by column chromatography to give the biaryl in high yield (81%). Intermediate **2.22** underwent an S_NAr reaction with primary amine **1.17**, in the presence of triethylamine in DMSO at 120 °C for 5 hours to give **2.23** (64%). Compound **2.24** was prepared through ester hydrolysis under basic conditions. Purification of compound **2.24** proved to be quite challenging due its aqueous solubility. Chloroform: IPA (5:1) was required to extract the product out of the aqueous layer and the organic layer was concentrated *in vacuo* to give the desired product **2.24** (88%) without further purification.

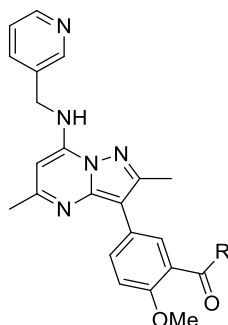


Scheme 2.2: Final step of the synthesis for activated phenolic esters

Final compounds **2.25**, **2.26** and **2.27** were synthesised through the coupling of carboxylic acid **2.24** with the appropriate phenol to form the corresponding phenolic ester. The compounds were purified by MDAP (formic method) to give the final compounds in low yields (3-14%), potentially due to the poor stability of the phenolic esters in the aqueous eluent of the MDAP purification process. In addition, the nucleophilicity associated with the phenol precursors led to poor overall conversion to the desired product. The expected activated intermediate was identified in all cases, however, attack of the phenolate proved to be a problematic step in the reaction. Other reaction conditions such as alternative coupling partner, solvent and temperature were explored but poor yields were still observed.

The first set of potential covalent inhibitors **2.25-2.27** and appropriate controls were screened in the PI4KIII β enzyme assay to determine their pIC₅₀ values. It was hypothesised that the activated phenolic esters could undergo nucleophilic addition with an appropriate nucleophile. By contrast, the carboxylic acid is unable to undergo such a reaction but can be used to identify potential hydrolysis products associated with the phenolic ester series. The methyl ester **2.23** was selected as a reversible control, a nucleophile attacking into the unactivated ester, is unlikely and so it can be used to establish potency differences between the potential covalent inhibitors. A description of the enzyme assay design is discussed in **Section 2.24**. The

physicochemical properties were also measured, to monitor the effect on the properties of introducing an additional aromatic ring to the molecule (see **Table 2.1**).



Entry	R	Cpd number	PI4KIII β pIC ₅₀	Kinetic sol. ($\mu\text{g}/\text{mL}$)	ChromLogD _{7.4}	AMP (nm/s)
1		2.24	5.7	>120	1.2	<3
2		2.23	6.8	>160	4.3	420
3		2.25	5.2	11	5.8	260
4		2.26	5.3	11	5.8	-
5		2.27	5.1	10	5.9	370

Table 2.1: Potency and physicochemical data of phenolic esters.

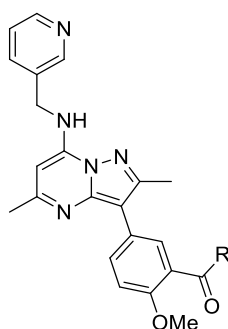
Compound **2.24** highlights the importance of the work carried out in Chapter 1 and the issues encountered with multiparameter optimisation. The presence of the carboxylic acid significantly altered the potency of the molecule (pIC₅₀ = 5.7). As a result, compound **2.24** had markedly reduced in the enzyme assay, and this was supported by methyl ester **2.23**, where the activity was approaching 100 nM in the enzyme assay (pIC₅₀ = 6.8).

The addition of an aromatic ring in the phenolic esters was detrimental to the physicochemical properties of final compounds **2.25**, **2.26** and **2.27** as shown in **Table 2.1**. In comparison to the methyl ester **2.23**, the solubility had dropped significantly

($\leq 11 \mu\text{g/mL}$), the ChromLogD (≥ 5.8) increased by one log-unit and the potency for the final compounds **2.25**, **2.26** and **2.27** was poor ($\text{pIC}_{50} \leq 5.3$).

As mentioned in **Section 2.4**, covalent modification is mechanistically a two-step process. The inhibitor initially reversibly binds in the active site, placing the ester in close proximity to the nucleophilic amino acid residue. This is the rate limiting step of the mechanism, therefore, the formation of the reversible complex between the inhibitor and protein is a time dependent process. In the enzyme assay, there was only a 40 min pre-incubation time before running the assay. These experimental conditions may not be suitable for this investigation due to the time dependent nature of achieving a covalent modification. An increased incubation time of the compound in the presence of the protein could be necessary for the inhibitor to covalently modify the protein.

Compounds shown in **Table 2.1** were subjected to a cellular based assay, the cytopathic effect (CPE) assay. The protocol for this assay is shown in **Section 2.24**. An important parameter to highlight is the incubation period. The cells and inhibitors were incubated for 2 days post infection at 33 °C. This prolonged assay gave the phenolic esters sufficient time to enter the cells, form the initial reversible complex and hence covalently modify PI4KIII β . The measured pIC_{50} values for the CPE assay are shown in **Table 2.2**.



Entry	R	Cpd number	PI4KIIIβ pIC ₅₀	CPE pIC ₅₀	Δ (CPE-PI4KIIIβ)
1		2.24	5.7	<5	-
2		2.23	6.8	6.5	-0.3
3		2.25	5.2	6.4	1.2
4		2.26	5.3	7	1.7
5		2.27	5.1	7	1.9

Table 2.2: Biochemical assay data of phenolic esters and control compounds.

High levels of intracellular ATP are present in the CPE assay (~ 10 mM). As previously mentioned (**Section 2.1**), ATP is the natural substrate for kinases and at high concentrations, it can outcompete other reversible competitive inhibitors. As a result, the measured pIC₅₀ values were likely to drop from the enzyme to CPE assay for reversible inhibitors of PI4KIIIβ. However, for covalent inhibition, it would be expected that the potency would translate or even increase from the enzyme assay to the CPE assay. A covalent bond in the active site of PI4KIIIβ would stop the inhibitor from disassociating and, this would prevent ATP from binding and consequently translate into increased activity.

The carboxylic acid control **2.24**, remained inactive in both the enzyme and cellular assay (**Table 2.2**), which suggests it was not tolerated in the active site of the protein

(poor permeability). Encouragingly, phenolic esters **2.25**, **2.26** and **2.27** gave rise to a significant boost in potency, suggesting an alternative mode of action for these compounds ($pIC_{50} \geq 6.4$). Unfortunately, due to a combination of high lipophilicity, low solubility and sub-optimal stability this series was not pursued further, and so alternative covalent warheads required exploration.

Jamieson and co-workers recently published on the amidation of unactivated ester derivatives mediated by trifluoroethanol.²³⁷ They were able to use trifluoroethanol to facilitate the condensation of esters with amines (**Figure 2.23**). The concept of this work was attractive, and was therefore investigated to determine if trifluoroethyl esters could be used to target the lysine residue of PI4KIII β .

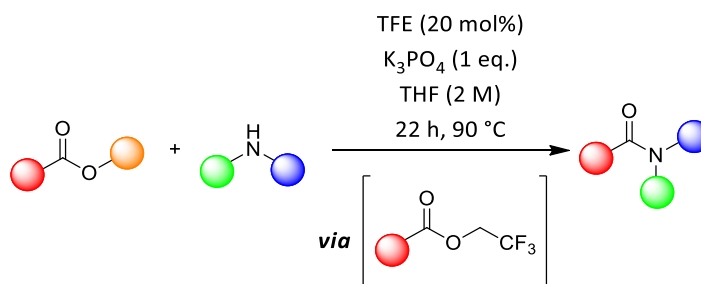
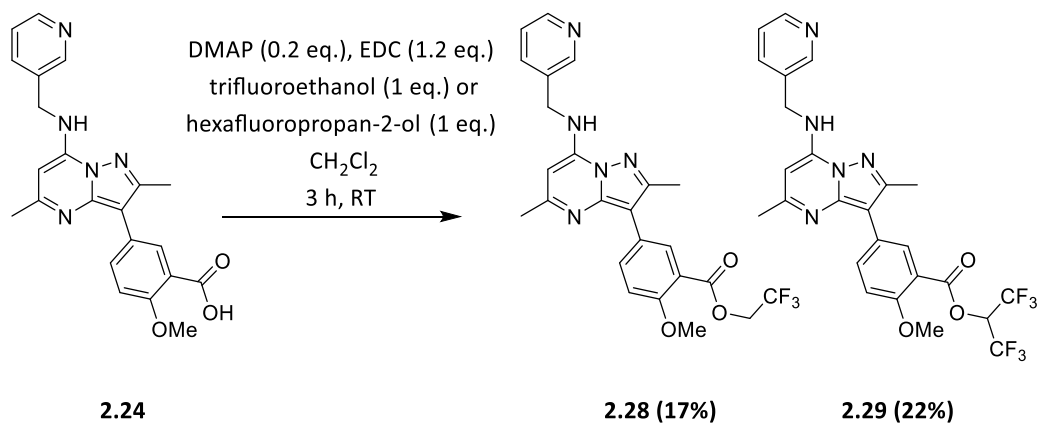


Figure 2.23: Trifluoroethanol mediated catalytic amidation.

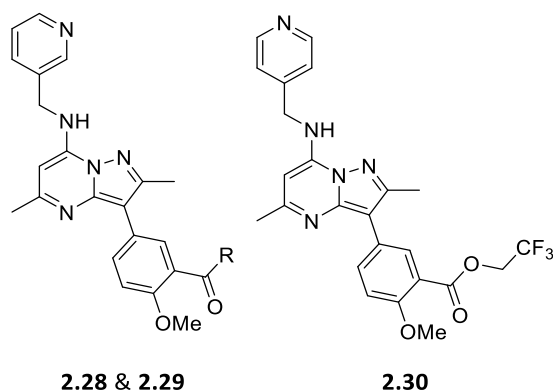
Based on this recent publication, trifluoroethyl and hexafluoropropan-2-yl esters **2.28** and **2.29** were synthesised (**Scheme 2.3**). The additional trifluoroethyl group would increase the electrophilicity of the carbonyl group of the ester, thus increasing the likelihood of the attack by the lysine.



Scheme 2.3: Synthesis of alternative activated esters.

The coupling reactions of compound **2.24** with trifluoroethanol and hexafluoropropan-2-ol progressed smoothly to synthesise compounds **2.28** (17%) and **2.29** (22%). The desired products were purified by MDAP (high pH method). However, the basic modifier in the eluent on the MDAP column may have potentially led to the hydrolysis of the activated ester, thus resulting in a poor overall yield. The final compounds were stored under nitrogen at 10 °C and no hydrolysis was observed over 12 months.

It was anticipated that the removal of the additional aromatic ring could help improve the solubility of the compounds. However, as shown in **Table 2.3** the physicochemical properties were not improved. Halogens are lipophilic substituents and the presence of multiple fluorine atoms was detrimental to the compound's physicochemical properties.



R	Cpd number	PI4KIIIβ pIC ₅₀	CPE pIC ₅₀	Kinetic sol. (μg/ mL)	ChromLogD _{7.4}	AMP (nm/s)
	2.28	6.0	6.3	21	5.6	180
	2.29	5.5	6.7	19	7.3	-
	2.30	7.0	7.2	24	5.6	170

Table 2.3: Enzyme and cellular biochemical data for alternative esters.

In both series, the potency for the trifluoroethyl ester (**2.28**, **2.30**) was quite comparable for both the enzyme and cellular assay. The *para*-pyridyl head group gave a log unit increase in activity, potentially due to the hydrogen bonding interaction with Tyr385 (**Figure 2.24**). The warhead may not have been optimal for the lysine to engage. In contrast, a significant potency increase was observed for the hexafluoropropan-2-yl ester **2.29** in the cellular assay. Hence, the incubation period influenced the compound's ability to interact with PI4KIIIβ. The size of the activated ester was considerably smaller in comparison to the phenolic esters but the strength of the electron withdrawing group was enhanced with terminal trifluoromethyl groups. However, due to the poor physicochemical properties associated with compound **2.29** (poor solubility and high ChromLogD) and the potential instability of the activated ester, alternative covalent warheads were examined.

Protein crystallography is an integral part of pharmaceutical research. It is used to obtain three-dimensional information for binary complexes involving crystallizable proteins and inhibitor molecules. Therefore, it can be used to identify hydrogen

bonding interactions between the compound and protein, lipophilic pockets and the binding mode of molecules. It is important to note that the resulting crystal structure obtained is based on a static conformation of the protein and does not consider the flexibility of the protein. However, it is an established technique for structure-based design in drug discovery and was used in this work to aid the design of potential lysine targeted covalent inhibitors. Compound **2.23** was selected as it possessed desirable physicochemical properties, which would therefore increase the probability of obtaining a crystal structure. Pleasingly, a crystal structure for the methyl ester control compound **2.23** in complex with PI4KIII β was obtained and is shown below in **Figure 2.24**.

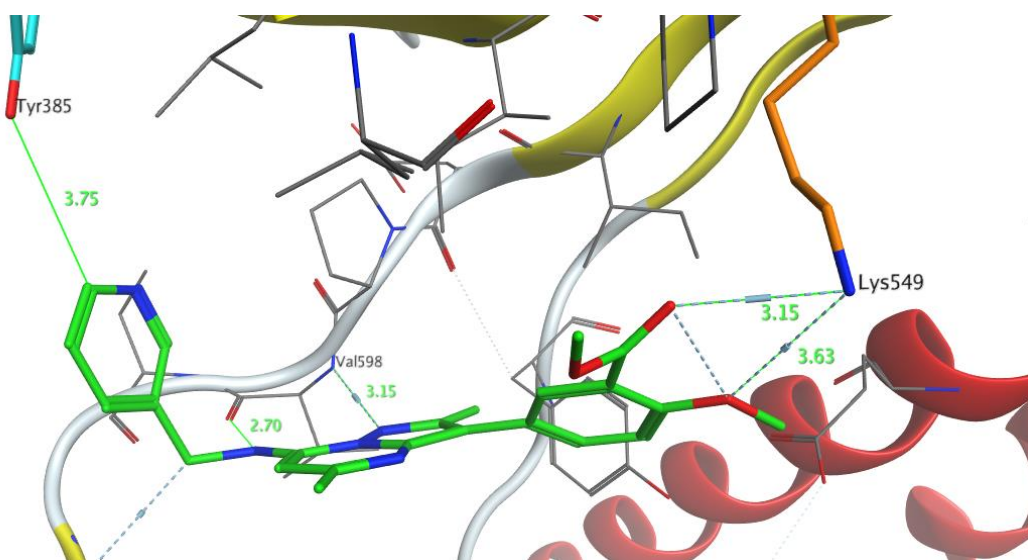
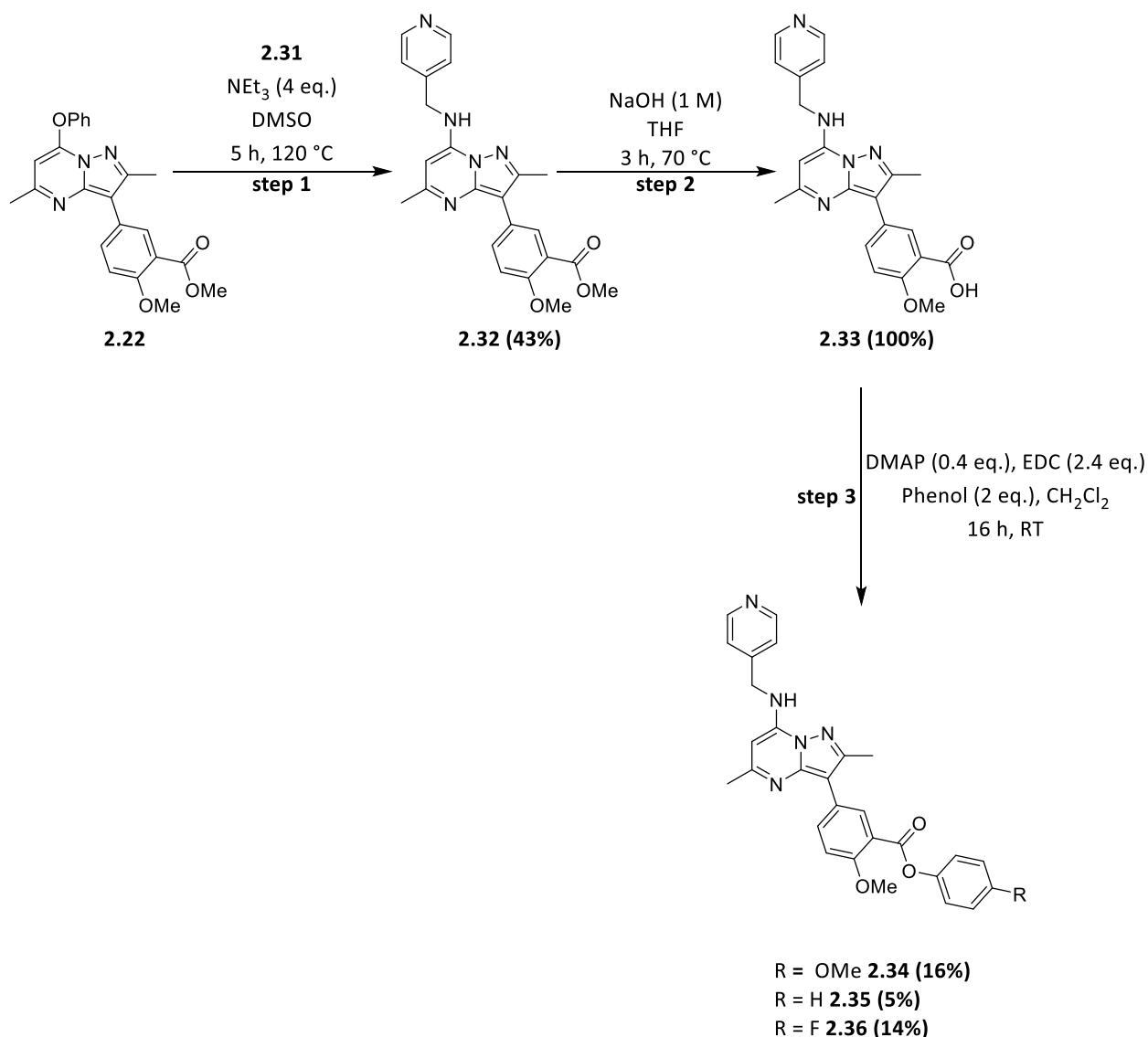


Figure 2.24: Crystal structure of compound **2.23** in the active site of PI4KIII β with resolution with 1.78Å.

Compound **2.23** showed the key acceptor/donor hinge binding interaction with the valine (Val598) backbone. The molecule rotated around the terminal aromatic ring to induce a bifurcated hydrogen bond with lysine (Lys549). The carbonyl group in the *meta*- position could form a slightly stronger hydrogen bonding interaction with the lysine residue suggesting that this is the optimal position for a covalent warhead to be introduced. Additionally, a nearby tyrosine (Tyr385) was identified and this

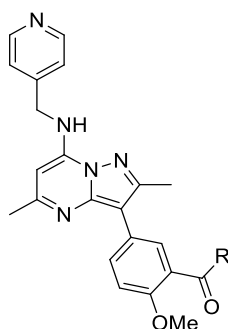
presented the opportunity to explore an additional hydrogen bonding interaction with the phenol group of the tyrosine. As a result, additional phenolic esters were synthesised, using a *para*-pyridyl head group. It was hypothesised that the additional hydrogen bonding interaction would lead to an increase in potency.

The synthetic route to the *para*-pyridyl series is shown in **Scheme 2.4**. The synthesis followed the previous route shown in **Scheme 2.4**, where the pyridyl head group was initially installed *via* an S_NAr reaction to give compound **2.32**, followed by basic ester hydrolysis to give the key intermediate **2.33**. Step 3 of the synthesis proved problematic and resulted in poor yields of the final compounds, however sufficient quantities of the target molecules were isolated in order to obtain biological and analytical data.



Scheme 2.4: Synthesis of the 4-pyridyl phenolic ester series.

The series of phenolic esters (**2.34**, **2.35** and **2.36**), along with the methyl ester **2.32** and carboxylic acid **2.33** were profiled in the biochemical assays. The physicochemical properties of the phenolic esters were not the focus and were expected to be similar to the previous series (compounds **2.25**, **2.26** and **2.27**), thus are not discussed. These compounds were designed as matched pairs to the previous series, which could identify the effects of potentially engaging the nearby tyrosine residue (Tyr385) shown in **Figure 2.24**. The enzyme and cellular data are shown in **Table 2.4**.



Entry	R	Cpd number	PI4KIII β pIC ₅₀	CPE pIC ₅₀	Δ (CPE-PI4KIII β)
1		2.33	6.8	<5	<-1.8
2		2.32	8	7.8	-0.2
3		2.34	5.3	6.7	1.4
4		2.35	6.3	7.6	1.3
5		2.36	6.1	7.8	1.7

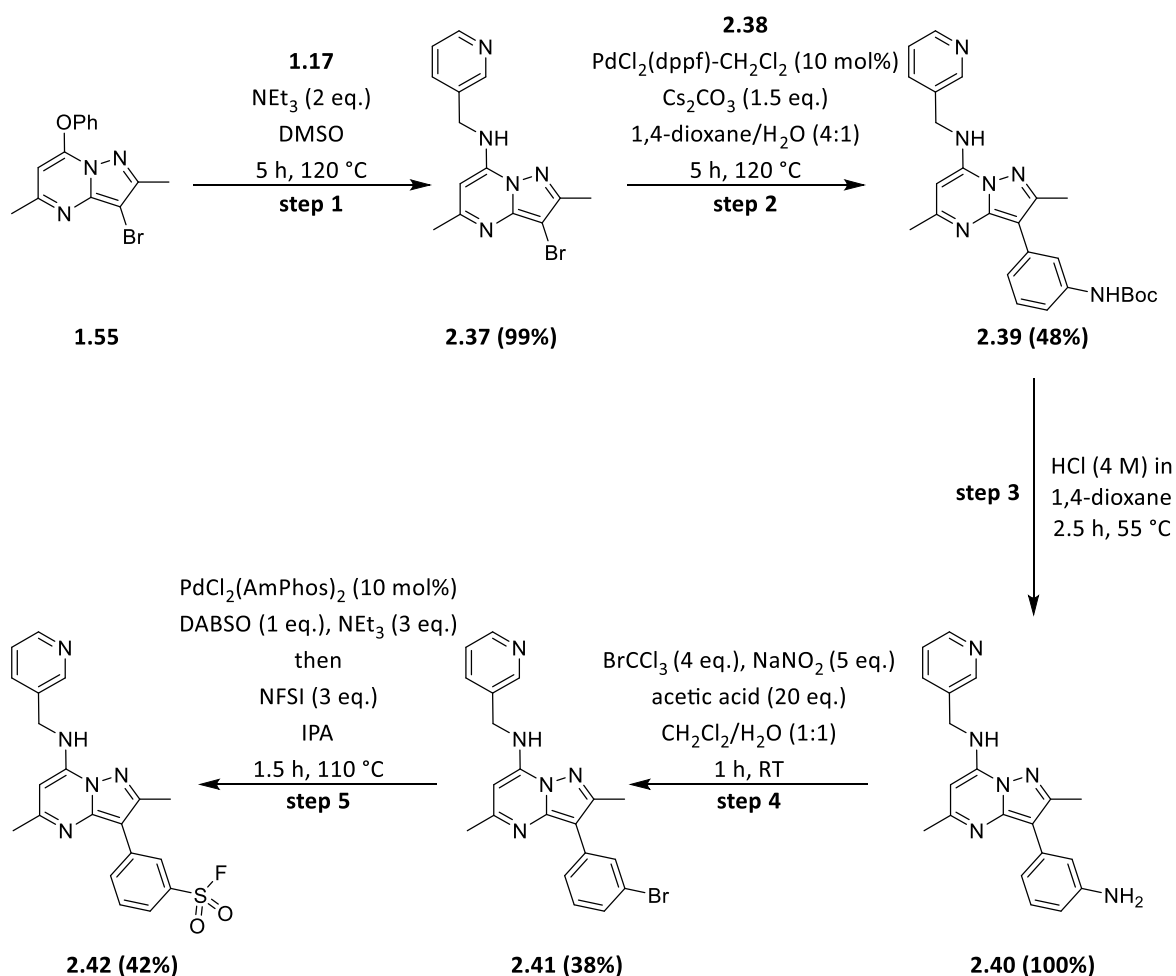
Table 2.4: Biochemical data for *para*-pyridyl series of phenolic esters and reversible control compounds.

Similar trends were observed as previously shown in **Table 2.2**, where the activity of reversible control compounds **2.32** and **2.33** dropped from the enzyme to the cellular assay, indicative of reversible competitive ATP binding. In contrast, the potential covalent inhibitors (**2.34**, **2.35** & **2.36**) displayed a consistent increase in activity translating from the enzyme to the cellular assay suggesting a time dependent mechanism. Interestingly, all the compounds shown in **Table 2.4** show a log unit (or greater) increase in activity in comparison to the *meta*-pyridyl series represented in **Table 2.2**. The data shown in **Table 2.4** strongly indicated that the *para*-pyridyl head group could form a favourable hydrogen bonding interaction with Try385 which was responsible for the boost in activity. Additionally, the electronics of the phenolic ester were varied which showed that decreasing the electrophilicity of the carbonyl group had a negative impact on the activity of the compounds. Overall, the data shown in

Table 2.4 was encouraging. However, the overriding suboptimal physicochemical properties limits this approach and therefore opens the opportunity to explore other lysine targeted covalent warheads.

2.11 Synthesis and characterisation of a sulfonyl fluoride inhibitor

Following exploration of the phenol ester derived series, our attention was turned to sulfonyl fluorides, an electrophile with high interest from multidisciplinary fields. This work was initiated before obtaining the crystallography data and so was carried out on the *meta*-pyridyl series.²³⁸ The warhead is sp³-hybridised at the sulfur atom and increasing the amount of sp³ character of drug molecules has been linked with improved physicochemical properties.⁴⁷ As previously discussed in **Section 2.7**, sulfonyl fluorides have been investigated for their potential to covalently label proteins. As a result, a sulfonyl fluoride warhead was appealing to investigate. The synthesis is shown in **Scheme 2.5**.



Scheme 2.5: Synthesis of sulfonyl fluoride **2.42**.

Step 1 of the synthesis shown in **Scheme 2.5** involved treating **1.55** with primary amine **1.17** to install the pyridyl head group of the molecule. The reaction progressed smoothly and led to the preparation of **2.37** in high yield (99%). Subsequently, a Suzuki cross coupling reaction was carried out on **2.37** with *N*-*Boc*-protected boronic acid **2.38** to give product **2.39** in moderate yield (48%). Compound **2.39** was deprotected with concentrated hydrochloric acid in dioxane for 2.5 hours at 55 °C to give the free aniline **2.40** (100%). Compound **2.40** was subjected to a Sandmeyer type reaction to install the aryl bromide to give compound **2.41** (38%).²³⁹ Excess acetic acid was used in this transformation which acted as a catalyst by assisting the formation of the diazonium intermediate. The highly reactive intermediate released nitrogen resulting in the aryl radical. This radical was then trapped by bromotrichloromethane

to give the desired brominated compound **2.41**. The product was purified by column chromatography to give the product **2.41** in a moderate yield (38%). Lastly, 3-(2,5-dimethyl-7-((pyridin-3-ylmethyl)amino)pyrazolo[1,5-*a*]pyrimidin-3-yl)benzene-1-sulfonyl fluoride **2.42** was prepared by palladium catalysed sulfonylation of the aryl bromide **2.41** using DABSO as an SO₂ source, followed by *in situ* treatment of the resultant sulfinate with an electrophilic fluorine source, NFSI.²⁴⁰ Compound **2.42** was purified by column chromatography but was susceptible to hydrolysis upon purification. The hydrolysed sulfonic acid was detected by LCMS and so compound **2.42** was stored under nitrogen at 10 °C.

All analytical data regarding compound **2.42** was obtained and profiled in terms of its activity towards PI4KIIIβ as shown in **Table 2.5**. The literature suggested that aryl sulfonyl fluorides are surprisingly stable. However, on the template investigated, the compound was susceptible to rapid hydrolysis and the sulfonic acid was observed by LCMS.²⁴⁰ Altering the substitution pattern around the aromatic ring was a possibility but due to the fast hydrolysis, the results obtained from this approach seemed unconvincing. In conclusion, the data generated for compound **2.42** was not deemed reliable and this series was put on hold.

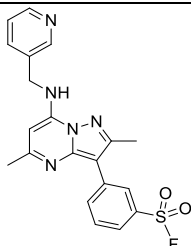
Series	Cpd number	PI4KIIIβ pIC ₅₀	CPE pIC ₅₀	Kinetic sol. (µg/ mL)	ChromLogD _{7.4}	AMP (nm/s)
	2.42	5.6	6	Failed	Failed	Not detected

Table 2.5: Biochemical and physicochemical data for compound **2.42**.

2.12 Fluorosulfate inhibitor design and characterisation

Fluorosulfates are a class of sulfur fluoride-based warheads which are currently generating much interest due to their enhanced stability and reduced reactivity in comparison to sulfonyl fluorides (**Figure 2.25**).²¹² The oxygen linker atom is capable of stabilising the sulfur, reducing its electrophilicity and therefore increasing its stability (**2.44**). To date, the reported literature methods for synthesising fluorosulfates are limited. Two approaches were investigated and are discussed further in this Section.^{241,242} In addition, there is very limiting data on the stability and reactivity of fluorosulfate containing compounds. This is important information for the field of covalent inhibition and so detailed stability and reactivity studies have been carried out.

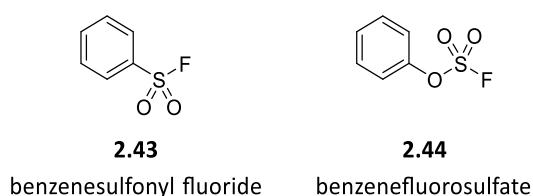


Figure 2.25: Aryl sulfonyl fluoride and fluorosulfate.

A series of fluorosulfate compounds were synthesised and the substituent *ortho* to the fluorosulfate group was varied in terms of electron donating ability e.g. OMe **2.45** through to electron withdrawing e.g. Cl **2.47** (**Figure 2.26**). Again, the *meta*-position was the selected vector for the covalent warhead to be attached, and this was designed based on the crystal structure (**Figure 2.24**) showing a hydrogen bonding interaction with a nearby lysine (Lys549).

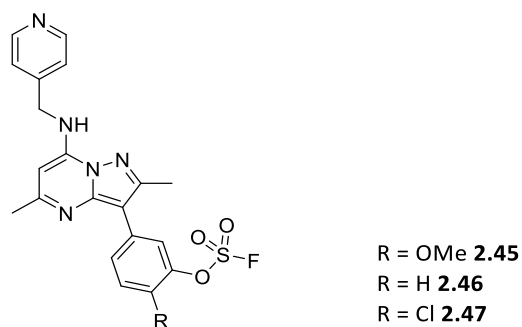
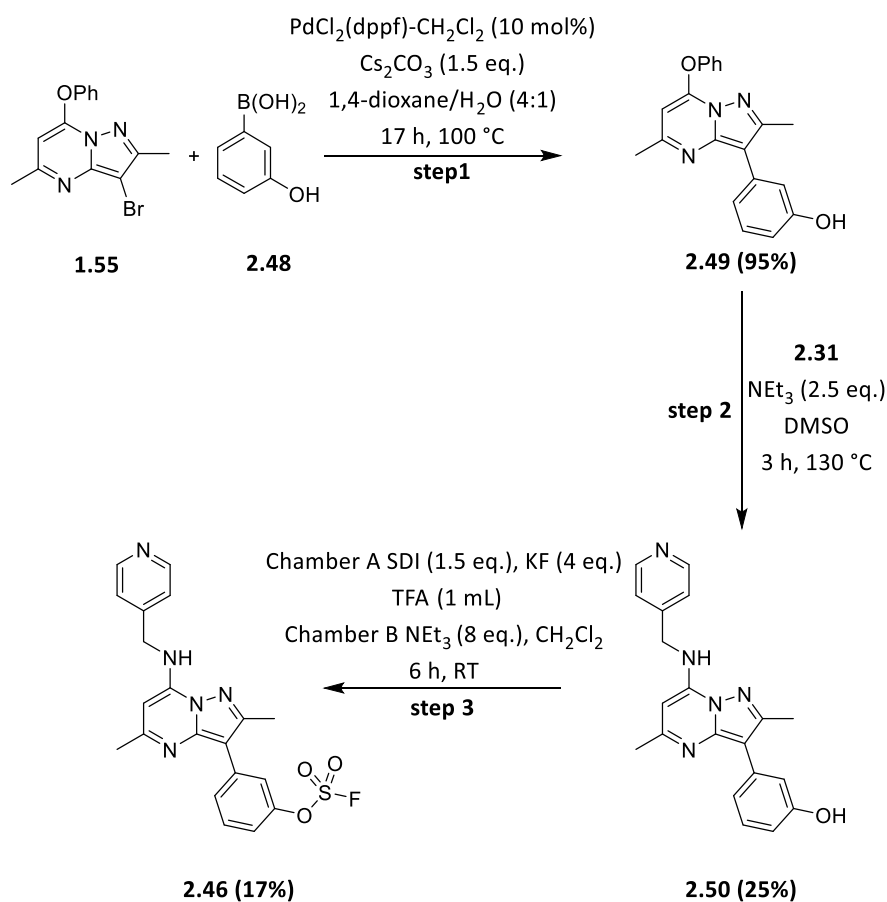


Figure 2.26: Initial fluorosulfate inhibitor design.

The synthesis for compound **2.46** is shown in **Scheme 2.6** and alternative fluorosulfate based inhibitors (**2.45** and **2.47**) were synthesised in analogous fashion.



Scheme 2.6: Synthesis of fluorosulfate **2.46**.

Compound **2.49** was prepared by a palladium catalysed cross coupling reaction of **1.55** with (3-hydroxyphenyl) boronic acid **2.48** under forcing reaction conditions to

give the product in high yield (95%). Step 2 of the synthesis involved an S_NAr reaction with **2.31** which was purified by column chromatography (25%). The target molecule **2.46** was synthesised using a **two-chamber reactor** through the generation of *ex situ* sulfonyl fluoride gas (shown in **Figure 2.27**).²⁴² The reaction was initiated by trifluoroacetic acid (TFA), which facilitated the generation of sulfonyl fluoride gas from sulfonyldiimidazole (SDI) which could pass into the adjacent chamber and react with the phenol group in compound **2.50** to generate the final compound **2.46**. It was important to stir the reaction at 1200 rpm to ensure efficient gas transfer across the chamber as shown in **Figure 2.27**.

COware has recently been developed for the *in situ* generation of low molecular weight gases such as carbon monoxide and hydrogen.²⁴³ Due to the safety concerns associated with these gases, the use of COware is appropriate. Sulfonyl fluoride gas is used to generate the final fluorosulfate compound, which is toxic and corrosive. Therefore, a sealed pressure system such as the COware reactor was a suitable piece of apparatus for synthesising compounds with the fluorosulfate warhead.

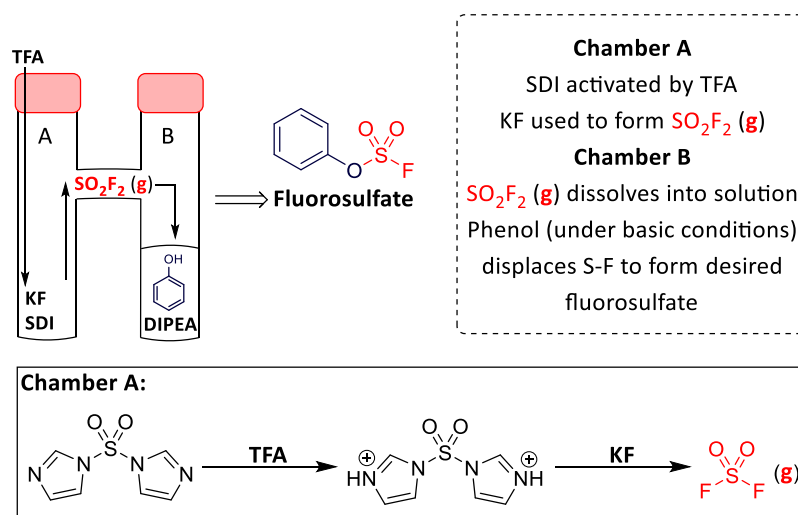
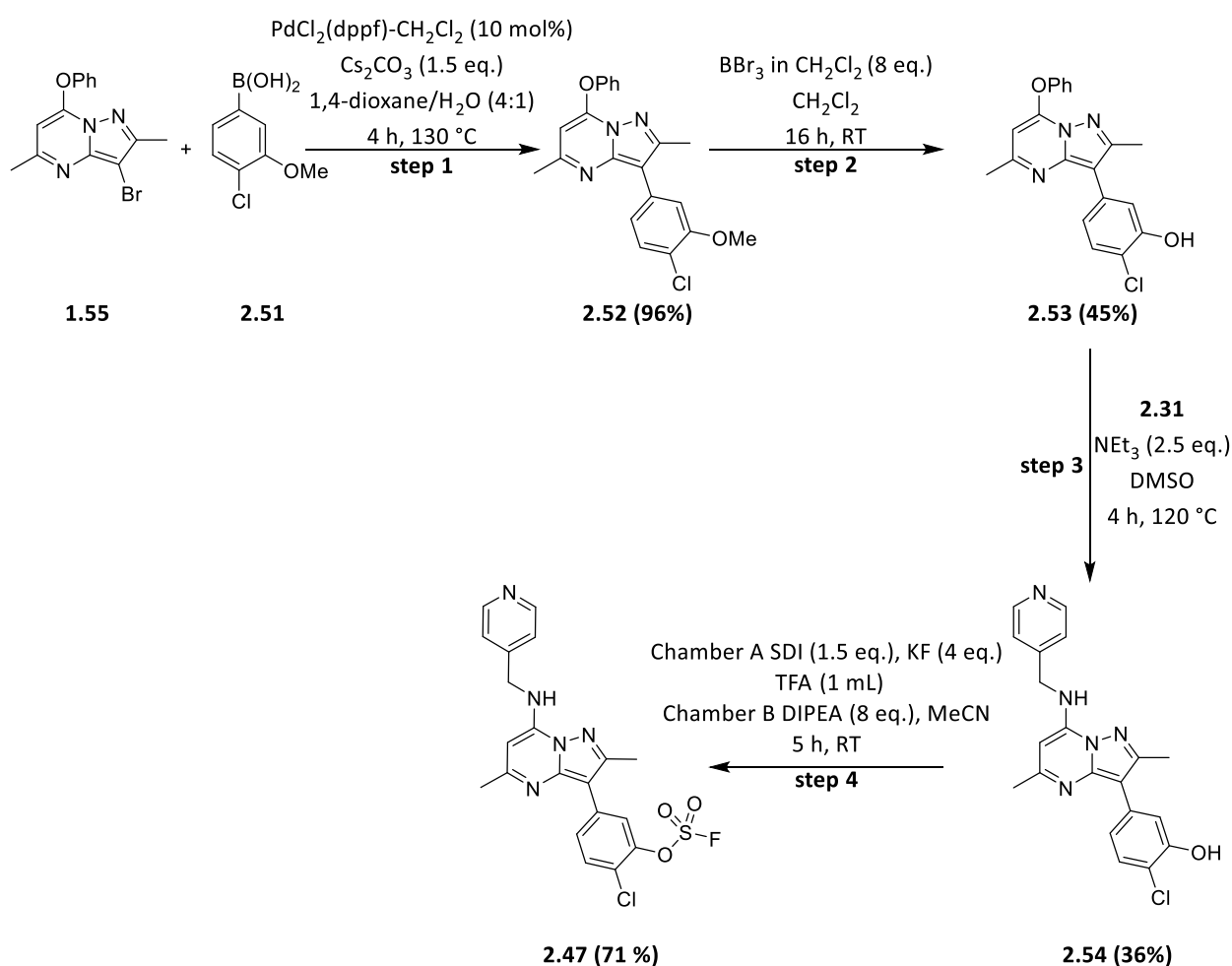


Figure 2.27: Use of a COware reactor to generate fluorosulfate compounds.

The method described using the COware apparatus shown in **Figure 2.27** worked efficiently for the synthesis of fluorosulfate containing compounds and was used

throughout this work. Chamber A contained the reagents used to generate SO_2F_2 (g) and Chamber B contained the phenol precursor stirred in MeCN/ CH_2Cl_2 in presence of excess DIPEA. The reaction was initiated by TFA to generate SO_2F_2 (g). The number of moles of gas could be calculated, and the maximum pressure was determined in the sealed pressure system to ensure safe and efficient gas transfer. The reagents for SO_2F_2 (g) generation and the desired reaction were segregated in their separate chambers and this led to a simple purification procedure. The synthesis of compound **2.47** was performed in a similar fashion and is shown below in **Scheme 2.7**.

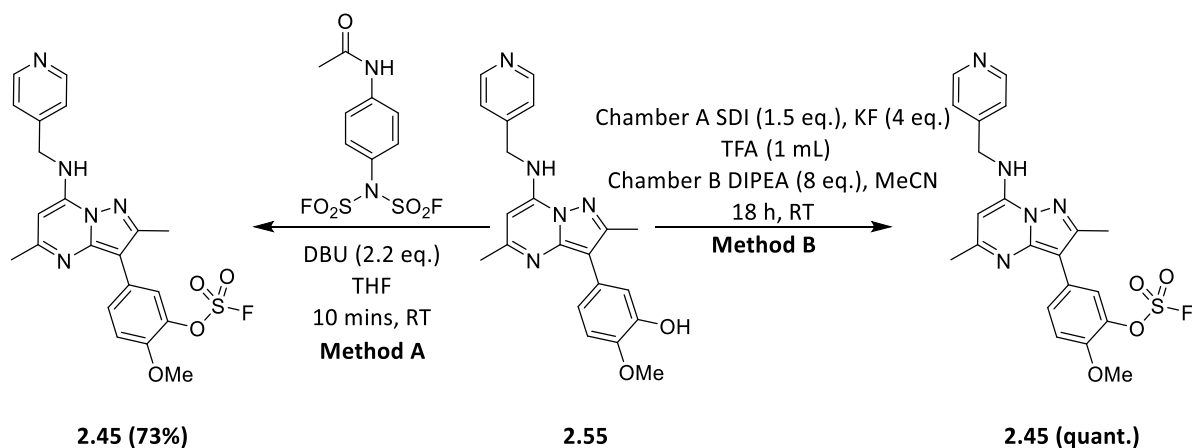


Scheme 2.7: Synthetic route to final compound **2.47**.

Biaryl **2.52** was assembled in 96% yield through a Suzuki cross-coupling reaction between compound **1.44** and boronic acid **2.51**. Treatment of product **2.52** with

tribromoborane solution gave the corresponding phenol product **2.53** in moderate yield (45%). The phenoxy group of compound **2.53** was displaced with pyridin-4-ylmethanamine **2.31** *via* an S_NAr reaction to give product **2.54** (36%). Intermediate **2.54** was subjected to the SO_2F_2 (g) conditions previously described to give the final compound **2.47** in high yield (71%).

Finally, the methoxy derivative **2.45** was prepared by two different synthetic routes. Key intermediate **2.55** was synthesised by an S_NAr reaction to install the pyridyl head group and the terminal aromatic ring was coupled onto the molecule through a palladium catalysed cross-coupling reaction in 44% yield for the two steps.

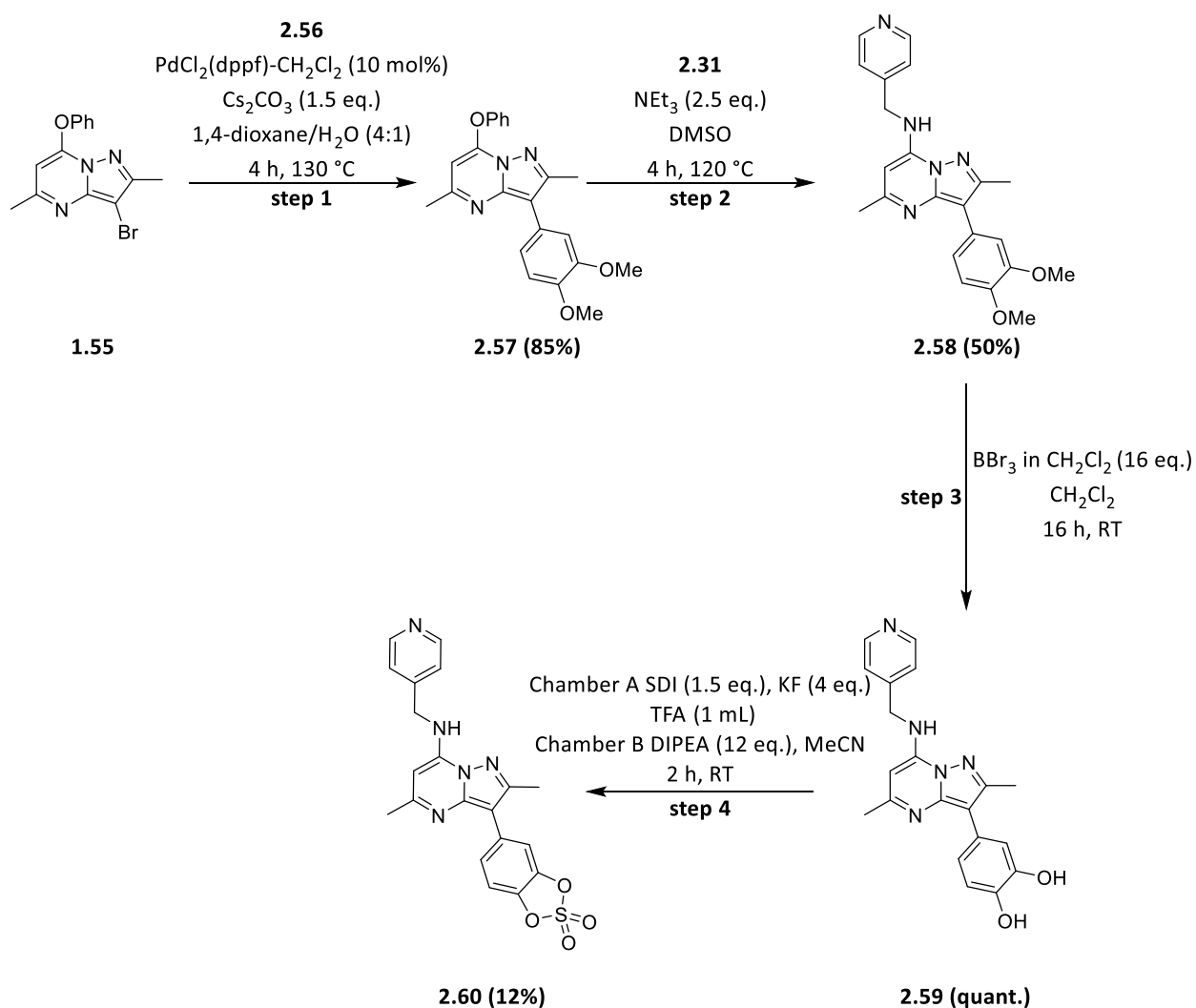


Scheme 2.8: Final compound **2.45**, synthesised *via* two different routes.

Fluorosulfate **2.45** was synthesised by Method A and Method B (**Scheme 2.8**).²⁴¹ [4-(Acetylamino)phenyl]imidodisulfuryldifluoride (AISF) the sulfonylating agent used in Method A is a bench stable commercially available solid. The reaction with AISF in the presence of DBU was complete within 10 minutes and no toxic gases were generated during the reaction. However, the aniline by-product of this reaction is genotoxic and was difficult to remove by column chromatography. Therefore, Method B was preferred and used to access **2.45** throughout the rest of this work. There are toxicity concerns with the generation of SO_2F_2 (g) however, the COware reactor was suitable

for this type of reaction as the gas was generated in a controlled fashion and contained in a sealed pressure vessel.

The reaction for synthesising the fluorosulfates from SO_2F_2 (g) using a phenol precursor was robust. Potentially, a bis-phenol precursor could be used to displace both fluoride groups to generate a cyclic sulfate group. Cyclic covalent warheads are of interest because the nucleophilic residue could add into the molecule in a traceless manner. This strategy has proven to be very successful, for example, the use of β -lactams in antibiotics.²⁴⁴ At this point, it was still uncertain whether the *meta* or *para* position of the aromatic ring was the optimal vector for appending a covalent warhead and so a cyclic warhead would cover both positions to increase the likelihood of engaging the lysine residue. The synthesis of cyclic sulfate **2.60** is shown in **Scheme 2.9**.



Scheme 2.9: Synthetic route to cyclic sulfate **2.60**.

The first step of the synthesis involved treating **1.55** with (3,4-dimethoxyphenyl) boronic acid **2.56** under palladium catalysed conditions to give the desired product **2.57** in high yield (85%). Compound **2.57** underwent an S_NAr reaction with amine **2.31** to give the desired product **2.58** (50%). Following this, compound **2.58** was stirred in a solution of tribromoborane under anhydrous conditions at room temperature for 16 hours to give the bis-phenol **2.59** (quant). The target cyclic sulfate **2.60** was prepared in a similar fashion to that shown in **Scheme 2.7**, but additional equivalents of DIPEA, KF and SDI were used. In the reaction, the bis-phenol displaces both fluoride atoms of the sulfonyl fluoride gas, giving the dioxathiole product **2.60**. However, there was an inherent instability associated with the final compound **2.60** and upon

purification the cyclic sulfate group hydrolysed and so compound **2.60** was obtained in only 12% overall yield and was stored under nitrogen at 10 °C.

The set of fluorosulfates (**2.45**, **2.46**, **2.47** and **2.60**) were screened in the biochemical and physicochemical assays to evaluate their potential as covalent modifiers. Compounds **2.45**, **2.46** and **2.47** were surprisingly stable and could be stored under ambient conditions. The biological data obtained is shown in **Table 2.6**.

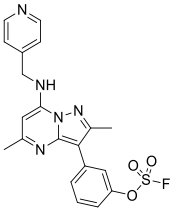
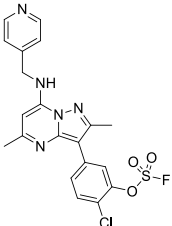
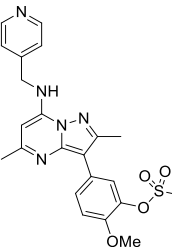
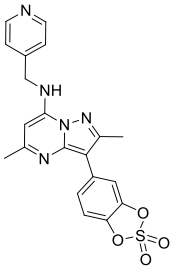
Entry	Cpd number	PI4KIII β pIC ₅₀	CPE pIC ₅₀	Δ (CPE-PI4KIII β)	Kinetic sol. ($\mu\text{g} / \text{mL}$)	ChromLogD _{7.4}	AMP (nm/s)
	2.46	6.5	7.3	0.8	15	6.3	290
	2.47	6.3	6.8	0.5	12	7.2	Not detected
	2.45	7.2	8.2	1.0	15	6.2	220
	2.60	7.3	6.2	-1.1	87	1.7	520

Table 2.6: Enzymatic and cellular data for compounds **2.45**, **2.46**, **2.47** and **2.60**.

Compounds **2.45**, **2.46** and **2.47** followed similar trends as identified for the phenolic ester series, where the activity increased from the enzyme assay to the cellular assay as evidenced by the Δ values, supporting the hypothesis that there could be a time dependency with the activities of these compounds. Although the physicochemical properties were not improved as anticipated, the boost in activity was encouraging and the compounds were surprisingly stable. Compound **2.45** was below 10 nanomolar activity in the CPE assay and became the lead compound for characterising the potential covalent adduct. Interestingly, the electrophilic centre of the fluorosulfate compounds was positioned one linker further out in comparison to the other activated phenolic esters. As shown in **Figure 2.24**, the lysine was approximately $\sim 3\text{-}4$ Å away from the electrophilic centre, therefore, the fluorosulfate warhead could be better positioned to engage with Lys549 explaining the improvement in the activity observed.

Cyclic sulfate **2.60** presented some interesting features, however, **2.60** was susceptible to rapid hydrolysis and formed the phenol by-product, where signs of hydrolysis were observed upon product isolation, reflected in the sub-optimal cellular potency. This was supported by the enhanced solubility and reduced ChromLogD (1.7). The stability of compound **2.60** in DMSO at 10 °C was investigated and 74% hydrolysis was observed after 2 weeks, therefore, no further investigation of this warhead was carried out.

Compound **2.45** was selected to be further profiled due to its promising initial results. In addition, necessary control compounds were synthesised in an analogous fashion to previous compounds and profiled as shown in **Table 2.7**. Compound **2.55**, the phenol control was more potent than compound **2.45** in the enzyme assay and a log unit less potent in the CPE assay. Both compounds **2.55** and **2.45** were permeable which eliminates the possibility of **2.55** not being able to enter the cell. This suggested that the increase in activity for compound **2.45** was not driven by hydrolysis of the

fluorosulfate group to the phenol within the cell, but indicated an alternative mode of action.

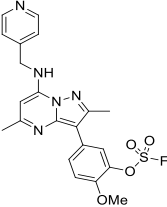
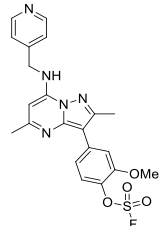
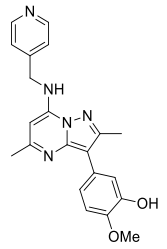
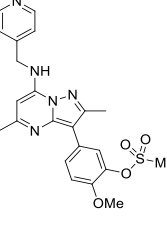
Entry	Cpd number	PI4KIII β pIC ₅₀	CPE pIC ₅₀	Δ (CPE-PI4KIII β)	AMP (nm/s)
	2.45	7.2	8.2	1.0	215
	2.61	6.5	6.3	-0.2	740
	2.55	7.9	7.0	-0.9	510
	2.62	8.1	7.6	-0.5	360

Table 2.7: Biochemical data for lead compound **2.45** and necessary control compounds **2.61**, **2.55** and **2.62**.

As shown in **Table 2.7**, compound **2.45**, was the only compound that showed an increase in activity from the enzyme to cellular assay. This strongly suggests an alternative mode of action to the other compounds examined. Compound **2.61** indicated that the *meta*-position was the appropriate vector for the warhead because the potency slightly dropped in the cellular assay, indicative of competitive reversible inhibition. Interestingly, compound **2.62** displayed the greatest activity in the enzyme

assay. The only difference between compound **2.45** and **2.62** was the presence of a methyl group instead of a fluorine atom. Fluorine is an electron withdrawing group and may have decreased the inhibitor's interactions with PI4KIII β , most likely due to reduced hydrogen bonding interactions between the oxygen atoms of the sulfate and the hydrogen atoms of the lysine. As a result, compound **2.62** displayed greater activity in the enzyme assay and a drop-in activity was observed from the enzyme to the cellular assay, supportive of the non-covalent interaction with the protein.

2.13 Lipid kinase selectivity of lead compound 2.45

Compound **2.45** was further profiled in terms of its selectivity over other lipid kinases through a commercial lipid kinase screen (see **Appendix 3.2** for full data set). The data is shown in **Figure 2.28**, where over 100-fold selectivity against other lipid kinases was achieved. The most significant off-target activity measured, was towards PI3K γ where the pIC₅₀ was 5.5, all other lipid kinases were less than this (pIC₅₀<5).

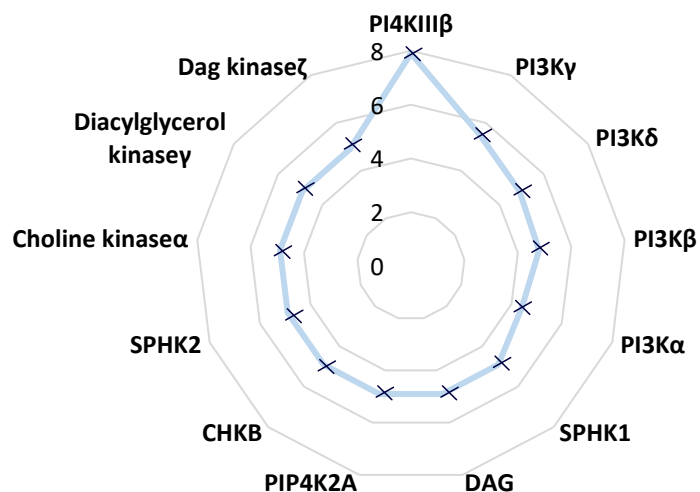


Figure 2.28: Lipid kinase pIC₅₀ data for **2.45**.

2.14 Stability screen of fluorosulfates

As previously mentioned, no detailed data of the stability and reactivity of fluorosulfate compounds has been reported. The compounds synthesised were surprisingly stable in comparison to the analogous sulfonyl fluoride compounds, where rapid hydrolysis to the sulfonic acid was observed after 24 h. To reduce the rate of hydrolysis for the sulfonyl fluoride (**2.42**), the compound was stored under nitrogen at 0 °C. The enhanced stability of the fluorosulfate group is probably due to the stabilisation effect of the oxygen linker of the fluorosulfate. As the electronics were varied around the phenyl ring for compounds **2.45**, **2.46** and **2.47** (shown in **Figure 2.29**), these features were investigated in terms of their stability. See general methods **Section 2.24** for further details of the experimental setup.

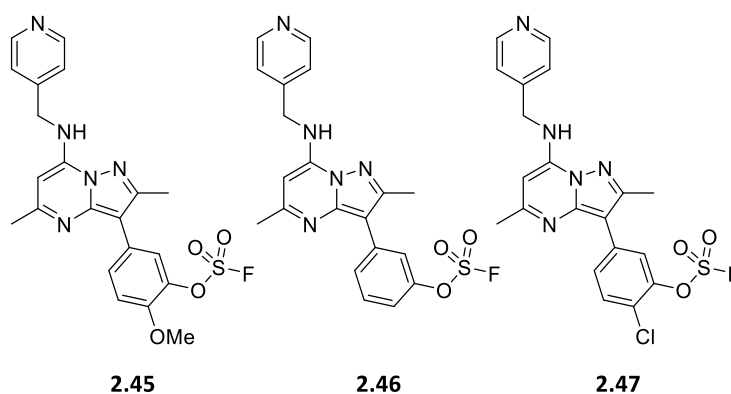


Figure 2.29: Compounds **2.45**, **2.46** and **2.47** profiled under the stability screen.

The compounds **2.45**, **2.46** and **2.47** were incubated in buffered solutions at different pHs in both the presence and absence of 20 mol% H₂O₂. An additional glutathione (GSH) reactivity experiment was conducted under neutral conditions. These studies were carried out at 40 °C and the data for compound **2.45** is shown in **Figure 2.30**.

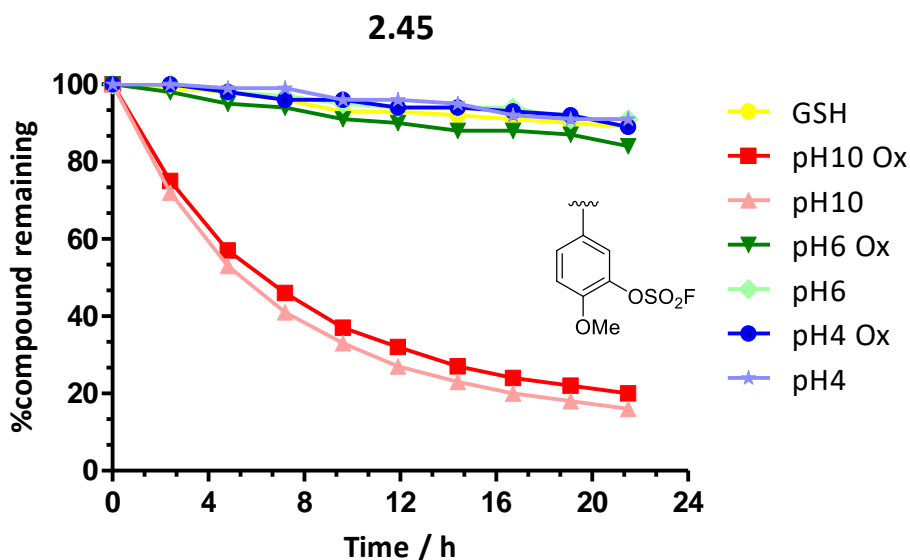


Figure 2.30: Stability plot of compound **2.45** under different conditions.

Compound **2.45** was stable to neutral and acidic conditions under these experimental conditions. Compound **2.45** did undergo a transformation under basic conditions at 40 °C with an approximate half-life of 7 hours. The adduct was not characterised but the formation of hydrolysed product was likely under the basic aqueous conditions. Interestingly, no reaction was observed with GSH under neutral conditions, which suggests the fluorosulfate group in compound **2.45** could be stable to nucleophilic cysteine residues. The fluorosulfate warhead could potentially act as a non-cysteine covalent modifier.

Subsequently, compound **2.47** was profiled under the same conditions (**Figure 2.31**).

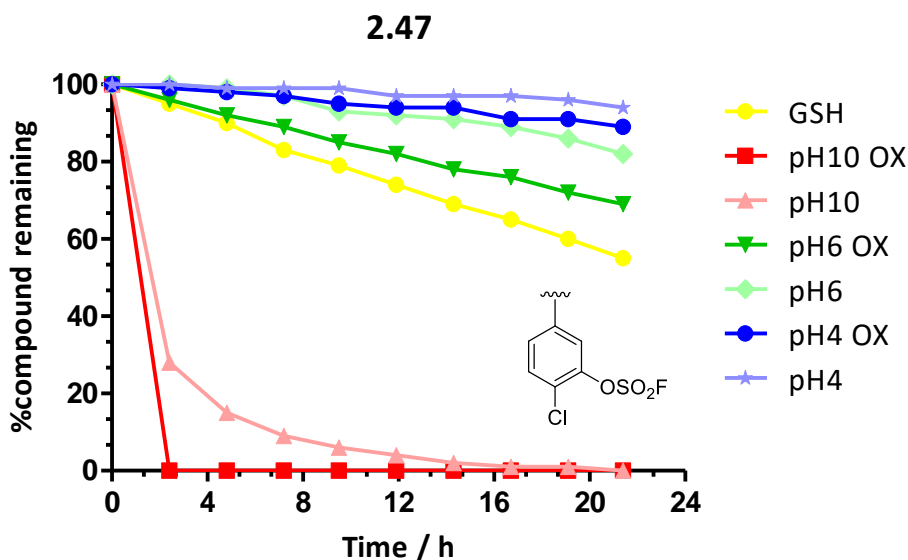


Figure 2.31: Stability plot of compound **2.47** under different conditions.

Compound **2.47**, containing an *ortho* chloro group exhibited an alternative profile under these experimental conditions when compared to compound **2.45**. The fluorosulfate warhead underwent a rapid transformation under basic conditions at 40 °C, showing an instability under basic conditions with an approximate half life of 2 h. **2.47** was stable to neutral and acidic conditions but was more susceptible to the oxidative conditions of the hydrogen peroxide in comparison to **2.45**. Compound **2.47** also appeared more reactive towards GSH under these experimental conditions. The adduct was not characterised and so the product of this transformation remains uncertain. The literature of aryl sulfonyl fluorides, suggests the formation of a thiosulfonate (not experimentally observed) which then undergoes rapid cleavage with cysteine to give the corresponding sulfinic acid (**Figure 2.32**).²¹² It could be possible for **2.47** to react with cysteine *via* a similar reaction mechanism, where a sulfurthioate intermediate could in principle be formed and then rapid cleavage to give the corresponding phenol by-product (as shown in **Figure 2.32**).

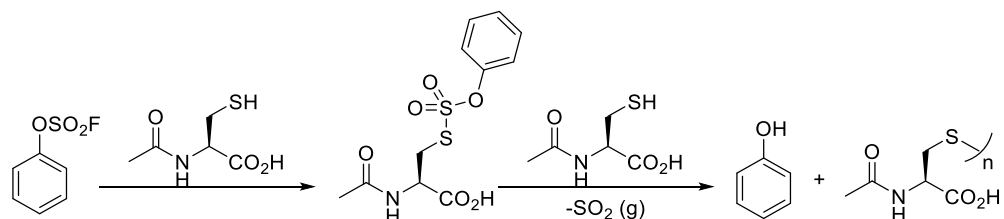
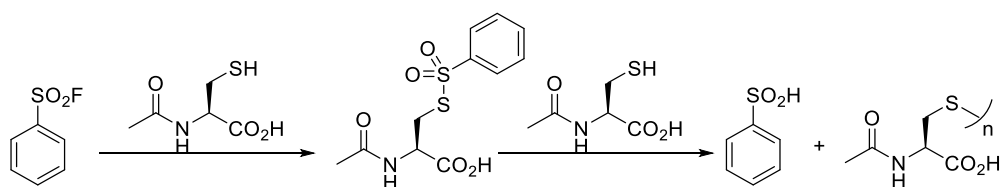


Figure 2.32: Reactivity aryl sulfonyl fluoride with *N*-acetyl-cysteine and potential reactivity of aryl fluorosulfate

Finally, compound **2.46**, an unsubstituted analogue, was profiled under the same stability conditions.

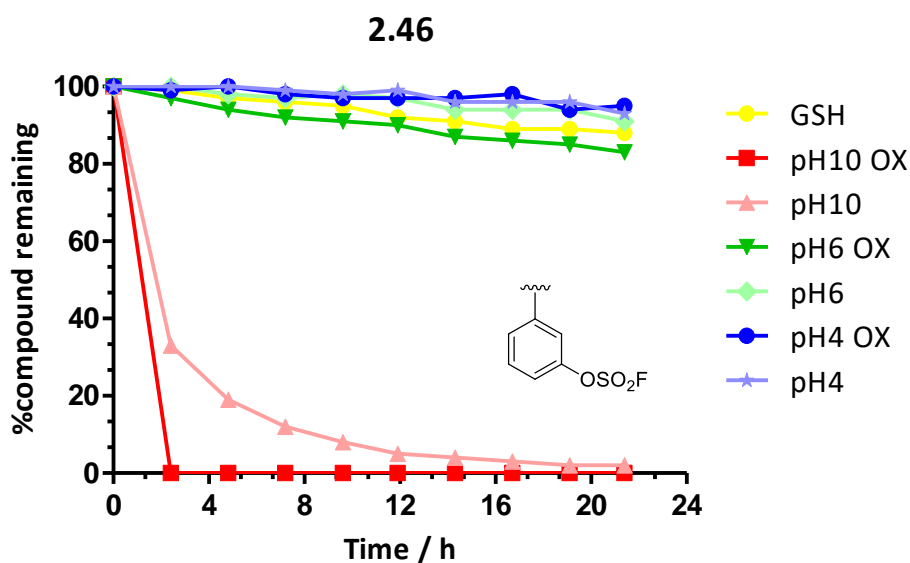


Figure 2.33: Stability plot of compound **2.46** under different conditions.

Compound **2.46** was stable to neutral and acidic conditions under these experimental conditions and underwent a rapid transformation under basic conditions (**Figure 2.33**). This data suggests an *ortho* substituent with electron donating capabilities was

necessary to increase the stability of the fluorosulfate group under basic conditions. This could potentially be due to the reduced electrophilicity of the sulfur atom. No adduct was observed with GSH under neutral conditions strengthening the case of the reduced reactivity of the fluorosulfate. As there was no substituent *ortho* to the fluorosulfate warhead this eliminates the possibility of steric hindrance influencing the reactivity of the fluorosulfate group with free thiol (this was later supported by reactivity studies with cysteine, see **Section 2.15**).

2.15 Amino acid screen

After the stability of the compounds **2.45**, **2.46** and **2.47** was established, the next step of this work involved understanding the reactivity of the fluorosulfate group with different amino acids. An amino acid screen was carried out on the lead compound **2.45** under basic and neutral conditions. The reactions were carried out under *pseudo first order* reaction conditions at RT and were monitored up to 48 h by LCMS (see **Section 2.24** for full experimental details). In the case of *N*-acetylcysteine, DTT was used to reduce any disulfide bonds formed, to ensure the free thiol was available to react. The results of the reactivity experiment are shown in **Figure 2.34**.

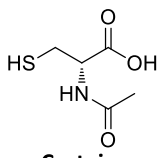
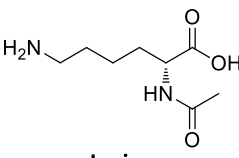
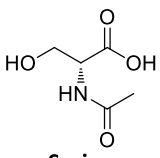
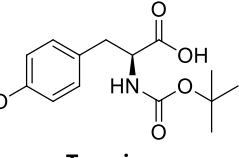
	 Cysteine	 Lysine	 Serine	 Tyrosine
pH7.4	✗	✗	✗	✗
pH10.1	✗	✓	✗	✓

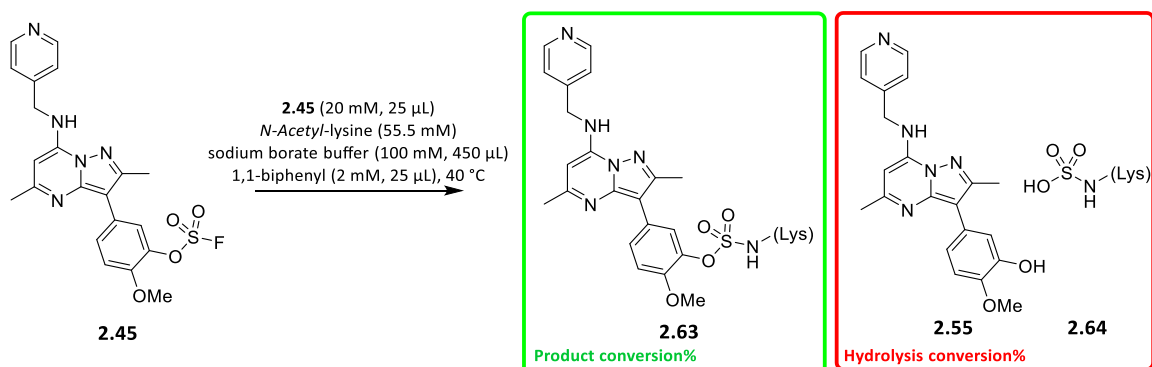
Figure 2.34: Amino acid screen of compound **2.45** under neutral and basic conditions.

Pleasingly, compound **2.45** was unreactive towards all the amino acids under neutral conditions. A concern with covalent drug design is the potential of the electrophilic warhead reacting with multiple residues. As no covalent adduct was identified under

physiological conditions, this minimises the risk of this being the case with this compound. Under basic conditions, compound **2.45** was reactive towards both lysine and tyrosine. The pH of the buffer was approximately equivalent to the pKa of the amino acids, suggesting if a lysine residue buried deeply in a hydrophobic pocket, where its pKa could be perturbed, a reaction with the fluorosulfate group could take place. The reactivity of the fluorosulfate group could therefore be dependent on the local protein microenvironment which would minimise its potential for promiscuous reactivity greatly enhancing its potential as a drug molecule.

2.16 HPLC reactivity assay

To understand the reactivity of compounds **2.45**, **2.46** and **2.47** against lysine, a more in-depth reactivity experiment was required. Pfizer have published work profiling a range of electrophilic moieties against *N*- α -acetyl-lysine to guide covalent drug design.¹⁴² These experimental conditions were replicated, carried out in duplicate alongside a control reaction where the compound was stirred in the buffered solution without any added lysine. The pH of the sodium borate buffered solution was measured at 10.18. After the addition of lysine (50 eq.), the pH was measured again at 10.2. Therefore, the pH of the buffer was approximately equivalent to the pKa of the lysine (~10.1) and so the lysine could act as a nucleophile. The reaction scheme and plot is shown below in **Figure 2.35**.



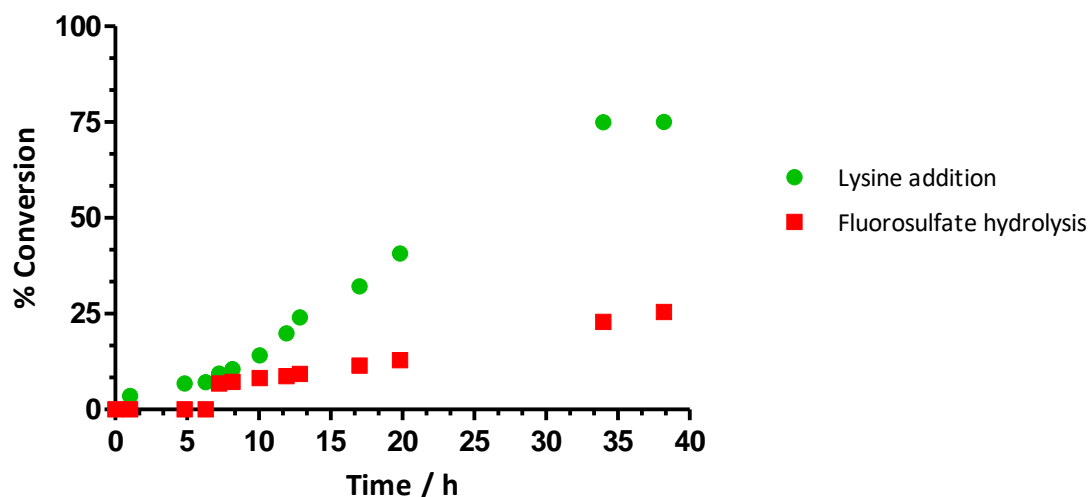


Figure 2.35: Compound **2.45** reactivity with *N-acetyl*-lysine, monitored by HPLC.

In an aqueous chemical environment at 40 °C, the reaction of compound **2.45** with lysine at pH10.2 occurred slowly. Approximately 50% conversion to the lysine adduct (**2.63**) was achieved after 24 h. If these results translated into the protein environment of PI4KIII β , it would suggest that the activity in the enzyme assay (with a 40-minute incubation period) was due to reversible interactions between compound **2.45** and PI4KIII β as the incubation period was not long enough to enable the covalent modification. Whereas, the activity from the CPE assay (48 h incubation period) could potentially come from the covalent modification itself. Interestingly, under these experimental conditions, compound **2.45** showed no signs of degradation in the absence of *N-acetyl*-lysine in the control experiment (see **Appendix 3.3**). This suggested that the hydrolysis (red line) must come from the lysine adduct itself and as shown, the hydrolysis of the product was relatively slow as approximately 25% hydrolysis was observed after 40 h (**2.64**). The desired sulfamate and hydrolysed phenol product of this reaction were characterised by LCMS and HRMS.

The observed hydrolysis of the sulfamate was consistent with the reported literature, where a collaboration at the Scripps Research Institute explored fluorosulfate probes

targeting a lysine residue in transthyretin (TTR).²⁰⁵ LC-ESI-MS was used to monitor the formation of the covalent modification with lysine after a 24 h incubation at 37 °C using 7.2 μM probe (**2.65**) against TTR. The desired conjugate adduct with TTR **2.66** was identified and then over time, the sulfamate adduct hydrolysed to give the sulfamic acid **2.67** and the corresponding phenol hydrolysis product as depicted in **Figure 2.36**. The authors concluded that the observed hydrolysis was an artefact of the protein and was catalysed by TTR itself.²⁰⁵

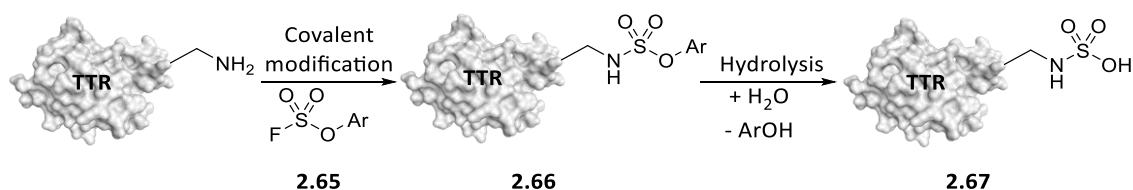
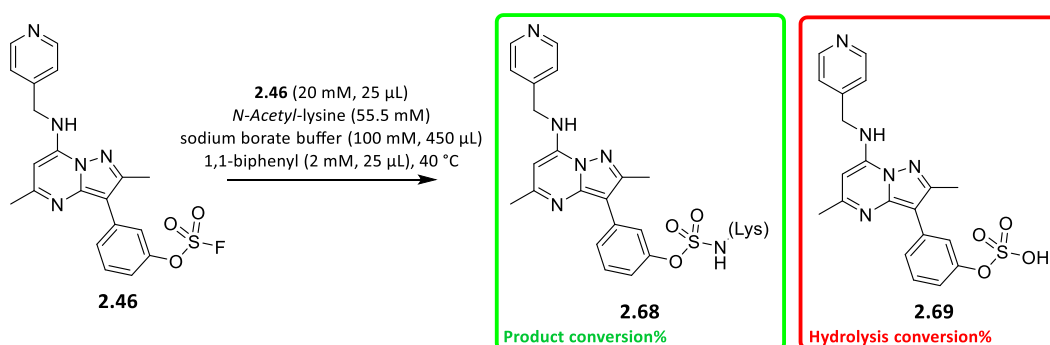


Figure 2.36: Covalent modification and hydrolysis of TTR with a fluorosulfate electrophile.

The result shown in **Figure 2.35** was promising as compound **2.45** showed potential for reacting with lysine residues. It also highlighted the question as to whether the hydrolytic transformation could take place in the active site of PI4KIIIβ. Subsequently, compound **2.46** was also profiled under the same experimental reaction conditions (**Figure 2.37**).



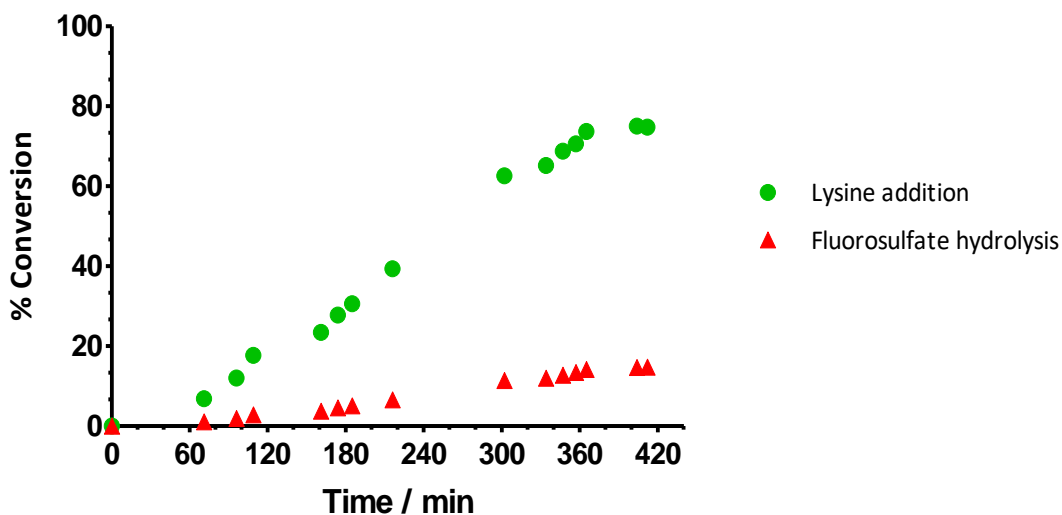


Figure 2.37: Compound **2.46** reactivity with *N*-acetyl-lysine, monitored by HPLC.

Compound **2.46**, without an *ortho* methoxy substituent showed an enhanced reactivity with lysine leading to approximately 50% conversion to the sulfamate adduct **2.68** after 4.5 hours. This suggested that the presence of an electron donating *ortho* substituent slowed down the rate of the reaction with lysine under these experimental conditions. In addition, approximately 20% hydrolysis was observed in the reaction (**2.69**). A control experiment was undertaken (without lysine) and approximately 20% hydrolysis was observed (see **Appendix 3.3**). This suggested that hydrolysis was associated with the starting material **2.46** rather than the lysine adduct, over this reduced time frame (sulfamate hydrolysis was identified over an extended time frame). Previous stability studies also highlighted the instability of compound **2.46** under basic aqueous conditions (see **Figure 2.31**). In addition, the expected phenol hydrolysis product was not observed, and it was in fact the sulfonic acid **2.69**, which was characterised by LCMS and HRMS. Therefore, compound **2.46** showed an enhancement in reactivity against lysine when compared to compound **2.45** but also a decreased stability under these experimental conditions, consistent with previous data.

Finally, compound **2.47** was profiled under the same reaction conditions, the results of which are shown in **Figure 2.38**.

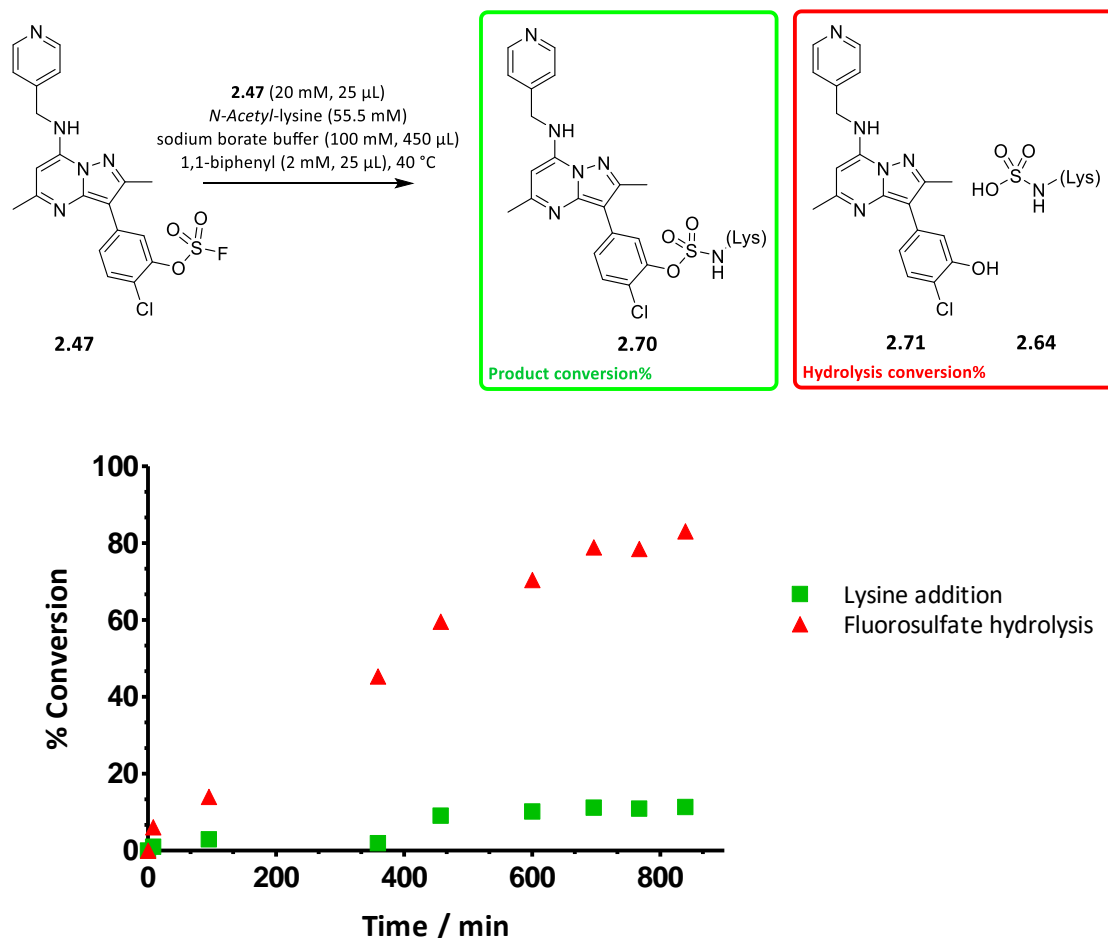


Figure 2.38: Compound **2.47** reactivity with *N*-acetyl-lysine, monitored by HPLC.

Compound **2.47** displayed a different reaction profile compared to **2.45** and **2.46**. The control reaction (see **Appendix 3.3**) displayed slow hydrolysis, where approximately 50% hydrolysis was observed after 900 minutes, in comparison to the profile for **2.47** where 50% hydrolysis was observed at approximately 400 minutes (**2.71**). Therefore, an enhancement in hydrolysis was observed in the presence of lysine. Additionally, the expected phenol hydrolysis product **2.71** was observed, consistent with sulfamate product hydrolysis **2.70**. The data suggested that the reaction of compound **2.47** with lysine under these experimental conditions was relatively rapid

which could be due to the increased electrophilicity of the sulfur atom. In addition, the data suggested that the sulfamate **2.70** had decreased stability in the presence of the *ortho*-chlorine substituent in comparison to the *ortho*-methoxy substituted analogue **2.45**.

A more detailed study into the stability of sulfamate esters under different conditions has been reported. Spillane and McCaw investigated kinetic and mechanistic aspects of sulfamate esters and their hydrolysis pathways.²⁴⁵ It was determined that sulfamate esters bearing a hydrogen on the nitrogen atom had pKa values of approximately 8 in water-organic media. Their work concluded that the hydrolysis pathway of sulfamate esters under aqueous basic conditions followed an E1cB type reaction. A proposed mechanism for the observed hydrolysis of compounds **2.45** and **2.47** is shown in **Figure 2.39**.

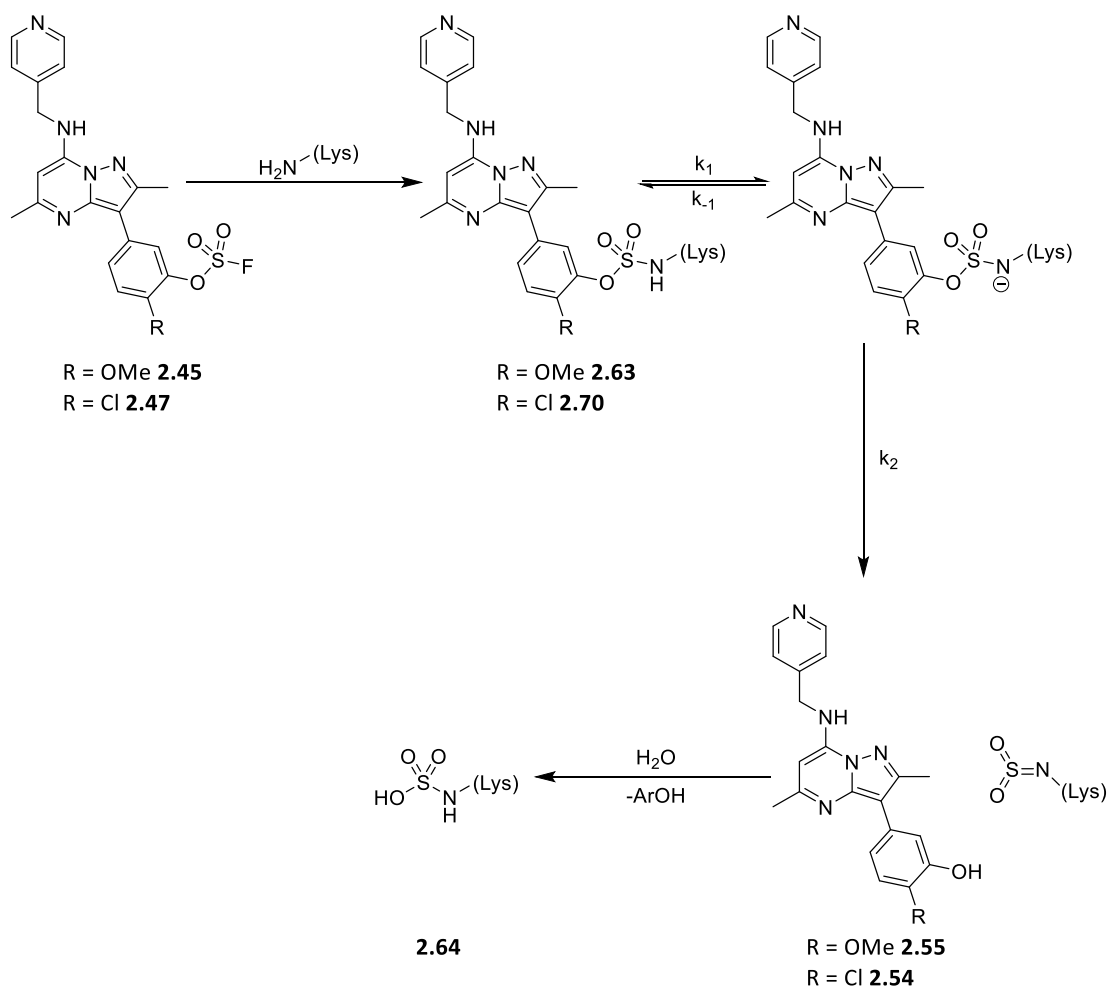


Figure 2.39: Proposed mechanism of hydrolysis under basic conditions.

The rate at which the sulfamate formed was dependent on whether R was OMe **2.63** or Cl **2.70**. Despite the reaction difference in forming the sulfamate, no significant variability in the pKa of the sulfamate was expected which could be correlated with the approximate value of 8 as previously determined by Spillane. The equilibrium for k_1/k_{-1} can be assumed to be in the same position for both **2.63** and **2.70**. Therefore, k_2 was key to the stability of the desired adduct formed with lysine. If R = Cl, the E1cB reaction (equilibrium shifted towards k_2) was more favourable because of the relatively good leaving group ability of the chloro substituted phenol (**2.54**). The chloro substituent inductively withdraws electron density increasing its leaving group ability. This can be correlated with a large k_2 value which was consistent with the data

represented in **Figure 2.39** and the opposing argument can be made if R = OMe (small k_2 , decreased formation of **2.55**).

Overall, interesting features of a potential covalent modification with lysine were identified with compounds **2.45**, **2.46** and **2.47**. However, it is important to note that the reactivity of the fluorosulfate compounds can change significantly in a biological environment and so no absolute conclusions could be drawn at this stage. As shown in **Equation 2.1**, covalent inhibition is a two-step process consisting of reversible binding to the protein of interest and then covalent attachment. The reversible interactions could play a major role in the covalent capability of the compounds and the biochemical data previously presented is not sufficient evidence for covalent binding, but more of an indicator for a potential alternative mechanism.

2.17 Mass spectrometry characterisation of lysine targeted inhibition

Based on all of the above, it was evident that compounds **2.45**, **2.46** and **2.47** showed promising features for covalent modification of a lysine residue. For the past 20 years, mass spectrometry has been used to analyse covalent interactions between ligands and proteins.²⁴⁶ To characterise the potential covalent interaction, intact protein mass spectrometry was carried out. This would determine if a covalent bond was formed between the inhibitor and PI4KIII β protein. Concentration and time dependant mass spectrometry experiments can be very useful tools for determining the selectivity of the covalent modification and also for providing an indication of the kinetics of covalent modification. If multiple covalent adducts with the protein were observed, this would be indicative of nonspecific binding and potential promiscuous covalent reactivity which represents a major challenge of non-reversible inhibition in drug discovery. The time taken to identify the labelling of proteins provides an insight on the mechanism of the covalent modification, i.e. fast onset vs slow onset of inhibition. A time course mass spectrometry experiment was carried out for compound **2.45** (5 μ M) with PI4KIII β (1 μ M) and is shown in **Figure 2.40**. See

experimental **Section 2.24** for the experimental procedure. Note, two peaks were observed in the mass spectrometry spectrum for recombinant PI4KIII β protein. Upon purification/expression of the protein a phosphate group (78 Da) is added to a surface residue of PI4KIII β .

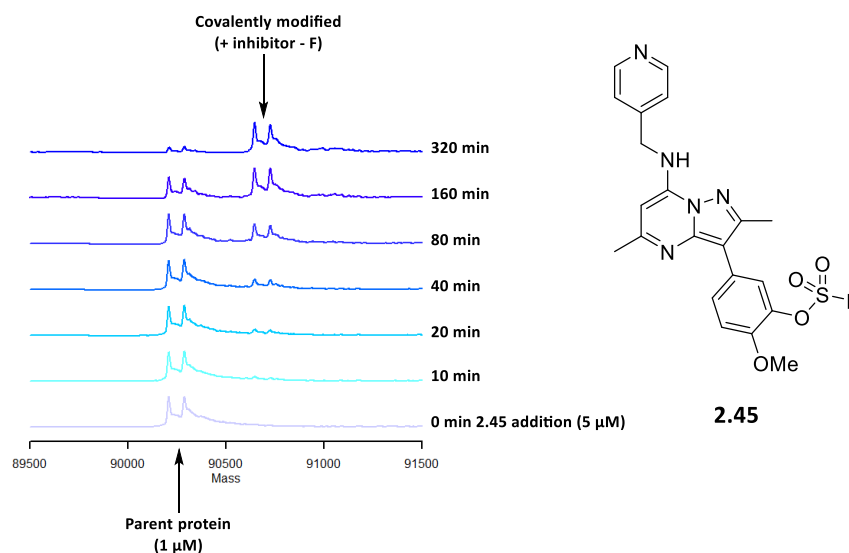


Figure 2.40: Time course of compound **2.45** reacting with recombinant PI4KIII β at 10 °C.

Pleasingly, as shown in **Figure 2.40**, compound **2.45** covalently modified recombinant PI4KIII β protein. The covalent modification took around 2 h to react 50% conversion with 5 eq. of the reactant **2.45** under neutral conditions at 10 °C. The mass shift was consistent with the addition of compound **2.45** minus the fluoride ion (90,688 Da), correlating with the attack of a nucleophilic residue onto the electrophilic sulfur atom, expelling the fluoride leaving group. In relation to the reactivity experiment previously carried out with an isolated *N*-acetyl-lysine (**Section 2.16**), a significant enhancement in the rate of reactivity of compound **2.45** was observed with recombinant PI4KIII β protein. This could be due to the local protein microenvironment, where the pKa of a deeply buried lysine may have been perturbed significantly, rendering it hyperreactive upon binding of compound **2.45** with the nucleophilic residue in close proximity of the electrophilic centre.

There are a total of 39 lysine residues in recombinant PI4KIII β protein which could lead to non-specific labelling of the protein with multiple warheads reacting.²⁴⁷ In order to investigate this, a large excess of compound **2.45** was used to incubate with enzyme to determine if the target engagement was selective. Only one covalent modification was observed indicative of a selective covalent attachment. Wortmannin, a known pan covalent PI3K inhibitor and other covalent warheads such as a vinyl sulfone showed multiple adduct formation as the concentration of the inhibitor and or time period of incubation was increased. Under the same mass spectrometry conditions, commercially available Wortmannin (5 μ M) was profiled against PI4KIII β (1 μ M) and the mass spectrum obtained is shown in **Figure 2.41**, showing multiple covalent adducts, highlighting the promiscuous covalent nature of Wortmannin in comparison with compound **2.45** where only one adduct was identified.

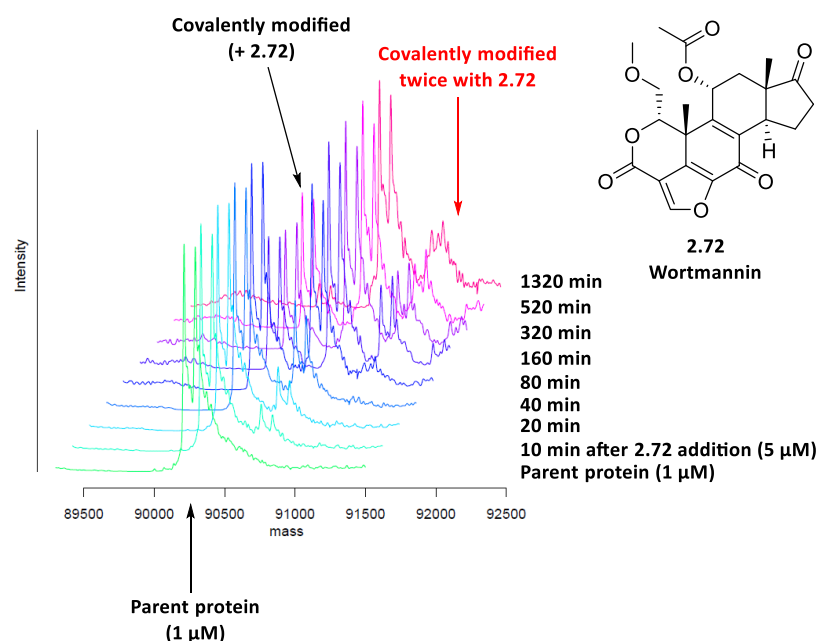


Figure 2.41: Mass spectrometry time course experiment with Wortmannin **2.72** with recombinant PI4KIII β at 10 °C.

Furthermore, protein mass spectrometry was used to assess the stability of the covalent adduct. Previous mass spectrometry conditions were replicated with

compound **2.45** (5 μM) and the adduct was identified by mass spectrometry. After the covalent modification was identified, the protein sample was saturated with high concentrations of competitive inhibitor ATP (10 mM) and the adduct was followed by mass spectrometry. Due to the high concentration of ATP used, if the covalent adduct was unstable, then ATP would compete in the active site of PI4KIII β reducing the covalent modification. The data shown in **Figure 2.42** suggests that the covalent adduct formed in PI4KIII β was stable and not susceptible to competitive inhibition.

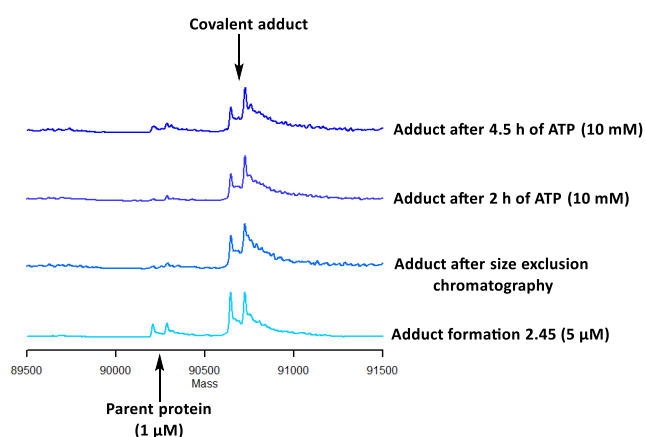


Figure 2.42: Covalent adduct between **2.45** and PI4KIII β stability experiment in the presence of ATP.

Compound **2.46** was subjected to the same time dependent mass spectrometry conditions described above. Pleasingly, it showed covalent modification of recombinant PI4KIII β protein (**Figure 2.43**). After 6 h, approximately 50% conversion was achieved, which was slower by 3-*fold* than that observed with **2.45**. In addition, the covalent adduct was stable after 48 h and there were no signs of hydrolysis or additional covalent adducts within the mass spectrum obtained.

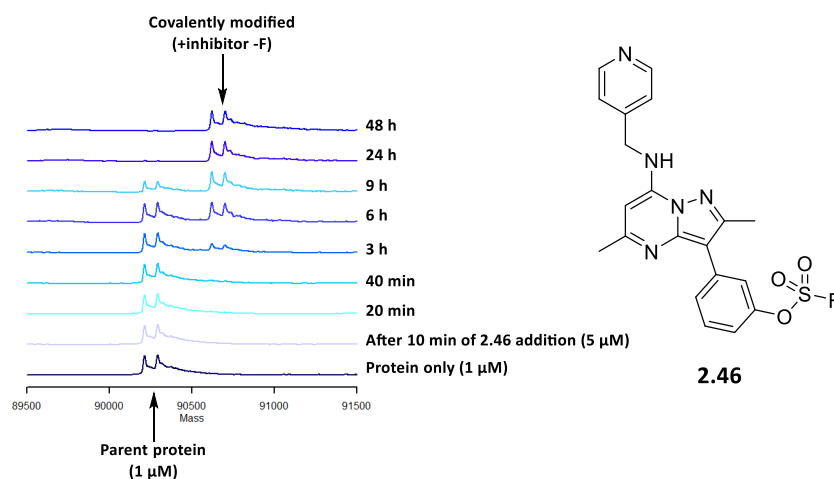


Figure 2.43: Time course of reaction of compound **2.46** with recombinant PI4KIII β at 10 °C.

Finally, compound **2.47** was profiled by mass spectrometry as shown in **Figure 2.44**. Interestingly, compound **2.47** displayed a significantly slower rate of covalent modification which took up to 24 h to reach 50% conversion. This suggests that the presence of the *ortho* chloro substituent hindered its ability to covalently link with PI4KIII β . Electronically, the presence of the chloro substituent would increase the electrophilicity of the sulfur atom and so it would be expected that the nucleophilic lysine would react more readily. Therefore, the reduced rate of covalent modification was possibly due to an alternative conformational arrangement of **2.47** disfavoring nucleophilic attack at the sulfur atom which can be supported by its decreased potency. This result shows the importance of the initial reversible interactions between an inhibitor and an enzyme and the implications it can have on covalent interaction.

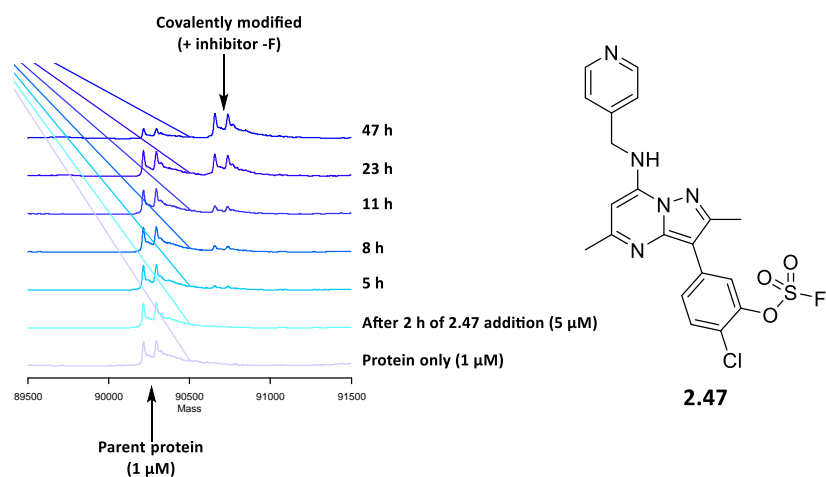


Figure 2.44: Time course of reaction of **2.47** with recombinant PI4KIII β at 10 °C.

The data shown in **Figure 2.40** disagrees with the previous reactivity experiments and the electronics of the molecule. The increased electron donating capability of the methoxy group would decrease the electrophilicity of the fluorosulfate, weakening the nucleophile interaction decreasing the overall rate of the covalent modification. However, inside the active site of PI4KIII β , the presence of the methoxy group of **2.45** increased the rate of covalent modification. In **Figure 2.24**, the distance of the methoxy group from Lys549 was 3.63 Å, therefore, the methoxy group could play a role in perturbing the pKa of the lysine residue through hydrogen bonding (**Figure 2.45**). This may have increased the nucleophilicity of the lysine and as a result, increased the rate of covalent modification.

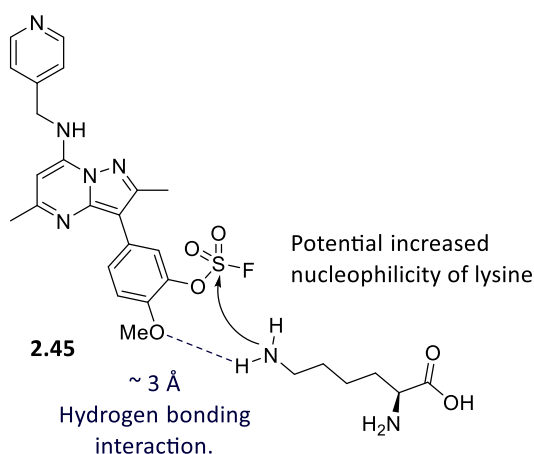


Figure 2.45: The *ortho*-methoxy group may have helped the increased rate of covalent modification.

In summary, the fluorosulfate containing inhibitors **2.45**, **2.46** and **2.47** demonstrated a selective covalent modification of PI4KIII β . The rate of covalent modification was surprisingly slow, and this phenomenon is supported by the recent literature around aryl fluorosulfate compounds targeting lysine residues.²⁴⁸ Pellecchia *et al* also observed the slow onset of aryl fluorosulfate containing inhibitors.²⁴⁸ Their reaction conditions were slightly different as they used a 1:10 protein-inhibitor ratio and incubated the mixture at 25 °C. After 6 h, full conversion to the covalent adduct was observed. Both findings are consistent with a reduced reactivity of the fluorosulfate containing inhibitor, highlighting the reversible interactions between the enzyme and inhibitor. Interesting, Pellecchia also disclosed the sulfonyl fluoride containing compounds used were reactive, but unstable in both aqueous buffer and in plasma. These results show a reduced reactivity of the fluorosulfate moiety to nucleophiles and their increased stability profile in comparison to sulfonyl fluorides. These attractive features of the fluorosulfate group render it an interesting area of research in covalent drug design.

2.18 PI4KIII β kinetic binding assay and characterisation of lysine inhibition

Once a selective covalent adduct for PI4KIII β had been obtained, it was important to understand the different binding parameters that contributed to the potency of the covalent inhibition. As shown in **Figure 2.46**, covalent inhibition is a two-step process.^{129,165}

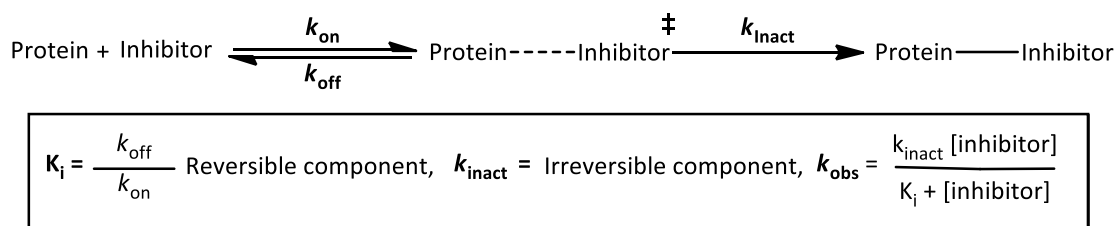
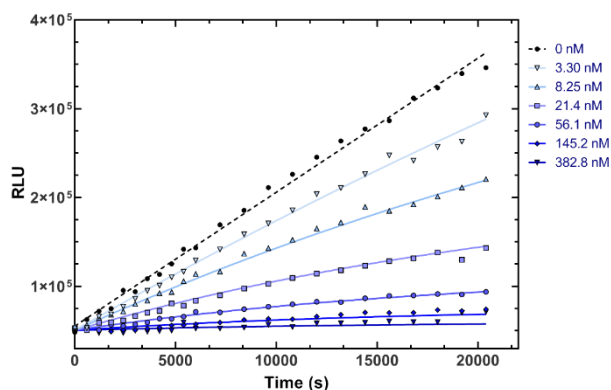


Figure 2.46: Two-step mechanism described by K_i , k_{inact} and k_{obs} .

To determine these parameters for PI4KIII β , a commercially available ADP-glo kit from Promega was used. In this experiment, compounds were profiled against a fixed concentration of recombinant PI4KIII β protein in a dose-dependent manner, and the effects of inhibition were measured by a discontinuous luminescent readout, in a time dependent manner (see **Section 2.24** for experimental details). There were two controls used in this experiment; A high control, which contained no-inhibitor. It was important that over the duration of the assay, the high control always remained linear, which ensured that the decrease in the fluorescent signal was due to the inhibition of the protein and was not from protein degradation; A low control, where the protein was fully inhibited over the duration of the assay with a known PI4KIII β inhibitor. The aim of the experiment was to measure the onset of inhibition which can be correlated with the luminescent readout. The raw data was fitted to the global progress curve analysis described in **Section 2.24** to derive an observed rate constant (k_{obs}). In addition, using the Cheng-Prusoff equation the k_{inact} and K_i were determined.²⁴⁹

Achieving linearity of the high control was difficult due to the prolonged onset of inhibition of compounds **2.46** and **2.47**, therefore, linearity over the duration of the assay was not possible. The measured onset of inhibition was only reliably measured for compound **2.45** and the data obtained is shown in **Figure 2.47**.



Cpd number	K_i (M)	k_{inact} (s^{-1})	k_{obs} ($s^{-1}M^{-1}$)
2.45	1.55×10^{-8}	6.5×10^{-5}	4.2×10^3

Figure 2.47: Measured onset of inhibition of compound **2.45**. See **Section 2.24** for equations used to generate rate and equilibrium constants.

The time course of the assay was significantly extended in comparison to previous literature methods.¹⁸⁹ The K_i value was determined using the Cheng-Prusoff equation and is a measure of the favourable reversible interactions. The smaller the K_i value, the equilibrium is driven more towards forming the initial protein inhibitor complex. The values of k_{on} and k_{off} are not explicitly determined and so the definition of K_i is the concentration of inhibitor required to achieve half-maximal rate of covalent inactivation under these conditions. The measured K_i was 15.5 nM which means the reversible interactions were favourable and a low concentration of **2.45** was required to achieve 50% inhibition. Despite this, the irreversible step, forming a covalent bond (described by k_{inact}), was measured to be $6.5 \times 10^{-5} s^{-1}$, which is orders of magnitude slower than literature precedent for a lipid kinase, thus, the rate of covalent bond formation was deemed to be slow.¹⁸⁹ This could be due to the nucleophilicity of the

lysine residue (potentially pKa related) and/ or the electrophilicity of the fluorosulfate. The previous reactivity experiments had shown that the fluorosulfate group was less reactive in comparison to analogous sulfonyl fluoride compounds.¹⁴² As a result, the overall observed rate described by k_{obs} was slow. Therefore, compound **2.45** is suitable for a slow-onset of inhibition with a prolonged duration of action.

A selective, stable and relatively slow covalent modification of compound **2.45** was observed. From the tool crystal structure shown in **Figure 2.24**, it was likely that compound **2.45** covalently modified Lys549. To have absolute certainty that Lys549 was covalently modified, either a trypsin digestion experiment or protein crystallography would be required. Additionally, to assess the nature of an irreversible compound, a jump dilution assay can be carried out.^{250,251} Whereby, the covalent adduct is forced to occur as the initial concentration of the inhibitor is equivalent to the pIC_{90} such that the fluorescent readout signal is weak. A series of dilution experiments is carried out to its pIC_{10} and for a reversible compound, the fluorescent readout regains signal as the dilution increases (**Figure 2.48**). Whereas, for an irreversible compound, the fluorescent signal should remain low. This experiment was carried out under a variety different experimental conditions. However, due to the slow onset of the compounds the assay was unsuccessful, as only the reversible interactions were captured before observing protein degradation under these experimental conditions.

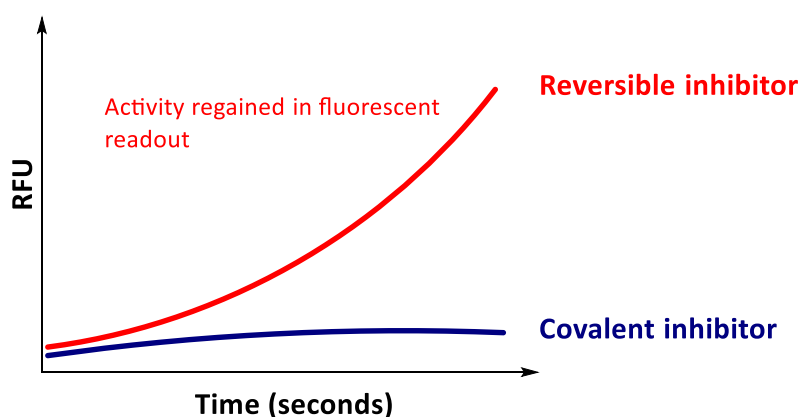


Figure 2.48: Schematic diagram of a jump dilution assay.

Protein crystallography was used in an attempt to identify the residue participating in the covalent modification. Co-crystallisation of compound **2.45** with PI4KIII β was required (crystallographer: Don O Somers).

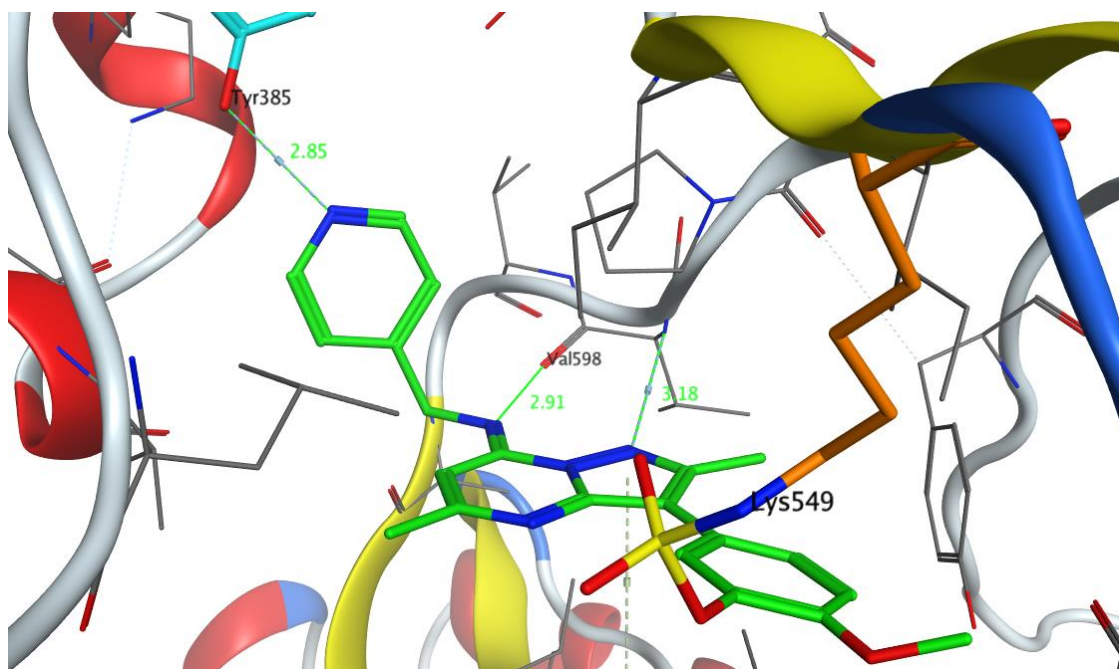
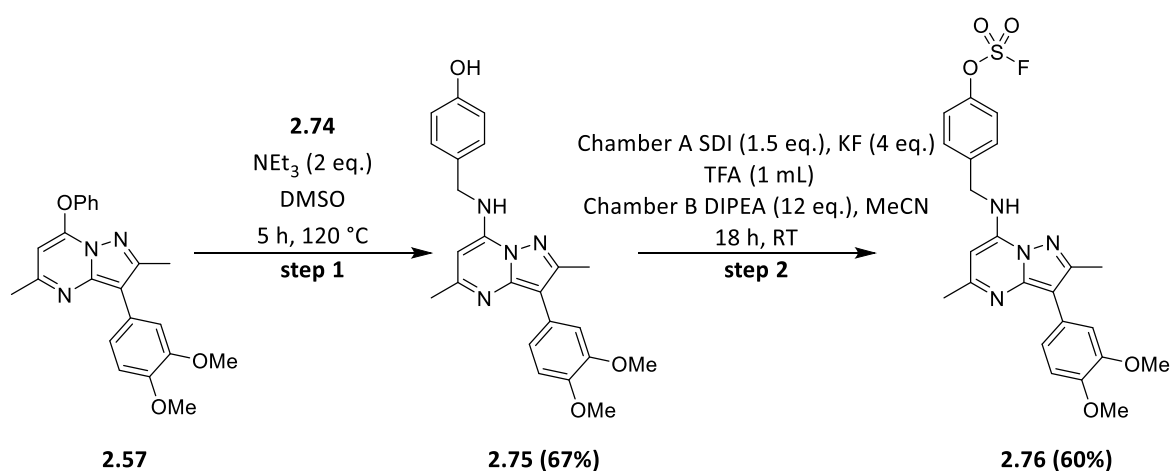


Figure 2.49: Crystal structure of compound **2.45** covalently modified Lys549 in PI4KIII β with resolution of 1.60Å.

Pleasingly, electron density consistent with compound **2.45** forming a covalent bond with Lys549 to form a sulfamate was observed (**Figure 2.49**). The oxygen linker directed the warhead to interact with Lys549; potentially the rotation about the fluorosulfate warhead was restricted due to the steric clash with the *ortho* methoxy substituent. Compound **2.45** bound similarly to compound **2.23** (**Figure 2.24**) through a hinge binding interaction between the valine backbone and the nitrogen donor/acceptor atoms of the heterocyclic core. In addition to this, the *para* pyridyl head group formed a favourable hydrogen bonding interaction with Tyr385. This gave rise to a log unit increase in potency as identified for the phenolic ester series (**Table 2.4**).

2.19 Targeting tyrosine

As previously discussed in **Section 2.15**, an amino acid screen was carried out where both lysine and tyrosine residues were shown to react with the fluorosulfate group under basic conditions. To date, there are two examples of a fluorosulfate containing compound reacting with lysine residue. The majority of the literature has shown fluorosulfate containing compounds to react with tyrosine residues.^{215,216,248} As shown in **Figure 2.49**, the *para*-pyridyl head group of compound **2.45** formed a favourable hydrogen bonding interaction with a nearby tyrosine residue (Tyr385). Based on the reported reactivity of fluorosulfate warheads targeting tyrosine and the crystal structure displaying a hydrogen bonding interaction with the phenol group of the tyrosine, it was hypothesised that Tyr385 could be covalently modified with our PI4KIII β scaffold. As a result, the next step was to synthesise an alternative inhibitor **2.76** to investigate its potential to covalently modify Tyr385. The synthesis of compound **2.76** is shown in **Scheme 2.10**.



Scheme 2.10: Synthesis of compound **2.43**.

Compound **2.76** and the appropriate control compounds **2.75** and **2.77** were screened in the standard project biochemical assays. The data is shown below in **Table 2.8**.

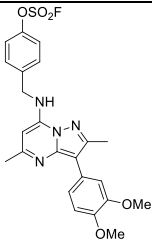
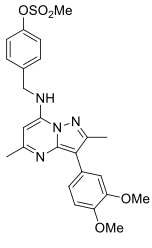
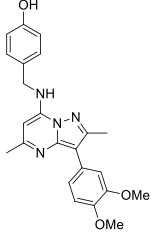
Entry	Cpd number	PI4KIII β pIC ₅₀	CPE pIC ₅₀	Δ (CPE-PI4KIII β)
	2.76	6.3	7.3	1.0
	2.77	6.5	6.7	0.2
	2.75	7.4	7.4	0

Table 2.8: Biochemical data for alternative covalent compound **2.76** and control compounds **2.77** and **2.75**.

As shown in **Table 2.8**, compound **2.76** followed the same trend in activity as observed for previous inhibitors, where a significant increase in potency was identified in progressing from the enzyme to the CPE assay. Control compounds **2.75** and **2.77** retained their activity in the CPE assay rather than increasing suggesting they are not covalent modifiers of the protein. It is important to note that potency in the CPE assay for compound **2.75** is similar to the potency of compound **2.76** in the CPE assay. This may suggest that once compound **2.76** entered the cell it underwent hydrolysis to give a phenol which could be responsible for the potency increase. The data represented in **Table 2.8** was encouraging, as the trends were consistent with previous data. The next step was to further profile compound **2.76** in terms of the potential covalent modification of Tyr385.

Before further biochemical evaluation, the stability and reactivity of compound **2.76** was determined. The substitution pattern about the fluorosulfate warhead is different to the previous inhibitors, and accordingly compound **2.76** could have a different stability. Compound **2.76** was profiled under the same stability conditions as previously used (see **Section 2.14**), where the pH and oxidative potential were varied (**Figure 2.50**).

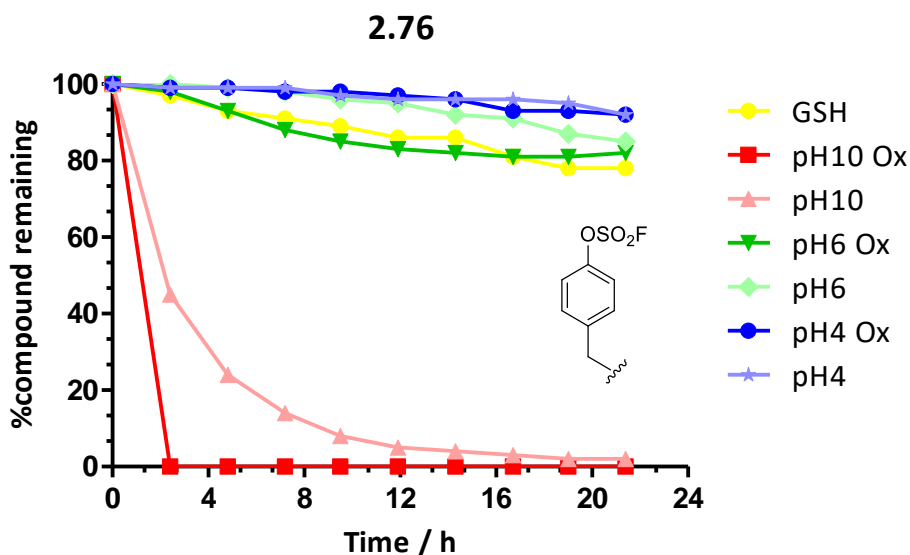


Figure 2.50: Stability plot of compound **2.76** under different conditions at 40 °C.

Compound **2.76** was stable under both neutral and acidic conditions. However, under basic conditions (pH 10), approximately 50% of the compound hydrolysed after 3 h and the rate of hydrolysis was enhanced in the presence of 20 mol% H₂O₂. The data shown in **Figure 2.50** is consistent with the stability data shown in **Section 2.14**, where the compounds were stable under neutral and acidic conditions but were susceptible to hydrolysis under basic conditions. The data suggested that **2.76** was stable under physiological conditions.

The reactivity of compound **2.76** was investigated using the same conditions previously used to profile compounds **2.45**, **2.46** and **2.47**. The substitution pattern for compound **2.76** was different to previous compounds. Encouraged by this, its reactivity was investigated. Initially we investigated lysine as a nucleophile to enable

comparison with previous compounds examined. The reactivity of **2.76** in the presence of lysine was determined as shown in **Figure 2.51** providing an approximate half-life of 60 minutes. The data for these reactivity experiments are shown in **Figure 2.51** and **Figure 2.52**.

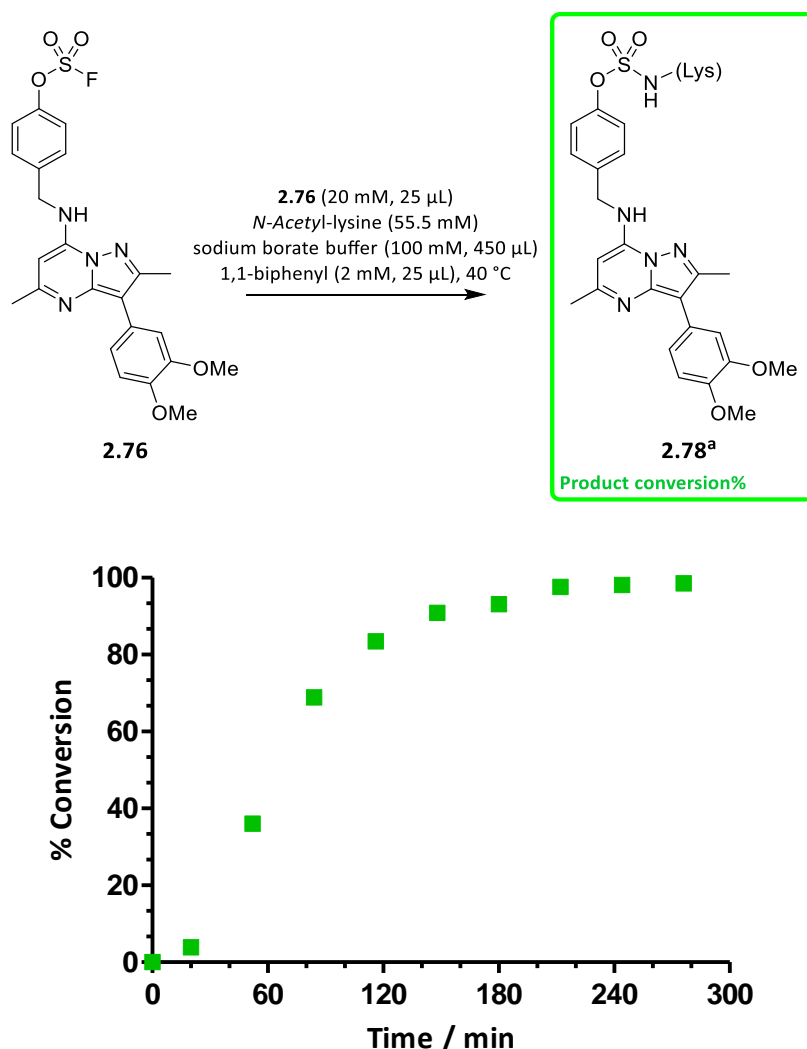


Figure 2.51: The reactivity results of compound **2.76** with *N*-acetyl lysine, monitored by HPLC.

Interestingly, the reactivity of compound **2.76** with protected lysine was enhanced (50% conversion was achieved after 60 minutes) in comparison to compound **2.46** (50% conversion was achieved after 270 minutes). Also, there was no evidence of hydrolysis of the fluorosulfate group, suggesting a *para*-methylphenyl substitution

pattern increased both the hydrolytic stability and reactivity with lysine under these experimental conditions.

Tyrosine was the target amino acid and so compound **2.76** was profiled against tyrosine as shown in **Figure 2.52**. The pH of the sodium borate buffered solution was measured at pH10.18. After the addition of tyrosine (50 eq.), the pH was reduced to pH9.9. Therefore, the pH of the buffer was approximately equivalent to the pKa to the phenol group of tyrosine (~10).

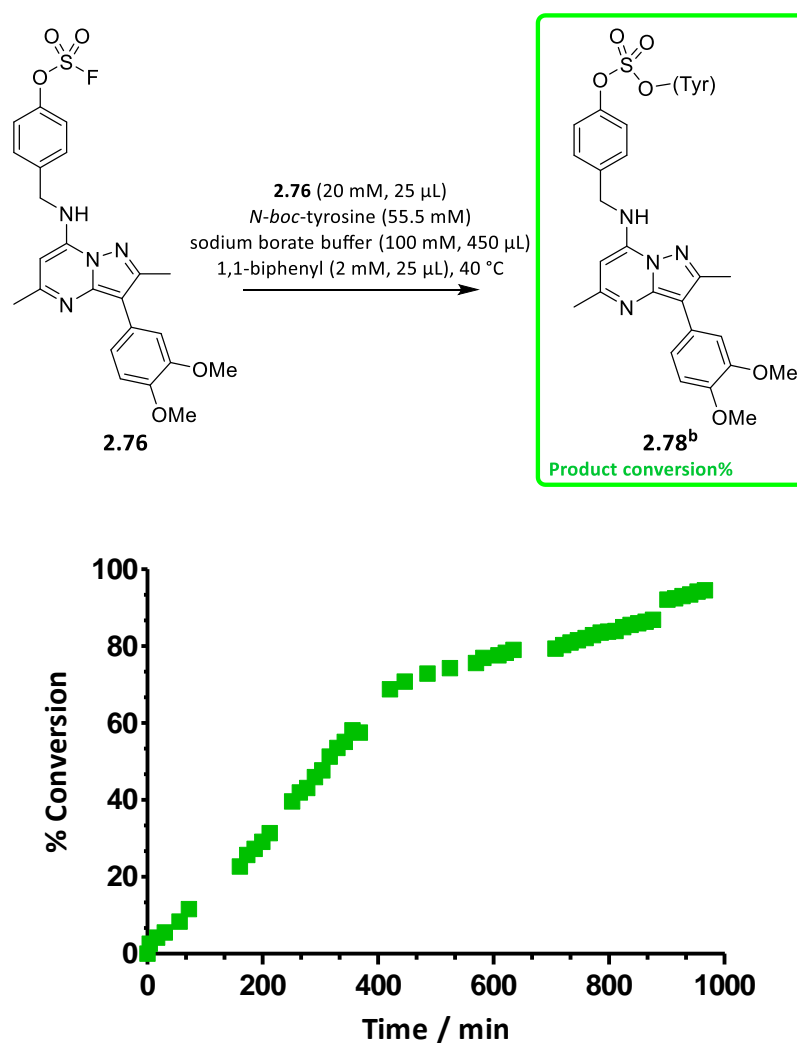
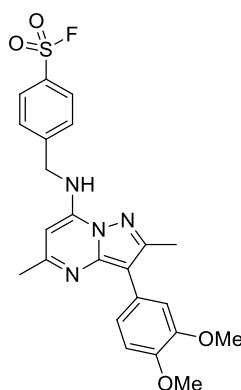


Figure 2.52: The reactivity of compound **2.76** with *N*-*Boc*-tyrosine monitored by HPLC.

A 5-fold decrease in the reactivity for compound **2.76** was observed for the reaction with tyrosine (50% conversion was achieved after 300 minutes) in comparison to the reaction with lysine (50% conversion was achieved after 60 minutes). This could be due to the different nucleophilicity of the phenol group at tyrosine and the free amine of lysine. No signs of hydrolysis was observed for compound **2.76** over the extended reaction time course, supporting the stability associated with a *para*-methylphenyl substituted fluorosulfate compound. These results indicate that compound **2.76** may require a longer incubation time to covalently link with Tyr385. However, as previously shown, the reaction profile can significantly differ from an aqueous buffered environment to a local protein microenvironment.

Compound **2.76** showed an increased stability profile in the reactivity experiments in comparison to the previous series of fluorosulfate covalent inhibitors (**2.45**, **2.46** and **2.47**). In light of this, a sulfonyl fluoride based inhibitor, compound **2.80** (shown in **Table 2.9**) was synthesised in high yield using our strategy. Compound **2.80** was moisture stable. Despite the increased stability associated with compound **2.80**, the physicochemical properties and biochemical data of the compound was poor, therefore, no further work was carried out on compound **2.80**.



Cpd number	PI4KIIIβ pIC ₅₀	CPE pIC ₅₀	Kinetic sol. (μg/ mL)	ChromLogD _{7.4}	AMP (nm/s)
2.80	<5	<5	-	-	-

Table 2.9: Biochemical and physicochemical data for compound **2.80**.

2.20 Characterisation of tyrosine targeted covalent inhibition

Mass spectrometry was again used to characterise the potential covalent interaction of compound **2.76** with Tyr385. The experimental conditions were the same as previously adopted (see experimental **Section 2.24** for the experimental procedure) and in **Figure 2.53** represents a mass spectrometry time course experiment for compound **2.76** with PI4KIII β protein.

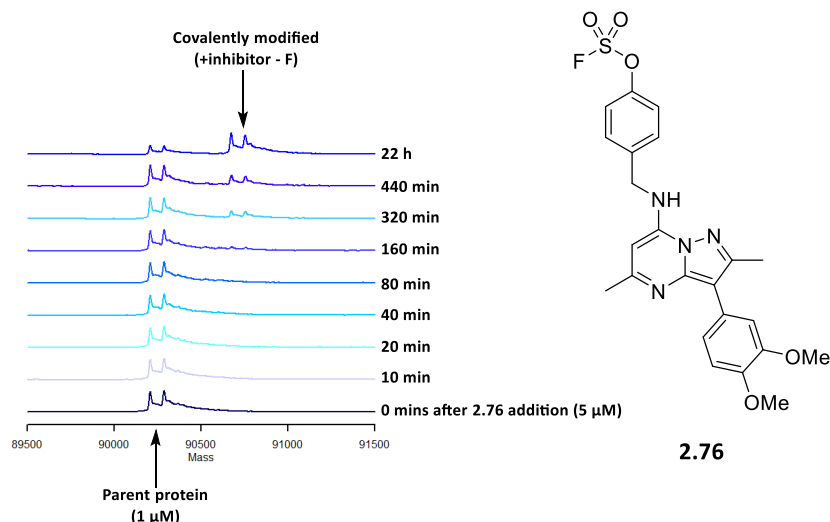
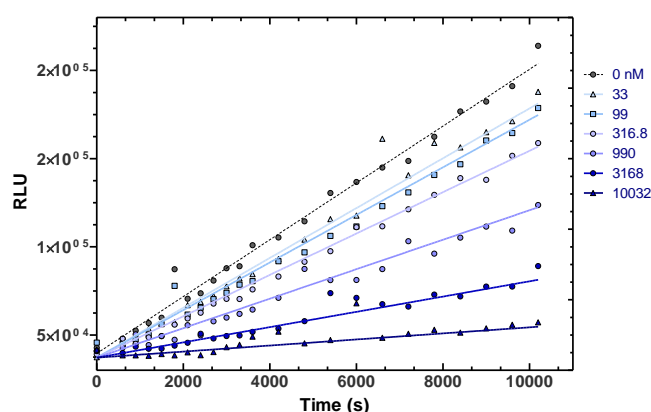


Figure 2.53: Time course of reaction of **2.76** with recombinant PI4KIII β at 10 °C.

Pleasingly, a covalent modification was detected with compound **2.76** and PI4KIII β with no signs of additional covalent adducts. It took approximately 22 h to achieve \sim 90% conversion and so a longer incubation time was required to engage with Tyr385. This could have been due to the reduced nucleophilicity of the tyrosine residue which is consistent with the reactivity experiment shown in **Figure 2.52**. Compound **2.76** was less potent in the biological assays in comparison with previous fluorosulfate inhibitors **2.45**, **2.46** and **2.47**. This suggests that the reversible interactions of **2.76** with PI4KIII β were less favourable which influenced the rate of the covalent modification of tyrosine.

After a covalent adduct was established using protein intact mass spectrometry, the next step involved understanding the rate of the covalent modification. As previously mentioned, the rate of covalent modification was considerably slower. To understand this phenomenon further, the kinetics of the reversible and irreversible steps were determined for compound **2.76** as shown in **Figure 2.54**.



Cpd number	K_i (M)	k_{inact} (s^{-1})	k_{obs} ($s^{-1}M^{-1}$)
2.76	1.35×10^{-6}	$\leq 1.6 \times 10^{-6}$	≤ 1.2

Figure 2.54: Measured onset of inhibition of compound **2.76**.

Compound **2.76** was significantly slower in forming the covalent adduct with the protein in comparison to compound **2.45** as shown by protein mass spectrometry. The reversible step K_i for **2.76** was approximately $\sim 1.4 \mu\text{M}$ and the irreversible step k_{inact} was $\leq 1.6 \times 10^{-6} s^{-1}$. This correlates to a much higher concentration of compound required to form the reversible complex in comparison to compound **2.45** (**Figure 2.47**), showing the reversible interactions to be less favourable. In addition, the inactivation step was an order of magnitude slower for compound **2.76** in comparison with **2.45**. This suggested that the formation of the covalent bond was significantly slower. Consistent with the previous reactivity and mass spectrometry experiments this is possibly due to the reduced nucleophilicity of the phenol group of tyrosine. As

a result, the overall observed rate described by k_{obs} for **2.76** was extremely slow (≤ 1.2).

To determine the site of covalent modification, X-ray crystallography was carried out on a cocrystal of PI4KIII β in complex with with compound **2.76**. As shown in **Figure 2.55**, Tyr385 was covalently modified by compound **2.76** through displacement of the sulfur fluoride bond as anticipated. The hinge binding interaction with the valine backbone was as expected and also, Lys549 formed a bifurcated hydrogen bonding interaction with the dimethoxy substituents. This result highlights the versatility of the fluorosulfate group, where two different amino acids were selectively covalently modified using the fluorosulfate group as a covalent warhead.

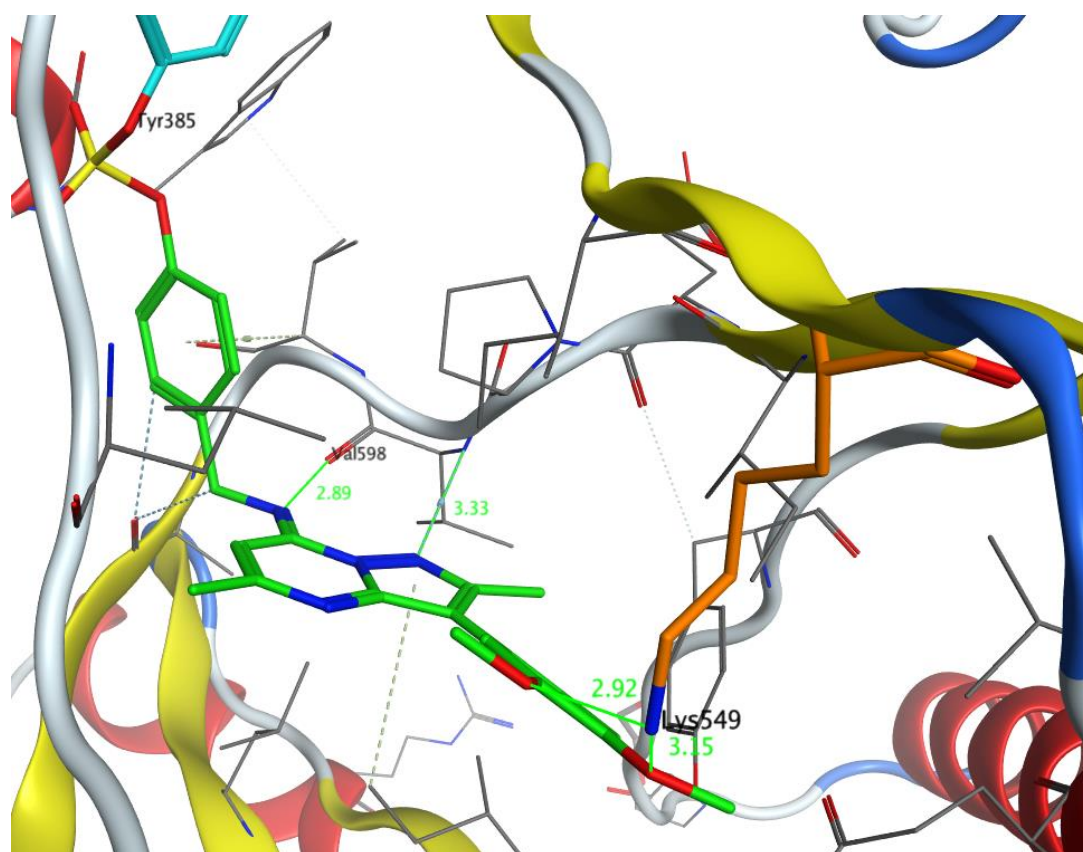
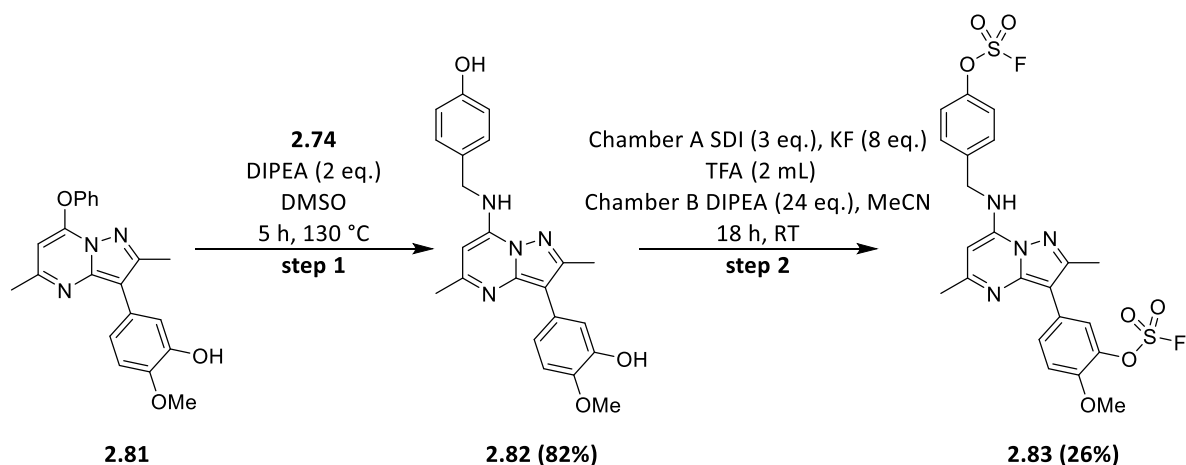


Figure 2.55: Crystal structure of compound **2.76** covalently modified Tyr385 in PI4KIII β with resolution of 1.77Å.

2.21 Dual covalent inhibitor

The next part of the work involved building upon the current knowledge of fluorosulfate containing compounds and PI4KIII β . So far, compound **2.45** covalently modified Lys549 and compound **2.76** covalently modified Tyr385. We were intrigued to discover if a compound containing two fluorosulfate warheads could target both Lys549 and Tyr385 at the same time, acting as a dual covalent PI4KIII β inhibitor **2.83**. The synthesis of this inhibitor follows a similar route as previously outlined (**Scheme 2.11**), additional equivalents of reagents were used to ensure sufficient amounts of SO₂F₂ (g) was generated in order to react with the bis-phenol **2.82**.



Scheme 2.11: Synthesis of dual covalent inhibitor **2.83**.

Sufficient quantities of **2.83** was obtained using the COware reactor and the compounds to test this hypothesis were profiled in the biochemical assays (**Table 2.10**), including the bis-phenol control **2.82**.

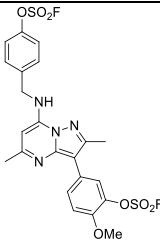
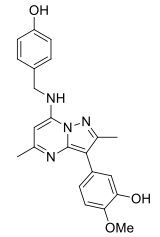
Entry	Cpd number	PI4KIIIβ pIC ₅₀	CPE pIC ₅₀	Δ (CPE-PI4KIIIβ)
	2.83	<5	6	>1.0
	2.82	6.6	6.4	-0.2

Table 2.10: Biochemical data for potential dual covalent inhibition.

Compound **2.83** followed the same trend as observed for previous covalent inhibitors, except compound **2.83** appeared inactive in the enzyme assay, but potency was observed in the CPE assay, indicative of time dependent inhibition. The reversible control compound **2.82** had similar potencies in both the enzyme and CPE assay. Also, compound **2.82** displayed greater activity in both assays suggesting the bis-fluorosulfate **2.83** may not be accommodated in the ATP binding pocket as effectively as the bis-phenol **2.82**.

To assess the ability of compound **2.83** acting as a dual covalent inhibitor, intact protein mass spectrometry was carried out. Time dependent mass spectrometry was carried out for compound **2.83**, with the expected covalent adduct molecular ion. The data for this experiment is shown in **Figure 2.56**.

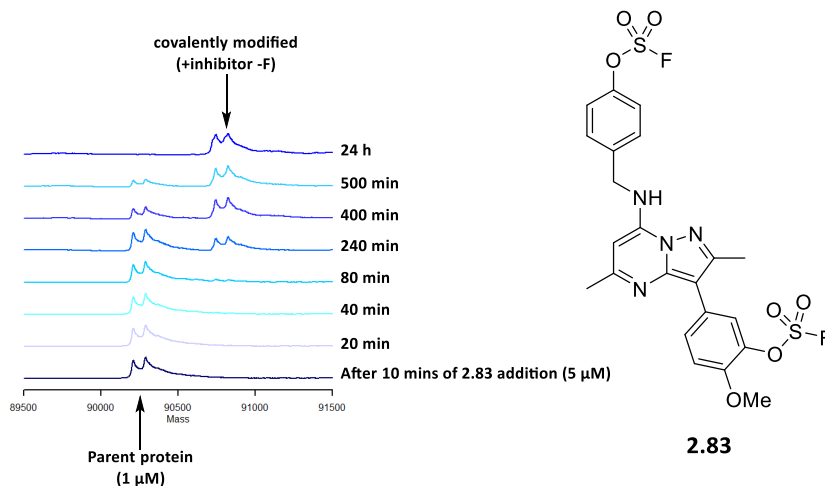


Figure 2.56: Time course of compound **2.83** with recombinant PI4KIII β at 10 °C.

Pleasingly, compound **2.83** covalently modified PI4KIII β , fully labelling the protein after 24 h. The slow rate of covalent modification was expected due to the weaker binding affinity of the compound, suggesting a higher concentration of inhibitor would be necessary to achieve the initial reversible complex. Two covalent modifications are expected to take place and based on the previous mass spectrometry evidence, it was anticipated that Lys549 would covalently modify **2.83** first, followed by the reaction of Tyr385. It is important to note that the loss of two fluorine atoms was expected, however, due to the high molecular weight of PI4KIII β (~ 90 kDa) and poor resolution of the mass spectrometry instrument, the mass shift of the loss of two fluorine atoms was not clear. To help investigate the possibility of a dual interaction in the protein, X-ray crystallography was again used as a technique to help characterise the adduct of **2.83** and PI4KIII β .

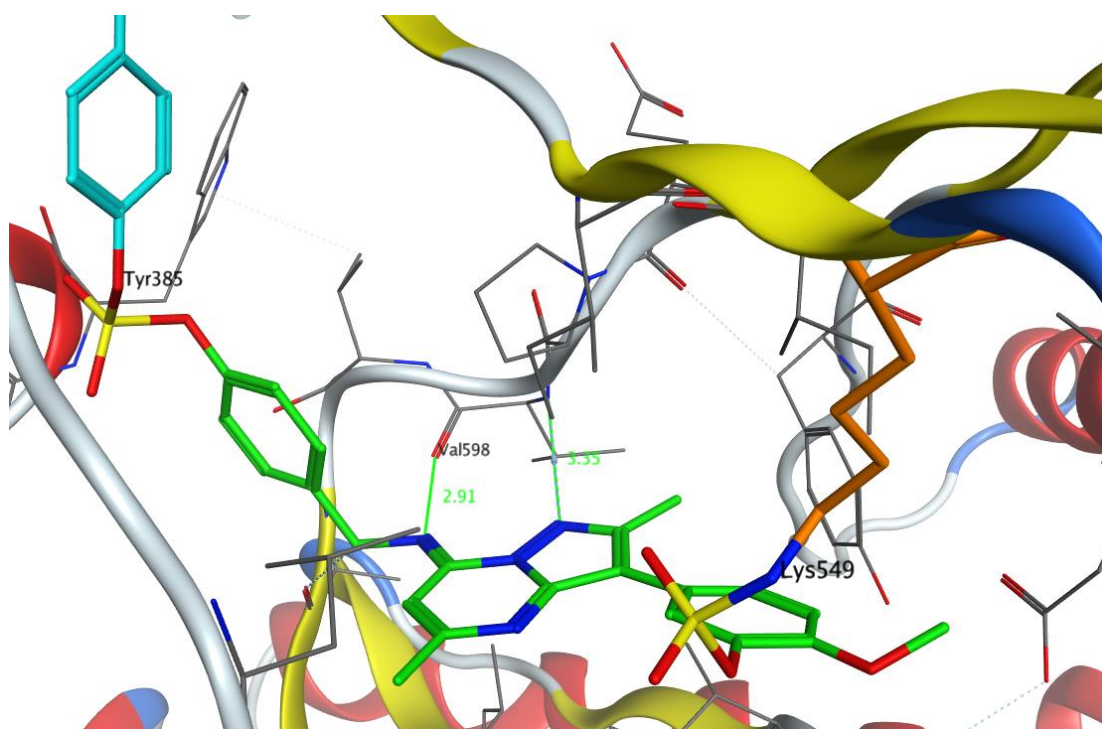


Figure 2.57: Crystal structure of dual covalent compound **2.83** engaged with Lys549 and Tyr385 in PI4KIII β with resolution with 2.09Å.

As shown in **Figure 2.57**, compound **2.83** adopted the expected binding mode covalently labelling both Lys549 & Tyr385. Overall, the research carried out highlights the potential of the fluorosulfate group as a covalent modifier targeting non-cysteine residues in proteins, an emerging area of research in drug discovery.²⁵² Recently, Lei wang and co-workers have reported the first unnatural amino acid containing a fluorosulfate warhead that undergoes sulfur fluoride exchange on proteins *in vivo*.²¹⁹ After a 48 h incubation at 37 °C, the fluorosulfate group was found to selectively react with proximal lysine, histidine and tyrosine residues, generating a covalent intra-protein bridge and inter-protein crosslink of interacting proteins directly in living cells as shown in **Figure 2.58**. They believe the genetically encoded amino acids containing fluorosulfate groups is the next generation of click chemistry, which can be further expanded in chemical biology and drug discovery. No cytotoxic effects were observed through incorporation fluorosulfate group up to high concentrations of the modified amino acid (1 mM). Therefore, it could be envisioned that dual containing

fluorosulfate molecules can be of interest through *in vivo* screening, in an attempt to engage with non-cysteine residues in single or multiple protein targets.

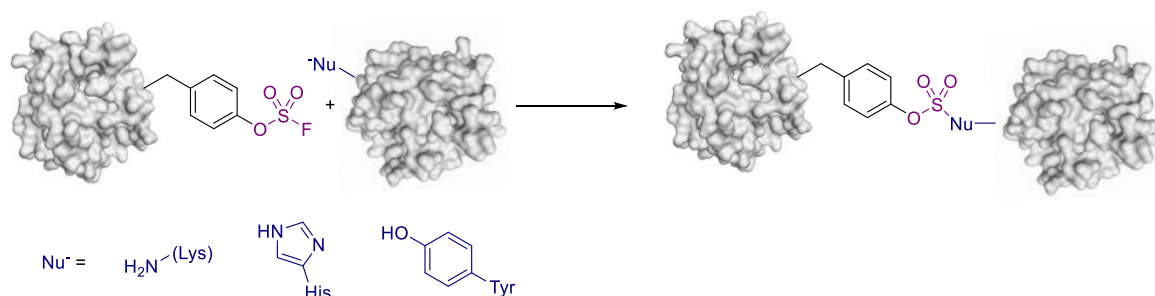


Figure 2.58: Genetically modified tyrosine containing a fluorosulfate warhead to crosslink with proteins.

The aim of this project was to develop a selective irreversible covalent inhibitor of PI4KIII β which targeted the conserved lysine in the ATP binding site. Outlined in previous sections of Part Two of this thesis, a selective covalent inhibitor targeting the lysine residue in PI4KIII β was achieved. Upon discovery of the fluorosulfate warhead, inhibitors (**2.45**, **2.46** and **2.47**) displayed a slow onset of inhibition, placing more emphasis on initial reversible interactions of the covalent modification where an inherent selectivity for the protein could be achieved. After identifying potential nucleophilic amino acids which the fluorosulfate warhead could react with, and the use of X-ray crystallography, an alternative inhibitor (**2.76**) was synthesised. Selective covalent modification of a tyrosine residue was observed, where the reactivity of the fluorosulfate warhead was lower for tyrosine in comparison to lysine. This data suggests that the reversible interactions of the fluorosulfate group are crucial for covalent attachment with the protein. Building upon this exciting finding, the inhibitors were merged to form the first dual covalent inhibitor (**2.83**) targeting both lysine and tyrosine. Where X-ray crystallography was used to support the proposed interaction, this exciting discovery broadens the scope of the potential of fluorosulfate based inhibitors in drug discovery.

2.22 Fragment library design

For the past 20 years, fragment based drug discovery has been implemented into the drug discovery process.²⁵³ The fragment-based approach consists of finding new potent small molecule ligands which bind to the protein target; usually through hydrophobic, Van der Waals and hydrogen bonding interactions.²²¹ When a 'hit' compound has been identified, it can usually serve as a starting point for optimising inhibitor protein interactions in the early stages of the drug development process. The use of fragments in drug discovery has translated into numerous compounds entering the clinic and so there is a demand to develop diverse fragment libraries.²⁵⁴ As shown in **Figure 2.59**, the small molecule ligands (shown in red) were initially identified for interacting with the protein target.²⁵³ X-ray crystallography and biochemical data typically assist the design of small molecules (shown in blue) where additional interactions can be explored. This has proven to be a successful approach for discovering potent small molecule candidates (**2.84** and **2.85**).²⁵³

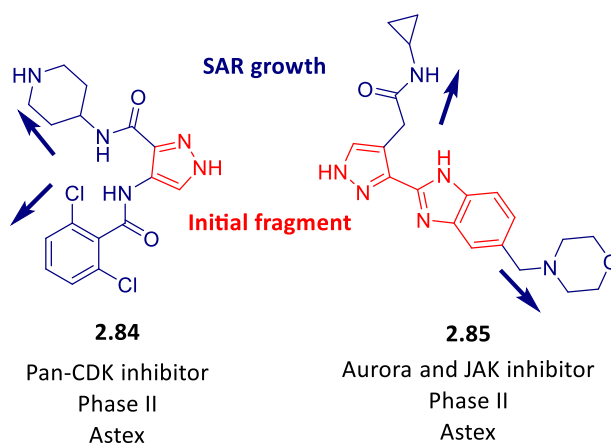


Figure 2.59: Examples of fragment based drug discovery derived drugs that have entered the clinic.

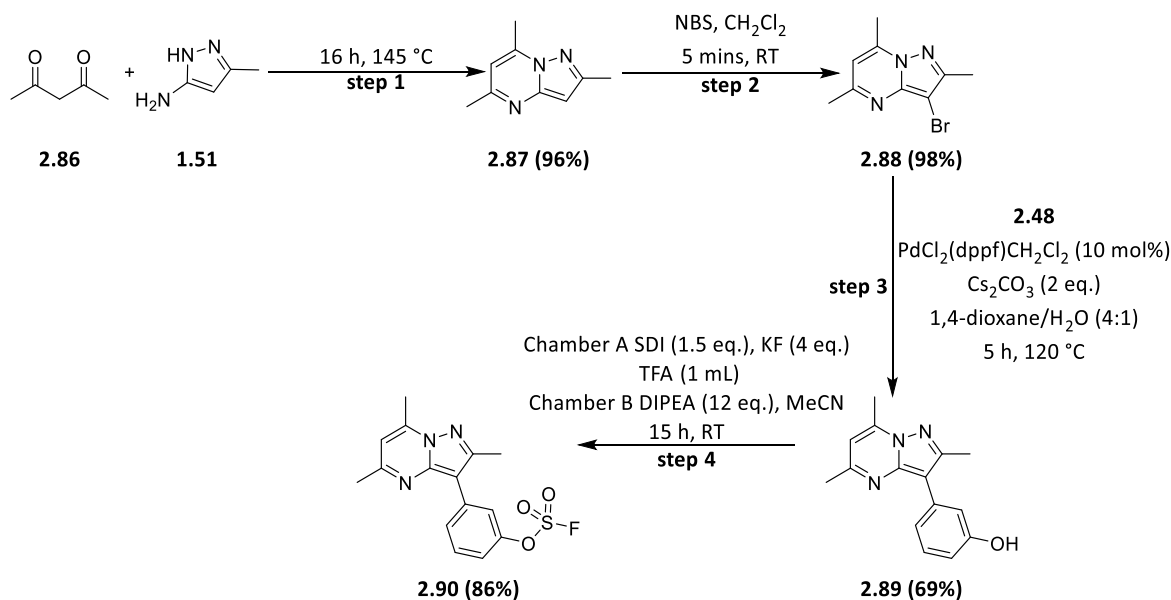
Generally, when synthesising a fragment library, the following criteria are considered:²⁵⁵

- Soluble at high concentrations (~ 500 μ M).
- MW ~200-300 Da.
- Stable over time.
- Small differences in chemical structure
- Simple to synthesise
- clogP <3

Once a fragment library has been synthesised, the fragments are then screened against protein targets. A variety of detection methods can be used to measure the protein fragment interactions: mass spectrometry (if covalent fragments are used), surface plasmon resonance (SPR), Thermal shift assay, X-ray crystallography and NMR (WaterLOGSY). After a fragment has been identified, then subsequent SAR can be carried out to establish potent inhibitors for the protein of interest.

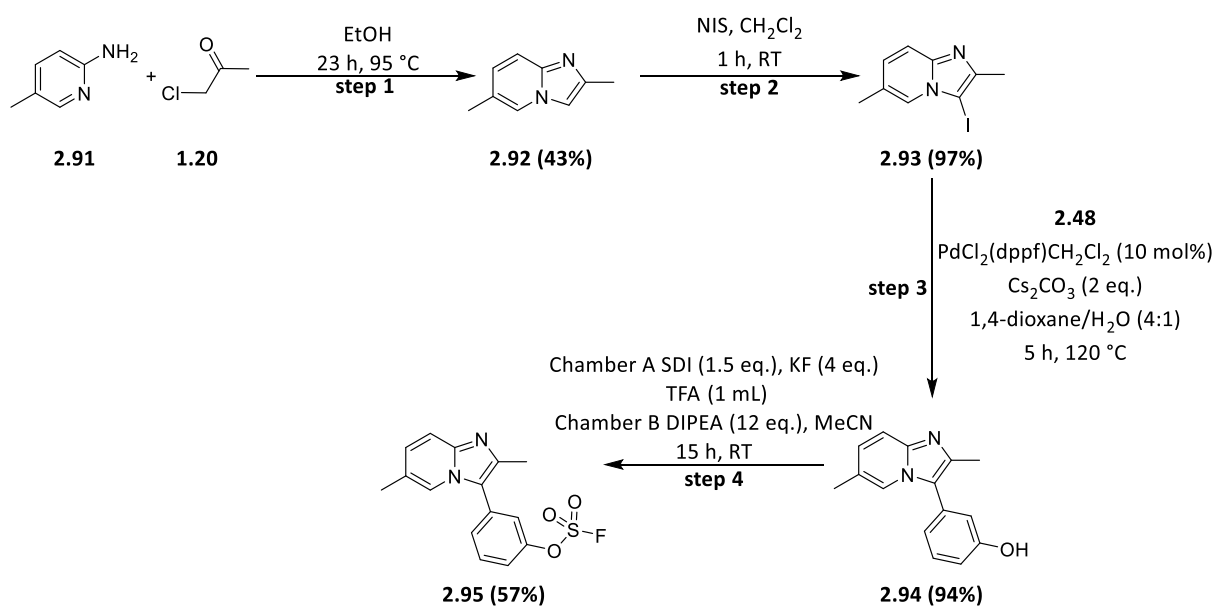
Recently, there has been increasing recent literature around covalent fragment libraries, particularly for targeting cysteine residues using α,β -unsaturated esters.²⁰¹ The high throughput nature of screening covalent fragments against protein targets is attractive, as the process is more time effective and mass spectrometry can be used to detect for covalent labelling. The next step of my project involved optimising a first generation fluorosulfate fragment library for screening against protein targets.²³⁵ PI4KIII β was selected as a model protein of interest for validating the concept of a covalent fluorosulfate fragment library due to our experience to date (**Section 2.21**). It was anticipated that molecules containing a fluorosulfate group of a cut-down PI4KIII β template could covalently modify the protein, thus validating the concept of the fragment library.

Fragment **2.90** was synthesised as shown in **Scheme 2.12**. This scaffold was selected in developing our covalent probes as it contained the equivalent pyrazolopyrimidine core (Core 4) used for previous PI4KIII β covalent inhibitors. It was anticipated that this template could still obtain similar recognition in the ATP binding site of PI4KIII β .



Scheme 2.12: Synthesis of PI4KIII β fragment **2.90**.

A supplementary fragment **2.95**, was prepared as shown in **Scheme 2.13**. The expected potencies for these fragment PI4KIII β covalent probes (**2.90** and **2.95**) was expected to drop significantly, due to the fact that the complexity of the molecule was reduced and so the protein inhibitor interactions would be weaker. **2.95** was synthesised to ensure that the covalent fragment was soluble at a high enough concentration to detect a covalent modification of PI4KIII β . As outlined in Section One of this thesis, Core 1 (**1.25-1.27**) offered improved solubility over the other templates investigated and due to the expected decreased binding affinity, a high concentration of these fragments could be required.



Scheme 2.13: Synthesis of PI4KIII β fragment **2.95**.

Fragments **2.90** and **2.95** were profiled in the PI4KIII β enzyme and cell assays, along with the physicochemical assays. The data is presented in **Table 2.11**.

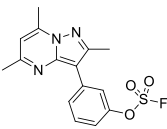
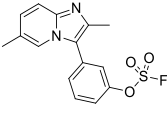
Entry	Cpd number	PI4KIII β pIC ₅₀	CPE pIC ₅₀	Kinetic sol. ($\mu\text{g/mL}$)	ChromLogD _{7.4}	AMP (nm/s)
	2.90	<5	5.4	6	7.2	820
	2.95	<5	<5	65	5.9	485

Table 2.11: The biochemical and physicochemical data for fragments **2.90** and **2.95**.

Compound **2.90**, with an additional methyl group, displayed less favourable physicochemical properties with a higher ChromLogD_{7.4} (increased lipophilicity) and low kinetic aqueous solubility (6 $\mu\text{g mL}^{-1}$). Whereas, fragment **2.95** displayed more

desirable properties with a smaller ChromLogD_{7.4} (5.9) and higher kinetic aqueous solubility (65 µg mL⁻¹). As anticipated, fragments **2.90** and **2.95** were inactive in the enzyme assay up to the concentration tested (10 µM final assay concentration, see **Section 2.24** for details) which could be due to the loss of the bidentate hinge binding interaction. Fragment molecules frequently need to be investigated at high concentrations in order to detect their binding. It was possible that the compound concentration used in this experiment may not have been high enough to detect binding. In both of the biological assays, ATP is present (kinase competitive inhibitor) at high concentrations (100 mM), which could potentially prevent fragments **2.90** and **2.95** from binding to the active site of PI4KIIIβ.

To account for the potential of weak binding, a serial dilution for fragments **2.90** and **2.95** was investigated against PI4KIIIβ using protein intact mass spectrometry as the detection method. The fragments were incubated with recombinant PI4KIIIβ protein at 10 °C for 24 h and were analysed by mass spectrometry (**Figure 2.60**). Compound **2.98** (**Scheme 2.14**) the control fragment in the mass spectrometry experiment showed no signs of covalently modifying PI4KIIIβ (see **Appendix 3.5**). This suggests that fragments **2.90** and **2.95** were bound to the active site of PI4KIIIβ and that the reversible interactions with the protein were important to enable covalent modification.

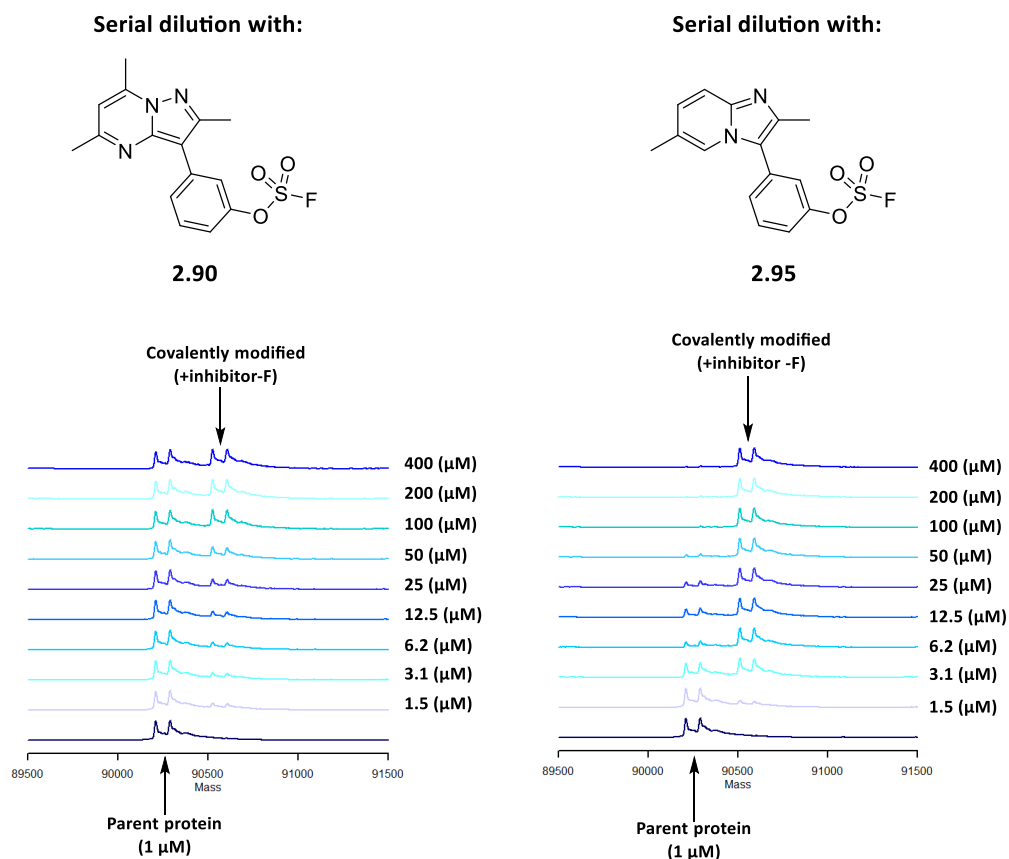


Figure 2.60: Mass spectrometry of fragment **2.90** and **2.95** after 24 h incubation with recombinant PI4KIII β at 10 °C.

Pleasingly, both fragments **2.90** and **2.95** covalently modified PI4KIII β only once after a 24-hour incubation (**Figure 2.60**). Interestingly, fragment **2.90** showed approximately 50% labelling of the protein at 100 μ M, whereas, for fragment **2.95**, the more soluble scaffold, approximately 50% labelling of the protein was observed at 3.1 μ M. **2.95** took up to 24 h to achieve 100% labelling of the protein at 100 μ M without additional covalent adduct formation at these high concentrations. Therefore, fragments **2.90** and **2.95** were significantly slower in covalently modifying PI4KIII β under these experimental conditions when compared to **2.45** (**Section 2.17**) which was most likely due to the weaker binding affinity.

It is proposed that the hydrophobic methyl group in **2.90** is not accommodated in the active site as well as the NH moiety, potentially due to a clash with Val598. A maximum of only 50% covalently modified PI4KIII β was achieved after 24 h. A longer

incubation time would be necessary to achieve full conversion with Lys549. For the larger molecules such as **2.46**, the NH donor group could form a favourable hydrogen bonding interaction with the carbonyl oxygen atom of Val598, increasing the binding affinity of the compound and as a result increasing the rate of covalent modification (shown in **Figure 2.61**).

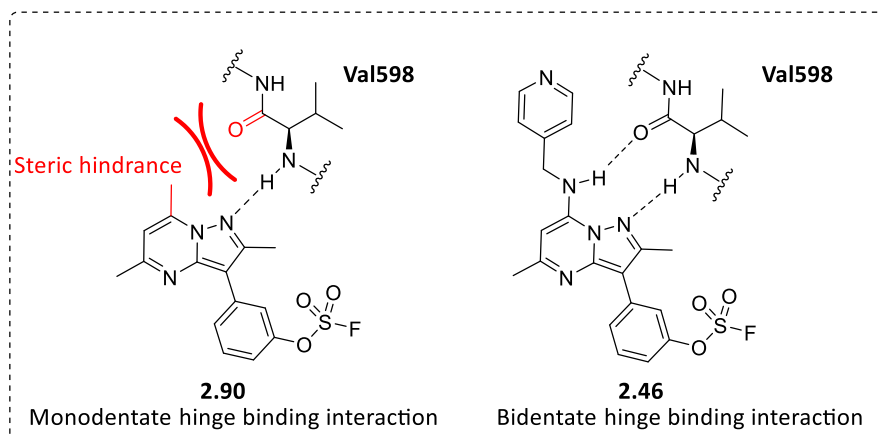


Figure 2.61: Different hinge binding interactions, potentially influencing the rate of covalent modification.

In an attempt to understand the binding modes of fragments **2.90** and **2.95**, they were soaked at high concentration into PI4KIII β crystals. Suitable electron density was obtained, and the fragments were overlaid to compare their modes of binding (**Figure 2.62**). Both fragments formed a monodentate hinge binding interaction with the amino group of Val598 through the nitrogen lone pair of the five membered ring. Compound **2.90**, which contained a methyl group, adopted a different binding mode to reduce the steric interaction with the oxygen of Val598, which was believed to be responsible for the slower rate of covalent modification observed. To validate this hypothesis, the methyl group in **2.90** could be replaced with a bulkier hydrophobic substituents e.g. an *iso*-propyl or *tert*-butyl group. It could be envisioned that the rate of the covalent modification could be reduced by changing the steric requirements at this position.

Both fragments **2.90** and **2.95** positioned the fluorosulfate group on the opposite face in comparison with compound **2.45** (see **Figure 2.49** and **Figure 2.62**). The presence of the *ortho*-methoxy group in **2.45** may have restricted the rotation about the oxygen sulfur bond, increasing the rate of the covalent modification. Whereas, in the case of **2.90** and **2.95**, the combination of lower binding affinity and unrestricted rotation about the oxygen sulfur bond contributed to the slower rate of covalent binding. The rate of the covalent modification could potentially be tuned by altering the substitution pattern on the *ortho*-methoxy substituent (**2.45**) e.g. an *iso*-propyl group. This change could help anchor the fluorosulfate warhead in a conformation to promote covalent modification with Lys549. This would be the type of change carried out during the optimisation of a fragment approach.

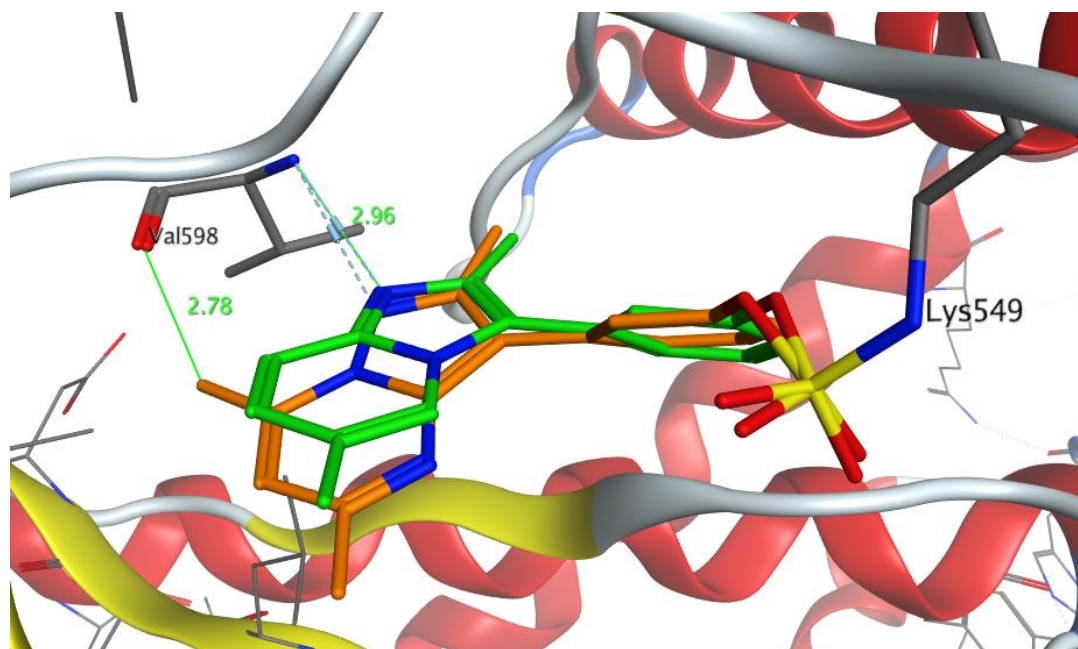


Figure 2.62: Crystal structure of fragments **2.90** and **2.95** engaged with Lys549 in PI4KIII β with resolution of 1.67Å.

In conclusion, this work demonstrated that low molecular weight fluorosulfate fragment molecules could label a lysine residue in a protein such as PI4KIII β . The weak covalent fragments could selectively bind to the lysine in PI4KIII β without labelling other residues. The reversible interaction between the protein and fragment

molecule enabled the selective covalent modification to occur at a single lysine within the protein.

To capitalise on this successful finding, we designed fragment molecules containing a fluorosulfate as part of a non-cysteine covalent fragment library. As previously shown, the effect of varying the *ortho* substituent can influence the reactivity of the fluorosulfate group significantly. This presents the risk of identifying the most reactive fragment i.e. most promiscuous covalent fragment, instead of the most compatible fragment (based on the reversible interactions) to the protein target of interest. Therefore, an unsubstituted phenyl ring was selected as the minimum pharmacophore necessary within the library. The next decision involved choosing the correct vector to attach the fluorosulfate warhead i.e. *ortho*, *meta* or *para* to the connective group. The *ortho* position was disregarded due to potential steric factors as outlined above. The *para*- and *meta*-positions cover different 3-dimensional spaces, therefore, both positions were selected for modification as shown below in **Figure 2.62**.

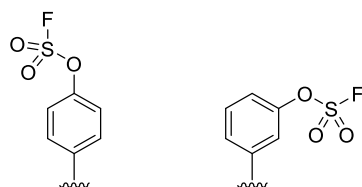
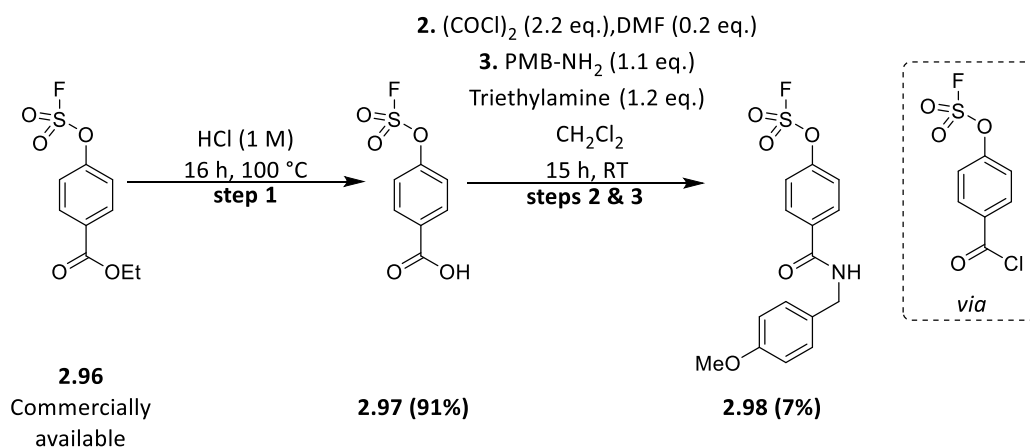


Figure 2.62: Initial design of a *meta*- and *para*-fluorosulfate fragment library.

Subsequently, the next point to address was how to connect the phenyl fluorosulfate groups to the fragment part of the molecule. In medicinal chemistry, it has been well established that the amide bond is one of the most useful bonds to introduce diversity.²⁵⁶ The amide bond is strong, stable and there are multiple ways of constructing it in high yield.²⁵⁷ Another important consideration was the synthetic sequence and to avoid potential hydrolysis of the fluorosulfate group. To date, the chemistry associated with the preparation of the fluorosulfate group is limited and requires a late stage functionalisation of a phenol. After searching through the

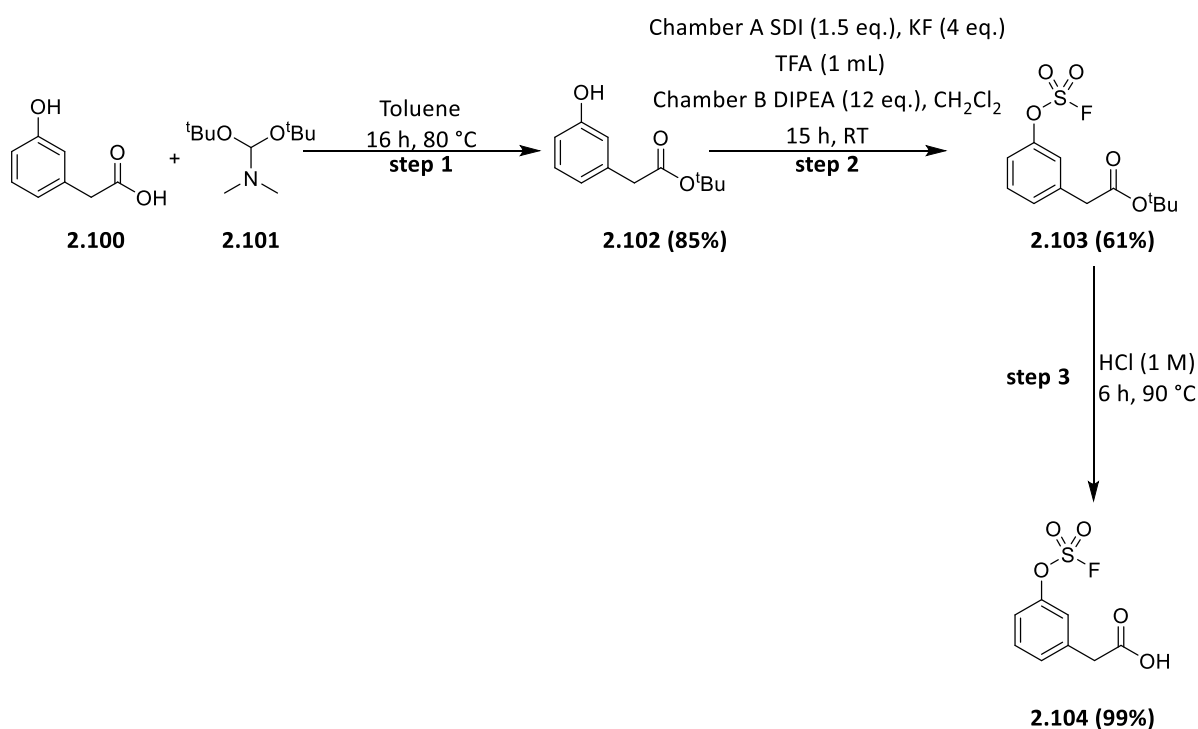
catalogues of Sigma-Aldrich, there was an interesting commercially available compound **2.96** and so this was used to investigate the potential of synthesising a fluorosulfate fragment library (**Scheme 2.14**).



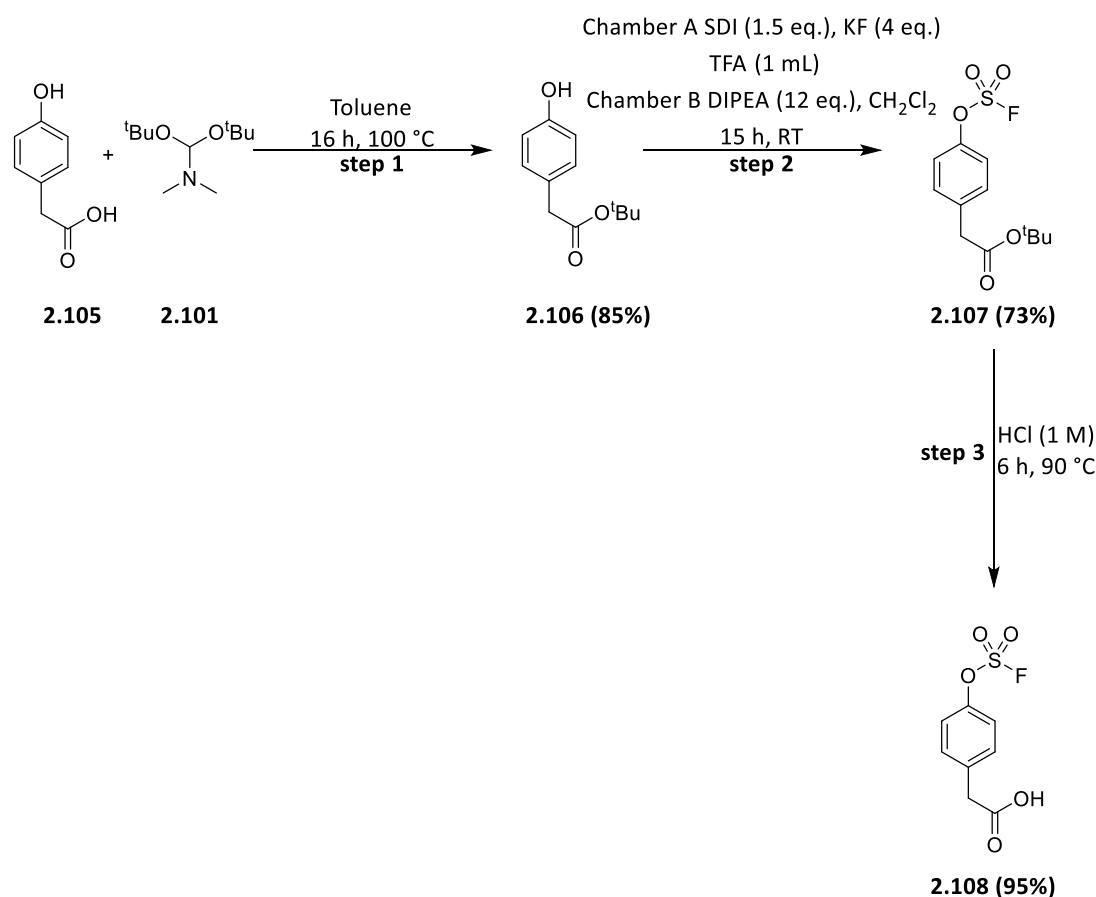
Scheme 2.14: Reaction scheme for the preparation of a fluorosulfate fragment library.

Commercially available ethyl 4-(fluorosulfonyloxy)benzoate **2.96** was treated with HCl (1 M) at 100 °C to give the corresponding carboxylic acid **2.97** without showing any signs of hydrolysis of the fluorosulfate group. Compound **2.97** was converted to the acid chloride which was reacted *in-situ* with *para*-methoxybenzylamine (PMB-NH₂) to give the corresponding amide **2.98**. Steps 2 and 3 of the synthesis gave a low overall yield, and so an alternative route to prepare the amide linker bond would be required for a library synthesis. Another important consideration was the rigidity of the fragment molecules; the flexibility of compound **2.98** is restricted. The carbonyl group of the amide bond is directly connected to the *para*-fluorosulfate aromatic ring and so planarity is embedded into compound **2.98**. The concept of the covalent fluorosulfate fragment library is for the fluorosulfate group to covalently modify nucleophilic residues in many potential protein targets of interest, therefore, a level of molecular flexibility would be important to allow the molecule to fit into a variety of pockets. As a result, it was decided that a phenylacetic acid would be used in the fragment library.

An alternative synthesis for the novel *meta*- and *para*-fluorosulfate fragment library was devised (**Scheme 2.15** and **Scheme 2.16**). The first step involved synthesising a *tert*-butyl ester **2.102**, which would be easier to hydrolyse under acidic conditions than the ethyl ester in the previous synthesis (**Scheme 2.14**). After examining alternative reaction conditions for preparing a *tert*-butyl ester, it was established that di-*tert*-butoxy-*N,N*-dimethylmethanamine **2.101** was the optimal reagent for this transformation. To add significant value to the fluorosulfate fragment library approach, we wanted to avoid carrying out a late stage functionalisation of phenols to construct the fluorosulfate warhead. A one pot strategy for synthesising key intermediates **2.104** and **2.108** was developed.



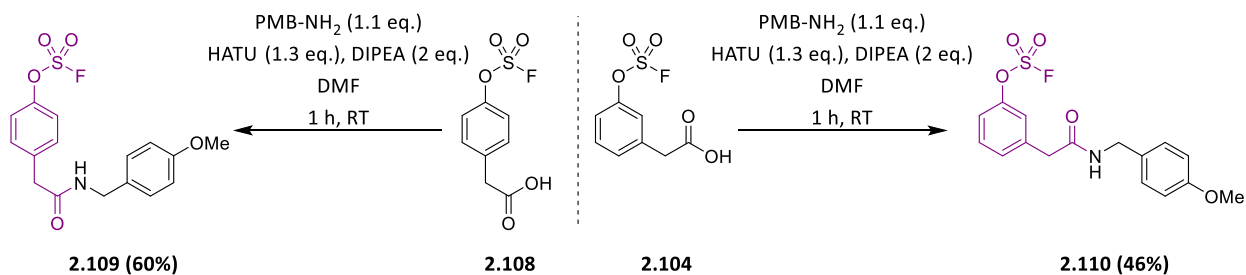
Scheme 2.15: Synthesis of 2-(3-((fluorosulfonyl)oxy)phenyl)acetic acid **2.104**.



Scheme 2.16: Synthesis of 2-(4-((fluorosulfonyl)oxy)phenyl)acetic acid **2.108**.

This route was appealing from a safety perspective as there would only be one reaction using sulfonyl fluoride gas as the fluorosulfate group was incorporated before the diversification step (**step 2**). In addition, the route could be rendered high throughput for preparing the amide bond in the final step. The *tert*-butyl ester of compounds **2.103** and **2.107** was hydrolysed under acidic conditions to give the corresponding carboxylic acids (**2.104** and **2.108**) in high yield (**step 3**).

The final step of the fragment library preparation involved synthesis of the amide bond. As shown in **Scheme 2.14**, the original route proceeded *via* an acid chloride intermediate which did not prove optimal. Therefore, alternative amide coupling reagents such as HATU and T3P were investigated and HATU was identified as the preferred amide coupling reagent. As shown in **Scheme 2.17**, the amide bond formation proceeded in reasonable yields to give **2.109** (60%) and **2.110** (46%).



Scheme 2.17: Scoping the synthesis of *meta*- and *para*-fluorosulfate fragment molecules.

A robust synthetic procedure had been developed to prepare a *meta*- and *para*-fluorosulfate fragment library. The subsequent steps involved deciding which protein targets and amine monomers would be suitable to investigate the potential of the fluorosulfate fragment library. Our attention was focused on in house photoaffinity fragments where known small molecule binders had been validated for specific protein targets.

Recently, in house photoaffinity fragment libraries have been used to identify new small molecules which display activity towards proteins of interest.²⁵⁸ As shown in **Figure 2.63**, different small molecule amines can be appended with a photoreactive group. The small molecule (**2.111**) binds to the protein target. The protein inhibitor mixture is subjected to UV-irradiation, typically 365 nm (dependent on photoreactive group). A highly reactive intermediate is formed and, dependent on the surrounding protein microenvironment, a covalent link with the protein target can be made, commonly known as photo-crosslinking. The covalent adduct can be profiled using mass spectrometry. This approach can be used as a high throughput platform to elucidate new small molecule ligands of protein targets.

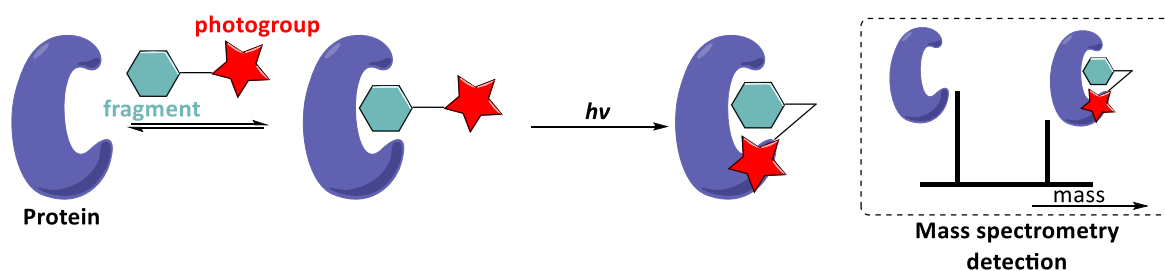


Figure 2.63: The workflow of a photoaffinity fragment screening library.²⁵⁸ Adapted from reference 258.

The BET protein BRD4 was identified as a potential target. In-house photoaffinity fragment libraries have identified groups which covalently modify BRD4. Protein X-ray crystallography was used to characterise the BRD4-fragment (**2.111**) interactions where an intermolecular hydrogen bond between the diazine (photoactivatable group) and Lys141 (**Figure 2.64**) was observed.

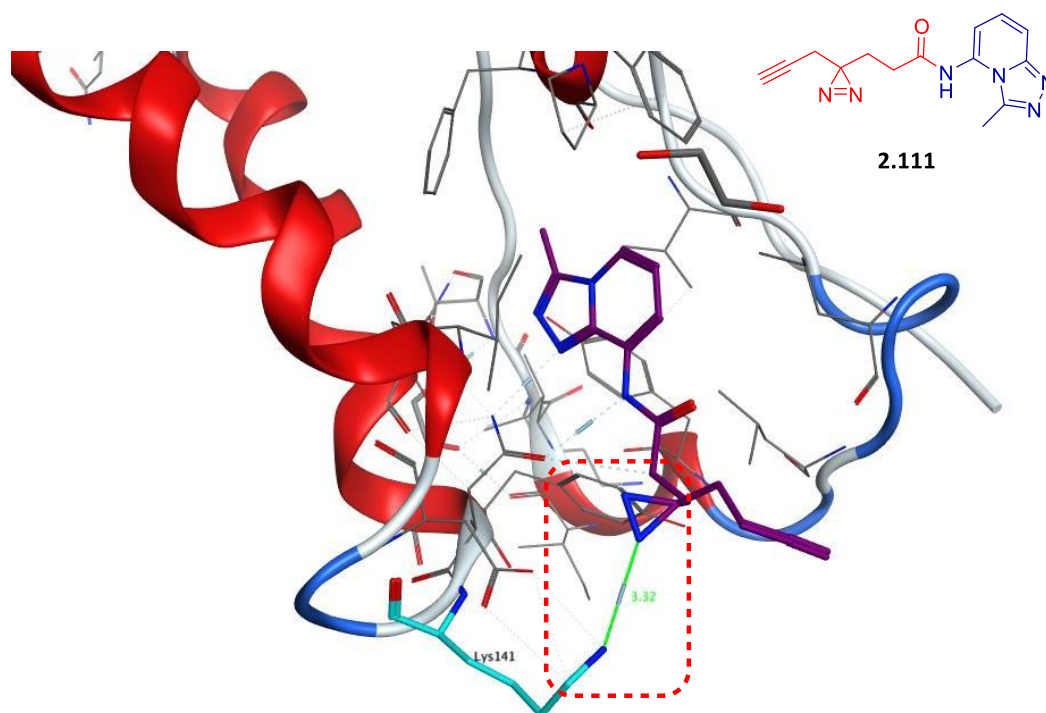


Figure 2.64: Crystal structure of **2.111** in the binding pocket of BRD4 highlighting a key hydrogen bonding interaction with Lys141 (PDB: 2N3K).

Fragment **2.111** used in the photoaffinity fragment library was selected as a group of interest as this bound to BRD4, close to a lysine residue (Lys141). The small molecule

amine monomer was appended with a fluorosulfate warhead to give fragment **2.121** (shown in **Figure 2.65**) in an attempt to engage with Lys141 in BRD4. Fragment **2.121**, and additional potent BRD4 fragments were explored to determine the potential of covalently modifying BRD4.

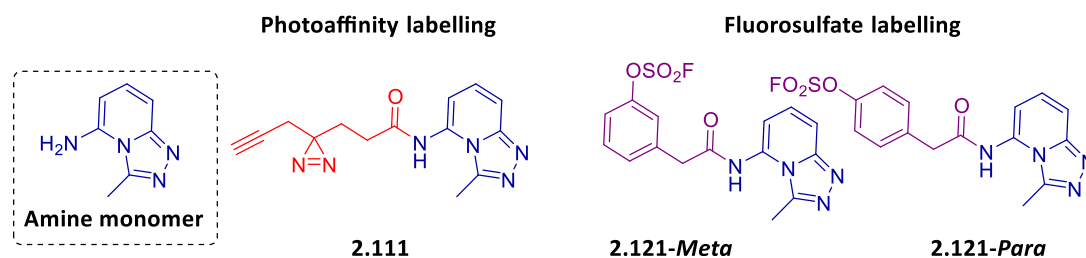
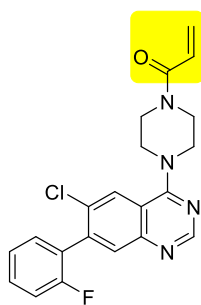


Figure 2.65: Photoaffinity fragment **2.111** and fluorosulfate fragment **2.121**.

A second protein target selected was KRAS, the most frequently mutated oncogene in cancer, appearing in 90% of pancreatic, 35% of lung and 45% of colon cancers.²⁵⁹ Therefore, the KRAS protein is deemed an important target in oncology. Early efforts in discovering small molecule inhibitors for targeting KRAS failed, which was due to the lack of well-defined hydrophobic pockets on the surface of the protein.²⁵⁹ The tractability of targeting this protein with small molecule inhibitors remains uncertain and alternative approaches for inhibiting KRAS require investigation. More recently, new strategies have been reported to develop KRAS-targeted therapies.²⁶⁰⁻²⁶² Compound **2.112** containing an acrylamide (**Figure 2.66**) was shown to covalently bind to Cys12 in the active site of KRAS^{G12C}-GDP.²⁶³



2.112

Figure 2.66: Compound **2.112**, a recent example of a KRAS covalent inhibitor targeting a cysteine residue.

KRAS is believed to be a difficult protein to target.²⁵⁹ However, due to its potential for various cancer treatments and the recently reported KRAS covalent inhibitors, KRAS represented an interesting target to explore. We decided to select amine monomers with KRAS pharmacophore elements in the fluorosulfate fragment library set. The amine monomers were chosen based on in-house knowledge of photoaffinity fragments. The protein crystal structure of KRAS is shown in **Figure 2.67**, where exposed nucleophilic residues have been highlighted (Lys104, Tyr71 and Tyr137). These residues represent potential nucleophilic sites which could be covalently modified by a fluorosulfate warhead.

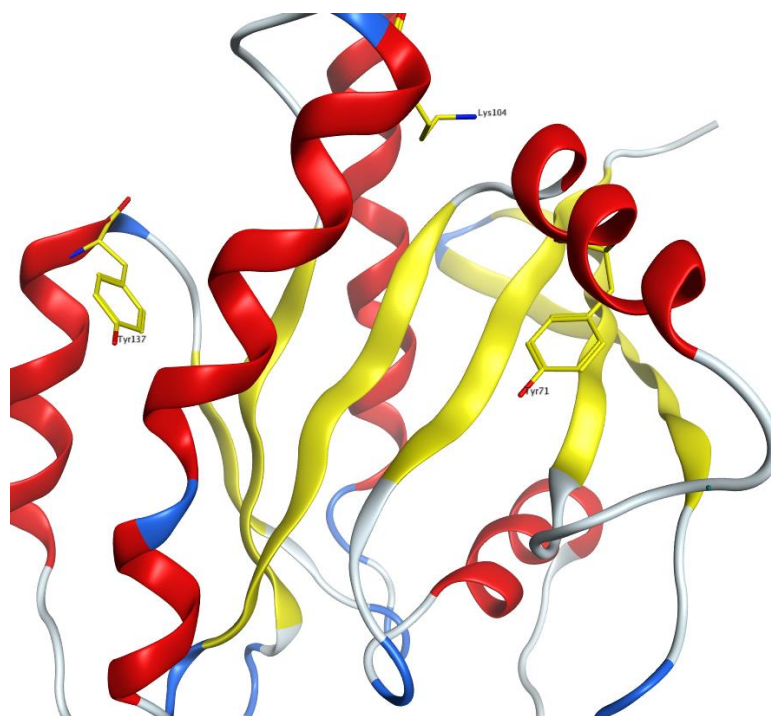


Figure 2.67: Crystal structure of KRAS highlighting potential nucleophilic residues Lys104, Tyr71 and Tyr137.

We now had a set of fragment warheads in which to introduce our fluorosulfate group. As shown in **General Procedure A** (see **Section 2.25**), the final amide bond formation was rendered high throughput. A focused set of 9 amine monomers which contained BRD4 and KRAS pharmacophoric elements were coupled onto the *meta* and *para* phenyl acetic fluorosulfate warheads **2.104** and **2.108**, giving a total of 18 final fragment molecules (**Figure 2.68, 2.113-2.121**).

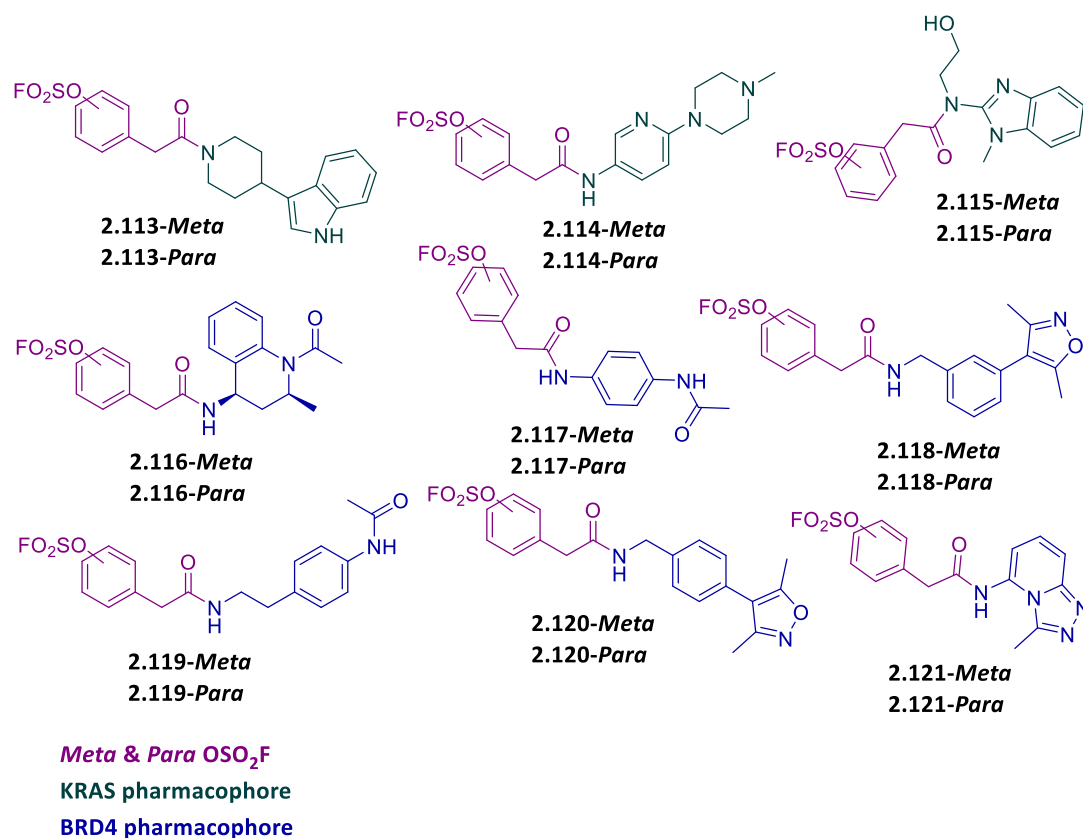


Figure 2.68: Fluorosulfate fragment library (2.113-2.121).

The fluorosulfate fragment library set (shown in **Figure 2.68**) at high concentrations (20 mM) were incubated for 24 h at 10 °C with recombinant BRD4 and KRAS proteins (1 μM protein). Subsequently, mass spectrometry was used as the detection method to determine any covalent modifications. Unfortunately, no covalent adducts were observed in PBS buffer with high concentrations of fragments (20 mM, shown in **Figure 2.69**). An alternative buffered solution, HEPES was used as the media to incubate the fragments and proteins, and no sign of a covalent modification was identified by mass spectrometry. As previously mentioned in **Section 2.5**, the pKa of a lysine is approximately 10, therefore, to help increase the nucleophilicity of lysine, TRIS base pH 8.6 was used to help enhance the nucleophilicity of the amino acid residues. However, no covalent mass adducts were identified for either BRD4 or KRAS.

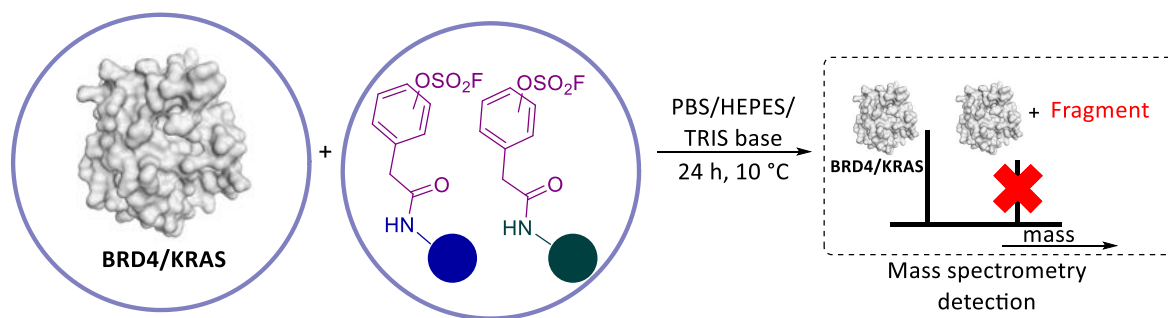


Figure 2.69: Fluorosulfate fragments incubated with BRD4 and KRAS proteins.

As shown in **Figure 2.64**, Lys141 in BRD4 is not deeply buried in the protein pocket and is solvent exposed.¹⁷⁶ It has been established that deeply buried lysine residues can have their pKa lowered by up to 5 units and so the reactivity of the lysine is largely dependent on its protein microenvironment. After carrying out this study, it was concluded that Lys141 was not situated in a suitable protein microenvironment and was therefore not sufficiently nucleophilic. Based on this, it was concluded that BRD4 was not a suitable protein target for exploring the potential of a fluorosulfate fragment library targeting non-cysteine residues.

KRAS is well known for its poor druggability, it wasn't the simplest of protein targets for examining the potential of a covalent fluorosulfate library.²⁶⁴ The reduced reactivity of the fluorosulfate warhead in comparison to sulfonyl fluorides may have hindered its ability in covalently modifying potential tyrosine residues. The lack of hydrophobic pockets in KRAS may disfavour the covalent interaction with the fluorosulfate warhead as the potential nucleophilicity associated with lysine/tyrosine could be limited.

As PI4KIII β had a suitable lysine to target, it was decided to screen fluorosulfate fragment library (**Figure 2.68**) with PI4KIII β protein under the same experimental conditions as outlined above. No covalent labelling of the protein was identified. This highlighted the specificity of the covalent modification with the PI4KIII β targeted compounds and fragments. This provides strong evidence that the fluorosulfate warhead required a certain conformation to engage with the nucleophilic lysine

residue. If the molecule cannot adopt this conformation in the protein then it won't bind and so there will be no chance to covalently modify the protein. The reduced reactivity of the fluorosulfate warhead minimises the potential for promiscuous reactivity and places more emphasis on the reversible interactions with the target protein. Therefore, as a fragment library, the number of 'hit' fragments against protein targets would be envisioned to be lower in comparison to photoaffinity fragment libraries. However, due to the reduced reactivity of the fluorosulfate warhead, the 'hit' fragment would be expected to be a valid fragment molecule for commencing a drug discovery project.

In conclusion, fragment compounds **2.90** and **2.95** covalently modified Lys549 in PI4KIII β at high concentrations. This acted as a proof of concept that a low molecular weight fluorosulfate fragment could actually label residues in proteins, with this very encouraging result, it gave an excellent rationale to design a potential covalent fluorosulfate fragment library. The synthesis of a *meta* and *para* phenylacetic derived fluorosulfate fragment library was robust and synthetically tractable. However, no absolute conclusions can be drawn on the application of the *meta* and *para* fluorosulfate fragment library derived from building blocks **2.104** and **2.108**. The focused fragment library was based on in-house knowledge and the library set was limited in terms of the number of fragments. Ideally, a larger fluorosulfate fragment library should be synthesised (hundreds of fragments) with a greater diversity of binding elements to determine its potential as a non-cysteine fragment covalent library. Further research into the covalent fluorosulfate warhead may be required (**2.222-2.224**). In this study, an unsubstituted phenyl ring was selected, however, alternative groups should be investigated, with perhaps additional functionality (**Figure 2.69**). For example, this could include HBA groups to make additional interactions with the protein target; striking a balance between physicochemical properties, reactivity and stability.

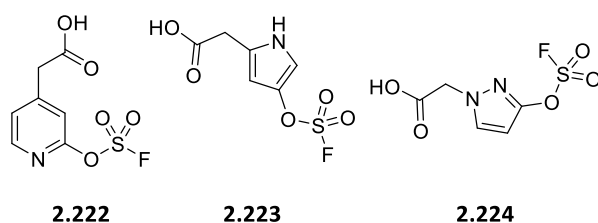


Figure 2.69: Alternative fluorosulfate covalent warhead groups to investigate.

2.23 Conclusions

In summary, a range of PI4KIII β covalent inhibitors were synthesised to initially target Lys549 in the ATP binding site of the protein. A range of electrophilic warheads were explored, and it was identified that the physicochemical properties of these activated phenolic esters were suboptimal and that other electrophiles required investigation. Sulfonyl fluorides were initially pursued as alternative covalent warhead, but hydrolysis to the sulfonic acid was observed. As a result of the poor stability of this compound class, they were deemed unsuitable. This led to an investigation into fluorosulfate containing molecules where novel fluorosulfate inhibitors such as **2.45**, **2.46** and **2.47** were synthesised using *ex-situ* generation of SO₂F₂ (g) in COWare to target Lys549.

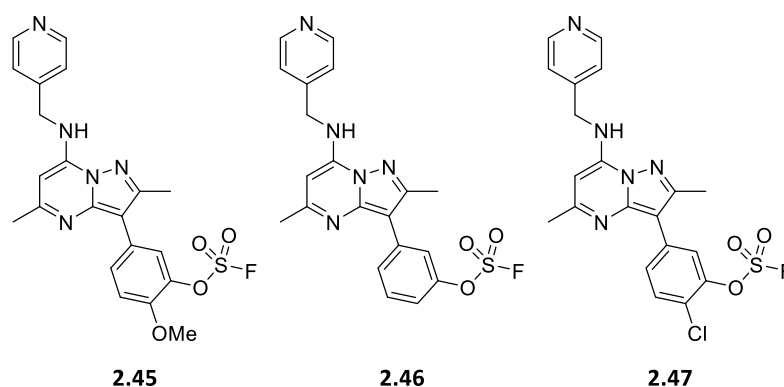


Figure 2.70: Lysine targeted fluorosulfate covalent inhibitors of PI4KIII β .

A robust synthetic procedure for the preparation of fluorosulfate compounds was established. The stability of compounds **2.45**, **2.46** and **2.47** to aqueous buffer were

investigated. No signs of hydrolysis were observed under neutral and acidic conditions. This was supported by an acidic ester hydrolysis transformation of compounds containing a fluorosulfate (**Scheme 2.14**) where no hydrolysis of the fluorosulfate group was observed. Under basic conditions, the fluorosulfate group was susceptible to slow hydrolysis. The rate of base hydrolysis could be slowed down further in the presence of an *ortho* methoxy substituent e.g. **2.45**. The increased steric contribution and reduced electrophilicity of the fluorosulfate group is believed to enhance the warhead stability.

Compounds **2.45**, **2.46** and **2.47** were profiled in terms of their reactivity. Excess lysine (50 eq.) under basic and neutral conditions (pH 10) was used to examine the compound's reactivity, where the fluorosulfate warhead was unreactive under neutral conditions. Under basic conditions, the fluorosulfate group could react with lysine and tyrosine. It was established that the reactivity of the fluorosulfate warhead with lysine was slow (even slower against tyrosine). After the stability and reactivity of the fluorosulfate warhead was measured, our attention turned to biochemical testing of the compounds with PI4KIII β .

Compounds (**2.45**, **2.46** and **2.47**) were screened through two key assays: enzyme and cell. In-house PI4KIII β biochemical assays alluded to an alternative mechanism of action as an increase in potency from the enzyme to cellular assay (which had a 48 h incubation period, compared to a 40 min incubation in the enzyme assay) was observed compared to control compounds. To investigate whether this increase in activity in the prolonged incubation in the assay was related to the fluorosulfate, characterisation of the covalent adduct with PI4KIII β was carried out using mass spectrometry. Pleasingly, protein labelled with the reacted warhead was observed which had only labelled PI4KIII β once. Lead compound **2.45** was further profiled in a lipid kinase panel screen where over 100-*fold* selectivity against other lipid kinases was achieved (**Section 2.13**).

Previous work carried out in Part One showed that the pyrazolopyrimidine template (Core 4) used was selective towards PI4KIII β . Therefore a covalent warhead was appended, and the conserved lysine was covalently modified. This revealed, a general approach to covalent kinase drug design, where the selectivity can be obtained through the core of the compound. A kinase with a potential nucleophilic residue could be selectively modified using a selective reversible template, appended with a fluorosulfate warhead targeting a non-cysteine residue, thus achieving selective covalent inhibition.

Biochemical mechanistic experiments were then carried out to determine the rates of the reversible and irreversible interactions for compounds **2.45** and **2.76**. The results gathered from the characterisation techniques were consistent, where the covalent bond forming step was slow (extremely slow for targeting tyrosine). Therefore, the inhibitors were suitable for a slow onset of inhibition with a prolonged duration of action. This could be due to poor nucleophilicity of the lysine/tyrosine and/or the reduced reactivity of the fluorosulfate warhead. The targeted covalent modification was guided by the reversible interactions between the inhibitor and protein (**Figure 2.71**). The fluorosulfate warhead required a specific conformation before the nucleophilic residue could engage which helped with the specificity of the covalent modification.

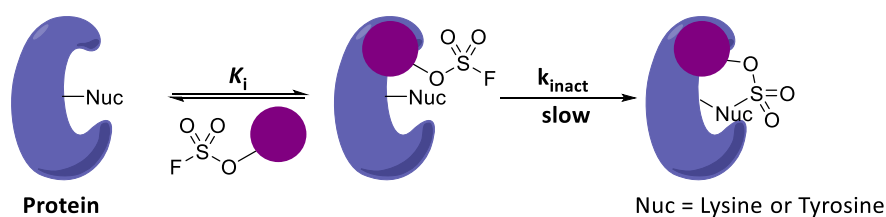


Figure 2.71: A generalised representation of a fluorosulfate warhead covalently modifying a protein target.

Protein crystallography enabled the design of alternative covalent fluorosulfate inhibitors targeting a tyrosine residue (**Figure 2.72**). A crucial hydrogen bonding

interaction between the *para* pyridyl head group and Tyr385 was identified (**Figure 2.24**). This led to the development of compound **2.76**. It was hypothesised that a dual covalent inhibitor molecule could potentially target both residues simultaneously (Lys549 and Tyr385). Compound **2.83** was synthesised, and pleasingly the covalent modification was detected by mass spectrometry and a crystal structure was obtained. This could have potential applications in chemical biology where a dual covalent compound could covalently link multiple residues in proteins to form a bivalent complex.

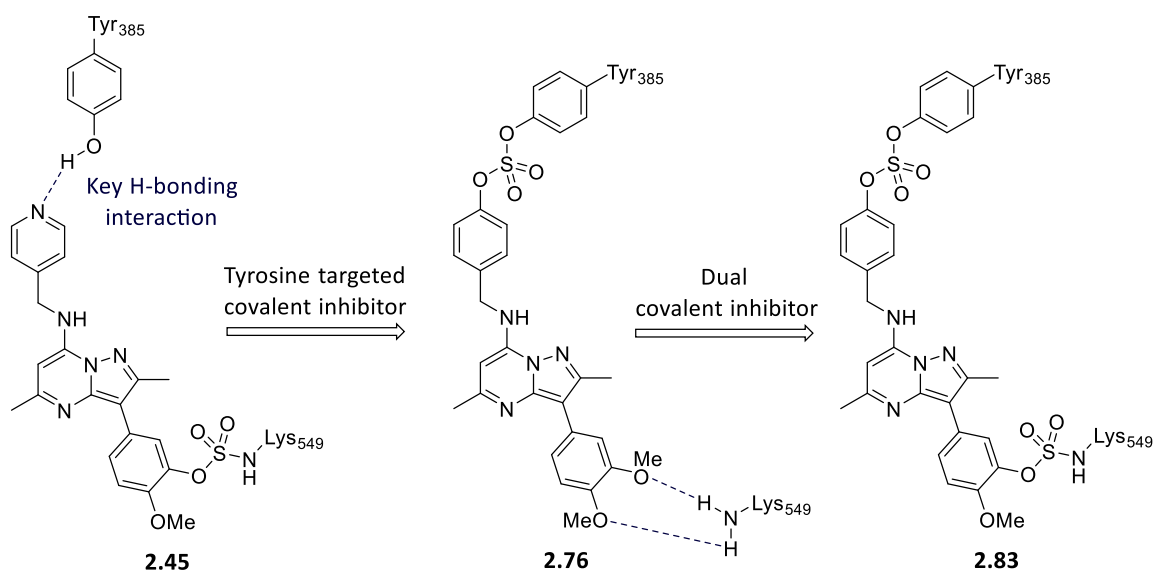


Figure 2.72: Design of alternative fluorosulfate inhibitors targeting Lys549 and Tyr385.

The final part of the research involved determining whether a covalent fluorosulfate fragment library technology could be a viable approach for identifying fragment 'hits' against proteins. PI4KIII β was used to validate the concept, where fragment like compounds based on Core One and Core Four were used to selectively covalently modify Lys549. After validating the concept of a fluorosulfate fragment library, a robust synthetic procedure was devised to prepare a covalent fluorosulfate fragment library. The use of in-house photoaffinity fragment libraries were used to identify fragment molecules which could be used to potentially modify a protein target of

interest.²⁵⁸ The potential of a fluorosulfate fragment library remains at an early stage as the focused fragment library set used in **Section 2.22** was limited. Ongoing research within our laboratories is investigating fluorosulfate containing molecules as tools within drug discovery research.

The work carried out has demonstrated the potential of introducing a fluorosulfate covalent warhead within a fragment library technology. In principle, PI4KIII β could have been targeted using a fragment fluorosulfate molecule **2.90** and then x-ray crystallography could have been used to design and explore further SAR. This could have established a more potent PI4KIII β covalent inhibitor **2.45** as shown in **Figure 2.73**.

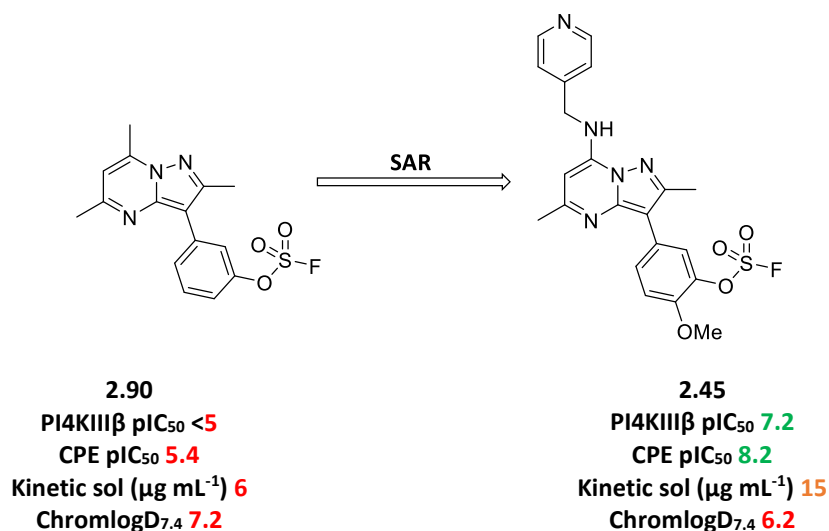


Figure 2.73: Fluorosulfate covalent PI4KIII β inhibitors **2.90** and **2.45**.

As result, this approach could be applied to other protein targets. Screening a set of fluorosulfate fragment molecules could identify a novel compound series for a particular target. Further SAR could induce a more potent inhibitor (reversible or irreversible) with a desirable profile which could lead to the development of novel drug molecules.

EXPERIMENTAL

2.24 General methods and assays

Enzymatic assay (PI4KIII β pIC₅₀) – Compound plates stamped with 60 nL stamp from 11-point titration (10 μ M final assay concentration), 60 nL of DMSO in control columns 6 and 18. Dispense 3 μ L of 2x substrate solution into all columns and add 3 μ L of assay buffer (25 mM HEPES pH7.5 (NaOH), 10 mM MgCl, 0.5 mM EGTA, 0.1% Triton X-100, 2 mM TCEP, 0.1 mg/mL BSA, 100 mM ATP (fresh)) to column 18 (no enzyme low control). Add 3 μ L of 2x enzyme solution to columns 1-17 and 19-24 and centrifuge plates at 1000 rpm for 1 min, apply plate seal to each plate and incubate for 180 min at room temperature. Centrifuge plates at 1000 rpm for 1 min prior to removal of plate seal and add 6 μ L of ADP-Glo 1 reagent +0.1% CHAPS to all wells. Centrifuge plates at 1000 rpm for 1 min and incubate for 60 min at room temperature. Add 12 μ L of ADP-Glo 2 reagent +0.1% CHAPS to all wells, centrifuge plates at 1000 rpm for 1 min and incubate for 40 min at room temperature. Read plates on Viewlux or PHERAstar (signal stable for 30-90 min following Glo 2 incubation). In the enzymatic assay, the ADP product is detected through a 2-step coupled detection with a luminescent read-out. In the first step the kinase reaction is quenched, and unused ATP substrate is converted to AMP, removing it from the detection system. In the second step, the ADP produced by the kinase reaction is converted back to ATP, and this is then detected *via* a luciferin/ luciferase reaction, as shown in **Figure 2.74**. The luminescent signal produced is proportional to the quantity of ADP produced, therefore correlating with PI4KIII β activity.

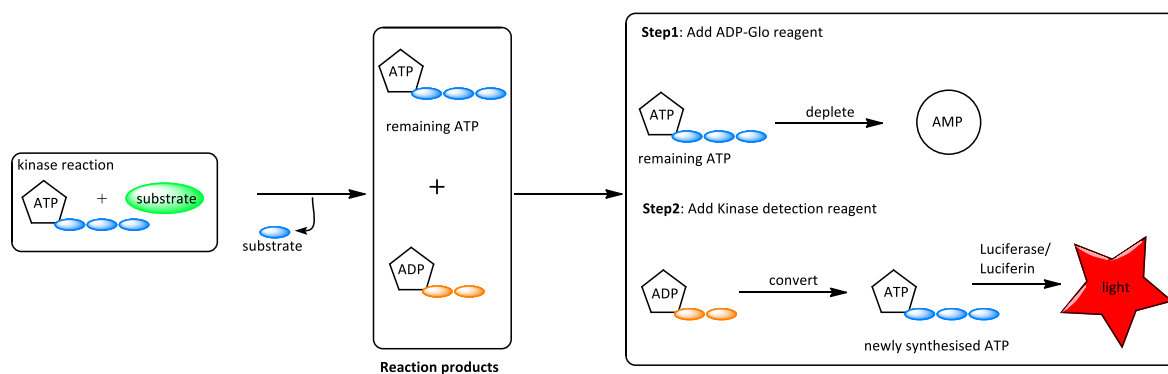


Figure 2.74: PI4KIII β enzyme assay.

Cellular based assay (CPE pIC₅₀) – 0.5 μ L of a 10 mM compound stock solution is stamped into compound plates. 3 mM top conc, 1:3 dilutions, 10 points with 0.5 μ L of 100% DMSO in columns 11 and 12. Remove the compound plates from the freezer, if necessary, and equilibrate to room temperature. Centrifuge briefly (bring up to 1000 rpm and then turn off the centrifuge). Remove the foil seals and pre-warm assay medium to 37 °C in sterile water bath. Wash confluent monolayer of HeLa cells with 10 mL of PBS and add 3 mL TrypLE to cover cells. Incubate 5 min at 37 °C and gently agitate flask to detach cells, then remove cells to 50 mL Falcon tube. Centrifuge 300 g for 5 min and re-suspend pellet in approx. 50 mL of media, then count the cells using Vicell. Adjust concentration to 6.6×10^4 cells/mL, for the 96-well assay, cells and virus are pre-mixed prior to dispensing into the compound plates. Add virus to moi 1 and HRV type A strain 16 stock, or a pre-diluted stock, is added to the 6.6×10^4 cells/mL suspension at the appropriate pre-determined dilution for the current virus stock to achieve an MOI of 1, or a suitable MOI for the current virus stock. Add 150 μ L of cell/virus suspension per well using a Multidrop to columns 1 to 11 and add 150 μ L of cell suspension per well using a multichannel pipette to columns 12. Incubate the plates at 33 °C, 5% CO₂, for 2 days post infection. Prepare fresh, or thaw frozen, CellTiter-Glo reagent. Avoid repeated freeze thaw cycles. Remove the 96-well plates from the 33 °C, 5% CO₂ incubator and equilibrate to room temperature. Dispense 60 μ L CellTiter-Glo reagent into all columns of the 96-well plates using a Multidrop. Cell Titer Glo reagent can be stored at RT or 4 °C for 8 hours. Once reconstituted can be stored at -20 °C for 21 weeks with ~3% loss of activity. Stable up to 10 freeze thaw

cycles with <10% loss of activity. After approximately 20 minutes of room temperature incubation, read the 96-well plates on the Envision using the Cell Titre Glo for CPE protocol to measure luminescence.²⁶⁵

Intact protein mass spectrometry – Intact protein masses were recorded by liquid chromatography-mass spectrometry (LC-MS) using a 6224 TOF (Agilent) Accurate Mass Series mass spectrometer, interfaced with an Agilent 1200 liquid chromatography and sample handling system. The protein sample was injected using an Agilent 1200 series AutoSampler (Model No. G1367B) with a 10 µL injection volume and maintained at a temperature of 10 °C. Chromatography was carried out on an Agilent Bio-HPLC PLRP-S (1000Å, 5 µm × 50 mm × 1.0 mm, PL1312-1502) reverse phase HPLC column at 70 °C. Using an Agilent 1200 series binary pump system (Model No. G1312B) the sample was eluted at 0.5 mL/min using a gradient system from Solvent A (water, 0.2 % (v/v) formic acid) to Solvent B (MeCN, 0.2 % (v/v) formic acid) according to the following conditions:

TIME (MIN)	%B	FLOW (ML/MIN)	PRESSURE
0	20	0.5	350
0.5	20	0.5	350
0.51	40	0.5	350
2.5	80	0.5	350
2.51	100	0.5	350
4	100	0.5	350
4.01	20	0.5	350
4.5	20	0.5	350

Table 2.12: Elution gradient (%B) used for intact protein LC-MS

The eluent was injected directly into an Agilent TOF mass spectrometer (Model No. G6224A) using a dual ESI source and scanning between 600-3200 Da with a scan rate of 1.03 s in positive mode. The following MS parameters were used: Capillary voltage limit – 4200; Desolvation temperature – 340 °C; Drying gas flow – 8.0 l/min. Data acquisition was carried out in 2GHz Extended Dynamic range mode. Spectra were processed using Mass Hunter Qualitative Analysis™ B06.00 (Agilent) software with

the Maximum Entropy method employed. The total ion chromatograms (TIC) were extracted (region containing protein) and the summed scans were deconvoluted over a m/z range with an expected mass range dependent on the protein (see below).

Table 2.13: Deconvolution conditions for PI4KIII β , BRD4 and KRAS^{G12D}.

PROTEIN	M/Z RANGE	EXPECTED MASS RANGE
PI4KIII β	850-2200	89000-93000
BRD4	850-2200	14000-17000
KRAS ^{G12D}	850-2000	18000-21000

The csv. files of deconvoluted spectra results were analysed using R Studio software to generate TIFF files of the spectra. Data Processing was carried out with assistance from Emma Grant.

X-ray crystallography – All crystal structures were determined by Don. O. Somers who is part of the structural and biophysical sciences, GlaxoSmithKline medicines research centre, Stevenage, UK. Email: don.o.somers@GSK.com for further information. The PDB files were analysed by MOE 2016.0802 to generate .jpg files for images.

Kinetic binding assay – This assay and data processing was carried out with assistance from Dr John P Evans (GSK). Human PI4KIII β (13-828, D316-330): GRITS48706 Stored at -80 °C. No known stability issues but should avoid repeated freeze/thaw cycles (>3). Molecular Weight: approx. 90,292 Da, BioCat ID 122258. The total protein concentration is approx. 1 mg/mL (Bradford; equivalent to 11.1 μ M). TCEP: Stored at -20 °C in reasonably sized aliquots. Bovine Serum Albumin (BSA) (Molecular Weight approx. 66,000 Da). Prepare 10 mg/mL in MilliQ water; stored at -20 °C in reasonably sized aliquots. Phosphatidylinositol (diC8), PI (Molecular Weight 608.6 Da). Dilute to 5 mM in MilliQ water and store at -80 °C in reasonably sized aliquots. ATP (10 mM). ADP-Glo kit, 0.1% CHAPS added to Glo1 and Glo2 reagents, stored at -20 °C. Buffered solution (contains 25 mM HEPES pH 7.5 (NaOH), 0.5 mM EGTA, 10 mM MgCl₂, 0.1 %

(v/v) Triton X-100). Add 2 mM TCEP and 0.1 mg/mL BSA on day of use. Compound stock solutions (10 mM) were dispensed using the HP digital dispenser using diluted stocks. The total final volume of DMSO added to each well was normalized across the plate to 60.8 nL (1%) in a total volume of 6 μ L. White Greiner 384 well low volume plates were used. The onset of inhibition at saturating ATP (1 mM to exacerbate slow association) using the ADP-Glo format. The substrate, enzyme, and quench additions were performed by the DragonFly liquid handling robot. Global progress curve fitting was used to determine the rate of onset of inhibition at increasing concentrations of inhibitor. The raw fluorescence data was fitted by the local progress curves analysis assuming a slow binding, irreversible inhibition. The notation for use of this equation in Graphpad Prism 5 is given below. Where k_{inact} denotes the rate constant for inactivation of the kinase in units of s^{-1} , and K_i is the concentration at which the half maximal rate of inactivation is achieved, in molar units to derive the k_{inact} . K_i values are an expression of an IC_{50} value as described by the Cheng-Prusoff relationship therefore k_{on}/k_{off} describes the change in K_i . $[S]$ is the concentration of substrate used. K_m is the Michaelis Menton constant, substrate concentration at which 50% of the maximal enzyme turnover rate is achieved. Therefore, for assays carried out at $K_m(ATP)$, the K_i is approximately 2-fold more potent than the measured value, which corresponds to roughly 0.3 log unit increase in pIC_{50} .

$$\text{Cheng Prusoff equation: } K_i = \frac{IC_{50}}{1 + \left(\frac{[S]}{K_m}\right)}$$

GraphPad notation:

$$vf = 0$$

$$vi = v0 / (1 + (\text{Compound} * 1e-9) / K_i)$$

$$k_{obs} = ((k_{inact} * (\text{Compound} * 1e-9)) / (K_i + (\text{Compound} * 1e-9)))$$

$$Y = \text{If}(X < X0, Y0, Y0 + vf * (X - X0) + ((vi - vf) / k_{obs}) * (1 - \exp(-k_{obs} * (X - X0))))$$

HPLC reactivity assay – Assay protocol: 25 µL of a 20 mM stock of inhibitor in DMSO was added to a stirred solution of internal standard (biphenyl, 25 µL of 2 mM stock in DMSO) (note: time added was recorded), 450 µL of 55.5 mM *acetyl*-lysine stock solution in 100 mM borate buffer at pH10.2 (*pseudo* first order reaction conditions). The reaction was stirred at 37 °C and analysed immediately by HPLC. The reactions were monitored frequently by HPLC and each reaction was carried out in at least duplicate. After reaction completion, the resulting reaction mixture was monitored by LCMS on a formic modifier and analysed by HRMS. The control reaction was ran under the same experimental conditions **without** added lysine.

HPLC Method: The liquid chromatography (LC) analysis was conducted on an Phenomenex Kinetex® XB-C18 column (50 mm x 3.0 mm internal diameter, 2.6 µm packing diameter) at 37 °C using a 0.5 µL injection volume. The solvents employed were A = 0.05% v/v solution of trifluoroacetic acid in water, and B = 0.05% v/v solution of trifluoroacetic acid in MeCN.

The gradient employed was:

TIME (MIN)	FLOW RATE (ML/MIN)	%A%B
Initial	1.0	97 3
1.5	1.0	100
1.9	1.0	100
2.0	1.0	97 3
2.3	1.0	97 3

The UV detection wavelength was at 260 nm.

Stability assay – Compound stock solutions (10 mM) were added to buffered solution at 40 °C to measure the stability under different degradation conditions. Buffers used, GSH: Phosphate buffer pH7.4 with 5 mM GSH. pH10 OX: Britton Robinson pH10 buffer with 20 molar% hydrogen peroxide. pH10: Britton Robinson pH10 buffer. pH6 OX: Britton Robinson pH6 buffer with 20 molar% hydrogen peroxide. pH6: Britton Robinson pH6 buffer. pH4 OX: Britton Robinson pH4 buffer with 20 molar% hydrogen

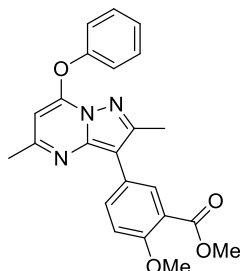
peroxide. pH4 OX: Britton Robinson pH4 buffer. The auto sampler was kept at 40 °C during the analysis time to speed up the kinetics of degradation. 10 mM solutions of compound in DMSO were diluted to 0.5 mM in MeCN. 440 µL of buffer were mixed in chromatography vials with 110 µL of 0.5 mM compound in MeCN. The contents were mixed using a Vortex. 550 µL was enough to inject the vial 10 times with an injection volume of 5 µL (full loop load ahead method), covering the length of the stability assay. The solutions were monitored by LCMS: Mobile Phase: A: 100% Water with 0.1% Formic Acid. B: 100% MeCN with 0.1% Formic Acid.

Time / min	Flow Rate / mL·min ⁻¹	% A	% B
0.00	1	100	0
8.00	1	5	95
8.01	1	100	0
10.00	1	100	0

Amino acid screen – All reactions were carried out in a low volume capped LCMS vial which contained 10 µL of stock compound (10 mM), 50 equivalents of the appropriate amino acid (*acetyl*-Cysteine, *acetyl*-Lysine, ((benzyloxy)carbonyl)-Serine or (*N*-Boc)-Tyrosine), 10 µL MeCN and 50 µL buffered solution (Total volume 70 µL). All reactions were carried out at RT and were monitored by LCMS (see liquid chromatography mass spectrometry for details) under a formic modifier after 3 h, 7 h, 20 h and 30 h. 2-(4-(2-Hydroxyethyl)piperazin-1-yl)ethanesulfonic acid referred to as HEPES (50 mM) was the buffered solution at pH7.4. Sodium tetraborate buffer solution known as borax (25 mM) was the buffered solution at pH10.1.

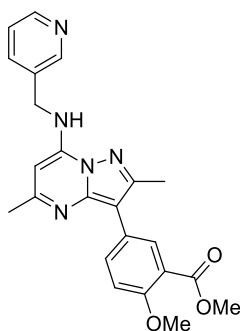
2.25 Synthesis

Methyl 5-(2,5-dimethyl-7-phenoxy-pyrazolo[1,5-*a*]pyrimidin-3-yl)-2-methoxybenzoate (2.22)



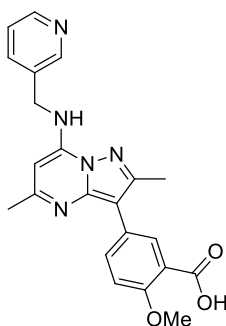
A microwave vial (20 mL) was charged with 3-bromo-2,5-dimethyl-7-phenoxy-pyrazolo[1,5-*a*]pyrimidine (1.52 g, 4.78 mmol), methyl 2-methoxy-5-(4,4,5,5-tetramethyl-1,3,2-dioxaborolan-2-yl)benzoate (3.07 g, 10.51 mmol), PdCl₂(dppf)-CH₂Cl₂ adduct (0.35 g, 0.43 mmol), cesium carbonate (3.42 g, 10.51 mmol), 1,4-dioxane (10 mL) and water (2.5 mL). The reaction vessel was sealed and heated in the microwave at 120 °C for 5 h. After cooling, the reaction mixture was passed through Celite™, diluted with EtOAc (20 mL) and washed with brine (20 mL). The organic layer was passed through a hydrophobic frit and concentrated *in vacuo*. The crude product was purified by column chromatography and eluted with EtOAc in cyclohexane (0-100% gradient). The appropriate fractions were combined and concentrated *in vacuo* to give methyl 5-(2,5-dimethyl-7-phenoxy-pyrazolo[1,5-*a*]pyrimidin-3-yl)-2-methoxybenzoate (2.07 g, 3.87 mmol, 81% yield). **¹H NMR** (400 MHz, DMSO-*d*₆) δ = 8.02 (d, *J* = 2.3 Hz, 1H), 7.93 - 7.89 (m, 1H), 7.60 (m, 2H), 7.49 - 7.43 (m, 3H), 7.31 - 7.26 (m, 1H), 5.97 (s, 1H), 3.89 (s, 3H), 3.84 (s, 3H), 2.56 (s, 3H), 2.42 (s, 3H). **¹³C NMR** (101 MHz, DMSO-*d*₆) δ = 166.8, 161.2, 156.8, 154.2, 152.3, 152.1, 147.7, 133.8, 131.2, 130.8, 127.4, 124.9, 121.3, 120.7, 113.3, 106.3, 90.8, 56.5, 52.4, 25.2, 14.7. **LCMS** (HpH) 100% desired product; *t*_{ret} = 1.16 min, MH⁺ 404.3.

Methyl 5-(2,5-dimethyl-7-((pyridin-3-ylmethyl)amino)pyrazolo[1,5-*a*]pyrimidin-3-yl)-2-methoxybenzoate (2.23)



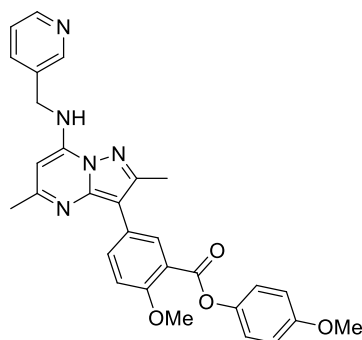
A microwave vial (20 mL) was charged with methyl 5-(2,5-dimethyl-7-phenoxy-pyrazolo[1,5-*a*]pyrimidin-3-yl)-2-methoxybenzoate (2.07 g, 5.14 mmol), pyridin-3-ylmethanamine (1.15 mL, 11.30 mmol), triethylamine (3.58 mL, 25.70 mmol) and DMSO (7 mL). The reaction vessel was sealed and heated in a microwave at 120 °C for 5 h. After cooling, the reaction mixture was diluted with EtOAc (20 mL) and washed with saturated aqueous sodium bicarbonate solution (20 mL). The organic layer was passed through a hydrophobic frit and concentrated *in vacuo* to give an oil. The crude product was purified by column chromatography and eluted with EtOAc in cyclohexane (0-100% gradient) and flushed with ethanol (1:3) EtOAc. The appropriate fractions were combined and concentrated *in vacuo* to give methyl 5-(2,5-dimethyl-7-((pyridin-3-ylmethyl)amino)pyrazolo[1,5-*a*]pyrimidin-3-yl)-2-methoxybenzoate (1.36 g, 1.33 mmol, 64% yield). ¹H NMR (400 MHz, DMSO-*d*₆) δ = 8.71 - 8.66 (m, 1H), 8.52 - 8.46 (m, 2H), 8.04 - 7.99 (m, 1H), 7.93 - 7.87 (m, 1H), 7.87 - 7.80 (m, 1H), 7.42 - 7.33 (m, 1H), 7.25 - 7.20 (m, 1H), 6.10 (s, 1H), 4.68 - 4.63 (m, 2H), 3.87 (s, 3H), 3.83 (s, 3H), 2.54 (s, 3H), 2.36 (s, 3H). ¹³C NMR (101 MHz, DMSO-*d*₆) δ = 167.0, 159.4, 156.4, 150.4, 149.2, 148.9, 146.5, 135.4, 134.4, 133.5, 130.6, 125.8, 124.0, 120.5, 113.2, 104.8, 86.0, 56.4, 55.3, 52.4, 42.7, 25.3, 14.7. LCMS (HpH) 98% desired product; *t*_{ret} = 0.98 min, MH⁺ 418.4.

5-(2,5-Dimethyl-7-((pyridin-3-ylmethyl)amino)pyrazolo[1,5-*a*]pyrimidin-3-yl)-2-methoxybenzoic acid (2.24)



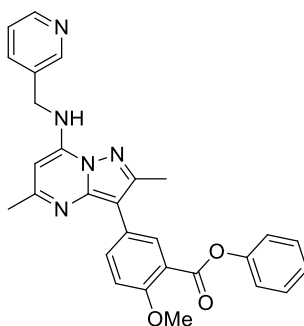
Methyl 5-(2,5-dimethyl-7-((pyridin-3-ylmethyl)amino)pyrazolo[1,5-*a*]pyrimidin-3-yl)-2-methoxybenzoate (1.24g, 2.96 mmol) in THF (8 mL) and aqueous sodium hydroxide (60 mL, 1 M) were heated at 55 °C for 3 h. After cooling, the solvent was concentrated *in vacuo* and the residue was re-dissolved in water (25 mL, pH = 14). The pH was lowered with acetic acid (pH = 4). The product was extracted out of the aqueous with EtOAc (2 x 30 mL) and the organic layer was concentrated *in vacuo*. The combined organics were concentrated *in vacuo* to give 5-(2,5-dimethyl-7-((pyridin-3-ylmethyl)amino)pyrazolo[1,5-*a*]pyrimidin-3-yl)-2-methoxybenzoic acid as an off-white solid (1.06 g, 2.60 mmol, 88% yield). **¹H NMR** (400 MHz, DMSO-*d*₆) δ = 8.70 - 8.66 (m, 1H), 8.51 - 8.43 (m, 2H), 7.86 - 7.81 (m, 1H), 7.81 - 7.78 (m, 1H), 7.74 - 7.66 (m, 1H), 7.41 - 7.34 (m, 1H), 7.13 - 7.09 (m, 1H), 6.08 (s, 1H), 4.68 - 4.62 (m, 2H), 3.82 (s, 3H), 2.35 (s, 3H), 1.90 (s, 3H). **¹³C NMR** (101 MHz, DMSO-*d*₆) δ = 172.7, 169.4, 159.2, 155.5, 150.4, 149.2, 148.9, 146.4, 146.1, 135.4, 134.4, 131.0, 129.9, 125.4, 124.0, 112.7, 85.9, 56.2, 42.5, 25.2, 22.0, 14.6. **LCMS** (HpH) 98% desired product; *t*_{ret} = 0.61 min, MH⁺ 404.3.

4-Methoxyphenyl 5-(2,5-dimethyl-7-((pyridin-3-ylmethyl)amino)pyrazolo[1,5- α]pyrimidin-3-yl)-2-methoxybenzoate (2.25)



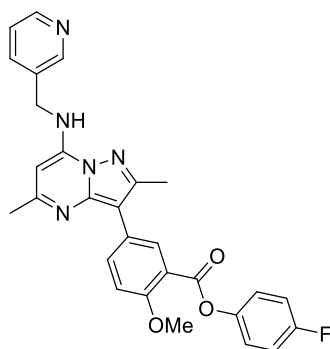
A microwave vial (5 mL) was charged with 5-(2,5-dimethyl-7-((pyridin-3-ylmethyl)amino)pyrazolo[1,5- α]pyrimidin-3-yl)-2-methoxybenzoic acid (136 mg, 0.34 mmol), 4-methoxyphenol (41.8 mg, 0.34 mmol), DMAP (8.24 mg, 0.07 mmol), EDC (77 mg, 0.37 mmol) and CH_2Cl_2 (3 mL). The reaction was stirred at RT for 3 h, additional 4-methoxyphenol (41.8 mg, 0.34 mmol) was added and the reaction was stirred for a further 2 h. The crude product was purified by MDAP (formic method). The appropriate fractions were combined and concentrated *in vacuo* to give 4-methoxyphenyl 5-(2,5-dimethyl-7-((pyridin-3-ylmethyl)amino)pyrazolo[1,5- α]pyrimidin-3-yl)-2-methoxybenzoate as a white solid (23 mg, 0.05 mmol, 14% yield). $^1\text{H NMR}$ (400 MHz, DMSO-d_6) δ = 8.69 - 8.64 (m, 1H), 8.55 - 8.45 (m, 2H), 8.27 - 8.25 (m, 1H), 8.03 - 7.94 (m, 1H), 7.88 - 7.79 (m, 1H), 7.41 - 7.34 (m, 1H), 7.33 - 7.28 (m, 1H), 7.18 (d, J = 9.3 Hz, 2H), 7.01 (d, J = 9.3 Hz, 2H), 6.13 - 6.10 (m, 1H), 4.68 - 4.62 (m, 2H), 3.94 - 3.89 (m, 3H), 3.79 (s, 3H), 2.57 (s, 3H), 2.35 (s, 3H). $^{13}\text{C NMR}$ (101 MHz, DMSO-d_6) δ = 165.0, 159.5, 157.4, 157.1, 150.4, 149.2, 148.9, 146.5, 146.2, 144.6, 135.5, 134.3, 134.2, 131.1, 125.9, 124.0, 123.2, 119.4, 114.9, 113.4, 104.6, 86.2, 56.6, 55.9, 55.4, 25.3, 14.8. **LCMS** (HpH) 96% desired product; t_{ret} = 1.19 min, MH^+ 510.4 **HRMS** ($\text{C}_{29}\text{H}_{27}\text{N}_5\text{O}_4$) $[\text{M}+\text{H}]^+$ requires 510.2141, found $[\text{M}+\text{H}]^+$ found 510.2150 ν_{max} (neat) / cm^{-1} 3380, 1738, 1588, 1186, 1046, 1022, 992, 823, 764, 521. **Mp** 132-135 °C.

Phenyl 5-(2,5-dimethyl-7-((pyridin-3-ylmethyl)amino)pyrazolo[1,5-*a*]pyrimidin-3-yl)-2-methoxybenzoate (2.26)



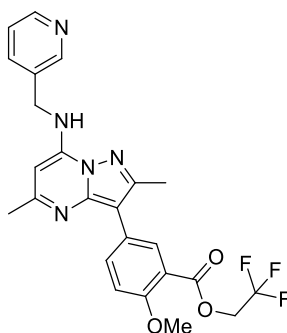
A microwave vial (5 mL) was charged with 5-(2,5-dimethyl-7-((pyridin-3-ylmethyl)amino)pyrazolo[1,5-*a*]pyrimidin-3-yl)-2-methoxybenzoic acid (208 mg, 0.52 mmol), phenol (58.2 mg, 0.62 mmol), DMAP (12.60 mg, 0.10 mmol), EDC (128 mg, 0.62 mmol) in DMSO (3 mL). The reaction mixture was stirred at RT for 17 h and additional phenol (116.4 mg, 1.24 mmol) and DMAP (12.60 mg, 0.10 mmol) were added. The reaction was stirred for a further 24 h and purified by MDAP (formic method). The appropriate fractions were combined and evaporated *in vacuo* to afford phenyl 5-(2,5-dimethyl-7-((pyridin-3-ylmethyl)amino)pyrazolo[1,5-*a*]pyrimidin-3-yl)-2-methoxybenzoate as a yellow oil (6 mg, 0.02 mmol, 3% yield). ¹H NMR (400 MHz, DMSO-*d*₆) δ = 8.68 (d, *J* = 1.5 Hz, 1H), 8.50 (br d, *J* = 1.5 Hz, 2H), 8.29 (d, *J* = 2.3 Hz, 1H), 8.01 (dd, *J* = 2.4, 8.7 Hz, 1H), 7.86 - 7.80 (m, 1H), 7.53 - 7.45 (m, 2H), 7.38 (ddd, *J* = 0.8, 4.8, 7.8 Hz, 1H), 7.35 - 7.24 (m, 4H), 6.13 (s, 1H), 4.69 - 4.63 (m, 2H), 3.96 - 3.90 (m, 3H), 2.58 (s, 3H), 2.36 (s, 3H). ¹³C NMR (151 MHz, DMSO-*d*₆) δ = 164.6, 159.5, 157.1, 151.1, 150.5, 149.2, 148.9, 146.6, 146.2, 135.4, 134.4, 134.3, 131.1, 130.0, 126.4, 125.8, 124.0, 122.4, 119.2, 113.5, 104.5, 86.2, 56.6, 42.5, 25.2, 14.7. LCMS (HpH) 96% desired product; *t*_{ret} = 1.21 min, MH⁺ 480.4 HRMS (C₂₈H₂₅N₅O₃) requires [M+H]⁺ 480.2036, found [M+H]⁺ 480.2039 *v*_{max} (neat) / cm⁻¹ 2967, 1738, 1618, 1585, 1260, 1191, 1033.

4-Fluorophenyl 5-(2,5-dimethyl-7-((pyridin-3-ylmethyl)amino)pyrazolo[1,5- α]pyrimidin-3-yl)-2-methoxybenzoate (2.27)



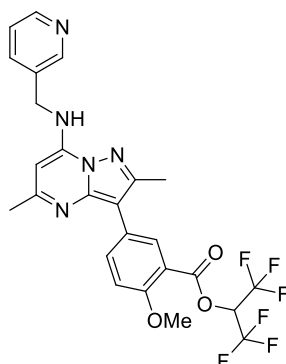
A microwave vial (5 mL) was charged with 5-(2,5-dimethyl-7-((pyridin-3-ylmethyl)amino)pyrazolo[1,5- α]pyrimidin-3-yl)-2-methoxybenzoic acid (190 mg, 0.47 mmol), 4-fluorophenol (63.4 mg, 0.57 mmol), DMAP (11.51 mg, 0.09 mmol), EDC (117 mg, 0.57 mmol) and DMSO (3 mL). The reaction was stirred at RT for 17 h. Additional 4-fluorophenol (63.4 mg, 0.57 mmol) was added and the reaction stirred for a further 2 h. The reaction mixture was purified by MDAP (formic method). The solvent was evaporated *in vacuo* to give 4-fluorophenyl 5-(2,5-dimethyl-7-((pyridin-3-ylmethyl)amino)pyrazolo[1,5- α]pyrimidin-3-yl)-2-methoxybenzoate as a colourless oil (16 mg, 0.03 mmol, 7% yield). ¹H NMR (600 MHz, DMSO-*d*₆) δ = 8.70 - 8.64 (m, 1H), 8.51 (s, 1H), 8.49 - 8.47 (m, 1H), 8.30 - 8.26 (m, 1H), 8.04 - 7.98 (m, 1H), 7.87 - 7.78 (m, 1H), 7.41 - 7.25 (m, 6H), 6.15 - 6.08 (m, 1H), 4.71 - 4.60 (m, 2H), 3.94 - 3.90 (m, 3H), 2.57 (s, 3H), 2.35 (s, 3H). ¹³C NMR (151 MHz, DMSO-*d*₆) δ = 164.7, 160.8, 159.5, 159.3, 157.2, 150.5, 149.2, 148.9, 147.2, 146.5, 146.2, 135.4, 134.5, 134.3, 131.2, 126.0, 118.9, 116.7, 116.5, 113.5, 104.6, 86.2, 56.6, 42.5, 25.3, 14.8. LCMS (HpH) 100% desired product; *t*_{ret} = 1.22 min, MH⁺ 498.4 HRMS (C₂₈H₂₄FN₅O₃) [M+H]⁺ requires 498.1941, found [M+H]⁺ found 498.1941 ν_{max} (neat) / cm⁻¹ 2989, 1743, 1618, 1584, 1503, 1261, 1181, 1033, 520.

2,2,2-Trifluoroethyl 5-(2,5-dimethyl-7-((pyridin-3-ylmethyl)amino)pyrazolo[1,5-*a*]pyrimidin-3-yl)-2-methoxybenzoate (2.28)



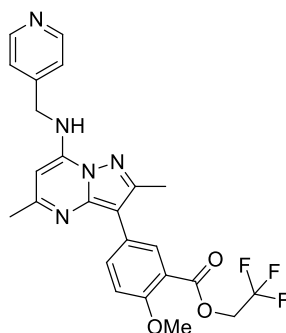
A microwave vial (20 mL) was charged with 5-(2,5-dimethyl-7-((pyridin-3-ylmethyl)amino)pyrazolo[1,5-*a*]pyrimidin-3-yl)-2-methoxybenzoic acid (206 mg, 0.51 mmol), EDC (108 mg, 0.56 mmol), DMAP (12.48 mg, 0.10 mmol), 2,2,2-trifluoroethanol (0.037 mL, 0.51 mmol) and CH₂Cl₂ (3 mL). The reaction was stirred at RT for 2.5 h, diluted with CH₂Cl₂ (15 mL) and washed with brine (15 mL). The organic layer was concentrated *in vacuo* and purified by MDAP (high pH method). The appropriate fractions were combined and evaporated *in vacuo* to afford 2,2,2-trifluoroethyl 5-(2,5-dimethyl-7-((pyridin-3-ylmethyl)amino)pyrazolo[1,5-*a*]pyrimidin-3-yl)-2-methoxybenzoate as a colourless oil (42 mg, 0.09 mmol, 17% yield). ¹H NMR (400 MHz, DMSO-*d*₆) δ = 8.70 - 8.65 (m, 1H), 8.55 - 8.43 (m, 2H), 8.24 (d, *J* = 2.4 Hz, 1H), 8.03 - 7.94 (m, 1H), 7.86 - 7.78 (m, 1H), 7.40 - 7.33 (m, 1H), 7.32 - 7.25 (m, 1H), 6.12 (s, 1H), 4.95 (q, *J* = 9.3 Hz, 2H), 4.65 (d, *J* = 6.8 Hz, 2H), 3.89 (s, 3H), 2.56 (s, 3H), 2.35 (s, 3H). ¹³C NMR (101 MHz, DMSO-*d*₆) δ = 164.2, 159.5, 157.1, 150.3, 149.2, 148.9, 146.4, 146.2, 135.4, 134.3, 134.2, 131.4-121.2, 126.0, 124.1, 118.1, 113.5, 104.3, 86.3, 60.7, 60.3, 56.5, 42.5, 25.2, 14.9. ¹⁹F NMR (376 MHz, DMSO-*d*₆) δ = -72.34 (s, 1F). LCMS (HpH) 99% desired product; *t*_{ret} = 1.17 min, MH⁺ 486.4 HRMS (C₂₄H₂₂F₃N₅O₃) requires [M+H]⁺ 486.1753, found [M+H]⁺ 486.1753. *v*_{max} (neat) / cm⁻¹ 2966, 1738, 1617, 1575, 1504, 1416, 1280, 1164, 1025, 969, 821, 625.

1,1,1,3,3,3-Hexafluoropropan-2-yl 5-(2,5-dimethyl-7-((pyridin-3-ylmethyl)amino)pyrazolo[1,5-*a*]pyrimidin-3-yl)-2-methoxybenzoate (2.29)



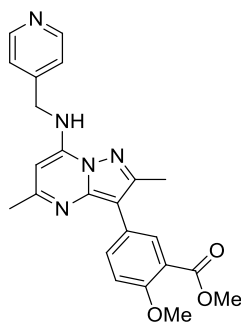
A microwave vial (20 mL) was charged with 5-(2,5-dimethyl-7-((pyridin-3-ylmethyl)amino)pyrazolo[1,5-*a*]pyrimidin-3-yl)-2-methoxybenzoic acid (190 mg, 0.47 mmol), EDC (99 mg, 0.52 mmol), DMAP (11.51 mg, 0.09 mmol) and 1,1,1,3,3,3-hexafluoropropan-2-ol (0.050 mL, 0.47 mmol) in CH₂Cl₂ (3 mL). The reaction was stirred at RT for 3 h, diluted with CH₂Cl₂ (15 mL) and washed with brine (15 mL). The organic layer was concentrated *in vacuo* and purified by MDAP (formic method). The appropriate fractions were combined and evaporated *in vacuo* to afford 1,1,1,3,3,3-hexafluoropropan-2-yl 5-(2,5-dimethyl-7-((pyridin-3-ylmethyl)amino)pyrazolo[1,5-*a*]pyrimidin-3-yl)-2-methoxybenzoate as a white solid (57 mg, 0.10 mmol, 22% yield). **¹H NMR** (400 MHz, DMSO-*d*₆) δ = 8.67 (d, *J* = 1.5 Hz, 1H), 8.56 - 8.51 (m, 1H), 8.50 - 8.46 (m, 1H), 8.42 (d, *J* = 2.4 Hz, 1H), 8.10 - 8.03 (m, 1H), 7.86 - 7.79 (m, 1H), 7.40 - 7.36 (m, 1H), 7.35 (s, 1H), 6.97 (spt, *J* = 6.4 Hz, 1H), 6.13 (s, 1H), 4.65 (d, *J* = 6.8 Hz, 2H), 3.92 (s, 3H), 2.57 (s, 3H), 2.34 (s, 3H). **¹³C NMR** (151 MHz, DMSO-*d*₆) δ = 161.8, 159.6, 157.8, 150.3, 149.2, 148.9, 146.5, 146.3, 135.4, 135.1, 134.3, 131.1, 126.3, 124.1, 115.8, 113.8, 103.8, 86.4, 67.1, 56.7, 42.5, 25.1, 14.9. **¹⁹F NMR** (376 MHz, DMSO-*d*₆) δ = -72.37 (d, *J* = 6.1 Hz, 1F). **LCMS** (Formic) 50% desired product; *t*_{ret} = 0.89 min, MH⁺ 554.3 **HRMS** (C₂₅H₂₁F₆N₅O₃) [M+H]⁺ requires 554.1627, found [M+H]⁺ 554.1633. *ν*_{max} (neat) / cm⁻¹ 2964, 1757, 1618, 1584, 1416, 1285, 1225, 1188, 1107, 1024, 821, 689. **Mp** 58-60 °C.

2,2,2-Trifluoroethyl 5-(2,5-dimethyl-7-((pyridin-4-ylmethyl)amino)pyrazolo[1,5-*a*]pyrimidin-3-yl)-2-methoxybenzoate (2.30)



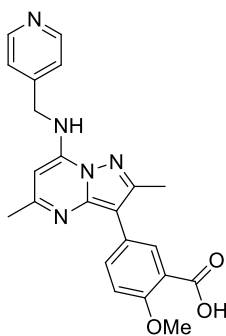
A microwave vial (5 mL) was charged with 5-(2,5-dimethyl-7-((pyridin-4-ylmethyl)amino)pyrazolo[1,5-*a*]pyrimidin-3-yl)-2-methoxybenzoic acid (300 mg, 0.74 mmol), 2,2,2-trifluoroethan-1-ol (0.06 mL, 0.82 mmol), DMAP (18.2 mg, 0.15 mmol), EDC (157 mg, 0.82 mmol) and CH₂Cl₂ (3 mL). The reaction mixture was stirred for 24 h at RT and was directly purified by MDAP (formic method). The appropriate fractions were combined and evaporated *in vacuo* to give 2,2,2-trifluoroethyl 5-(2,5-dimethyl-7-((pyridin-4-ylmethyl)amino)pyrazolo[1,5-*a*]pyrimidin-3-yl)-2-methoxybenzoate as a colourless oil (20 mg, 0.05 mmol, 6% yield). ¹H NMR (400 MHz, DMSO-*d*₆) δ = 8.56 - 8.50 (m, 3H), 8.26 - 8.22 (m, 1H), 7.99 (dd, *J* = 2.4, 8.7 Hz, 1H), 7.41 - 7.35 (m, 2H), 7.32 - 7.27 (m, 1H), 6.00 - 5.98 (m, 1H), 4.95 (q, *J* = 9.0 Hz, 2H), 4.66 (d, *J* = 6.5 Hz, 2H), 3.89 (s, 3H), 2.57 (s, 3H), 2.32 (s, 3H). ¹³C NMR (101 MHz, DMSO-*d*₆) δ = 164.2, 159.5, 157.1, 150.4, 150.2, 147.8, 146.4, 146.4, 134.1, 130.8, 126.0, 122.4, 118.2, 113.5, 104.3, 86.3, 60.7, 60.3, 56.6, 43.9, 25.2, 14.9. ¹⁹F NMR (376 MHz, DMSO-*d*₆) δ = -72.34 (s, 1F). LCMS (Formic) 95% desired product; *t*_{ret} = 0.64 min, MH⁺ 486.4. HRMS (C₂₄H₂₂F₃N₅O₃) [M+H]⁺ requires 486.1753, found [M+H]⁺ 486.1752 *v*_{max} (neat) / cm⁻¹ 3251, 1739, 1583, 1263, 1148, 996, 829, 660, 493.

Methyl 5-(2,5-dimethyl-7-(2-(pyridin-4-yl)ethyl)pyrazolo[1,5-*a*]pyrimidin-3-yl)-2-methoxybenzoate (2.32)



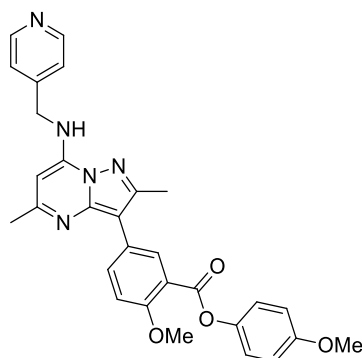
A microwave vial (20 mL) was charged with methyl 5-(2,5-dimethyl-7-phenoxy-pyrazolo[1,5-*a*]pyrimidin-3-yl)-2-methoxybenzoate (2.9 g, 7.19 mmol), pyridin-4-ylmethanamine (0.803 mL, 7.91 mmol), triethylamine (2.204 mL, 15.81 mmol) and DMSO (7 mL). The reaction vessel was sealed and heated in a microwave at 120 °C for 5 h. After cooling, the reaction mixture was diluted with EtOAc (20 mL) and washed with saturated aqueous sodium bicarbonate solution (20 mL). The organic layer was concentrated *in vacuo*, re-dissolved in a minimum amount of MeCN, followed by the addition of water which led to product precipitation to give methyl 5-(2,5-dimethyl-7-(2-(pyridin-4-yl)ethyl)pyrazolo[1,5-*a*]pyrimidin-3-yl)-2-methoxybenzoate as a white solid (1.28 g, 3.09 mmol, 43% yield). **¹H NMR** (400 MHz, DMSO-*d*₆) δ = 8.54 - 8.48 (m, 3H), 8.02 - 7.98 (m, 1H), 7.93 - 7.87 (m, 1H), 7.40 - 7.35 (m, 2H), 7.26 - 7.21 (m, 1H), 5.98 (s, 1H), 4.71 - 4.59 (m, 2H), 3.86 (s, 3H), 3.82 (s, 3H), 2.54 (s, 3H), 2.32 (s, 3H). **¹³C NMR** (101 MHz, DMSO-*d*₆) δ = 166.9, 159.5, 156.5, 150.5, 150.1, 147.8, 146.4, 146.4, 133.5, 130.5, 125.7, 122.4, 120.5, 113.2, 104.8, 86.2, 56.4, 52.4, 44.0, 25.2, 14.7. **LCMS** (HpH) 100% desired product; *t*_{ret} = 0.98 min, MH⁺ 418.4 **HRMS** (C₂₃H₂₃N₅O₃) [M+H]⁺ requires 418.1879 found [M+H]⁺ 418.1874.

5-(2,5-Dimethyl-7-((pyridin-4-ylmethyl)amino)pyrazolo[1,5-*a*]pyrimidin-3-yl)-2-methoxybenzoic acid (2.33)



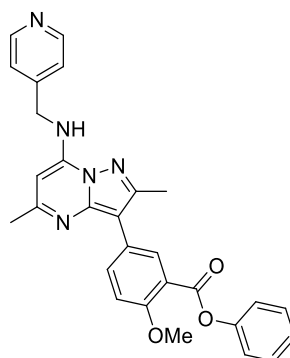
An RBF (100 mL) was charged with methyl 5-(2,5-dimethyl-7-((pyridin-4-ylmethyl)amino)pyrazolo[1,5-*a*]pyrimidin-3-yl)-2-methoxybenzoate (1.20 g, 2.86 mmol), THF (10 mL) and sodium hydroxide (60 mL, 2.86 mmol). The reaction was heated at 70 °C for 3 h and the reaction mixture was concentrated *in vacuo*. The residue was re-dissolved in water (pH = 14), the pH was lowered with acetic acid (pH = 4) and the desired product was extracted out of the aqueous layer with 5:1 chloroform: IPA (50:10 mL). The organic layer was passed through a hydrophobic frit and concentrated *in vacuo* to give 5-(2,5-dimethyl-7-((pyridin-4-ylmethyl)amino)pyrazolo[1,5-*a*]pyrimidin-3-yl)-2-methoxybenzoic acid in quantitative yield (2.6 g, 6.41 mmol). ¹H NMR (400 MHz, DMSO-*d*₆) δ = 8.54 - 8.46 (m, 3H), 7.92 (d, *J* = 2.4 Hz, 1H), 7.81 (dd, *J* = 2.4, 8.8 Hz, 1H), 7.37 (d, *J* = 6.4 Hz, 2H), 7.17 (d, *J* = 8.8 Hz, 1H), 5.96 (s, 1H), 4.67 - 4.62 (m, 2H), 3.84 (s, 3H), 2.53 (s, 3H), 2.31 (s, 3H). ¹³C NMR (101 MHz, DMSO-*d*₆) δ = 168.3, 159.3, 156.2, 150.4, 150.2, 147.8, 146.4, 146.3, 132.5, 130.4, 125.6, 123.0, 122.4, 113.0, 105.2, 86.1, 56.3, 43.9, 25.3, 14.7. LCMS (HpH) 86% desired product; *t*_{ret} = 0.6 min, MH⁺ 404.2.

4-Methoxyphenyl 5-(2,5-dimethyl-7-((pyridin-4-ylmethyl)amino)pyrazolo[1,5- α]pyrimidin-3-yl)-2-methoxybenzoate (2.34)



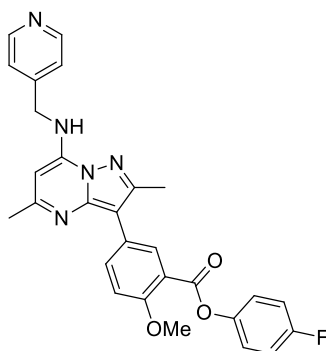
A microwave vial (5 mL) was charged with 5-(2,5-dimethyl-7-((pyridin-4-ylmethyl)amino)pyrazolo[1,5- α]pyrimidin-3-yl)-2-methoxybenzoic acid (200 mg, 0.50 mmol), 4-methoxyphenol (61.5 mg, 0.50 mmol), DMAP (12.1 mg, 0.09 mmol), EDC (105 mg, 0.55 mmol) and CH_2Cl_2 (3 mL). The reaction was stirred for 12 h at RT. Additional 4-methoxyphenol (61.5 mg, 0.50 mmol), DMAP (12.1 mg, 0.10 mmol) and EDC (105 mg, 0.55 mmol) were added and the reaction was stirred for a further 12 h. The reaction mixture was diluted with CH_2Cl_2 (15 mL) and washed with saturated aqueous sodium bicarbonate solution (10 mL) (pH = 9). The organic layer was passed through a concentrated *in vacuo* and purified by MDAP (formic method). The appropriate fractions were combined and concentrated *in vacuo* to give 4-methoxyphenyl 5-(2,5-dimethyl-7-((pyridin-4-ylmethyl)amino)pyrazolo[1,5- α]pyrimidin-3-yl)-2-methoxybenzoate as a yellow/brown oil (40 mg, 0.08 mmol, 16% yield). $^1\text{H NMR}$ (600 MHz, DMSO-d_6) δ = 8.77 (d, J = 6.6 Hz, 2H), 8.13 - 8.09 (m, 1H), 7.90 - 7.85 (m, 1H), 7.80 (d, J = 5.9 Hz, 2H), 7.36 (d, J = 8.8 Hz, 1H), 7.18 (d, J = 9.2 Hz, 2H), 7.01 (d, J = 8.8 Hz, 2H), 6.32 (s, 1H), 4.94 (d, J = 6.2 Hz, 2H), 3.94 (s, 3H), 3.79 (s, 3H), 2.53 (s, 3H), 2.41 (s, 3H) (*NH proton not observed). $^{13}\text{C NMR}$ (151 MHz, DMSO-d_6) δ = 164.8, 159.0, 158.8, 158.6, 158.3, 158.0, 157.4, 145.5, 144.5, 135.1, 132.1, 124.3, 123.1, 119.6, 117.2, 115.4, 115.0, 113.7, 104.7, 87.0, 56.7, 55.9, 55.4, 44.6, 14.1. **LCMS** (Formic) 99% desired product; t_{ret} = 0.69 min, MH^+ 510.4 **HRMS** ($\text{C}_{29}\text{H}_{27}\text{N}_5\text{O}_4$) $[\text{M}+\text{H}]^+$ requires 510.2141, found $[\text{M}+\text{H}]^+$ 510.2139 ν_{max} (neat) / cm^{-1} 3006, 1609, 1505, 1261, 1180, 1133, 1024, 825, 799, 720.

Phenyl 5-(2,5-dimethyl-7-((pyridin-4-ylmethyl)amino)pyrazolo[1,5- σ]pyrimidin-3-yl)-2-methoxybenzoate (2.35)



A microwave vial (5 mL) was charged with 5-(2,5-dimethyl-7-((pyridin-4-ylmethyl)amino)pyrazolo[1,5- σ]pyrimidin-3-yl)-2-methoxybenzoic acid (200 mg, 0.50 mmol), phenol (46.7 mg, 0.50 mmol), DMAP (12.1 mg, 0.10 mmol), EDC (105 mg, 0.55 mmol) and CH_2Cl_2 (3 mL). The reaction was stirred for 12 h at RT. Additional phenol (46.7 mg, 0.50 mmol), DMAP (12.1 mg, 0.10 mmol) and EDC (105 mg, 0.55 mmol) were added and the reaction was stirred for a further 12 h. The reaction mixture was diluted with CH_2Cl_2 (15 mL) and washed with saturated aqueous sodium bicarbonate solution (10 mL) (pH = 9). The organic layer was concentrated *in vacuo* and purified by MDAP (formic method). The appropriate fractions were combined and evaporated *in vacuo* to afford phenyl 5-(2,5-dimethyl-7-((pyridin-4-ylmethyl)amino)pyrazolo[1,5- σ]pyrimidin-3-yl)-2-methoxybenzoate as a colourless oil (10 mg, 0.02 mmol, 5% yield). $^1\text{H NMR}$ (400 MHz, DMSO-d_6) δ = 8.56 - 8.49 (m, 3H), 8.32 - 8.27 (m, 1H), 8.04 - 7.98 (m, 1H), 7.51 - 7.45 (m, 2H), 7.37 (d, J = 6.4 Hz, 2H), 7.34 - 7.25 (m, 4H), 5.99 (s, 1H), 4.71 - 4.61 (m, 2H), 3.92 (s, 3H), 2.58 (s, 3H), 2.33 (s, 3H). $^{13}\text{C NMR}$ (101 MHz, DMSO-d_6) δ = 164.7, 159.5, 157.2, 151.2, 150.2, 147.8, 146.5, 146.4, 134.4, 131.2, 130.0, 126.3, 126.0, 122.4, 122.4, 119.2, 113.5, 104.6, 86.2, 56.6, 55.4, 43.9, 25.3, 14.8. **LCMS** (Formic) 92% desired product; t_{ret} = 0.67 min, MH^+ 480.4 **HRMS** ($\text{C}_{28}\text{H}_{25}\text{N}_5\text{O}_3$) $[\text{M}+\text{H}]^+$ requires 480.2036, found $[\text{M}+\text{H}]^+$ 480.2032. ν_{max} (neat) / cm^{-1} 3006, 1609, 1505, 1261, 1133, 1180, 1049, 824, 719, 539.

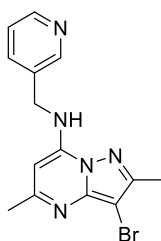
4-Fluorophenyl 5-(2,5-dimethyl-7-((pyridin-4-ylmethyl)amino)pyrazolo[1,5-*a*]pyrimidin-3-yl)-2-methoxybenzoate (2.36)



A microwave vial (5 mL) was charged with 5-(2,5-dimethyl-7-((pyridin-4-ylmethyl)amino)pyrazolo[1,5-*a*]pyrimidin-3-yl)-2-methoxybenzoic acid (215 mg, 0.53 mmol), 4-fluorophenol (59.7 mg, 0.53 mmol), DMAP (13 mg, 0.11 mmol), EDC (112 mg, 0.59 mmol) and CH₂Cl₂ (3 mL). The reaction was stirred for 12 h at RT. Additional EDC (112 mg, 0.59 mmol), DMAP (13 mg, 0.11 mmol) and 4-fluorophenol (59.7 mg, 0.53 mmol) were added and the reaction was stirred for a further 12 h. The reaction mixture was directly purified by MDAP (formic method). The appropriate fractions were combined and evaporated *in vacuo* to give 4-fluorophenyl 5-(2,5-dimethyl-7-((pyridin-4-ylmethyl)amino)pyrazolo[1,5-*a*]pyrimidin-3-yl)-2-methoxybenzoate as white solid (37 mg, 0.07 mmol, 14% yield). ¹H NMR (400 MHz, DMSO-*d*₆) δ = 8.56 - 8.50 (m, 3H), 8.29 (d, *J* = 2.5 Hz, 1H), 8.02 (dd, *J* = 2.5, 8.8 Hz, 1H), 7.38 (d, *J* = 6.0 Hz, 2H), 7.35 - 7.28 (m, 5H), 5.99 (s, 1H), 4.76 - 4.60 (m, 2H), 3.92 (s, 3H), 2.58 (s, 3H), 2.33 (s, 3H). ¹³C NMR (101 MHz, DMSO-*d*₆) δ = 164.6, 163.5, 159.5, 157.3, 150.5, 150.2, 147.8, 146.4, 134.5, 131.2, 126.0, 124.2, 124.1, 122.4, 118.9, 116.7, 116.5, 113.5, 104.5, 86.2, 56.6, 44.0, 25.3, 14.8. ¹⁹F NMR (376 MHz, DMSO-*d*₆) δ = -117.25 (s, 1F). LCMS (Formic) 98% desired product; *t*_{ret} = 0.71 min, MH⁺ 498.4 HRMS (C₂₈H₂₄FN₅O₃) [M+H]⁺ requires 498.1941, found [M+H]⁺ 498.1941 *v*_{max} (neat) / cm⁻¹. 3377, 1741, 1618, 1580, 1500, 1258, 1178, 1023, 820, 623, 482. Mp 96-98 °C.

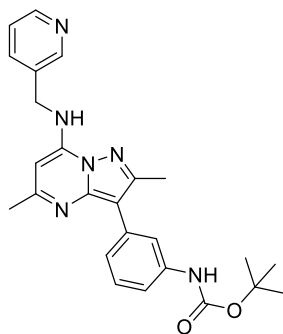
3-Bromo-2,5-dimethyl-N-(pyridin-3-ylmethyl)pyrazolo[1,5-*a*]pyrimidin-7-amine

(2.37)



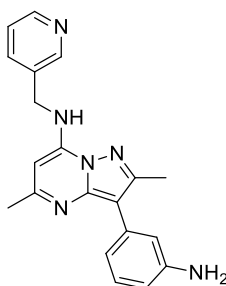
A microwave vial (20 mL) was charged with 3-bromo-2,5-dimethyl-7-phenoxypyrazolo[1,5-*a*]pyrimidine (1.54 g, 4.83 mmol), pyridin-3-ylmethanamine (0.54 mL, 5.32 mmol), triethylamine (1.48 mL, 10.63 mmol) and dimethyl sulfoxide (7 mL). The reaction vessel was sealed and heated in a microwave at 120 °C for 5 h. After cooling, the reaction mixture was diluted with EtOAc (25 mL) and washed with saturated aqueous sodium bicarbonate solution (25 mL). The organic layer was passed through a hydrophobic frit and concentrated *in vacuo*. The residue was dissolved in a minimum amount of MeCN and upon addition of water, precipitation occurred, and the product was collected by vacuum filtration (1.6 g, 4.80 mmol, 99% yield). ¹H NMR (400 MHz, CHLOROFORM-*d*) δ = 8.61 (d, *J* = 1.5 Hz, 1H), 8.55 (dd, *J* = 1.7, 4.7 Hz, 1H), 7.67 - 7.62 (m, 1H), 7.30 - 7.25 (m, 1H), 6.77 (br t, *J* = 5.9 Hz, 1H), 5.75 (s, 1H), 4.57 (d, *J* = 6.4 Hz, 2H), 2.46 (s, 3H), 2.39 (s, 3H). ¹³C NMR (101 MHz, CHLOROFORM-*d*) δ = 160.6, 152.0, 149.5, 148.7, 145.8, 145.7, 134.9, 132.0, 123.8, 86.0, 82.2, 43.7, 25.2, 13.2. LCMS (HpH) 100% desired product; *t*_{ret} = 0.86 min, MH⁺ 333.1.

Tert-butyl (3-(2,5-dimethyl-7-((pyridin-3-ylmethyl)amino)pyrazolo[1,5-*a*]pyrimidin-3-yl)phenyl)carbamate (2.39)



A microwave vial (5 mL) was charged with 3-bromo-2,5-dimethyl-*N*-(pyridin-3-ylmethyl)pyrazolo[1,5-*a*]pyrimidin-7-amine (188 mg, 0.57 mmol), (3-((*tert*-butoxycarbonyl)amino)phenyl)boronic acid (201 mg, 0.85 mmol), PdCl₂(dppf)-CH₂Cl₂ adduct (46.2 mg, 0.06 mmol), cesium carbonate (277 mg, 0.85 mmol), 1,4-dioxane (2 mL) and water (0.5 mL). The reaction vessel was sealed and heated in a microwave at 120 °C for 5 h. After cooling, the reaction mixture was passed through Celite™, diluted with EtOAc (20 mL) and washed with brine (20 mL). The organic layer was concentrated *in vacuo* and the crude product was purified by column chromatography eluting with EtOAc in cyclohexane (0-100% gradient). The appropriate fractions were combined and concentrated *in vacuo* to give *tert*-butyl (3-(2,5-dimethyl-7-((pyridin-3-ylmethyl)amino)pyrazolo[1,5-*a*]pyrimidin-3-yl)phenyl)carbamate as an oil (119 mg, 0.27 mmol, 48% yield). ¹H NMR (400 MHz, DMSO-*d*₆) δ = 9.30 (s, 1H), 8.71 - 8.66 (m, 1H), 8.52 - 8.43 (m, 2H), 7.85 - 7.79 (m, 1H), 7.72 - 7.69 (m, 1H), 7.42 - 7.34 (m, 3H), 7.31 - 7.25 (m, 1H), 6.10 - 6.08 (m, 1H), 4.67 - 4.62 (m, 2H), 2.53 (s, 3H), 2.35 (s, 3H), 1.49 (s, 9H). ¹³C NMR (101 MHz, DMSO-*d*₆) δ = 159.4, 153.3, 150.6, 149.2, 148.9, 146.6, 146.1, 139.8, 135.4, 134.4, 133.9, 128.7, 124.0, 122.9, 118.7, 115.8, 106.1, 86.1, 79.3, 42.5, 28.7, 25.2, 14.9. LCMS (HpH) 97% desired product; *t*_{ret} = 1.18 min, MH⁺ 445.4.

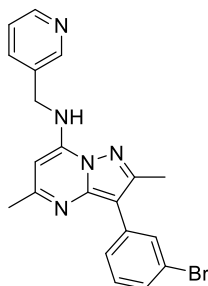
3-(3-Aminophenyl)-2,5-dimethyl-*N*-(pyridin-3-ylmethyl)pyrazolo[1,5-*a*]pyrimidin-7-amine (2.40)



A microwave vial (20 mL) was charged with *tert*-butyl (3-(2,5-dimethyl-7-((pyridin-3-ylmethyl)amino)pyrazolo[1,5-*a*]pyrimidin-3-yl)phenyl)carbamate (110 mg, 0.25 mmol) and 1,4-dioxane (4 mL). To this, HCl (2 mL, 4 M) in 1,4-dioxane (4 mL) was added and the reaction was heated at 55 °C for 2.5 h. After cooling, the reaction

mixture was diluted with EtOAc (3 x 20 mL) and washed with saturated aqueous sodium bicarbonate solution (20 mL). The combined organics was concentrated *in vacuo* to give 3-(3-aminophenyl)-2,5-dimethyl-*N*-(pyridin-3-ylmethyl)pyrazolo[1,5-*a*]pyrimidin-7-amine in quantitative yield (90 mg, 0.25 mmol). **¹H NMR** (400 MHz, DMSO-*d*₆) δ = 8.70 - 8.65 (m, 1H), 8.51 - 8.46 (m, 1H), 8.44 - 8.38 (m, 1H), 7.85 - 7.79 (m, 1H), 7.39 - 7.33 (m, 1H), 7.09 - 7.02 (m, 1H), 6.93 - 6.89 (m, 1H), 6.87 - 6.81 (m, 1H), 6.50 - 6.43 (m, 1H), 6.06 (s, 1H), 5.00 - 4.95 (m, 2H), 4.68 - 4.60 (m, 2H), 3.57 (s, 3H), 2.34 (s, 3H). **¹³C NMR** (101 MHz, DMSO-*d*₆) δ = 158.9, 150.6, 149.2, 148.9, 148.8, 146.4, 146.1, 135.4, 134.4, 134.0, 128.9, 124.1, 117.2, 114.8, 107.0, 85.7, 66.8, 42.6, 25.3, 14.8. **LCMS** (HpH) 94% desired product; *t*_{ret} = 0.85 min, MH⁺ 345.3.

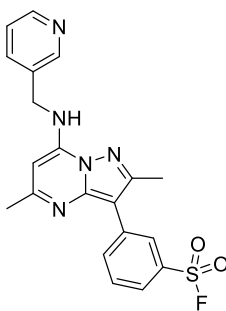
3-(3-Bromophenyl)-2,5-dimethyl-*N*-(pyridin-3-ylmethyl)pyrazolo[1,5-*a*]pyrimidin-7-amine (2.41)



An RBF (50 mL) was charged with 3-(3-aminophenyl)-2,5-dimethyl-*N*-(pyridin-3-ylmethyl)pyrazolo[1,5-*a*]pyrimidin-7-amine (706 mg, 2.05 mmol) and CH₂Cl₂ (5 mL). To this, water (5 mL) was added, followed by bromotrichloromethane (0.808 mL, 8.20 mmol) and sodium nitrite (707 mg, 10.25 mmol). The reaction mixture was stirred for 5 mins and then acetic acid (2.347 mL, 41.0 mmol) was added dropwise. The reaction mixture was stirred vigorously at RT for 1 h. The reaction mixture was diluted with CH₂Cl₂ (3 x 15 mL) and washed with brine (15 mL). The organic layer was concentrated *in vacuo* and the crude product was purified by column chromatography eluting with EtOAc in cyclohexane (0-100% gradient). The appropriate fractions were combined and concentrated *in vacuo* to give 3-(3-bromophenyl)-2,5-dimethyl-*N*-(pyridin-3-ylmethyl)pyrazolo[1,5-*a*]pyrimidin-7-amine (316 mg, 0.78 mmol, 38% yield). **¹H NMR** (600 MHz, DMSO-*d*₆) δ = 8.69 - 8.65 (m, 1H), 8.58 - 8.53 (m, 1H), 8.51 - 8.46 (m, 1H),

8.04 - 8.00 (m, 1H), 7.85 - 7.80 (m, 1H), 7.76 - 7.73 (m, 1H), 7.43 - 7.35 (m, 3H), 6.15 (s, 1H), 4.70 - 4.61 (m, 2H), 2.57 (s, 3H), 2.37 (s, 3H). ^{13}C NMR (151 MHz, DMSO- d_6) δ = 160.0, 150.8, 149.2, 148.9, 146.7, 146.2, 136.3, 135.4, 134.3, 130.8, 130.6, 128.3, 127.1, 124.1, 122.1, 104.3, 86.5, 42.4, 25.3, 14.9. LCMS (HpH) 96% desired product; t_{ret} = 1.24 min, MH^+ 408.0 HRMS ($\text{C}_{20}\text{H}_{18}\text{BrN}_5$) $[\text{M}+\text{H}]^+$ requires 408.0824 found $[\text{M}+\text{H}]^+$ 408.0821.

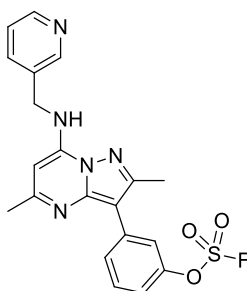
3-(2,5-Dimethyl-7-((pyridin-3-ylmethyl)amino)pyrazolo[1,5- α]pyrimidin-3-yl)benzene-1-sulfonyl fluoride (2.42)



A microwave vial (5 mL) was charged with 3-(3-bromophenyl)-2,5-dimethyl-*N*-(pyridin-3-ylmethyl)pyrazolo[1,5- α]pyrimidin-7-amine (106 mg, 0.26 mmol), bis(*tert*-butyl(4-dimethylaminophenyl)phosphine)-dichloropalladium(II) (16.54 mg, 0.02 mmol), 1,4-diazabicyclo[2.2.2]octane bis(sulfur dioxide)-adduct (62.4 mg, 0.26 mmol), *N,N*-dicyclohexylmethylamine (0.167 mL, 0.78 mmol) and isopropanol (2 mL). The reaction was heated in a microwave at 110 °C for 1.5 h. After cooling, *N*-fluorobenzenesulfonamide (246 mg, 0.78 mmol) was added and the reaction was stirred at RT for 13 h. The reaction mixture was diluted with EtOAc (20 mL) and passed through a CeliteTM and the organic layer was washed with brine (20 mL) and concentrated *in vacuo*. The crude product was purified by column chromatography eluting with EtOAc in cyclohexane (0-100% gradient). The appropriate fractions were combined and concentrated *in vacuo* to afford 3-(2,5-dimethyl-7-((pyridin-3-ylmethyl)amino)pyrazolo[1,5- α]pyrimidin-3-yl)benzene-1-sulfonyl fluoride as a colourless oil (44 mg, 0.11 mmol, 42% yield). ^1H NMR (600 MHz, DMSO- d_6) δ = 8.69 - 8.64 (m, 3H), 8.50 - 8.46 (m, 1H), 8.35 - 8.31 (m, 1H), 7.95 - 7.91 (m, 1H), 7.87 - 7.80 (m, 2H), 7.40 - 7.35 (m, 1H), 6.23 (s, 1H), 4.70 - 4.63 (m, 2H), 2.64 (s, 3H), 2.39 (s, 3H).

¹³C NMR (151 MHz, DMSO-d₆) δ = 160.6, 151.1, 149.2, 149.0, 147.0, 146.4, 136.2, 135.4, 135.0, 134.2, 132.3, 130.8, 126.7, 124.6, 123.9, 102.9, 87.1, 42.4, 25.3, 15.2. **LCMS** (Formic) 98% desired product; t_{ret} = 0.78 min, MH⁺ 412.3 **HRMS** (C₂₀H₁₈FN₅O₂S) [M+H]⁺ requires 412.1243 found [M+H]⁺ 412.1241 ν_{max} (neat) / cm⁻¹ 3391, 1617, 1583, 1393, 1203, 1026, 998, 792, 734, 588, 488.

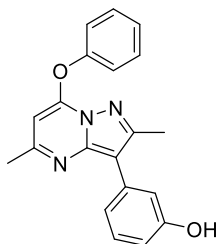
3-(2,5-Dimethyl-7-((pyridin-3-ylmethyl)amino)pyrazolo[1,5-*a*]pyrimidin-3-yl)phenyl sulfofluoridate (2.18)



Chamber A of the COware flask reactor was charged with sulfonyldiimidazole (0.263 g, 1.33 mmol) and potassium fluoride (0.205 g, 3.53 mmol). Chamber B of the COware flask reactor was charged with 3-(2,5-dimethyl-7-((pyridin-3-ylmethyl)amino)pyrazolo[1,5-*a*]pyrimidin-3-yl)phenol (0.305 g, 0.88 mmol), triethylamine (0.246 mL, 1.77 mmol) and CH₂Cl₂ (4 mL). Trifluoroacetic acid (1 mL) was added to chamber A *via* syringe injection. The reaction was stirred vigorously at RT for 18 h. The reaction was brought to a stop and the pressure was released. Chamber B was decanted into an RBF (50 mL) and chamber A was quenched with concentrated aqueous NaOH. The reaction mixture was concentrated *in vacuo*, diluted with CH₂Cl₂ (15 mL) and washed with brine (15 mL). The organic layer was concentrated *in vacuo* and purified by MDAP (formic method). The appropriate fractions were combined and concentrated *in vacuo* to give 3-(2,5-dimethyl-7-((pyridin-3-ylmethyl)amino)pyrazolo[1,5-*a*]pyrimidin-3-yl)phenyl sulfofluoridate (179 mg, 0.42 mmol, 48% yield). ¹H NMR (400 MHz, DMSO-d₆) δ = 8.67 (d, *J* = 1.0 Hz, 1H), 8.59 (br t, *J* = 6.7 Hz, 1H), 8.48 (br d, *J* = 3.5 Hz, 1H), 8.05 (s, 1H), 7.93 (td, *J* = 1.1, 8.1 Hz, 1H), 7.82 (br d, *J* = 8.0 Hz, 1H), 7.62 (t, *J* = 8.2 Hz, 1H), 7.42 - 7.34 (m, 2H), 6.18 (s, 1H), 4.65 (d, *J* = 6.5 Hz, 2H), 2.60 (s, 3H), 2.37 (s, 3H). ¹³C NMR (151 MHz, DMSO-

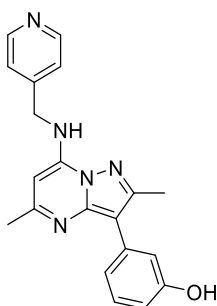
d_6) δ = 160.3, 151.0, 150.4, 149.2, 149.0, 146.9, 146.3, 136.8, 135.4, 134.2, 130.9, 128.2, 124.0, 119.7, 117.4, 103.7, 86.8, 42.5, 25.3, 15.1. **^{19}F NMR** (376 MHz, DMSO- d_6) δ = 38.52 (s, 1F). **LCMS** (Formic) 98% desired product; t_{ret} = 0.83 min, MH^+ 428.3. **HRMS** ($\text{C}_{20}\text{H}_{18}\text{FN}_5\text{O}_3\text{S}$) $[\text{M}+\text{H}]^+$ requires 428.1193 found $[\text{M}+\text{H}]^+$ 428.1193 ν_{max} (neat) / cm^{-1} 3183, 1614, 1545, 1418, 1228, 1039, 926, 682, 572.

3-(2,5-Dimethyl-7-phenoxy-pyrazolo[1,5- α]pyrimidin-3-yl)phenol (2.49)



An RBF (50 mL) was charged with 3-bromo-2,5-dimethyl-7-phenoxy-pyrazolo[1,5- α]pyrimidine (1 g, 3.14 mmol), (3-hydroxyphenyl)boronic acid (0.650 g, 4.71 mmol), $\text{PdCl}_2(\text{dppf})\text{-CH}_2\text{Cl}_2$ adduct (0.180 g, 0.22 mmol), cesium carbonate (1.536 g, 4.71 mmol), 1,4-dioxane (16 mL) and water (4 mL). The reaction was heated at 100 °C for 17 h. After cooling, the reaction mixture was passed through CeliteTM, diluted with EtOAc (30 mL) and washed with brine (25 mL). The organic layer was concentrated *in vacuo* and purified by column chromatography eluting with EtOAc in cyclohexane (0-100% gradient). The appropriate fractions were combined and concentrated *in vacuo* to give 3-(2,5-dimethyl-7-phenoxy-pyrazolo[1,5- α]pyrimidin-3-yl)phenol (987 mg, 2.98 mmol, 95% yield). **^1H NMR** (400 MHz, DMSO- d_6) δ = 9.39 (s, 1H), 7.58 (br d, J = 7.8 Hz, 2H), 7.47 - 7.42 (m, 3H), 7.25 (s, 1H), 7.20 (s, 2H), 6.74 - 6.67 (m, 1H), 5.97 - 5.91 (m, 1H), 2.55 (s, 3H), 2.42 (s, 3H). **^{13}C NMR** (101 MHz, DMSO- d_6) δ = 161.0, 157.7, 154.1, 152.3, 152.2, 147.8, 134.0, 131.2, 129.5, 127.5, 121.3, 119.5, 115.9, 113.5, 107.6, 90.7, 25.2, 14.9. **LCMS** (HpH) 82% desired product; t_{ret} = 1.08 min, MH^+ 332.23.

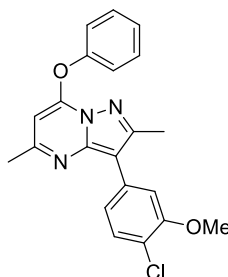
3-(2,5-Dimethyl-7-((pyridin-4-ylmethyl)amino)pyrazolo[1,5-*a*]pyrimidin-3-yl)phenol (2.50)



A microwave vial (5 mL) was charged with 3-(2,5-dimethyl-7-phenoxy-pyrazolo[1,5-*a*]pyrimidin-3-yl)phenol (309 mg, 0.93 mmol), pyridin-4-ylmethanamine (0.142 mL, 1.40 mmol), DIPEA (0.326 mL, 1.87 mmol) and DMSO (3 mL). The reaction vessel was sealed and heated in a microwave at 130 °C for 5 h. After cooling, the reaction was diluted with EtOAc (25 mL) and washed with saturated aqueous sodium bicarbonate solution (25 mL). The organic layer was concentrated *in vacuo* and the crude product was purified by column chromatography eluting with EtOAc in cyclohexane (0-100% gradient). The appropriate fractions were combined and concentrated *in vacuo* to give 3-(2,5-dimethyl-7-((pyridin-4-ylmethyl)amino)pyrazolo[1,5-*a*]pyrimidin-3-yl)phenol (80 mg, 0.23 mmol, 25% yield). ¹H NMR (400 MHz, DMSO-*d*₆) δ = 9.33 - 9.26 (m, 1H), 8.67 (d, *J* = 2.0 Hz, 1H), 8.49 - 8.43 (m, 2H), 7.82 (td, *J* = 1.8, 8.2 Hz, 1H), 7.41 - 7.34 (m, 1H), 7.23 - 7.17 (m, 2H), 7.16 - 7.12 (m, 1H), 6.66 - 6.62 (m, 1H), 6.09 (s, 1H), 4.64 (br d, *J* = 5.4 Hz, 2H), 2.53 (s, 3H), 2.36 (s, 3H). ¹³C NMR (101 MHz, DMSO-*d*₆) δ = 159.3, 157.6, 150.6, 149.2, 148.9, 146.5, 135.4, 134.4, 129.4, 124.1, 119.6, 115.7, 112.9, 106.2, 86.1, 42.5, 25.3, 14.9. LCMS (HpH) 99% desired product; *t*_{ret} = 0.87 min, MH⁺ 346.1 HRMS (C₂₀H₁₉N₅O) [M+H]⁺ requires 346.1668 found [M+H]⁺ 346.1665 *v*_{max} (neat) / cm⁻¹ 3371, 2664, 1605, 1576, 1414, 1326, 781, 463.

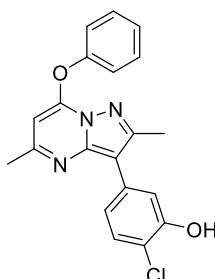
3-(4-Chloro-3-methoxyphenyl)-2,5-dimethyl-7-phenoxyprazolo[1,5-*a*]pyrimidine

(2.52)



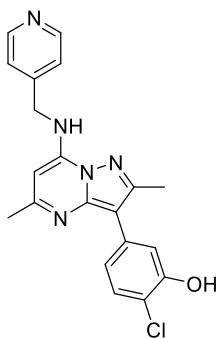
A microwave vial (20 mL) was charged with 3-bromo-2,5-dimethyl-7-phenoxyprazolo[1,5-*a*]pyrimidine (0.92 g, 2.89 mmol), (4-chloro-3-methoxyphenyl)boronic acid (0.808 g, 4.34 mmol), PdCl₂(dppf)-CH₂Cl₂ adduct (0.189 g, 0.23 mmol), cesium carbonate (1.413 g, 4.34 mmol), 1,4-dioxane (10 mL) and water (2.5 mL). The reaction vessel was sealed and heated in a microwave at 130 °C for 4 h. After cooling, the reaction mixture was passed through Celite™, diluted with EtOAc (25 mL) and washed with brine (25 mL). The organic layer was passed through a hydrophobic frit and concentrated *in vacuo* to give 3-(4-chloro-3-methoxyphenyl)-2,5-dimethyl-7-phenoxyprazolo[1,5-*a*]pyrimidine (1.05 g, 2.77 mmol, 96% yield). ¹H NMR (400 MHz, DMSO-*d*₆) δ = 7.63 - 7.56 (m, 3H), 7.52 - 7.47 (m, 1H), 7.46 - 7.41 (m, 3H), 7.39 - 7.34 (m, 1H), 6.00 (s, 1H), 3.93 (s, 3H), 2.61 (s, 3H), 2.44 (s, 3H). ¹³C NMR (101 MHz, DMSO-*d*₆) δ = 161.6, 154.8, 154.2, 152.4, 152.2, 147.9, 133.2, 131.2, 130.1, 127.4, 121.5, 121.3, 118.9, 113.0, 106.4, 91.1, 56.4, 25.3, 15.1. LCMS (HpH) 95% desired product; t_{ret} = 1.41 min, MH⁺ 380.1. HRMS (C₂₁H₁₈ClN₃O₂) [M+H]⁺ requires 380.1166, found [M+H]⁺ 380.1162.

2-Chloro-5-(2,5-dimethyl-7-phenoxyprazolo[1,5-*a*]pyrimidin-3-yl)phenol (2.53)



An RBF (50 mL) was charged with 3-(4-chloro-3-methoxyphenyl)-2,5-dimethyl-7-phenoxy-pyrazolo[1,5-*a*]pyrimidine (100 mg, 0.26 mmol) and anhydrous CH₂Cl₂ (6 mL). The solution was stirred in an acetone-dry ice bath for 5 minutes, before removal of the ice-bath, tribromoborane solution in CH₂Cl₂ (0.360 mL, 2.11 mmol) was added and the reaction was left to stir at RT for 16 h. The reaction mixture was diluted with CH₂Cl₂ (15 mL) and washed with saturated aqueous sodium bicarbonate solution (15 mL). The organic layer was concentrated *in vacuo* and purified by MDAP (formic method). The appropriate fractions were combined and evaporated *in vacuo* to give 2-chloro-5-(2,5-dimethyl-7-phenoxy-pyrazolo[1,5-*a*]pyrimidin-3-yl)phenol (43 mg, 0.12 mmol, 45% yield). ¹H NMR (400 MHz, DMSO-*d*₆) δ = 7.58 (d, *J* = 7.8 Hz, 2H), 7.47 - 7.42 (m, 4H), 7.39 (d, *J* = 8.3 Hz, 1H), 7.23 - 7.18 (m, 1H), 5.97 (s, 1H), 2.55 (s, 3H), 2.43 (s, 3H) (OH signal not observed). ¹³C NMR (101 MHz, DMSO-*d*₆) δ = 161.3, 154.2, 153.6, 152.3, 152.2, 147.8, 132.7, 131.2, 130.0, 127.4, 121.4, 120.3, 117.8, 117.0, 106.6, 90.9, 25.2, 15.0. LCMS (HpH) 100% desired product; *t*_{ret} = 1.20 min, MH⁺ 366.1. HRMS (C₂₀H₁₆ClN₃O₂) [M+H]⁺ requires 366.1009 found [M+H]⁺ 366.1004.

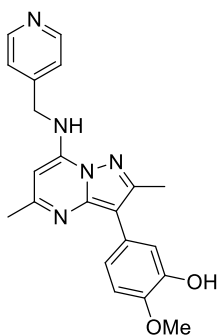
2-Chloro-5-(2,5-dimethyl-7-((pyridin-4-ylmethyl)amino)pyrazolo[1,5-*a*]pyrimidin-3-yl)phenol (2.54)



A microwave vial (5 mL) was charged with 2-chloro-5-(2,5-dimethyl-7-phenoxy-pyrazolo[1,5-*a*]pyrimidin-3-yl)phenol (43 mg, 0.12 mmol), pyridin-4-ylmethanamine (0.013 mL, 0.13 mmol), triethylamine (0.025 mL, 0.18 mmol) and DMSO (3 mL). The reaction vessel was sealed and heated in a microwave at 120 °C for 4 h. After cooling, the reaction mixture was diluted with EtOAc (10 mL) and washed with saturated aqueous sodium bicarbonate solution (10 mL). The organic

layer was concentrated *in vacuo* and purified by MDAP (formic method). The appropriate fractions were combined and concentrated *in vacuo* to give 2-chloro-5-(2,5-dimethyl-7-((pyridin-4-ylmethyl)amino)pyrazolo[1,5-*a*]pyrimidin-3-yl)phenol (16 mg, 0.04 mmol, 36% yield). **¹H NMR** (400 MHz, DMSO-*d*₆) δ = 8.55 - 8.47 (m, 3H), 7.44 (d, *J* = 2.0 Hz, 1H), 7.40 - 7.36 (m, 2H), 7.34 (d, *J* = 8.3 Hz, 1H), 7.21 (dd, *J* = 2.0, 8.3 Hz, 1H), 5.99 (s, 1H), 4.65 (d, *J* = 6.5 Hz, 2H), 2.55 (s, 3H), 2.34 (s, 3H) (OH signal not observed). **¹³C NMR** (101 MHz, DMSO-*d*₆) δ = 159.5, 153.3, 150.6, 150.2, 147.8, 146.5, 146.3, 133.6, 129.8, 122.4, 120.3, 117.1, 116.7, 105.1, 86.3, 43.9, 25.3, 15.1. **LCMS** (Formic) 97% desired product; *t*_{ret} = 0.52 min, MH⁺ 380.4. **HRMS** (C₂₀H₁₈ClN₅O) [M+H]⁺ requires 380.1278 found [M+H]⁺ 380.1282.

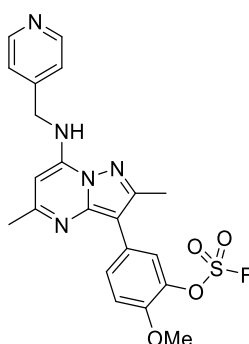
5-(2,5-Dimethyl-7-((pyridin-4-ylmethyl)amino)pyrazolo[1,5-*a*]pyrimidin-3-yl)-2-methoxyphenol (2.55)



A microwave vial (20 mL) was charged with 5-(2,5-dimethyl-7-phenoxy)pyrazolo[1,5-*a*]pyrimidin-3-yl)-2-methoxyphenol (1.04 g, 2.88 mmol), pyridin-4-ylmethanamine (0.321 mL, 3.17 mmol), triethylamine (0.88 mL, 6.33 mmol) and DMSO (10 mL). The reaction vessel was sealed and heated in a microwave at 120 °C for 4 h. After cooling, the reaction mixture was diluted with EtOAc (20 mL) and washed with saturated aqueous sodium bicarbonate solution (20 mL). The organic layer was concentrated *in vacuo* and purified by column chromatography eluting with EtOAc in cyclohexane (0-100% gradient). The appropriate fractions were combined and concentrated *in vacuo* to give 5-(2,5-dimethyl-7-((pyridin-4-ylmethyl)amino)pyrazolo[1,5-*a*]pyrimidin-3-yl)-2-methoxyphenol (865 mg, 2.31 mmol, 80% yield) as a colourless oil. **¹H NMR** (400 MHz, DMSO-*d*₆) δ = 8.55-8.50 (m, 2H), 8.45-8.42 (m, 1H), 7.37 (d, *J* = 5.9 Hz, 2H), 7.20

(d, $J = 2.4$ Hz, 1H), 7.12 - 7.05 (m, 1H), 6.97 (d, $J = 8.3$ Hz, 1H), 5.93 (s, 1H), 4.64 (d, $J = 6.4$ Hz, 2H), 3.80 (s, 3H), 2.52 (s, 3H), 2.31 (s, 3H) (OH signal not observed). ^{13}C NMR (DMSO- d_6 , 101 MHz) $\delta = 160.6, 154.1, 152.1, 150.2, 147.6, 146.8, 146.7, 131.1, 127.4, 125.6, 121.3, 116.6, 112.9, 94.9, 90.5, 89.9, 56.2, 25.2, 14.8$. LCMS (Formic) 97% desired product; $t_{\text{ret}} = 0.87$ min, MH^+ 376.3 HRMS ($\text{C}_{21}\text{H}_{21}\text{N}_5\text{O}_2$) $[\text{M}+\text{H}]^+$ requires 376.1773 found $[\text{M}+\text{H}]^+$ 376.1769 ν_{max} (neat) / cm^{-1} 3402, 2921, 1617, 1582, 1410, 1326, 1250, 1010, 796, 558, 473.

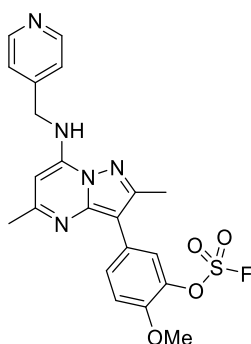
5-(2,5-Dimethyl-7-((pyridin-4-ylmethyl)amino)pyrazolo[1,5- α]pyrimidin-3-yl)-2-methoxyphenyl sulfofluoridate (2.45)



Chamber A of the COware flask reactor was charged with sulfonyldiimidazole (118 mg, 0.56 mmol) and potassium fluoride (92 mg, 1.59 mmol). Chamber B of the COware flask reactor was charged with 5-(2,5-dimethyl-7-((pyridin-4-ylmethyl)amino)pyrazolo[1,5- α]pyrimidin-3-yl)-2-methoxyphenol (149 mg, 0.40 mmol), DIPEA (0.83 mL, 4.76 mmol) and MeCN (3 mL). Trifluoroacetic acid (1 mL) was added to chamber A *via* syringe injection. The reaction was stirred vigorously at RT for 18 h. Chamber B was decanted into an RBF (50 mL) and chamber A was quenched with concentrated aqueous NaOH. The reaction mixture was concentrated *in vacuo* and purified by MDAP (formic method). The appropriate fractions were combined and concentrated *in vacuo* to give 5-(2,5-dimethyl-7-((pyridin-4-ylmethyl)amino)pyrazolo[1,5- α]pyrimidin-3-yl)-2-methoxyphenyl sulfofluoridate in quantitative yield (260 mg, 0.57 mmol). ^1H NMR (400 MHz, DMSO- d_6) $\delta = 8.75$ (br s, 1H), 8.63 - 8.58 (m, 2H), 7.97 (d, $J = 1.5$ Hz, 1H), 7.82 (dd, $J = 2.2, 8.6$ Hz, 1H), 7.52 (d, $J = 5.9$ Hz, 2H), 7.43 (d, $J = 8.8$ Hz, 1H), 6.08 (s, 1H), 4.74 (d, $J = 6.8$ Hz, 2H), 3.95 (s,

3H), 2.58 (s, 3H), 2.35 (s, 3H). ^{13}C NMR (151 MHz, DMSO- d_6) δ = 160.1, 151.0, 150.6, 150.2, 147.7, 146.8, 146.5, 136.1, 136.1, 122.5, 122.4, 120.6, 113.7, 104.4, 86.7, 56.8, 43.9, 25.3, 15.2. ^{19}F NMR (376 MHz, DMSO- d_6) δ = 40.36 (s, 1F). LCMS (Formic) 100% desired product; t_{ret} = 0.74 min, MH^+ 458.3 HRMS ($\text{C}_{21}\text{H}_{20}\text{FN}_5\text{O}_4\text{S}$) $[\text{M}+\text{H}]^+$ requires 458.1298 found $[\text{M}+\text{H}]^+$ 458.1293 ν_{max} (neat) / cm^{-1} 3286, 1616, 1585, 1543, 1452, 1227, 1104, 1014, 923, 835, 802, 763, 543. Mp 109-111 °C.

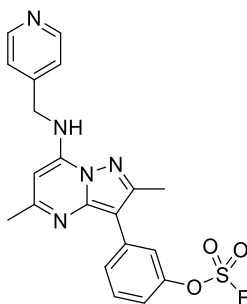
5-(2,5-Dimethyl-7-((pyridin-4-ylmethyl)amino)pyrazolo[1,5- α]pyrimidin-3-yl)-2-methoxyphenyl sulfofluoridate (2.45)



A microwave vial (5 mL) was charged with 5-(2,5-dimethyl-7-((pyridin-4-ylmethyl)amino)pyrazolo[1,5- α]pyrimidin-3-yl)-2-methoxyphenol (203 mg, 0.54 mmol) and THF (3 mL). To this, (4-acetamidophenyl)(fluorosulfonyl)sulfamoyl fluoride (204 mg, 0.65 mmol) was added, followed by the addition of (*Z*)-3,4,5,6,8,9,10,11-octahydro-2*H*-pyrido[1,2- α][1,3]diazocine (0.2 mL, 1.19 mmol). The reaction was stirred for 10 minutes at RT. The reaction mixture was concentrated *in vacuo* and the residue was dissolved in CH_2Cl_2 (20 mL) and washed with brine (10 mL). The organic layer was concentrated *in vacuo* and the crude product was purified by MDAP (formic method). The appropriate fractions were combined and concentrated *in vacuo* to give 5-(2,5-dimethyl-7-((pyridin-4-ylmethyl)amino)pyrazolo[1,5- α]pyrimidin-3-yl)-2-methoxyphenyl sulfofluoridate (179 mg, 0.40 mmol, 73% yield). ^1H NMR (400 MHz, DMSO- d_6) δ = 8.74 (br s, 1H), 8.64 - 8.57 (m, 2H), 7.96 (d, J = 1.8 Hz, 1H), 7.82 (dd, J = 2.1, 8.7 Hz, 1H), 7.51 (d, J = 6.3 Hz, 2H), 7.42 (d, J = 8.8 Hz, 1H), 6.07 (s, 1H), 4.73 (d, J = 6.5 Hz, 2H), 3.98 - 3.91 (m, 3H), 2.57 (s, 3H), 2.34 (s, 3H). ^{13}C NMR (151 MHz, DMSO- d_6) δ = 160.1, 151.0, 150.6, 150.2, 147.7, 146.8, 146.5, 136.1,

136.1, 122.5, 122.4, 120.6, 113.7, 104.4, 86.7, 56.8, 43.9, 25.3, 15.2. ¹⁹F NMR (376 MHz, DMSO-d₆) δ = 40.35 (s, 1F). LCMS (Formic) 100% desired product; t_{ret} = 0.74 min, MH⁺ 458.1. HRMS (C₂₁H₂₀FN₅O₄S) [M+H]⁺ requires 458.1298 found [M+H]⁺ 458.1296. ν_{max} (neat) / cm⁻¹ 3286, 1616, 1585, 1543, 1452, 1227, 1104, 1014, 923, 835, 802, 763, 543. Mp 109-111 °C.

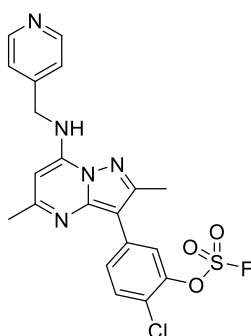
3-(2,5-Dimethyl-7-((pyridin-4-ylmethyl)amino)pyrazolo[1,5-*a*]pyrimidin-4-yl)phenyl sulfofluoridate (2.46)



Chamber A of the COware flask reactor was charged with sulfonyldiimidazole (112 mg, 0.57 mmol) and potassium fluoride (87 mg, 1.51 mmol). Chamber B of the COware flask reactor was charged with 3-(2,5-dimethyl-7-((pyridin-4-ylmethyl)amino)pyrazolo[1,5-*a*]pyrimidin-3-yl)phenol (130 mg, 0.38 mmol), triethylamine (0.31 mL, 3.01 mmol) and CH₂Cl₂ (4 mL). Trifluoroacetic acid (1 mL) was added to chamber A *via* syringe injection. The reaction mixture was stirred vigorously at RT for 6 h. The reaction was brought to a stop and the pressure was released. Chamber B was decanted into an RBF (50 mL) and chamber A was quenched with concentrated aqueous NaOH. The reaction mixture was concentrated *in vacuo*, diluted with CH₂Cl₂ (15 mL) and washed with brine (15 mL). The organic layer was concentrated *in vacuo* and purified by MDAP (formic method). The appropriate fractions were combined and concentrated *in vacuo* to give 3-(2,5-dimethyl-7-((pyridin-4-ylmethyl)amino)pyrazolo[1,5-*a*]pyrimidin-3-yl)phenyl sulfofluoridate (26 mg, 0.06 mmol, 17% yield). ¹H NMR (400 MHz, DMSO-d₆) δ = 8.75 - 8.67 (m, 1H), 8.59 (br d, *J* = 5.4 Hz, 2H), 8.05 (s, 1H), 7.97 - 7.91 (m, 1H), 7.65 (t, *J* = 8.1 Hz, 1H), 7.50 (d, *J* = 6.4 Hz, 2H), 7.44 (br d, *J* = 2.4 Hz, 1H), 6.10 (s, 1H), 4.73 (d, *J* = 6.8 Hz, 2H), 2.62 (s, 3H), 2.36 (s, 3H). ¹³C NMR (101 MHz, DMSO-d₆) δ = 160.1, 151.2, 150.4, 149.7, 148.8,

146.6, 136.6, 131.0, 128.4, 122.9, 119.9, 117.6, 103.8, 86.9, 55.4, 44.0, 25.1, 15.1. ¹⁹F NMR (376 MHz, DMSO-d₆) δ = 38.52 (s, 1F). LCMS (Formic) 96% desired product; t_{ret} = 0.78 min, MH⁺ 428.4 HRMS (C₂₀H₁₈FN₅O₃S) [M+H]⁺ requires 428.1193 found [M+H]⁺ 428.1187 ν_{max} (neat) / cm⁻¹ 3455, 1674, 1451, 1198, 1173, 1126, 1027, 931, 828, 799, 719, 518. Mp 110-112 °C.

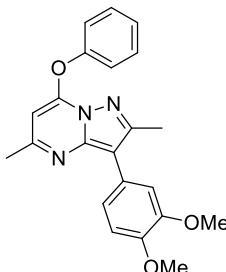
2-Chloro-5-(2,5-dimethyl-7-((pyridin-4-ylmethyl)amino)pyrazolo[1,5-*a*]pyrimidin-3-yl)phenyl sulfofluoridate (2.47)



Chamber A of the COware flask reactor was charged with sulfonyldiimidazole (258 mg, 1.30 mmol) and potassium fluoride (202 mg, 3.48 mmol). Chamber B of the COware flask reactor was charged with 2-chloro-5-(2,5-dimethyl-7-((pyridin-4-ylmethyl)amino)pyrazolo[1,5-*a*]pyrimidin-3-yl)phenol (330 mg, 0.87 mmol), DIPEA (1.21 mL, 6.95 mmol) and MeCN (4 mL). Trifluoroacetic acid (1 mL) was added to chamber A *via* syringe injection. The reaction mixture was stirred vigorously for 5 h at RT, chamber B was decanted into an RBF (50 mL) and chamber A was quenched with concentrated aqueous NaOH. The reaction mixture was concentrated *in vacuo* and purified by MDAP (formic method). The appropriate fractions were combined and concentrated *in vacuo* to afford 2-chloro-5-(2,5-dimethyl-7-((pyridin-4-ylmethyl)amino)pyrazolo[1,5-*a*]pyrimidin-3-yl)phenyl sulfofluoridate as a colourless oil (282 mg, 0.62 mmol, 71% yield). ¹H NMR (400 MHz, DMSO-d₆) δ = 9.05 - 8.97 (m, 1H), 8.80 (d, *J* = 6.5 Hz, 2H), 8.29 - 8.26 (m, 1H), 7.97 - 7.82 (m, 4H), 6.22 (s, 1H), 4.93 (d, *J* = 6.5 Hz, 2H), 2.63 (s, 3H), 2.38 (s, 3H). ¹³C NMR (DMSO-d₆, 151 MHz) δ = 160.0, 151.7, 146.8, 145.5, 144.3, 134.9, 131.7, 129.7, 124.6, 121.9, 117.2, 115.3, 102.9, 87.4, 44.4, 24.6, 15.0 (one carbon signal not observed). ¹⁹F NMR (376 MHz, DMSO-

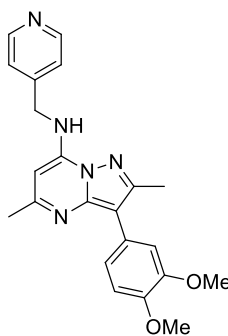
$\delta = 41.57$ (s, 1F). **LCMS** (Formic) 100% desired product; $t_{\text{ret}} = 0.92$ min, $\text{MH}^+ 462.3$
HRMS ($\text{C}_{20}\text{H}_{17}\text{ClFN}_5\text{O}_3\text{S}$) $[\text{M}+\text{H}]^+$ requires 462.0803 found $[\text{M}+\text{H}]^+ 462.0803$ v_{max} (neat)
/ cm^{-1} 2989, 1610, 1452, 1261, 1178, 1139, 932, 719, 583.

3-(3,4-Dimethoxyphenyl)-2,5-dimethyl-7-phenoxy-pyrazolo[1,5-*a*]pyrimidine (2.57)



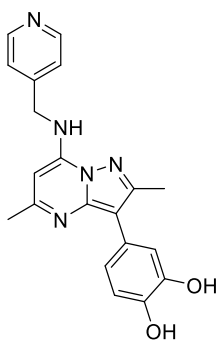
A microwave vial (20 mL) was charged with 3-bromo-2,5-dimethyl-7-phenoxy-pyrazolo[1,5-*a*]pyrimidine (1.5 g, 4.71 mmol), (3,4-dimethoxyphenyl)boronic acid (1.29 g, 7.07 mmol), $\text{PdCl}_2(\text{dppf})\text{-CH}_2\text{Cl}_2$ adduct (0.308 g, 0.38 mmol), cesium carbonate (2.30 g, 7.07 mmol), 1,4-dioxane (10 mL) and water (2.5 mL). The reaction vessel was sealed and heated in a microwave at 130 °C for 4 h. After cooling, the reaction mixture was passed through CeliteTM, diluted with EtOAc (30 mL) and washed with brine (30 mL). The organic layer was passed through a hydrophobic frit and concentrated *in vacuo* to give 3-(3,4-dimethoxyphenyl)-2,5-dimethyl-7-phenoxy-pyrazolo[1,5-*a*]pyrimidine (1.51 g, 4.0 mmol, 85% yield). **¹H NMR** (400 MHz, DMSO-d_6) $\delta = 7.63 - 7.54$ (m, 2H), 7.47 - 7.36 (m, 4H), 7.27 - 7.20 (m, 1H), 7.10 - 7.00 (m, 1H), 5.94 (s, 1H), 3.82 (s, 3H), 3.80 (s, 3H), 2.57 (s, 3H), 2.41 (s, 3H). **¹³C NMR** (101 MHz, DMSO-d_6) $\delta = 160.8, 154.1, 152.3, 152.1, 149.1, 147.8, 147.6, 131.1, 127.4, 125.5, 121.3, 113.2, 112.6, 107.5, 90.6, 56.1, 56.1, 55.4, 25.2, 14.8$. **LCMS** (HpH) 93% desired product; $t_{\text{ret}} = 1.12$ min, $\text{MH}^+ 376.4$.

3-(3,4-Dimethoxyphenyl)-2,5-dimethyl-N-(pyridin-4-ylmethyl)pyrazolo[1,5-*a*]pyrimidin-7-amine (2.58)



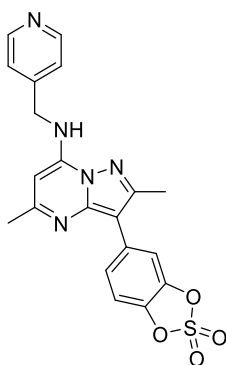
The microwave vial (20 mL) was charged with 3-(3,4-dimethoxyphenyl)-2,5-dimethyl-7-phenoxy-pyrazolo[1,5-*a*]pyrimidine (2 g, 5.33 mmol), pyridin-4-ylmethanamine (0.60 mL, 5.86 mmol), triethylamine (1.63 mL, 11.72 mmol) and DMSO (10 mL). The reaction vessel was sealed and heated in a microwave at 120 °C for 4 h. After cooling, the reaction was diluted with EtOAc (20 mL) and washed with saturated aqueous sodium bicarbonate solution (20 mL). The organic layer was concentrated *in vacuo* and the crude product was purified by column chromatography eluting with EtOAc in cyclohexane (0-100% gradient). The column was flushed with EtOAc/ethanol (3:1) to elute the product off the column. The appropriate fractions were combined and concentrated *in vacuo* to give 3-(3,4-dimethoxyphenyl)-2,5-dimethyl-N-(pyridin-4-ylmethyl)pyrazolo[1,5-*a*]pyrimidin-7-amine (1.02 g, 2.67 mmol, 50% yield). ¹H NMR (400 MHz, DMSO-*d*₆) δ = 8.55 - 8.50 (m, 2H), 8.49 - 8.43 (m, 1H), 7.45 - 7.40 (m, 1H), 7.39 - 7.33 (m, 2H), 7.25 - 7.19 (m, 1H), 7.05 - 7.00 (m, 1H), 5.95 (s, 1H), 4.65 (d, *J* = 6.5 Hz, 2H), 3.80 (s, 3H), 3.79 (s, 3H), 2.56 (s, 3H), 2.32 (s, 3H). ¹³C NMR (101 MHz, DMSO-*d*₆) δ = 159.1, 150.4, 150.2, 149.0, 147.9, 147.3, 146.3, 126.4, 122.4, 121.0, 113.1, 112.5, 106.0, 85.9, 56.1, 56.0, 55.4, 43.8, 25.3, 14.9. LCMS (Formic) 96% desired product; *t*_{ret} = 0.44 min, MH⁺ 390.4.

4-(2,5-Dimethyl-7-((pyridin-4-ylmethyl)amino)pyrazolo[1,5-*a*]pyrimidin-3-yl)benzene-1,2-diol (2.59)



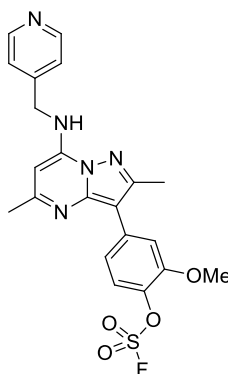
An RBF (50 mL) was charged with 4-(2,5-dimethyl-7-phenoxy-pyrazolo[1,5-*a*]pyrimidin-3-yl)benzene-1,2-diol (240 mg, 0.69 mmol), pyridin-4-ylmethanamine (0.077 mL, 0.76 mmol), triethylamine (0.144 mL, 1.04 mmol) and DMSO (3 mL). The reaction vessel was sealed and heated in a microwave at 120 °C for 5 h. After cooling, the reaction mixture was diluted with EtOAc (15 mL) and washed with saturated aqueous sodium bicarbonate solution (15 mL). The organic layer was concentrated *in vacuo* to quantitatively give 4-(2,5-dimethyl-7-((pyridin-4-ylmethyl)amino)pyrazolo[1,5-*a*]pyrimidin-3-yl)benzene-1,2-diol as a yellow oil. **¹H NMR** (400 MHz, DMSO-*d*₆) δ = 8.81 (s, 1H), 8.74 (s, 1H), 8.53 - 8.51 (m, 2H), 8.43 (s, 1H), 7.38 (d, *J* = 5.8 Hz, 2H), 7.14 (d, *J* = 2.3 Hz, 1H), 6.93 (dd, *J* = 2.1, 8.2 Hz, 1H), 6.79 (d, *J* = 8.0 Hz, 1H), 5.92 (s, 1H), 4.64 (d, *J* = 6.5 Hz, 2H), 2.31 (s, 3H) (one CH₃ signal under DMSO solvent residue signal, not reported). **¹³C NMR** (101 MHz, DMSO-*d*₆) δ = 178.9, 163.4, 158.8, 150.1, 147.9, 146.3, 145.3, 143.8, 122.4, 120.2, 116.7, 115.9, 106.7, 85.7, 55.4, 43.9, 25.2, 14.8. **LCMS** (Formic) 100% desired product; *t*_{ret} = 0.33 min, MH⁺ 362.3. **HRMS** (C₂₀H₁₉N₅O₂) [M+H]⁺ requires 362.1617 found [M+H]⁺ 362.1617.

5-(2,5-Dimethyl-7-((pyridin-4-ylmethyl)amino)pyrazolo[1,5-*a*]pyrimidin-3-yl)benzo[*d*][1,3,2]dioxathiole 2,2-dioxide (2.60)



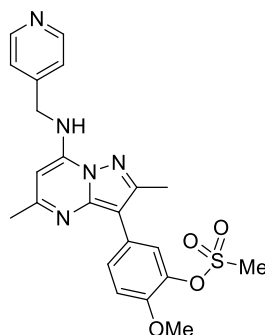
Chamber A of the COware flask reactor was charged with sulfonyldiimidazole (240 mg, 1.21 mmol) and potassium fluoride (188 mg, 3.23 mmol). Chamber B of the COware flask reactor was charged with 4-(2,5-dimethyl-7-((pyridin-4-ylmethyl)amino)pyrazolo[1,5-*a*]pyrimidin-3-yl)benzene-1,2-diol (292 mg, 0.81 mmol), DIPEA (1.69 mL, 9.70 mmol) and MeCN (3 mL). Trifluoroacetic acid (1 mL) was added to chamber A *via* syringe injection. The reaction mixture was stirred vigorously at RT for 2 h, chamber B was decanted into an RBF (50 mL) and chamber A was quenched with concentrated aqueous NaOH. The reaction mixture was concentrated *in vacuo* and purified by MDAP (formic method). The solvent was concentrated *in vacuo* to afford 5-(2,5-dimethyl-7-((pyridin-4-ylmethyl)amino)pyrazolo[1,5-*a*]pyrimidin-3-yl)benzo[*d*][1,3,2]dioxathiole 2,2-dioxide as a colourless oil (39 mg, 0.1 mmol, 12% yield). **¹H NMR** (400 MHz, DMSO-*d*₆) δ = 9.17 - 9.08 (m, 1H), 8.78 (br d, *J* = 5.9 Hz, 2H), 7.96 (s, 1H), 7.83 (d, *J* = 6.4 Hz, 2H), 7.71 - 7.68 (m, 2H), 6.23 (s, 1H), 4.91 (d, *J* = 6.4 Hz, 2H), 2.59 (s, 3H), 2.39 (s, 3H). **¹³C NMR** (101 MHz, DMSO-*d*₆) δ = 158.6, 155.1, 151.8, 147.0, 145.0, 142.5, 140.3, 131.3, 126.2, 124.4, 112.9, 112.3, 104.1, 87.2, 44.4, 40.9, 24.0, 14.6. **LCMS** (Formic) 98% desired product; t_{ret} = 0.69 min, MH^+ 424.3 **HRMS** ($\text{C}_{20}\text{H}_{17}\text{N}_5\text{O}_4\text{S}$) $[\text{M}+\text{H}]^+$ requires 424.1079 found $[\text{M}+\text{H}]^+$ 424.1073. ν_{max} (neat) / cm^{-1} 3096, 1609, 1298, 1134, 1044, 824, 763, 582.

4-(2,5-Dimethyl-7-((pyridin-4-ylmethyl)amino)pyrazolo[1,5-*a*]pyrimidin-3-yl)-2-methoxyphenyl sulfofluoridate (2.61)



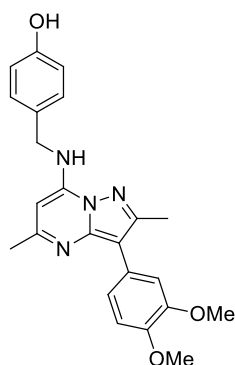
Chamber A of the COware flask reactor was charged with sulfonyldiimidazole (95 mg, 0.48 mmol) and potassium fluoride (74.3 mg, 1.28 mmol). Chamber B of the COware flask reactor was charged with 4-(2,5-dimethyl-7-((pyridin-4-ylmethyl)amino)pyrazolo[1,5-*a*]pyrimidin-3-yl)-2-methoxyphenol (60 mg, 0.16 mmol), DIPEA (0.34 mL, 1.92 mmol) and MeCN (3 mL). Trifluoroacetic acid (1 mL) was added to chamber A *via* syringe injection. The reaction was stirred vigorously at RT for 16 h. Chamber B was decanted into an RBF (50 mL) and chamber A was quenched with concentrated aqueous NaOH. The reaction mixture was concentrated *in vacuo* and purified by MDAP (formic method). The appropriate fractions were combined and concentrated *in vacuo* to afford 4-(2,5-dimethyl-7-((pyridin-4-ylmethyl)amino)pyrazolo[1,5-*a*]pyrimidin-3-yl)-2-methoxyphenyl sulfofluoridate as a colourless oil (6 mg, 0.01 mmol, 9% yield). **¹H NMR** (600 MHz, DMSO-*d*₆) δ = 8.61 (t, *J* = 6.6 Hz, 1H), 8.53 (d, *J* = 4.8 Hz, 2H), 7.80 (d, *J* = 1.8 Hz, 1H), 7.59 (d, *J* = 8.8 Hz, 1H), 7.48 (dd, *J* = 2.0, 8.6 Hz, 1H), 7.38 (d, *J* = 5.9 Hz, 2H), 6.05 (s, 1H), 4.67 (d, *J* = 6.6 Hz, 2H), 3.96 (s, 3H), 2.64 (s, 3H), 2.36 (s, 3H). **¹³C NMR** (151 MHz, DMSO-*d*₆) δ = 160.1, 151.0, 150.6, 150.2, 147.7, 146.8, 146.5, 136.2, 136.1, 122.5, 122.4, 120.6, 113.7, 104.4, 86.7, 56.8, 43.9, 25.3, 15.2. **¹⁹F NMR** (376 MHz, DMSO-*d*₆) δ = 40.01 (s, 1F). **LCMS** (Formic) 100% desired product; *t*_{ret} = 0.77 min, MH⁺ 458.3 **HRMS** (C₂₁H₂₀FN₅O₄S) [M+H]⁺ requires 458.1298 found [M+H]⁺ 458.1295. ν_{\max} (neat) / cm⁻¹ 3285, 1616, 1585, 1543, 1452, 1227, 1104, 1014, 903, 835, 802, 763, 627, 474.

5-(2,5-Dimethyl-7-((pyridin-4-ylmethyl)amino)pyrazolo[1,5-*a*]pyrimidin-3-yl)-2-methoxyphenyl methanesulfonate (2.62)



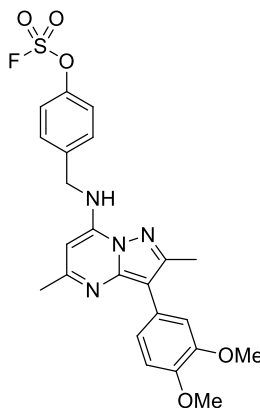
A microwave vial (5 mL) was charged with 5-(2,5-dimethyl-7-((pyridin-4-ylmethyl)amino)pyrazolo[1,5-*a*]pyrimidin-3-yl)-2-methoxyphenol (50 mg, 0.13 mmol), methanesulfonyl chloride (0.012 mL, 0.16 mmol), DIPEA (0.047 mL, 0.27 mmol) and CH₂Cl₂ (2 mL). The reaction was stirred at RT for 16 h, diluted with CH₂Cl₂ (10 mL) and washed with brine (10 mL). The organic layer was concentrated *in vacuo* and purified by column chromatography eluting with EtOAc/ethanol (3:1). The appropriate fractions were combined and concentrated *in vacuo* to give 5-(2,5-dimethyl-7-((pyridin-4-ylmethyl)amino)pyrazolo[1,5-*a*]pyrimidin-3-yl)-2-methoxyphenyl methanesulfonate (13 mg, 0.03 mmol, 22% yield). **¹H NMR** (400 MHz, DMSO-*d*₆) δ = 8.56 - 8.51 (m, 3H), 7.72 - 7.67 (m, 2H), 7.39 - 7.35 (m, 2H), 7.31 - 7.27 (m, 1H), 5.99 (s, 1H), 4.66 (d, *J* = 6.9 Hz, 2H), 3.89 (s, 3H), 3.39 (s, 3H), 2.57 (s, 3H), 2.33 (s, 3H). **¹³C NMR** (101 MHz, DMSO-*d*₆) δ = 159.5, 150.0, 149.6, 148.0, 146.4, 138.2, 128.1, 123.6, 122.5, 114.1, 110.0, 104.5, 86.3, 56.5, 43.9, 38.7, 25.2, 14.8 **LCMS** (Formic) 85% desired product; *t*_{ret} = 0.52 min, MH⁺ 454.4. **HRMS** (C₂₂H₂₃N₅O₄S) [M+H]⁺ requires 454.1549 found [M+H]⁺ 454.1551.

4-(((3-(3,4-Dimethoxyphenyl)-2,5-dimethylpyrazolo[1,5-*a*]pyrimidin-7-yl)amino)methyl)phenol (2.75)



A microwave vial was charged with 3-(3,4-dimethoxyphenyl)-2,5-dimethyl-7-phenoxy-pyrazolo[1,5-*a*]pyrimidine (500 mg, 1.33 mmol), 4-(aminomethyl)phenol (246 mg, 2.0 mmol) and DIPEA (0.465 mL, 2.66 mmol). The reaction vessel was sealed and heated in a microwave at 120 °C for 5 h. After cooling, the reaction mixture was diluted with EtOAc (20 mL) and washed with brine (20 mL). The organic layer was concentrated *in vacuo* and purified by column chromatography eluting with EtOAc gradient (0-50%) cyclohexane. The appropriate fractions were combined and concentrated *in vacuo* to give the give 4-(((3-(3,4-dimethoxyphenyl)-2,5-dimethylpyrazolo[1,5-*a*]pyrimidin-7-yl)amino)methyl)phenol (361 mg, 0.89 mmol, 67% yield). ¹H NMR (400 MHz, DMSO-*d*₆) δ = 9.31 (s, 1H), 8.22 (s, 1H), 7.42 (d, *J* = 2.0 Hz, 1H), 7.27 - 7.19 (m, 3H), 7.01 (d, *J* = 8.4 Hz, 1H), 6.75 - 6.71 (m, 2H), 5.99 (s, 1H), 4.47 (d, *J* = 6.4 Hz, 2H), 3.80 (s, 3H), 3.79 (s, 3H), 2.54 (s, 3H), 2.34 (s, 3H). ¹³C NMR (101 MHz, DMSO-*d*₆) δ = 158.9, 157.0, 150.2, 149.0, 147.3, 146.3, 146.3, 128.9, 126.5, 120.9, 115.7, 113.1, 112.6, 105.9, 86.0, 56.1, 56.0, 44.5, 25.4, 14.9 (1 carbon signal not observed). LCMS (Formic) 98% desired product; *t*_{ret} = 1.08 min, MH⁺ 405.3. HRMS (C₂₃H₂₄N₄O₃) [M+H]⁺ requires 405.1927 found [M+H]⁺ 405.1928 *v*_{max} (neat) / cm⁻¹ 3391, 2932, 1610, 1583, 1365, 1227, 1025, 791, 626, 494.

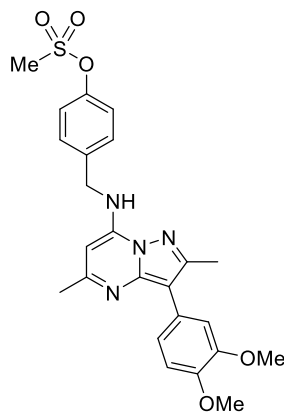
4-(((3-(3,4-Dimethoxyphenyl)-2,5-dimethylpyrazolo[1,5-*a*]pyrimidin-7-yl)amino)methyl)phenyl sulfofluoridate (2.76)



Chamber A of the COware flask reactor was charged with Sulfonyldiimidazole (110 mg, 0.55 mmol) and potassium fluoride (86 mg, 1.47 mmol). Chamber B of the COware flask reactor was charged with 4-(((3-(3,4-dimethoxyphenyl)-2,5-dimethylpyrazolo[1,5-*a*]pyrimidin-7-yl)amino)methyl)phenol (149 mg, 0.37 mmol), DIPEA (0.77 mL, 4.42 mmol) and MeCN (3 mL). Trifluoroacetic acid (1 mL) was added to chamber A *via* syringe injection and the reaction was stirred at RT for 18 h. After pressure release, chamber B was decanted into an RBF (50 mL) and chamber A was quenched with aqueous concentrated NaOH. The reaction mixture was concentrated *in vacuo*, diluted with CH₂Cl₂ (10 mL) and washed with brine (10 mL). The organic layer was concentrated *in vacuo* and purified by MDAP (formic method). The appropriate vials were combined and concentrated *in vacuo* to afford 4-(((3-(3,4-dimethoxyphenyl)-2,5-dimethylpyrazolo[1,5-*a*]pyrimidin-7-yl)amino)methyl)phenyl sulfofluoridate (107 mg, 0.22 mmol, 60% yield). ¹H NMR (600 MHz, DMSO-*d*₆) δ = 8.55 - 8.43 (m, 1H), 7.63 - 7.55 (m, 4H), 7.40 (d, *J* = 1.8 Hz, 1H), 7.22 (dd, *J* = 1.8, 8.4 Hz, 1H), 7.02 (d, *J* = 8.4 Hz, 1H), 6.04 (s, 1H), 4.68 (d, *J* = 6.6 Hz, 2H), 3.80 (s, 3H), 3.79 (s, 3H), 2.55 (s, 3H), 2.34 (s, 3H). ¹³C NMR (151 MHz, DMSO-*d*₆) δ = 163.4, 159.1, 150.4, 149.1, 149.0, 147.3, 146.3, 140.3, 129.8, 126.4, 121.6, 121.0, 113.1, 112.6, 106.0, 85.9, 56.1, 56.0, 44.0, 31.2, 14.9. ¹⁹F NMR (376 MHz, DMSO-*d*₆) δ = 38.46 (s, 1F). LCMS (Formic) 100% desired product; *t*_{ret} = 0.94 min, MH⁺ 487.1. HRMS (C₂₃H₂₃FN₄O₅S)

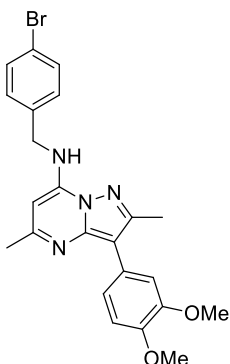
[M+H]⁺ requires 487.1451 found [M+H]⁺ 487.1454 ν_{\max} (neat) / cm⁻¹ 3370, 2933, 1617, 1582, 1504, 1446, 1329, 1251, 1233, 1141, 1027, 915, 771.

4-(((3-(3,4-Dimethoxyphenyl)-2,5-dimethylpyrazolo[1,5-*a*]pyrimidin-7-yl)amino)methyl)phenyl methanesulfonate (2.77)



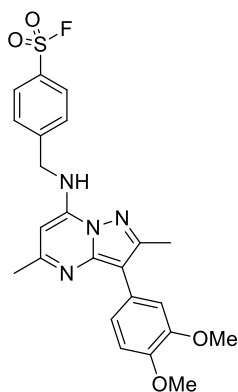
A microwave vial (5 mL) was charged with 4-(((3-(3,4-dimethoxyphenyl)-2,5-dimethylpyrazolo[1,5-*a*]pyrimidin-7-yl)amino)methyl)phenol (71 mg, 0.18 mmol), methanesulfonyl chloride (0.02 mL, 0.21 mmol), DIPEA (0.06 mL, 0.35 mmol) and CH₂Cl₂ (2 mL). The reaction was stirred at RT for 16 h, diluted with CH₂Cl₂ (10 mL) and washed with brine (10 mL). The organic layer was concentrated *in vacuo* and purified by column chromatography eluting with EtOAc in cyclohexane (0-100% gradient). The appropriate fractions were combined and concentrated *in vacuo* to give 4-(((3-(3,4-dimethoxyphenyl)-2,5-dimethylpyrazolo[1,5-*a*]pyrimidin-7-yl)amino)methyl)phenyl methanesulfonate (82 mg, 0.17 mmol, 97% yield). ¹H NMR (400 MHz, DMSO-*d*₆) δ = 8.43 (s, 1H), 7.56 - 7.48 (m, 2H), 7.41 (d, *J* = 2.5 Hz, 1H), 7.37 - 7.29 (m, 2H), 7.22 (dd, *J* = 2.0, 8.4 Hz, 1H), 7.02 (d, *J* = 8.4 Hz, 1H), 6.04 (s, 1H), 4.68 - 4.59 (m, 2H), 3.80 (s, 3H), 3.79 (s, 3H), 3.36 (s, 3H), 2.55 (s, 3H), 2.34 (s, 3H). ¹³C NMR (151 MHz, DMSO-*d*₆) δ = 159.1, 150.4, 148.9, 148.6, 147.3, 146.3, 138.2, 129.1, 126.5, 122.8, 121.0, 113.1, 112.6, 105.8, 85.9, 56.1, 56.0, 44.2, 37.9, 31.1, 25.3, 14.8. LCMS (Formic) 99% desired product; *t*_{ret} = 0.73 min, MH⁺ 483.3. HRMS (C₂₄H₂₆N₄O₅S) [M+H]⁺ requires 483.1702 found [M+H]⁺ 483.1693.

***N*-(4-Bromobenzyl)-3-(3,4-dimethoxyphenyl)-2,5-dimethylpyrazolo[1,5-*a*]pyrimidin-7-amine (2.79)**



A microwave vial (5 mL) was charged with 3-(3,4-dimethoxyphenyl)-2,5-dimethyl-7-phenoxy-pyrazolo[1,5-*a*]pyrimidine (409 mg, 1.09 mmol), (4-bromophenyl)methanamine (0.206 mL, 1.63 mmol), DIPEA (0.38 mL, 2.18 mmol) and DMSO (3 mL). The reaction vessel was sealed and heated in a microwave at 130 °C for 5 h. After cooling, the reaction mixture was diluted with EtOAc (15 mL) and washed with brine (15 mL), the organic layer was concentrated *in vacuo* and purified by column chromatography eluting with EtOAc in cyclohexane (0-100% gradient). The appropriate fractions were combined and concentrated *in vacuo* to give *N*-(4-bromobenzyl)-3-(3,4-dimethoxyphenyl)-2,5-dimethylpyrazolo[1,5-*a*]pyrimidin-7-amine (465 mg, 1.0 mmol, 91% yield). ¹H NMR (400 MHz, DMSO-*d*₆) δ = 8.47 - 8.38 (m, 1H), 7.57 - 7.51 (m, 2H), 7.41 (d, *J* = 2.0 Hz, 1H), 7.39 - 7.34 (m, 2H), 7.25 - 7.19 (m, 1H), 7.05 - 6.99 (m, 1H), 5.99 - 5.95 (m, 1H), 4.60 - 4.55 (m, 2H), 3.80 (s, 3H), 3.79 (s, 3H), 2.55 (s, 3H), 2.36 - 2.30 (s, 3H). ¹³C NMR (101 MHz, DMSO-*d*₆) δ = 159.0, 150.4, 149.0, 147.3, 146.3, 146.2, 138.3, 131.8, 129.7, 126.5, 121.0, 120.6, 113.1, 112.6, 106.0, 86.0, 56.1, 56.0, 44.1, 25.3, 14.8. LCMS (Formic) 100% desired product; *t*_{ret} = 0.90 min, MH⁺ 469.2. HRMS (C₂₃H₂₃BrN₄O₂) [M+H]⁺ requires 467.1083 found [M+H]⁺ 467.1081 *v*_{max} (neat) / cm⁻¹ 3400, 2995, 1578, 623.

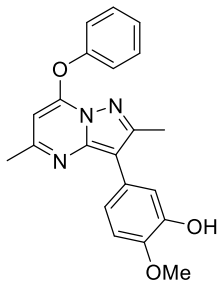
4-(((3-(3,4-Dimethoxyphenyl)-2,5-dimethylpyrazolo[1,5-*a*]pyrimidin-7-yl)amino)methyl)benzene-1-sulfonyl fluoride (2.80)



A microwave vial (5 mL) was charged with *N*-(4-bromobenzyl)-3-(3,4-dimethoxyphenyl)-2,5-dimethylpyrazolo[1,5-*a*]pyrimidin-7-amine (73 mg, 0.16 mmol), DABSO (38 mg, 0.16 mmol) and bis(di-*tert*-butyl(4-dimethylaminophenyl)phosphine)dichloropalladium(II) (11 mg, 0.02 mmol). Triethylamine (0.22 mL, 1.6 mmol) and isopropanol (3 mL) were added and nitrogen was bubbled through the solution for a couple of minutes. The reaction vessel was sealed and heated in a microwave at 120 °C for 4 h. After cooling, *N*-fluorobenzenesulfonimide (148 mg, 0.47 mmol) was added and the reaction was stirred at RT for 2.5 h. The reaction mixture was passed through Celite™, diluted with EtOAc (15 mL) and washed with water (15 mL). The organic layer was concentrated *in vacuo* and purified by column chromatography eluting with EtOAc in cyclohexane (0-100% gradient). The appropriate fractions were combined and concentrated *in vacuo* to give 4-(((3-(3,4-dimethoxyphenyl)-2,5-dimethylpyrazolo[1,5-*a*]pyrimidin-7-yl)amino)methyl)benzene-1-sulfonyl fluoride (48 mg, 0.10 mmol, 66% yield). ¹H NMR (400 MHz, DMSO-*d*₆) δ = 8.61 - 8.54 (m, 1H), 8.16 - 8.11 (m, 2H), 7.81 - 7.76 (m, 2H), 7.42 - 7.39 (m, 1H), 7.26 - 7.20 (m, 1H), 7.06 - 7.00 (m, 1H), 6.00 (s, 1H), 4.83 - 4.77 (m, 2H), 3.80 (s, 3H), 3.79 (s, 3H), 2.57 (s, 3H), 2.33 (s, 3H). ¹³C NMR (176 MHz, DMSO-*d*₆) δ = 158.7, 150.0, 148.4, 148.1, 146.8, 145.8, 145.7, 128.5, 125.9, 120.5, 112.6, 112.1, 105.6, 85.40, 55.6, 55.5, 43.9, 30.6, 24.8, 22.0, 14.4. ¹⁹F NMR (376 MHz, DMSO-*d*₆) δ = 66.54 (s, 1F). LCMS (Formic) 94% desired product; *t*_{ret} = 0.87 min, MH⁺ 471.3.

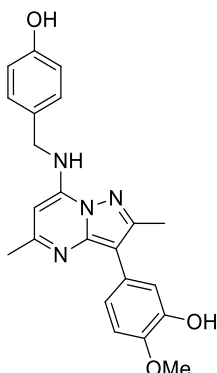
HRMS (C₂₃H₂₃FN₄O₄S) [M+H]⁺ requires 471.1502 found [M+H]⁺ 471.1502 *v*_{max} (neat) / cm⁻¹ 3405, 3002, 1710, 1619, 1585, 1411, 1362, 1214, 1028, 770.

5-(2,5-Dimethyl-7-phenoxy-pyrazolo[1,5-*a*]pyrimidin-3-yl)-2-methoxyphenol (2.81)



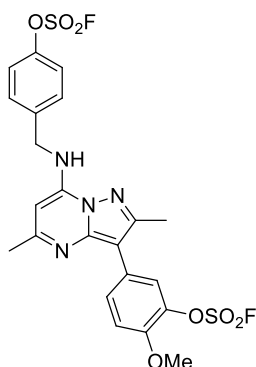
The microwave vial (20 mL) was charged with 3-bromo-2,5-dimethyl-7-phenoxy-pyrazolo[1,5-*a*]pyrimidine (260 mg, 0.82 mmol), 2-methoxy-5-(4,4,5,5-tetramethyl-1,3,2-dioxaborolan-2-yl)phenol (225 mg, 0.90 mmol), PdCl₂(dppf)-CH₂Cl₂ adduct (53.4 mg, 0.07 mmol), cesium carbonate (399 mg, 1.23 mmol) in 1,4-dioxane (8 mL) and water (2 mL). The reaction vessel was sealed and heated in a microwave at 130 °C for 5 h. After cooling, the reaction mixture was passed through Celite™ and concentrated *in vacuo*. The crude product was purified by column chromatography eluting with EtOAc in cyclohexane (0-60% gradient). The appropriate fractions were combined and concentrated *in vacuo* to give 5-(2,5-dimethyl-7-phenoxy-pyrazolo[1,5-*a*]pyrimidin-3-yl)-2-methoxyphenol (290 mg, 0.80 mmol, 98% yield). **¹H NMR** (400 MHz, DMSO-*d*₆) δ = 8.98 (br s, 1H), 7.58 (t, *J* = 7.1 Hz, 2H), 7.46 - 7.40 (m, 3H), 7.24 - 7.22 (m, 1H), 7.13 - 7.08 (m, 1H), 7.03 - 6.99 (m, 1H), 5.91 (s, 1H), 3.82 (s, 3H), 2.54 (s, 3H), 2.41 (s, 3H). **¹³C NMR** (DMSO-*d*₆, 101 MHz) δ = 160.6, 154.1, 152.3, 152.1, 147.6, 146.8, 146.6, 131.1, 129.8, 127.3, 125.6, 121.3, 120.0, 116.7, 115.7, 112.9, 90.5, 56.2, 55.3, 25.2, 14.8. **LCMS** (Formic) 90% desired product; *t*_{ret} = 1.05 min, MH⁺ 362.3. **HRMS** (C₂₁H₁₉N₃O₃) [M+H]⁺ requires 362.1505 found [M+H]⁺ 362.1497.

5-(7-((4-Hydroxybenzyl)amino)-2,5-dimethylpyrazolo[1,5-*a*]pyrimidin-3-yl)-2-methoxyphenol (2.82)



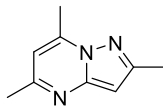
A microwave vial (20 mL) was charged with 5-(2,5-dimethyl-7-phenoxy-pyrazolo[1,5-*a*]pyrimidin-3-yl)-2-methoxyphenol (520 mg, 1.44 mmol), 4-(aminomethyl)phenol (266 mg, 2.16 mmol), DIPEA (0.503 mL, 2.88 mmol) and DMSO (11 mL). The reaction vessel was sealed and heated in a microwave at 130 °C for 5 h. After cooling, the reaction mixture was diluted with EtOAc (15 mL) and washed with brine (15 mL). The organic layer was concentrated *in vacuo* and purified by column chromatography eluting with EtOAc in cyclohexane (0-100% gradient). The appropriate fractions were combined and concentrated *in vacuo* to 5-(7-((4-hydroxybenzyl)amino)-2,5-dimethylpyrazolo[1,5-*a*]pyrimidin-3-yl)-2-methoxyphenol (459 mg, 1.18 mmol, 82% yield). **¹H NMR** (400 MHz, DMSO-*d*₆) δ = 9.35 (s, 1H), 8.91 (s, 1H), 7.23 (d, *J* = 8.9 Hz, 2H), 7.16 (d, *J* = 2.0 Hz, 1H), 7.04 (d, *J* = 2.0 Hz, 1H), 6.99 - 6.95 (m, 1H), 6.73 (d, *J* = 8.4 Hz, 2H), 6.02 (s, 1H), 4.48 (d, *J* = 6.4 Hz, 2H), 3.79 (s, 3H), 2.48 (s, 3H), 2.34 (s, 3H). **¹³C NMR** (101 MHz, DMSO-*d*₆) δ = 163.4, 157.1, 146.8, 129.0, 128.4, 120.1, 119.7, 116.6, 115.7, 113.0, 106.0, 86.3, 84.2, 71.6, 56.3, 44.6, 31.1, 21.2, 14.5 (one carbon signal not observed). **LCMS** (Formic) 99% desired product; *t*_{ret} = 0.6 min, MH⁺ 391.3. **HRMS** (C₂₂H₂₂N₄O₃) [M+H]⁺ requires 391.1770 found [M+H]⁺ 391.1767.

4-(((3-(3-Sulfofluoridate-4-methoxyphenyl)-2,5-dimethylpyrazolo[1,5-*a*]pyrimidin-7-yl)amino)methyl)phenyl sulfofluoridate (2.83)



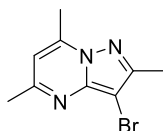
Chamber A was charged with Sulfonyldiimidazole (104 mg, 0.52 mmol) and potassium fluoride (81 mg, 1.39 mmol). Chamber B was charged with 5-(7-((4-hydroxybenzyl)amino)-2,5-dimethylpyrazolo[1,5-*a*]pyrimidin-3-yl)-2-methoxyphenol (68 mg, 0.17 mmol), MeCN (3 mL) and DIPEA (0.73 mL, 4.18 mmol). Trifluoroacetic acid (2 mL) was added to chamber A *via* syringe injection and the reaction was stirred at RT for 16 h. Chamber B was concentrated *in vacuo*, diluted with CH₂Cl₂ (15 mL) and washed with brine (15 mL). The organic layer was concentrated *in vacuo* and purified by MDAP (formic method). The appropriate fractions were combined and concentrated *in vacuo* to afford 4-(((3-(3-sulfofluoridate-4-methoxyphenyl)-2,5-dimethylpyrazolo[1,5-*a*]pyrimidin-7-yl)amino)methyl)phenyl sulfofluoridate (25 mg, 0.05 mmol, 26% yield). ¹H NMR (700 MHz, DMSO-*d*₆) δ = 8.57 (t, *J* = 6.7 Hz, 1H), 7.98 (d, *J* = 2.1 Hz, 1H), 7.83 (dd, *J* = 2.1, 8.7 Hz, 1H), 7.62 - 7.59 (m, 2H), 7.59 - 7.54 (m, 2H), 7.41 (d, *J* = 8.9 Hz, 1H), 6.10 (s, 1H), 4.67 (d, *J* = 6.6 Hz, 2H), 3.94 (s, 3H), 2.57 (s, 3H), 2.34 (s, 3H). ¹³C NMR (176 MHz, DMSO-*d*₆) δ = 159.3, 150.0, 148.6, 147.9, 146.0, 145.8, 139.7, 138.0, 129.3, 129.1, 126.7, 121.1, 121.0, 114.3, 103.2, 85.9, 56.4, 43.5, 24.8, 14.3. ¹⁹F NMR (500 MHz, DMSO-*d*₆) δ = 40.31 (s, 1F), 38.43 (s, 1F). LCMS (Formic) 99% desired product; *t*_{ret} = 1.22 min, MH⁺ 555.3. HRMS (C₂₂H₂₀F₂N₄O₇S₂) [M+H]⁺ requires 555.0820 found [M+H]⁺ 555.0818 *v*_{max} (neat) / cm⁻¹ 2928, 1711, 1618, 1580, 1442, 1290, 1228, 1140, 1018, 930, 840, 800.

2,5,7-Trimethylpyrazolo[1,5-*a*]pyrimidine (2.87)



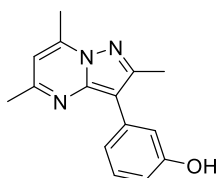
The RBF (100 mL) was charged with 3-methyl-1H-pyrazol-5-amine (1.5 g, 15.44 mmol) and pentane-2,4-dione (1.745 ml, 16.99 mmol). The reaction was heated at 145 °C for 16 h. After cooling, the reaction mixture was concentrated *in vacuo* to give 2,5,7-trimethylpyrazolo[1,5-*a*]pyrimidine (2.4 g, 14.91 mmol, 96% yield). ¹H NMR (400 MHz, CDCl₃) δ = 6.49 (s, 1H), 6.37 (s, 1H), 2.72 (s, 3H), 2.55 (s, 3H), 2.54 (s, 3H). ¹³C NMR (101 MHz, CDCl₃) δ = 158.0, 154.5, 149.4, 144.7, 107.5, 95.1, 24.5, 17.1, 14.7.

3-Bromo-2,5,7-trimethylpyrazolo[1,5-*a*]pyrimidine (2.88)



The RBF (150 mL) was charged with 2,5,7-trimethylpyrazolo[1,5-*a*]pyrimidine (2.3 g, 14.27 mmol), *N*-bromosuccinimide (3.05 g, 17.12 mmol) and CH₂Cl₂ (50 mL). The reaction was stirred at RT for 5mins. The reaction mixture was washed with aqueous sodium thiosulfate solution and the organic layer was concentrated *in vacuo* to give 3-bromo-2,5,7-trimethylpyrazolo[1,5-*a*]pyrimidine (3.36 g, 14.06 mmol, 98% yield). ¹H NMR (400 MHz, CDCl₃) δ = 6.56 (s, 1H), 2.72 (s, 3H), 2.62 (s, 3H), 2.52 (s, 3H). ¹³C NMR (101 MHz, CDCl₃) δ = 159.5, 152.8, 145.7, 145.2, 108.6, 83.5, 24.7, 16.5, 13.3. LCMS (Formic) 100% desired product; *t*_{ret} = 0.86 min, MH⁺ 242.0.

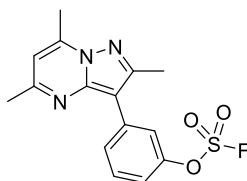
3-(2,5,7-Trimethylpyrazolo[1,5-*a*]pyrimidin-3-yl)phenol (2.89)



A microwave vial (5 mL) was charged with 3-bromo-2,5,7-trimethylpyrazolo[1,5-*a*]pyrimidine (432 mg, 1.80 mmol), (3-hydroxyphenyl)boronic acid (248 mg, 1.80

mmol), PdCl₂(dppf)-CH₂Cl₂ adduct (147 mg, 0.18 mmol), cesium carbonate (1.17 g, 3.60 mmol), 1,4-dioxane (4 mL) and water (1 mL). The reaction vessel was sealed and heated in a microwave at 120 °C for 5 h. After cooling, the reaction mixture was passed through Celite™, diluted with EtOAc (15 mL) and washed with brine (15 mL). The organic layer was concentrated *in vacuo* and purified by column chromatography eluting with EtOAc (0-50% gradient) cyclohexane. The appropriate fractions were combined and concentrated *in vacuo* to give 3-(2,5,7-trimethylpyrazolo[1,5-*a*]pyrimidin-3-yl)phenol (313 mg, 1.24 mmol, 69% yield). ¹H NMR (400 MHz, CDCl₃) δ = 7.25 (d, *J* = 7.9 Hz, 1H), 7.23 - 7.19 (m, 1H), 7.15 - 7.11 (m, 1H), 6.72 - 6.67 (m, 1H), 6.53 (s, 1H), 2.76 (s, 3H), 2.61 (s, 3H), 2.55 (s, 3H) (OH signal not observed). ¹³C NMR (101 MHz, CDCl₃) δ = 158.7, 156.3, 152.2, 145.8, 145.0, 133.6, 129.5, 121.0, 116.3, 113.7, 108.6, 108.2, 24.3, 17.1, 14.1. LCMS (Formic) 100% desired product; *t*_{ret} = 0.88 min, MH⁺ 254.1.

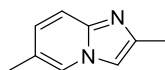
3-(2,5,7-Trimethylpyrazolo[1,5-*a*]pyrimidin-3-yl)phenyl sulfofluoridate (2.90)



Chamber A of the COware flask reactor was charged with sulfonyldiimidazole (154 mg, 0.78 mmol) and potassium fluoride (120 mg, 2.07 mmol). Chamber B of the COware flask reactor was charged with 3-(2,5,7-trimethylpyrazolo[1,5-*a*]pyrimidin-3-yl)phenol (131 mg, 0.52 mmol), DIPEA (0.72 mL, 4.14 mmol) and MeCN (4 mL). Trifluoroacetic acid (1 mL) was added to chamber A *via* syringe injection and the reaction was stirred at RT for 15 h. After pressure release, chamber B was decanted into an RBF (50 mL) and the reaction mixture was concentrated *in vacuo*. The crude product was purified by column chromatography eluting with EtOAc (0-30% gradient) cyclohexane. The appropriate fractions were combined and concentrated *in vacuo* to give 3-(2,5,7-trimethylpyrazolo[1,5-*a*]pyrimidin-3-yl)phenyl sulfofluoridate as a white solid (150 mg, 0.39 mmol, 86% yield). ¹H NMR (400 MHz, DMSO-*d*₆) δ = 8.04 - 8.00 (m, 1H), 7.97 - 7.91 (m, 1H), 7.68 (t, *J* = 7.9 Hz, 1H), 7.52 - 7.45 (m, 1H), 6.97 - 6.92 (m,

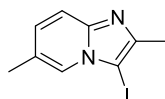
1H), 2.71 (s, 3H), 2.62 (s, 3H), 2.54 (s, 3H). ¹³C NMR (101 MHz, DMSO-d₆) δ = 159.9, 151.6, 150.3, 146.0, 145.7, 136.1, 131.2, 128.7, 120.2, 118.2, 109.4, 105.1, 24.9, 16.9, 15.0. ¹⁹F NMR (376 MHz, DMSO-d₆) δ = 38.57 (s, 1F). LCMS (Formic) 100% desired product; t_{ret} = 1.31 min, MH⁺ 336.1. HRMS (C₁₅H₁₄N₃O₃FS) [M+H]⁺ requires 336.0818 found [M+H]⁺ 336.0831 ν_{max} (neat) / cm⁻¹ 3065, 1617, 1561, 1438, 1230, 1137, 922, 838, 791, 681, 573.

2,6-Dimethylimidazo[1,2-a]pyridine (2.92)



5-Methylpyridin-2-amine (990 mg, 9.15 mmol) was added to the RBF (100 mL), the RBF was degassed and under atmosphere of nitrogen. Anhydrous ethanol (8 mL) and 1-chloropropan-2-one (1.46 mL, 18.31 mmol) were added and the reaction was heated at 95 °C for 23 h. After cooling, the reaction mixture was concentrated, diluted with CH₂Cl₂ (20 mL) and washed with saturated aqueous sodium bicarbonate solution (20 mL). The organic layer was concentrated *in vacuo* and purified by column chromatography eluting with EtOAc in cyclohexane (0-100% gradient). The appropriate fractions were combined and concentrated *in vacuo* to give 2,6-dimethylimidazo[1,2-a]pyridine (570 mg, 3.90 mmol, 43% yield). ¹H NMR (400 MHz, CDCl₃) δ = 7.82 (s, 1H), 7.41 (d, *J* = 9.4 Hz, 1H), 7.25 (s, 1H), 6.96 (dd, *J* = 1.7, 9.4 Hz, 1H), 2.45 (s, 3H), 2.30 (s, 3H). ¹³C NMR (101 MHz, CDCl₃) δ = 144.2, 143.1, 126.9, 122.9, 121.2, 116.1, 109.1, 18.0, 14.3. LCMS (HpH) 89% desired product; t_{ret} = 0.74 min, MH⁺ 147.1. HRMS (C₉H₁₀N₂) [M+H]⁺ requires 146.0922 found [M+H]⁺ 147.0925.

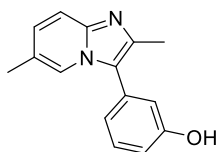
3-Iodo-2,6-dimethylimidazo[1,2-a]pyridine (2.93)



The RBF (100 mL) was charged with 2,6-dimethylimidazo[1,2-a]pyridine (556 mg, 3.80 mmol) and CH₂Cl₂ (20 mL). Cold *N*-iodosuccinimide (856 mg, 3.80 mmol) was added and the reaction was stirred for 1 h at RT. The reaction mixture was

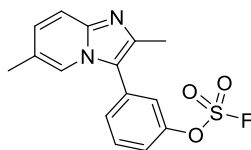
concentrated, diluted with CH₂Cl₂ (10 mL) and washed with water (20 mL). The organic layer was concentrated *in vacuo* to give 3-iodo-2,6-dimethylimidazo[1,2-*a*]pyridine (1.0 g, 3.68 mmol, 97% yield). ¹H NMR (400 MHz, CDCl₃) δ = 7.83 (d, *J* = 1.0 Hz, 1H), 7.44 (d, *J* = 8.9 Hz, 1H), 7.06 (dd, *J* = 1.5, 8.9 Hz, 1H), 2.49 (s, 3H), 2.39 (d, *J* = 1.0 Hz, 3H). ¹³C NMR (101 MHz, CDCl₃) δ = 128.0, 123.8, 122.4, 116.2, 108.7, 60.8, 29.6, 18.2, 14.8. LCMS (HpH) 100% desired product; *t*_{ret} = 1.01 min, MH⁺ 273.0. HRMS (C₉H₉N₂I) [M+H]⁺ requires 272.9889 found [M+H]⁺ 272.9897.

3-(2,6-Dimethylimidazo[1,2-*a*]pyridin-3-yl)phenol (2.94)



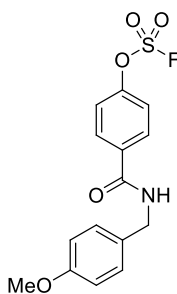
A microwave vial (20 mL) was charged with 3-iodo-2,6-dimethylimidazo[1,2-*a*]pyridine (325 mg, 1.19 mmol), (3-hydroxyphenyl)boronic acid (165 mg, 1.19 mmol), PdCl₂(dppf)-CH₂Cl₂ adduct (98 mg, 0.12 mmol), cesium carbonate (778 mg, 2.39 mmol), 1,4-dioxane (4 mL) and water (1 mL). The reaction vessel was sealed and heated in a microwave at 120 °C for 5 h. After cooling, the reaction mixture was passed through Celite™, diluted with EtOAc (15 mL) and washed with aqueous sodium thiosulfate solution (15 mL). The organic layer was concentrated *in vacuo* and purified by column chromatography eluting with EtOAc in cyclohexane (0-100% gradient). The appropriate fractions were combined and concentrated *in vacuo* to give 3-(2,6-dimethylimidazo[1,2-*a*]pyridin-3-yl)phenol (267 mg, 1.12 mmol, 94% yield). ¹H NMR (400 MHz, CDCl₃) δ = 7.93 (s, 1H), 7.45 (d, *J* = 9.4 Hz, 1H), 7.38 (t, *J* = 7.9 Hz, 1H), 7.08 - 7.02 (m, 2H), 6.99 (dd, *J* = 1.5, 9.4 Hz, 1H), 6.92 (d, *J* = 7.9 Hz, 1H), 2.41 (s, 3H), 2.23 (s, 3H) (OH signal not observed). ¹³C NMR (101 MHz, CDCl₃) δ = 158.8, 143.0, 139.5, 130.3, 130.1, 127.7, 121.7, 121.3, 120.1, 116.7, 116.1, 115.5, 30.9, 18.2, 13.4. LCMS (HpH) 85% desired product; *t*_{ret} = 0.9 min, MH⁺ 239.1.

3-(2,6-Dimethylimidazo[1,2-*a*]pyridin-3-yl)phenyl sulfofluoridate (2.95)



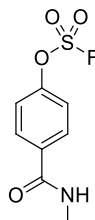
Chamber A of the COware flask reactor was charged with sulfonyldiimidazole (231 mg, 1.17 mmol) and potassium fluoride (180 mg, 3.11 mmol). Chamber B of the COware flask reactor was charged with 3-(2,6-dimethylimidazo[1,2-*a*]pyridin-3-yl)phenol (185 mg, 0.78 mmol), DIPEA (1.09 mL, 6.21 mmol) and MeCN (4 mL). Trifluoroacetic acid (1 mL) was added to chamber A *via* syringe injection. The reaction was stirred at RT for 15 h. After pressure release, chamber B was decanted into an RBF (50 mL) and concentrated *in vacuo*. The crude product was purified by column chromatography eluting with EtOAc (0-80% gradient) cyclohexane. The appropriate fractions were combined and concentrated *in vacuo* to give 3-(2,6-dimethylimidazo[1,2-*a*]pyridin-3-yl)phenyl sulfofluoridate as a colourless oil (140 mg, 0.44 mmol, 57% yield). **¹H NMR** (400 MHz, DMSO-*d*₆) δ = 8.13 (d, *J* = 1.5 Hz, 1H), 7.83 (s, 1H), 7.81 - 7.74 (m, 1H), 7.75 - 7.71 (m, 1H), 7.70 - 7.65 (m, 1H), 7.48 (d, *J* = 8.9 Hz, 1H), 7.16 (dd, *J* = 1.5, 9.4 Hz, 1H), 2.38 (s, 3H), 2.28 (d, *J* = 1.0 Hz, 3H). **¹³C NMR** (101 MHz, DMSO-*d*₆) δ = 150.5, 143.6, 141.7, 132.3, 132.1, 130.0, 128.3, 122.2, 122.1, 121.5, 120.6, 119.1, 116.3, 18.1, 14.4. **¹⁹F NMR** (376 MHz, DMSO-*d*₆) δ = 38.79 (s, 1F). **LCMS** (Formic) 100% desired product; t_{ret} = 0.64 min, MH^+ 321.1. **HRMS** (C₁₅H₁₃N₂O₃FS) [M+H]⁺ requires 321.0709 found [M+H]⁺ 321.0714 ν_{max} (neat) / cm⁻¹ 3022, 2923, 1560, 1441, 1425, 1229, 1128, 923, 832, 791, 697, 545.

4-((4-Methoxybenzyl)carbamoyl)phenyl sulfofluoridate (2.98)



A microwave vial (5 mL) was charged with ((fluorosulfonyl)oxy)benzoic acid (100 mg, 0.45 mmol) in CH₂Cl₂ (4 mL) and oxalyl chloride (0.087 mL, 0.10 mmol). DMF (7.03 μL, 0.09 mmol) was slowly added and the reaction was stirred for 16 h at RT. (4-Methoxyphenyl)methanamine (0.059 mL, 0.45 mmol) and triethylamine (0.076 mL, 0.55 mmol) were added and the reaction was stirred for a further 50 mins at RT. The reaction mixture was diluted with CH₂Cl₂ (15 mL) and washed with brine (15 mL). The organic layer was concentrated *in vacuo* and purified by MDAP (formic method). The appropriate fractions were combined and concentrated *in vacuo* to give 4-((4-methoxybenzyl)carbamoyl)phenyl sulfofluoridate as a white solid (10 mg, 0.03 mmol, 7% yield). ¹H NMR (600 MHz, CDCl₃) δ = 7.95 - 7.90 (m, 2H), 7.43 (d, *J* = 8.4 Hz, 2H), 7.30 (d, *J* = 8.4 Hz, 2H), 6.95 - 6.89 (m, 2H), 6.31 (br s, 1H), 4.61 (d, *J* = 5.5 Hz, 2H), 3.84 (s, 3H). ¹³C NMR (151 MHz, CDCl₃) δ = 165.4, 159.3, 151.8, 135.0, 129.4, 129.3, 121.2, 114.3, 65.1, 53.4, 43.9. ¹⁹F NMR (376 MHz, CDCl₃) δ = 38.48 (s, 1F). LCMS (Formic) 95% desired product; *t*_{ret} = 1.07 min, MH⁺ 340.1. HRMS (C₁₅H₁₄NO₅FS) [M+H]⁺ requires 340.0655 found [M+H]⁺ 340.0652.

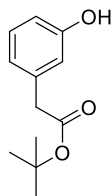
4-(Methylcarbamoyl)phenyl sulfofluoridate (2.99)



A microwave vial (5 mL) was charged with 4-((fluorosulfonyl)oxy)benzoic acid (20 mg, 0.09 mmol) in CH₂Cl₂ (1 mL) and oxalyl chloride (0.017 mL, 0.20 mmol). DMF (1.41 μL, 0.02 mmol) was slowly added and the reaction was stirred for 1 h at RT. Methanamine in MeOH (0.045 mL, 0.09 mmol) was added and the reaction was stirred for a further 1.5 h at RT. The reaction mixture was directly purified by MDAP (formic method). The appropriate fractions were combined and concentrated *in vacuo* to give 4-(methylcarbamoyl)phenyl sulfofluoridate (6 mg, 0.03 mmol, 29% yield). ¹H NMR (400 MHz, CDCl₃) δ = 7.92 - 7.89 (m, 2H), 7.46 - 7.42 (m, 2H), 3.06 (d, *J* = 4.9 Hz, 3H). ¹³C NMR (151 MHz, CDCl₃) δ = 166.3, 151.7, 134.8, 129.2, 121.2, 27.0. ¹⁹F NMR (376 MHz,

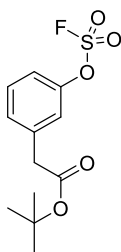
CDCl₃) δ = 38.47 (s, 1F). **LCMS** (Formic) 93% desired product; t_{ret} = 0.78 min, MH⁺ 234.1. **HRMS** (C₈H₈NO₄FS) [M+H]⁺ requires 234.0236 found [M+H]⁺ 234.0242 ν_{max} (neat) / cm⁻¹ 3323, 1643, 1555, 1436, 1230, 1140, 917, 856, 810, 655, 578.

***tert*-Butyl 2-(3-hydroxyphenyl)acetate (2.102)**



An RBF (50 mL) was charged with 2-(3-hydroxyphenyl)acetic acid (5 g, 32.9 mmol), 1,1-di-*tert*-butoxy-*N,N*-dimethylmethanamine (17.33 mL, 72.3 mmol) and toluene (80 mL). The reaction was heated at 80 °C for 16 h. The reaction mixture was concentrated, and the crude product was purified by column chromatography eluting with EtOAc (0-30% gradient) cyclohexane. The appropriate fractions were combined and concentrated *in vacuo* to give *tert*-butyl 2-(3-hydroxyphenyl)acetate (5.82 g, 28.0 mmol, 85% yield). **¹H NMR** (400 MHz, CDCl₃) δ = 7.17 (t, J = 7.6 Hz, 1H), 6.83 (d, J = 6.9 Hz, 1H), 6.79 - 6.70 (m, 2H), 3.50 (s, 2H), 1.47 (s, 9H). **¹³C NMR** (101 MHz, CDCl₃) δ = 171.6, 156.0, 136.0, 129.6, 121.3, 116.3, 114.1, 81.3, 42.6, 28.0. **LCMS** (HpH) 100% desired product; t_{ret} = 1.00 min, MH⁻ 207.1.

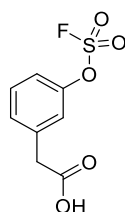
***tert*-Butyl 2-(3-((fluorosulfonyl)oxy)phenyl)acetate (2.103)**



Chamber A of the COware flask reactor was charged with sulfonyldiimidazole (1.26 g, 6.36 mmol) and potassium fluoride (985 mg, 16.96 mmol). Chamber B of the COware flask reactor was charged with *tert*-butyl 2-(3-hydroxyphenyl)acetate (883 mg, 4.24 mmol), DIPEA (4.44 mL, 25.40 mmol) and CH₂Cl₂ (12 mL). Trifluoroacetic acid (4 mL)

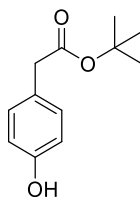
was injected into chamber A and the reaction was stirred for 1 h at RT. After pressure release, chamber B was diluted with CH₂Cl₂ (20 mL) and washed with brine (20 mL). The organic layer was concentrated *in vacuo* and purified by column chromatography eluting with EtOAc (0-50% gradient) cyclohexane. The appropriate fractions were combined and concentrated *in vacuo* to give *tert*-butyl 2-(3-((fluorosulfonyl)oxy)phenyl)acetate (740 mg, 2.55 mmol, 61% yield). ¹H NMR (400 MHz, CDCl₃) δ = 7.48 - 7.42 (m, 1H), 7.37 - 7.31 (m, 2H), 7.28 - 7.25 (m, 1H), 3.60 (s, 2H), 1.47 (s, 9H). ¹³C NMR (101 MHz, CDCl₃) δ = 169.6, 150.0, 137.7, 130.2, 129.6, 121.7, 119.3, 81.6, 42.2, 28.0. ¹⁹F NMR (376 MHz, CDCl₃) δ = 37.65 (s, 1F). LCMS (Formic) 100% desired product; t_{ret} = 1.31 min, MH⁺ 308.2.

2-(3-((Fluorosulfonyl)oxy)phenyl)acetic acid (2.104)



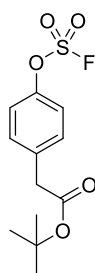
An RBF (25 mL) was charged with *tert*-butyl 2-(3-((fluorosulfonyl)oxy)phenyl)acetate (177 mg, 0.61 mmol) and HCl (5.3 ml, 5.31 mmol). The reaction was heated at 80 °C for 6 h. The reaction mixture was diluted with 3:1 chloroform:IPA (20 mL), washed with brine (20 mL) and the pH adjusted to pH4. The organic layer was concentrated *in vacuo* to give 2-(3-((fluorosulfonyl)oxy)phenyl)acetic acid (142 mg, 0.61 mmol, 99% yield) as a white solid. ¹H NMR (400 MHz, DMSO-d₆) δ = 7.58 - 7.52 (m, 1H), 7.52 - 7.46 (m, 2H), 7.45 - 7.40 (m, 1H), 3.70 (s, 2H) (COOH signal not observed). ¹³C NMR (101 MHz, DMSO-d₆) δ = 172.4, 150.0, 139.2, 130.9, 122.3, 119.5, 28.1 (one carbon signal under solvent residue peak). ¹⁹F NMR (376 MHz, DMSO-d₆) δ = 38.59 (s, 1F). LCMS (Formic) unambiguous peak shape; t_{ret} = 0.90 min, MH⁻ 233.0. ν_{max} (neat) / cm⁻¹ 2919, 2671, 1706, 1443, 1205, 1117, 906, 883, 792, 751, 626, 534.

***tert*-Butyl 2-(4-hydroxyphenyl)acetate (2.106)**



The RBF (50 mL) was charged with 2-(4-hydroxyphenyl)acetic acid (5 g, 32.9 mmol), 1,1-di-*tert*-butoxy-*N,N*-dimethylmethanamine (17.33 mL, 72.3 mmol) and toluene (80 mL). The reaction was heated at 100 °C for 48 h. After cooling, the reaction mixture was concentrated, diluted with CH₂Cl₂ (30 mL) and precipitation occurred. The solid was isolated from the filtrate and the filtrate was concentrated *in vacuo*. The concentrated filtrate was purified by column chromatography eluting with EtOAc (0-30%) in cyclohexane. The appropriate fractions were combined and concentrated *in vacuo* to give *tert*-butyl 2-(4-hydroxyphenyl)acetate as an oil (3.8 g, 18.17 mmol, 56% yield). ¹H NMR (400 MHz, DMSO-*d*₆) δ = 9.26 (br s, 1H), 7.03 (d, *J* = 8.4 Hz, 2H), 6.70 (d, *J* = 8.4 Hz, 2H), 3.40 (s, 2H), 1.39 (s, 9H). ¹³C NMR (101 MHz, DMSO-*d*₆) δ = 171.3, 156.5, 130.5, 125.3, 115.6, 80.3, 41.3, 28.2. LCMS (HpH) 87% desired product; *t*_{ret} = 1.01 min, MH⁺ 207.2. HRMS (C₁₂H₁₆O₃) [M+H]⁺ requires 209.1178 found [M+H]⁺ 209.1178 *v*_{max} (neat) / cm⁻¹ 3252, 2982, 2706, 1702, 1612, 1524, 1404, 1234, 1210, 858, 822, 788, 653, 513.

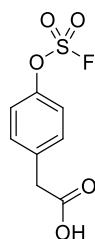
***tert*-Butyl 2-(4-((fluorosulfonyl)oxy)phenyl)acetate (2.107)**



Chamber A of the COware flask reactor was charged with sulfonyldiimidazole (1.2 g, 6.22 mmol) and potassium fluoride (964 mg, 16.59 mmol). Chamber B of the COware flask reactor was charged with *tert*-butyl 2-(4-hydroxyphenyl)acetate (864 mg, 4.15 mmol), DIPEA (4.35 mL, 24.89 mmol) and CH₂Cl₂ (12 mL). Trifluoroacetic acid (4 mL)

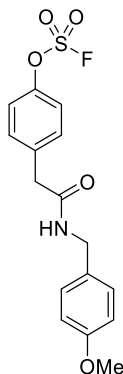
was injected into chamber A and the reaction was stirred for 1 h at RT. After pressure release, chamber B was diluted with CH₂Cl₂ (20 mL) and washed with brine (20 mL). The organic layer was concentrated *in vacuo* and purified by column chromatography eluting with EtOAc (0-50% gradient) cyclohexane. The appropriate fractions were combined and concentrated *in vacuo* to give *tert*-butyl 2-(4-((fluorosulfonyl)oxy)phenyl)acetate (879 mg, 3.03 mmol, 73% yield). **¹H NMR** (400 MHz, CDCl₃) δ = 7.44 - 7.36 (m, 2H), 7.35 - 7.29 (m, 2H), 3.59 (s, 2H), 1.47 (s, 9H). **¹³C NMR** (101 MHz, CDCl₃) δ = 170.0, 149.0, 135.6, 131.2, 120.8, 81.4, 41.8, 28.0. **¹⁹F NMR** (376 MHz, CDCl₃) δ = 37.44 (s, 1F). **LCMS** (Formic) 96% desired product; *t*_{ret} = 1.31 min, MH⁺ 308.2.

2-(4-((Fluorosulfonyl)oxy)phenyl)acetic acid (2.108)



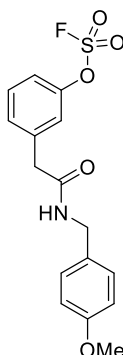
An RBF (25 mL) was charged with *tert*-butyl 2-(4-((fluorosulfonyl)oxy)phenyl)acetate (165 mg, 0.57 mmol) and HCl (5.3 ml, 5.31 mmol). The reaction mixture was heated at 80 °C for 16 h. After cooling, the reaction mixture was diluted with 3:1 chloroform:IPA (20 mL), washed with brine (20 mL) and the pH was adjusted to pH 4. The organic layer was concentrated *in vacuo* to give 2-(4-((Fluorosulfonyl)oxy)phenyl)acetic acid as a white solid (127 mg, 0.52 mmol, 95% yield). **¹H NMR** (400 MHz, DMSO-d₆) δ = 12.46 (br s, 1H), 7.56 - 7.51 (m, 2H), 7.51 - 7.46 (m, 2H), 3.69 (s, 2H). **¹³C NMR** (101 MHz, DMSO-d₆) δ = 172.6, 148.8, 137.0, 132.3, 121.2, 31.1. **¹⁹F NMR** (376 MHz, DMSO-d₆) δ = 38.34 (s, 1F). **LCMS** (Formic) 100% desired product; *t*_{ret} = 0.90 min, MH⁻ 233.0. **HRMS** (C₈H₇O₅FS) [M-H]⁻ requires 232.9925 found [M-H]⁻ 232.9924 *v*_{max} (neat) / cm⁻¹ 2917, 2849, 1694, 1503, 1443, 1231, 1136, 900, 811, 615, 571, 510.

4-(2-((4-Methoxybenzyl)amino)-2-oxoethyl)phenyl sulfofluoridate (2.109)



A microwave vial (5 mL) was charged with DMF (1 mL), HATU (60.9 mg, 0.16 mmol), 2-(4-((fluorosulfonyl)oxy)phenyl)acetic acid (30 mg, 0.13 mmol) and DIPEA (44.7 μ L, 0.26 mmol). The reaction was stirred for 5 min before the addition of (4-methoxyphenyl)methanamine (16.74 μ L, 0.13 mmol). The reaction was stirred for 16 h at RT. The reaction mixture was directly purified by MDAP (formic method). The appropriate vials were combined and concentrated *in vacuo* to give 4-(2-((4-methoxybenzyl)amino)-2-oxoethyl)phenyl sulfofluoridate (27 mg, 0.08 mmol, 60% yield). $^1\text{H NMR}$ (600 MHz, CDCl_3) δ = 7.42 (d, J = 8.4 Hz, 2H), 7.34 (br d, J = 8.4 Hz, 2H), 7.17 (d, J = 8.4 Hz, 2H), 6.90 - 6.85 (m, 2H), 5.71 - 5.59 (m, 1H), 4.39 (d, J = 5.9 Hz, 2H), 3.82 (s, 3H), 3.62 (s, 2H). $^{13}\text{C NMR}$ (151 MHz, CDCl_3) δ = 169.4, 159.2, 149.2, 135.8, 131.3, 129.9, 129.1, 121.3, 114.2, 55.3, 43.4, 42.9. $^{19}\text{F NMR}$ (376 MHz, CDCl_3) δ = 37.95 (s, 1F). **LCMS** (Formic) 100% desired product; t_{ret} = 1.07 min, MH^+ 354.1. **HRMS** ($\text{C}_{16}\text{H}_{16}\text{NO}_5\text{FS}$) $[\text{M}+\text{H}]^+$ requires 354.0811 found $[\text{M}+\text{H}]^+$ 354.0811.

3-(2-((4-Methoxybenzyl)amino)-2-oxoethyl)phenyl sulfofluoridate (2.110)

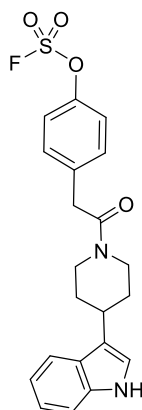


A microwave vial (5 mL) was charged DMF (1 mL), HATU (64.9 mg, 0.17 mmol), 2-(3-((fluorosulfonyl)oxy)phenyl)acetic acid (32 mg, 0.14 mmol) and DIPEA (0.048 mL, 0.27 mmol). The reaction was stirred for 5 min before the addition of (4-methoxyphenyl)methanamine (0.018 mL, 0.14 mmol). The reaction was left to stir for 1 h at RT. The reaction mixture was directly purified by MDAP (formic method). The appropriate vials were combined and concentrated *in vacuo* to give 3-(2-((4-methoxybenzyl)amino)-2-oxoethyl)phenyl sulfofluoridate (22 mg, 0.06 mmol, 46% yield). **¹H NMR** (400 MHz, CDCl₃) δ = 7.50 - 7.45 (m, 1H), 7.37 (d, *J* = 7.9 Hz, 1H), 7.32 - 7.29 (m, 2H), 7.17 (d, *J* = 8.9 Hz, 2H), 6.90 - 6.84 (m, 2H), 5.71 (br s, 1H), 4.39 (d, *J* = 5.9 Hz, 2H), 3.82 (s, 3H), 3.64 (s, 2H). **¹³C NMR** (176 MHz, CDCl₃) δ = 169.16, 159.20, 150.22, 137.88, 130.72, 129.79, 129.63, 129.11, 121.72, 119.67, 114.19, 55.30, 43.43, 43.08. **¹⁹F NMR** (376 MHz, CDCl₃) δ = 37.95 (s, 1F). ν_{\max} (neat) / cm⁻¹ 3287, 2925, 1638, 1513, 1438, 1230, 1117, 958, 895, 557. **LCMS** (Formic) 100% desired product; t_{ret} = 1.04 min, MH⁺ 354.3. **HRMS** (C₁₆H₁₆NO₅FS) [M+H]⁺ requires 354.0811 found [M+H]⁺ 354.0813 ν_{\max} (neat) / cm⁻¹ 3287, 2924, 1638, 1438, 1230, 1210, 958, 806, 768, 557.

General procedure A: Stock solution of 2-(4-((fluorosulfonyl)oxy)phenyl)acetic acid (0.028 g, 0.12 mmol)/2-(3-((fluorosulfonyl)oxy)phenyl)acetic acid (0.028 g, 0.12 mmol) in DMF (3.3 mL) were prepared. Stock solution of HATU (0.057 g, 0.15 mmol) in DMF (3.3 mL) was prepared. 2-(4-((Fluorosulfonyl)oxy)phenyl)acetic acid or 2-(3-((fluorosulfonyl)oxy)phenyl)acetic acid (300 μL) was transferred into 11 reaction vials, followed by DIPEA (0.042 mL, 0.24 mmol). HATU (300 μL) was added to each of the reaction vials followed by the addition of the appropriate amine (200 μL, 0.144 mmol). Note, additional DIPEA (0.042 mL, 0.24 mmol) was added to reactions containing amines stored as HCl salts. The reaction vials were sealed and stirred at RT for 4 h. The reaction mixture was directly purified by MDAP (formic method). The appropriate vials were combined and concentrated *in vacuo* to give the following products.

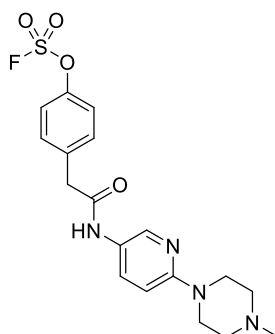
4-(2-(4-(1H-Indol-3-yl)piperidin-1-yl)-2-oxoethyl)phenyl sulfofluoridate (2.113-

Para)



Prepared by **General Procedure A**. 4-(2-(4-(1H-indol-3-yl)piperidin-1-yl)-2-oxoethyl)phenyl sulfofluoridate (3.8 mg, 9.12 μmol , 8% yield). $^1\text{H NMR}$ (600 MHz, $\text{DMSO-}d_6$) δ = 10.78 (br s, 1H), 7.56 - 7.52 (m, 3H), 7.47 (d, J = 8.4 Hz, 2H), 7.33 (d, J = 8.1 Hz, 1H), 7.08 - 7.04 (m, 2H), 6.99 - 6.94 (m, 1H), 4.52 (br d, J = 12.5 Hz, 1H), 4.08 (br d, J = 13.6 Hz, 1H), 3.85 (s, 2H), 3.21 (br t, J = 11.9 Hz, 1H), 3.07 - 3.00 (m, 1H), 2.78 - 2.71 (m, 1H), 1.99 - 1.91 (m, 2H), 1.53 - 1.42 (m, 2H). $^{13}\text{C NMR}$ (176 MHz, $\text{DMSO-}d_6$) δ = 168.0, 148.2, 137.7, 136.3, 131.5, 126.1, 120.8, 120.6, 120.6, 118.9, 118.5, 118.0, 111.4, 46.0, 42.0, 38.6, 33.1, 33.0, 32.3. **LCMS** (Formic) 100% desired product; t_{ret} = 1.21 min, MH^+ 417.2.

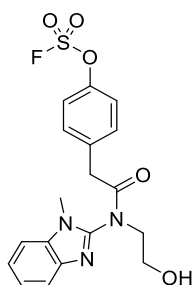
4-(2-((6-(4-Methylpiperazin-1-yl)pyridin-3-yl)amino)-2-oxoethyl)phenyl sulfofluoridate (2.114-Para)



Prepared by **General procedure A**. 4-(2-((6-(4-Methylpiperazin-1-yl)pyridin-3-yl)amino)-2-oxoethyl)phenyl sulfofluoridate (10.1 mg, 0.03 mmol, 21% yield). $^1\text{H NMR}$ (600 MHz, $\text{DMSO-}d_6$) δ = 10.10 (s, 1H), 8.29 (d, J = 2.6 Hz, 1H), 7.77 (dd, J =

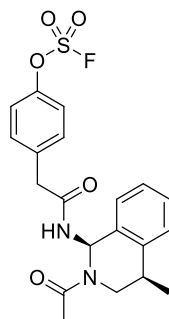
2.6, 9.2 Hz, 1H), 7.58 - 7.50 (m, 4H), 6.83 (d, $J = 9.2$ Hz, 1H), 3.71 (s, 2H), 2.62 - 2.54 (m, 4H), 2.40 - 2.29 (m, 4H) (CH₃ signal under DMSO residue peak). ¹³C NMR (101 MHz, DMSO-d₆) $\delta = 168.7, 163.5, 155.6, 148.9, 139.5, 137.8, 132.0, 130.5, 129.8, 127.6, 121.3, 120.9, 107.7, 53.7, 44.3, 42.4$. LCMS (Formic) 100% desired product; $t_{ret} = 0.57$ min, MH⁺ 409.2.

4-(2-((2-Hydroxyethyl)(1-methyl-1H-benzo[d]imidazol-2-yl)amino)-2-oxoethyl)phenyl sulfofluoridate (2.115-Para)



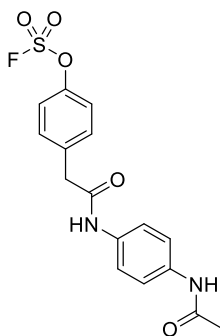
Prepared by **General Procedure A**. 4-(2-((2-Hydroxyethyl)(1-methyl-1H-benzo[d]imidazol-2-yl)amino)-2-oxoethyl)phenyl sulfofluoridate (12.9 mg, 0.03 mmol, 27% yield). ¹H NMR (600 MHz, DMSO-d₆) $\delta = 8.84 - 8.54$ (m, 1H), 7.52 - 7.39 (m, 6H), 7.32 - 7.23 (m, 2H), 4.32 (t, $J = 5.3$ Hz, 2H), 3.78 (s, 2H), 3.71 (q, $J = 5.1$ Hz, 2H), 3.58 (s, 3H). ¹³C NMR (176 MHz, DMSO-d₆) $\delta = 170.7, 150.5, 148.5, 135.4, 131.7, 131.7, 123.1, 122.7, 120.7, 120.5, 111.8, 109.7, 62.3, 41.8, 40.4, 29.0$. LCMS (Formic) 100% desired product; $t_{ret} = 0.7$ min, MH⁺ 408.1.

4-(2-(((1R,4R)-2-Acetyl-4-methyl-1,2,3,4-tetrahydroisoquinolin-1-yl)amino)-2-oxoethyl)phenyl sulfofluoridate (2.116-Para)



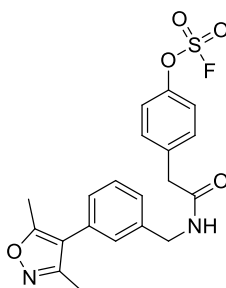
Prepared by **General procedure A**. 4-(2-(((1*R*,4*R*)-2-Acetyl-4-methyl-1,2,3,4-tetrahydroisoquinolin-1-yl)amino)-2-oxoethyl)phenyl sulfofluoridate (12.1 mg, 0.03 mmol, 24% yield). **¹H NMR** (600 MHz, DMSO-*d*₆) δ = 8.57 (br d, *J* = 8.4 Hz, 1H), 7.56 (d, *J* = 3.3 Hz, 4H), 7.34 - 7.25 (m, 2H), 7.22 - 7.16 (m, 1H), 7.10 - 7.04 (m, 1H), 4.70 - 4.55 (m, 2H), 3.69 (d, *J* = 16.9 Hz, 2H), 2.48 - 2.41 (m, 1H), 2.03 (s, 3H), 1.27 - 1.17 (m, 1H), 1.04 (d, *J* = 6.2 Hz, 3H). **¹³C NMR** (176 MHz, DMSO-*d*₆) δ = 169.5, 168.4, 148.4, 137.7, 136.1, 131.3, 126.9, 126.0, 125.2, 122.7, 120.8, 54.8, 46.5, 44.7, 41.4, 22.5, 21.1 (1 carbon signal not observed). **LCMS** (Formic) 100% desired product; *t*_{ret} = 1.02 min, MH⁺ 421.2.

4-(2-((4-Acetamidophenyl)amino)-2-oxoethyl)phenyl sulfofluoridate (2.117-*Para*)



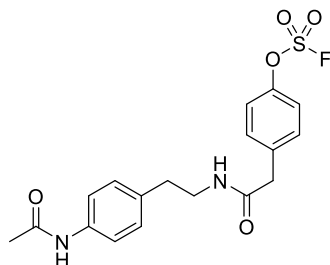
Prepared by following **General procedure A**. 4-(2-((4-Acetamidophenyl)amino)-2-oxoethyl)phenyl sulfofluoridate (23.5 mg, 0.06 mmol, 53% yield). **¹H NMR** (600 MHz, DMSO-*d*₆) δ = 10.15 (s, 1H), 9.86 (s, 1H), 7.54 (br d, *J* = 5.9 Hz, 4H), 7.50 - 7.48 (m, 4H), 3.71 (s, 2H), 2.01 (s, 3H). **¹³C NMR** (101 MHz, DMSO-*d*₆) δ = 172.6, 168.5, 148.9, 137.9, 136.9, 135.4, 134.7, 132.3, 132.0, 121.3, 120.0, 42.7, 24.3. **LCMS** (Formic) 100% desired product; *t*_{ret} = 0.92 min, MH⁺ 367.1.

4-(2-((3-(3,5-Dimethylisoxazol-4-yl)phenyl)amino)-2-oxoethyl)phenyl sulfofluoridate (2.118-Para)



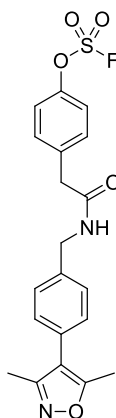
Prepared by **General Procedure A**. 4-(2-((3-(3,5-dimethylisoxazol-4-yl)phenyl)amino)-2-oxoethyl)phenyl sulfofluoridate (10.4 mg, 0.03 mmol, 21% yield). $^1\text{H NMR}$ (600 MHz, $\text{DMSO-}d_6$) δ = 8.68 (br t, J = 5.9 Hz, 1H), 7.55 - 7.46 (m, 4H), 7.41 (t, J = 7.7 Hz, 1H), 7.27 - 7.22 (m, 2H), 7.20 (s, 1H), 4.33 (d, J = 5.9 Hz, 2H), 3.58 (s, 2H), 2.35 (s, 3H), 2.18 (s, 3H). $^{13}\text{C NMR}$ (176 MHz, $\text{DMSO-}d_6$) δ = 169.5, 165.0, 157.9, 148.3, 140.0, 137.7, 131.3, 129.8, 128.8, 127.5, 127.2, 126.2, 120.7, 115.7, 42.1, 41.3, 11.2, 10.4. **LCMS** (Formic) 100% desired product; t_{ret} = 1.12 min, MH^+ 419.2.

4-(2-((4-Acetamidophenethyl)amino)-2-oxoethyl)phenyl sulfofluoridate (2.119-Para)



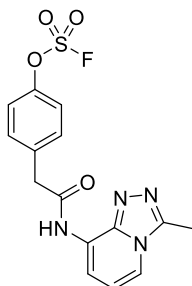
Prepared by **General Procedure A**. 4-(2-((4-Acetamidophenethyl)amino)-2-oxoethyl)phenyl sulfofluoridate (9.7 mg, 0.03 mmol, 21% yield). $^1\text{H NMR}$ (600 MHz, $\text{DMSO-}d_6$) δ = 9.89 - 9.82 (m, 1H), 8.16 (br t, J = 5.5 Hz, 1H), 7.47 (dd, J = 8.6, 15.6 Hz, 4H), 7.38 (d, J = 8.8 Hz, 2H), 7.08 (d, J = 8.4 Hz, 2H), 3.45 (s, 2H), 3.26 (q, J = 6.7 Hz, 2H), 2.65 (t, J = 7.2 Hz, 2H), 2.02 (s, 3H). $^{13}\text{C NMR}$ (176 MHz, $\text{DMSO-}d_6$) δ = 169.2, 168.0, 148.2, 137.8, 137.4, 133.8, 131.2, 128.7, 120.6, 119.0, 41.4, 40.2, 34.4, 23.8. **LCMS** (Formic) 100% desired product; t_{ret} = 0.89 min, MH^+ 395.1.

**4-(2-((4-(3,5-Dimethylisoxazol-4-yl)phenyl)amino)-2-oxoethyl)phenyl
sulfofluoridate (2.120-Para)**



Prepared by **General procedure A**. 4-(2-((4-(3,5-Dimethylisoxazol-4-yl)phenyl)amino)-2-oxoethyl)phenyl sulfofluoridate (9.4 mg, 0.02 mmol, 19% yield). **¹H NMR** (600 MHz, DMSO-*d*₆) δ = 8.70 - 8.64 (m, 1H), 7.57 - 7.47 (m, 4H), 7.33 (s, 4H), 4.32 (d, *J* = 5.9 Hz, 2H), 3.59 (s, 2H), 2.38 (s, 3H), 2.21 (s, 3H). **¹³C NMR** (176 MHz, DMSO-*d*₆) δ = 169.5, 164.9, 158.0, 148.3, 138.5, 137.7, 131.3, 128.8, 128.3, 127.7, 120.7, 115.6, 42.0, 41.3, 11.2, 10.4. **LCMS** (Formic) 100% desired product; *t*_{ret} = 1.12 min, MH⁺ 419.2.

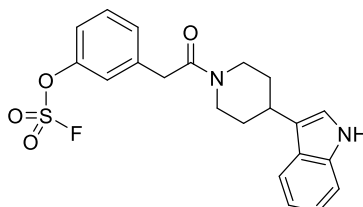
**4-(2-((3-Methyl-[1,2,4]triazolo[4,3-*a*]pyridin-8-yl)amino)-2-oxoethyl)phenyl
sulfofluoridate (2.121-Para)**



Prepared by **General procedure A**. 4-(2-((3-Methyl-[1,2,4]triazolo[4,3-*a*]pyridin-8-yl)amino)-2-oxoethyl)phenyl sulfofluoridate (10 mg, 0.03 mmol, 23% yield). **¹H NMR** (600 MHz, DMSO-*d*₆) δ = 10.70 - 10.66 (m, 1H), 8.08 (d, *J* = 7.0 Hz, 1H), 7.99 (d, *J* = 7.3 Hz, 1H), 7.61 - 7.53 (m, 4H), 6.93 (t, *J* = 7.0 Hz, 1H), 4.00 (s, 2H), 2.70 (s, 3H). **¹³C NMR** (101 MHz, DMSO-*d*₆) δ = 170.7, 149.0, 145.1, 144.5, 137.6, 132.1, 126.2, 121.3,

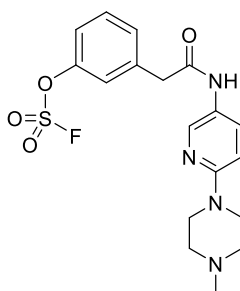
119.0, 114.2, 113.2, 42.3, 10.3. **LCMS** (Formic) 100% desired product; $t_{\text{ret}} = 0.9$ min, MH^+ 365.1.

3-(2-(4-(1*H*-indol-3-yl)piperidin-1-yl)-2-oxoethyl)phenyl sulfofluoridate (2.113-*Meta*)



Prepared by **General procedure A**. 3-(2-(4-(1*H*-indol-3-yl)piperidin-1-yl)-2-oxoethyl)phenyl sulfofluoridate (24.7 mg, 0.06 mmol, 50% yield). **¹H NMR** (600 MHz, $\text{DMSO-}d_6$) $\delta = 10.78$ (br s, 1H), 7.57 - 7.52 (m, 2H), 7.50 - 7.45 (m, 2H), 7.43 (d, $J = 7.7$ Hz, 1H), 7.33 (d, $J = 8.1$ Hz, 1H), 7.08 - 7.03 (m, 2H), 6.99 - 6.93 (m, 1H), 4.52 (br d, $J = 12.5$ Hz, 1H), 4.08 (br d, $J = 13.6$ Hz, 1H), 3.93 - 3.84 (m, 2H), 3.25 - 3.18 (m, 1H), 3.04 (br s, 1H), 2.75 (br s, 1H), 1.98 - 1.91 (m, 2H), 1.54 - 1.40 (m, 2H). **¹³C NMR** (176 MHz, $\text{DMSO-}d_6$) $\delta = 167.7, 149.5, 139.7, 136.3, 130.4, 130.1, 126.1, 121.5, 120.8, 120.5, 118.9, 118.8, 118.5, 118.0, 111.4, 45.9, 42.0, 38.9, 33.1, 33.0, 32.3$. **LCMS** (Formic) 100% desired product; $t_{\text{ret}} = 1.20$ min, MH^+ 417.2.

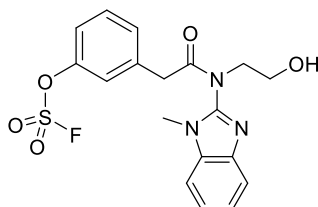
3-(2-((6-(4-Methylpiperazin-1-yl)pyridin-3-yl)amino)-2-oxoethyl)phenyl sulfofluoridate (2.114-*Meta*)



Prepared by **General Procedure A**. 3-(2-((6-(4-Methylpiperazin-1-yl)pyridin-3-yl)amino)-2-oxoethyl)phenyl sulfofluoridate (8.9 mg, 0.02 mmol, 19% yield). **¹H NMR** (600 MHz, $\text{DMSO-}d_6$) $\delta = 10.13$ (s, 1H), 8.32 (d, $J = 2.6$ Hz, 1H), 7.80 (dd, $J = 2.6, 9.2$ Hz, 1H), 7.59 - 7.53 (m, 2H), 7.51 - 7.46 (m, 2H), 6.89 (d, $J = 9.2$ Hz, 1H), 3.75 (s,

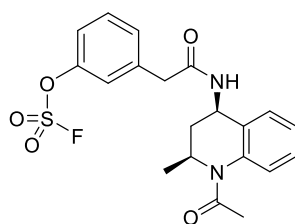
2H), 2.94 - 2.87 (m, 2H), 2.61 - 2.55 (m, 2H). ^{13}C NMR (176 MHz, DMSO- d_6) δ = 168.0, 162.9, 154.7, 149.5, 139.1, 139.0, 130.5, 130.1, 130.1, 127.4, 121.5, 119.1, 107.5, 52.5, 43.0, 42.0. LCMS (Formic) 100% desired product; t_{ret} = 0.57 min, MH^+ 409.2.

3-(2-((2-Hydroxyethyl)(1-methyl-1H-benzo[d]imidazol-2-yl)amino)-2-oxoethyl)phenyl sulfofluoridate (2.115-*Meta*)



Prepared by **General Procedure A**. 3-(2-((2-Hydroxyethyl)(1-methyl-1H-benzo[d]imidazol-2-yl)amino)-2-oxoethyl)phenyl sulfofluoridate (17.5 mg, 0.04 mmol, 36% yield). ^1H NMR (600 MHz, DMSO- d_6) δ = 8.78 - 8.64 (m, 1H), 7.52 - 7.49 (m, 1H), 7.48 - 7.44 (m, 2H), 7.44 - 7.40 (m, 2H), 7.40 - 7.36 (m, 1H), 7.32 - 7.25 (m, 2H), 4.33 (t, J = 5.1 Hz, 2H), 3.83 (s, 2H), 3.71 (br d, J = 5.5 Hz, 2H), 3.59 (s, 3H). ^{13}C NMR (176 MHz, DMSO- d_6) δ = 170.5, 150.4, 149.4, 137.4, 131.6, 130.5, 130.3, 123.2, 122.7, 121.8, 119.3, 111.7, 109.7, 62.4, 41.9, 29.0. LCMS (Formic) 100% desired product; t_{ret} = 0.70 min, MH^+ 408.1.

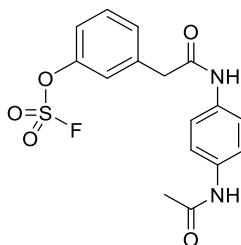
3-(2-(((2S,4R)-1-Acetyl-2-methyl-1,2,3,4-tetrahydroquinolin-4-yl)amino)-2-oxoethyl)phenyl sulfofluoridate (2.116-*Meta*)



Prepared by **General Procedure A**. 3-(2-(((2S,4R)-1-Acetyl-2-methyl-1,2,3,4-tetrahydroquinolin-4-yl)amino)-2-oxoethyl)phenyl sulfofluoridate (13.2 mg, 0.03 mmol, 27% yield). ^1H NMR (600 MHz, DMSO- d_6) δ = 8.61 - 8.55 (m, 1H), 7.61 - 7.55 (m, 2H), 7.53 - 7.48 (m, 2H), 7.33 - 7.26 (m, 2H), 7.22 - 7.15 (m, 1H), 7.13 - 7.06 (m, 1H), 4.71 - 4.58 (m, 2H), 3.77 - 3.67 (m, 2H), 2.48 - 2.42 (m, 1H), 2.03 (s, 3H), 1.27

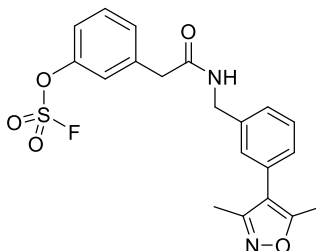
- 1.19 (m, 1H), 1.04 (d, $J = 6.6$ Hz, 3H). $^{13}\text{C NMR}$ (176 MHz, DMSO-d_6) $\delta = 169.2, 168.4, 149.6, 139.6, 136.1, 130.6, 130.0, 126.9, 126.0, 125.2, 122.7, 121.2, 119.0, 46.5, 44.8, 41.6, 22.5, 21.2$. **LCMS** (Formic) 100% desired product; $t_{\text{ret}} = 1.02$ min, $\text{MH}^+ 421.2$.

3-(2-((4-Acetamidophenyl)amino)-2-oxoethyl)phenyl sulfofluoridate (2.117-*Meta*)



Prepared by **General Procedure A**. 3-(2-((4-Acetamidophenyl)amino)-2-oxoethyl)phenyl sulfofluoridate (13.9 mg, 0.04 mmol, 32% yield). $^1\text{H NMR}$ (600 MHz, DMSO-d_6) $\delta = 10.17$ (s, 1H), 9.87 (s, 1H), 7.58 - 7.53 (m, 2H), 7.49 (s, 6H), 3.75 (s, 2H), 2.01 (s, 3H). $^{13}\text{C NMR}$ (176 MHz, DMSO-d_6) $\delta = 167.9, 167.8, 149.5, 139.3, 134.9, 134.2, 130.5, 130.0, 121.5, 119.5, 119.3, 119.0, 42.3, 23.8$. **LCMS** (Formic) 100% desired product; $t_{\text{ret}} = 0.92$ min, $\text{MH}^+ 367.1$.

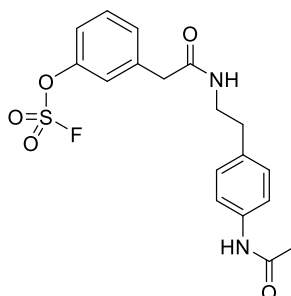
3-(2-((3-(3,5-Dimethylisoxazol-4-yl)benzyl)amino)-2-oxoethyl)phenyl sulfofluoridate (2.118-*Meta*)



Prepared by **General Procedure A**. 3-(2-((3-(3,5-Dimethylisoxazol-4-yl)benzyl)amino)-2-oxoethyl)phenyl sulfofluoridate (9.7 mg, 0.02 mmol, 20% yield). $^1\text{H NMR}$ (600 MHz, DMSO-d_6) $\delta = 8.68$ (br s, 1H), 7.54 - 7.39 (m, 5H), 7.27 - 7.23 (m, 2H), 7.21 - 7.18 (m, 1H), 4.34 (d, $J = 5.5$ Hz, 2H), 3.62 (s, 2H), 2.35 (s, 3H), 2.18 (s, 3H). $^{13}\text{C NMR}$ (176 MHz, DMSO-d_6) $\delta = 169.3, 164.9, 157.9, 149.5, 139.9, 139.6, 130.5, 129.9, 129.8, 128.8, 127.5, 127.2, 126.3, 121.2, 118.9, 115.7, 42.1, 41.5, 11.2, 10.3$. **LCMS** (Formic) 100% desired product; $t_{\text{ret}} = 1.12$ min, $\text{MH}^+ 419.2$.

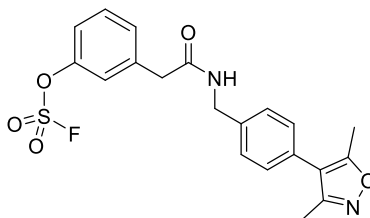
3-(2-((4-Acetamidophenethyl)amino)-2-oxoethyl)phenyl sulfofluoridate (2.119-

Meta)



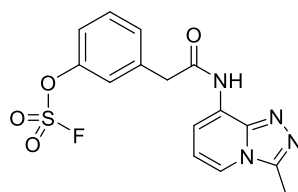
Prepared by **General Procedure A**. 3-(2-((4-Acetamidophenethyl)amino)-2-oxoethyl)phenyl sulfofluoridate (20.6 mg, 0.05 mmol, 44% yield). ¹H NMR (600 MHz, DMSO_{1p7}mm) δ = 9.88 - 9.81 (m, 1H), 8.21 - 8.14 (m, 1H), 7.53 - 7.49 (m, 1H), 7.48 - 7.41 (m, 4H), 7.36 - 7.32 (m, 1H), 7.10 - 7.06 (m, 2H), 3.50 (s, 2H), 3.26 (br d, *J* = 6.6 Hz, 2H), 2.65 (t, *J* = 7.3 Hz, 2H), 2.02 (s, 3H). ¹³C NMR (176 MHz, DMSO-*d*₆) δ = 169.0, 168.0, 149.5, 139.8, 137.4, 133.8, 130.4, 129.8, 128.7, 121.2, 119.0, 118.8, 41.6, 40.3, 34.4, 23.9. LCMS (Formic) 100% desired product; *t*_{ret} = 0.89 min, MH⁺ 395.1.

3-(2-((4-(3,5-Dimethylisoxazol-4-yl)benzyl)amino)-2-oxoethyl)phenyl sulfofluoridate (2.120-Meta)



Prepared by **General Procedure A**. 3-(2-((4-(3,5-Dimethylisoxazol-4-yl)benzyl)amino)-2-oxoethyl)phenyl sulfofluoridate (9.3 mg, 0.02 mmol, 19% yield). ¹H NMR (600 MHz, DMSO_{1p7}mm) δ = 8.72 - 8.65 (m, 1H), 7.54 (d, *J* = 7.7 Hz, 1H), 7.49 (br d, *J* = 10.3 Hz, 2H), 7.45 (d, *J* = 7.3 Hz, 1H), 7.37 - 7.27 (m, 4H), 4.33 (d, *J* = 5.9 Hz, 2H), 3.62 (s, 2H), 2.38 (s, 3H), 2.21 (s, 3H). ¹³C NMR (176 MHz, DMSO-*d*₆) δ = 169.2, 164.9, 158.0, 149.5, 139.6, 138.5, 130.5, 129.9, 128.8, 128.3, 127.7, 121.2, 119.0, 115.6, 42.0, 41.5, 11.2, 10.4. LCMS (Formic) 100% desired product; *t*_{ret} = 1.12 min, MH⁺ 419.2.

3-(2-((3-Methyl-[1,2,4]triazolo[4,3-*a*]pyridin-8-yl)amino)-2-oxoethyl)phenyl sulfonfluoridate (2.121-*Meta*)



Prepared by **General Procedure A**. 3-(2-((3-Methyl-[1,2,4]triazolo[4,3-*a*]pyridin-8-yl)amino)-2-oxoethyl)phenyl sulfonfluoridate (10.2 mg, 0.03 mmol, 24% yield). **¹H NMR** (600 MHz, DMSO-*d*₆) δ = 10.74 (s, 1H), 8.25 - 8.20 (m, 1H), 8.04 - 7.98 (m, 1H), 7.62 - 7.49 (m, 4H), 7.10 - 7.05 (m, 1H), 4.02 (s, 2H), 2.74 (s, 3H). **¹³C NMR** (176 MHz, DMSO-*d*₆) δ = 169.8, 149.5, 145.0, 143.1, 138.8, 130.6, 130.3, 125.1, 121.7, 119.4, 119.2, 115.9, 114.6, 41.8, 9.8. **LCMS** (Formic) 100% desired product; *t*_{ret} = 0.9 min, MH⁺ 365.1

REFERENCES

- (74) Duong-Ly, K. C.; Peterson, J. R. *The human kinome and kinase inhibition*; Wiley Online Library, **2013**; Vol. Chapter 2.
- (75) Weinmann, H.; Metternich, R. *Chembiochem* **2005**, *6*, 455.
- (76) Reiterer, V.; Eysers, P. A.; Farhan, H. *Trends Cell Biol* **2014**, *24*, 489.
- (77) Fabbro, D.; Cowan-Jacob, S. W.; Moebitz, H. *Br J Pharmacol* **2015**, *172*, 2675.
- (78) Shchemelinin, I.; Sefc, L.; Necas, E. *Folia biologica* **2006**, *52*, 81.
- (79) Dorian, F.; Sandra, W.; Cowan-Jacob; Henrik, M. *J. Pharm* **2015**, *172*, 2675.
- (80) Fleuren, E. D.; Zhang, L.; Wu, J.; Daly, R. J. *Nat Rev Cancer* **2016**, *16*, 83.
- (81) Kwarcinski, F. E.; Steffey, M. E.; Fox, C. C.; Soellner, M. B. *ACS Med Chem Lett* **2015**, *6*, 898.
- (82) Zhang Jianming, Y. L. P.; Gray, S. N. *Nature review* **2009**, *9*, 28.
- (83) Pflug, A.; de Oliveira, T. M.; Bossemeyer, D.; Engh, R. A. *Biochem J* **2011**, *440*, 85.
- (84) Gaßel, M.; Breitenlechner, C. B.; Rüger, P.; Jucknischke, U.; Schneider, T.; Huber, R.; Bossemeyer, D.; Engh, R. A. *J Mol Biol* **2003**, *329*, 1021.
- (85) Manning, G.; Whyte, D. B.; Martinez, R.; Hunter, T.; Sudarsanam, S. *Science* **2002**, *298*, 1912.
- (86) Huang, D.; Zhou, T.; Lafleur, K.; Nevado, C.; Caflisch, A. *Bioinformatics* **2010**, *26*, 198.
- (87) Santiago-Tirado, F. H.; Bretscher, A. *Trends Cell Biol* **2011**, *21*, 515.
- (88) Adams, J. L.; Bamborough, P.; Drewry, D. H.; Shewchuk, L.; John Wiley & Sons, Inc.: Hoboken, NJ, USA, 2008, p 119.
- (89) Mindy I Davis, J. P. H., Sanna Herrgard, Pietro Ciceri, Lisa M Wodicka, Gabriel Pallares, Michael Hocker, Daniel K Treiber, Patrick P Zarrinkar *Nature Biotechnology* **2011**, *29*, 1046.
- (90) Bamborough, P.; Brown, M. J.; Christopher, J. A.; Chung, C. W.; Mellor, G. W. *J Med Chem* **2011**, *54*, 5131.
- (91) Campbell, R. M.; Anderson, B. D.; Brooks, N. A.; Brooks, H. B.; Chan, E. M.; De Dios, A.; Gilmour, R.; Graff, J. R.; Jambrina, E.; Mader, M.; McCann, D.; Na, S.; Parsons, S. H.; Pratt, S. E.; Shih, C.; Stancato, L. F.; Starling, J. J.; Tate, C.; Velasco, J. A.; Wang, Y.; Ye, X. S. *Mol Cancer Ther* **2014**, *13*, 364.
- (92) Yaish, P.; Gazit, A.; Gilon, C.; Levitzki, A. *Science* **1988**, *242*, 933.
- (93) O'Brien, Z.; Fallah Moghaddam, M. *Expert Opin Drug Metab Toxicol* **2013**, *9*, 1597.
- (94) Lindsay, M. A. *Nat Rev Drug Discov* **2003**, *2*, 831.
- (95) Wu, P.; Nielsen, T. E.; Clausen, M. H. *Drug Discov Today* **2016**, *21*, 5.
- (96) Bamborough, P. *Expert Opin Drug Discov* **2012**, *7*, 1053.
- (97) Bhullar, K. S.; Lagaron, N. O.; McGowan, E. M.; Parmar, I.; Jha, A.; Hubbard, B. P.; Rupasinghe, H. P. V. *Mol Cancer* **2018**, *17*, 48.
- (98) Hopkins, A. L.; Groom, C. R. *Nat Rev Drug Discov* **2002**, *1*, 727.

- (99) Loo, L.; Wright, B. D.; Zylka, M. J. *Pain* **2015**, *156 Suppl 1*, S2.
- (100) Suh, B. C.; Hille, B. *Annu Rev Biophys* **2008**, *37*, 175.
- (101) Whitman, M.; Downes, C. P.; Keeler, M.; Keller, T.; Cantley, L. *Nature* **1988**, *332*, 644.
- (102) Yang, Q.; Modi, P.; Newcomb, T.; Queva, C.; Gandhi, V. *Clin Cancer Res* **2015**, *21*, 1537.
- (103) Walker, E. H.; Perisic, O.; Ried, C.; Stephens, L.; Williams, R. L. *Nature* **1999**, *402*, 313.
- (104) Williams, R. L.; Walker, E. H.; Perisic, O.; Ried, C.; Stephens, L.; Aggarwal, G. *Nature* **1999**, *402*, 313.
- (105) Vanhaesebroeck, B.; Whitehead, M. A.; Pineiro, R. *J Mol Med* **2016**, *94*, 5.
- (106) Wymann, M. P.; Marone, R. *Curr Opin Cell Biol* **2005**, *17*, 141.
- (107) Fruman, D. A.; Chiu, H.; Hopkins, B. D.; Bagrodia, S.; Cantley, L. C.; Abraham, R. T. *Cell* **2017**, *170*, 605.
- (108) Samuels, Y.; Wang, Z.; Bardelli, A.; Silliman, N.; Ptak, J.; Szabo, S.; Yan, H.; Gazdar, A.; Powell, S. M.; Riggins, G. J.; Willson, J. K. V.; Markowitz, S.; Kinzler, K. W.; Vogelstein, B.; Velculescu, V. E. *Science* **2004**, *304*, 554.
- (109) Morrow, A. A.; Alipour, M. A.; Bridges, D.; Yao, Z.; Saltiel, A. R.; Lee, J. M. *Mol Cancer Res* **2014**, *12*, 1492.
- (110) Heath, C. M.; Stahl, P. D.; Barbieri, M. A. *Histol Histopathol* **2003**, *18*, 989.
- (111) Altan-Bonnet, N.; Balla, T. *Trends Biochem Sci* **2012**, *37*, 293.
- (112) Weixel, K. M.; Blumental-Perry, A.; Watkins, S. C.; Aridor, M.; Weisz, O. A. *J Biol Chem* **2005**, *280*, 10501.
- (113) Godi, A.; Pertile, P.; Meyers, R.; Marra, P.; Di Tullio, G.; Iurisci, C.; Luini, A.; Corda, D.; De Matteis, M. A. *Nat Cell Biol* **1999**, *1*, 280.
- (114) Chu, K. M.; Minogue, S.; Hsuan, J. J.; Waugh, M. G. *Cell Death Dis* **2010**, *1*, e106.
- (115) Balla, A.; Balla, T. *Trends Cell Biol* **2006**, *16*, 351.
- (116) Klima, M.; Baumlova, A.; Chalupska, D.; Hrebabecky, H.; Dejmek, M.; Nencka, R.; Boura, E. *Acta Crystallogr D Biol Crystallogr* **2015**, *71*, 1555.
- (117) Wong, K.; Meyers, R.; Cantley, L. C. *J Biol Chem* **1997**, *272*, 13236.
- (118) Baumlova, A.; Gregor, J.; Boura, E. *Physiological research* **2016**, *65*, 987.
- (119) Bojjireddy, N.; Botyanszki, J.; Hammond, G.; Creech, D.; Peterson, R.; Kemp, D. C.; Snead, M.; Brown, R.; Morrison, A.; Wilson, S.; Harrison, S.; Moore, C.; Balla, T. *J Biol Chem* **2014**, *289*, 6120.
- (120) den Boon, J. A.; Ahlquist, P. *Annu Rev Microbiol* **2010**, *64*, 241.
- (121) Delang, L.; Paeshuyse, J.; Neyts, J. *Biochem Pharmacol* **2012**, *84*, 1400.
- (122) Boura, E.; Nencka, R. *Exp Cell Res* **2015**, *337*, 136.
- (123) Jacobs, S. E.; Lamson, D. M.; St George, K.; Walsh, T. J. *Clinical microbiology reviews* **2013**, *26*, 135.
- (124) Lindenbach, B. D.; Rice, C. M. *Nature* **2005**, *436*, 933.

- (125) van der Schaar, H. M.; Leyssen, P.; Thibaut, H. J.; de Palma, A.; van der Linden, L.; Lanke, K. H.; Lacroix, C.; Verbeken, E.; Conrath, K.; Macleod, A. M.; Mitchell, D. R.; Palmer, N. J.; van de Poel, H.; Andrews, M.; Neyts, J.; van Kuppeveld, F. J. *Antimicrob Agents Chemother* **2013**, *57*, 4971.
- (126) Mathers, C. D.; Loncar, D. *PLoS Med* **2006**, *3*, e442.
- (127) Vijayan, V. K. *Indian J Med Res* **2013**, *137*, 251.
- (128) Seemungal, T. A. R.; Harper-Owen, R.; Bhowmik, A.; Sapsford, R.; Jeffries, D. J.; Wedzicha, J. A. *Thorax* **1999**, *54*.
- (129) Singh, J.; Petter, R. C.; Baillie, T. A.; Whitty, A. *Nat Rev Drug Discov* **2011**, *10*, 307.
- (130) Long, M. J. C.; Aye, Y. *Cell Chem Biol* **2017**, *24*, 787.
- (131) Yocum, R. R.; Rasmussen, J. R.; Strominger, J. L. *J Biol Chem* **1980**, *255*, 3977.
- (132) Vane, J. R.; Botting, R. M. *Thrombosis Research* **2003**, *110*, 255.
- (133) Gonzalez-Bello, C. *ChemMedChem* **2016**, *11*, 22.
- (134) Bradshaw, J. M.; McFarland, J. M.; Paavilainen, V. O.; Bisconte, A.; Tam, D.; Phan, V. T.; Romanov, S.; Finkle, D.; Shu, J.; Patel, V.; Ton, T.; Li, X.; Loughhead, D. G.; Nunn, P. A.; Karr, D. E.; Gerritsen, M. E.; Funk, J. O.; Owens, T. D.; Verner, E.; Brameld, K. A.; Hill, R. J.; Goldstein, D. M.; Taunton, J. *Nat Chem Biol* **2015**, *11*, 525.
- (135) Shin, J. M.; Cho, Y. M.; Sachs, G. *J Am Chem Soc* **2004**, *126*, 7800.
- (136) Howden, C. W. *Clin Pharmacokinet* **1991**, *20*, 38.
- (137) Olbe, L.; Carlsson, E.; Lindberg, P. *Nat Rev Drug Discov* **2003**, *2*, 132.
- (138) Wallmark, B.; Brändström, A.; Larsson, H. *Scand J Gastroentero* **2009**, *21*, 59.
- (139) Vasudevan, A.; Argiriadi, M. A.; Baranczak, A.; Friedman, M. M.; Gavriilyuk, J.; Hobson, A. D.; Hulce, J. J.; Osman, S.; Wilson, N. S. In *Progress in Medicinal Chemistry*; Witty, D. R., Cox, B., Eds.; Elsevier: **2019**; Vol. 58, p 1.
- (140) Sanderson, K. *Nature Reviews Drug Discovery* **2013**, *12*, 649.
- (141) Johnson, D. S.; Weerapana, E.; Cravatt, B. F. *Future Med Chem* **2010**, *2*, 949.
- (142) Dahal, U. P.; Gilbert, A. M.; Obach, R. S.; Flanagan, M. E.; Chen, J. M.; Garcia-Irizarry, C.; Starr, J. T.; Schuff, B.; Uccello, D. P.; Young, J. A. *MedChemComm* **2016**, *7*, 864.
- (143) Lee, C. U.; Grossmann, T. N. *Angew Chem Int Ed Engl* **2012**, *51*, 8699.
- (144) Kalgutkar, A. S.; Dalvie, D. K. *Expert Opin Drug Discov* **2012**, *7*, 561.
- (145) Miller, J. A. *Drug Metab. Rev* **1998**, *30*, 645.
- (146) Barf, T.; Kaptein, A. *J Med Chem* **2012**, *55*, 6243.
- (147) Singh, J.; Petter, R. C.; Kluge, A. F. *Curr Opin Chem Biol* **2010**, *14*, 475.
- (148) Potashman, M. H.; Duggan, M. E. *J Med Chem* **2009**, *52*, 1231.
- (149) Doorn, J. A.; Petersen, D. R. *Chem Res Toxicol* **2002**, *15*, 1445.
- (150) Abranyi-Balogh, P.; Petri, L.; Imre, T.; Szijj, P.; Scarpino, A.; Hrast, M.; Mitrovic, A.; Fonovic, U. P.; Nemeth, K.; Barreteau, H.; Roper, D. I.; Horvati, K.; Ferenczy, G. G.; Kos, J.; Ilas, J.; Gobec, S.; Keseru, G. M. *Eur J Med Chem* **2018**, *160*, 94.

- (151) Ghosh, A. K.; Samanta, I.; Mondal, A.; Liu, W. R. *ChemMedChem* **2019**, *14*, 889.
- (152) Lonsdale, R.; Burgess, J.; Colclough, N.; Davies, N. L.; Lenz, E. M.; Orton, A. L.; Ward, R. A. *J Chem Inf Model* **2017**, *57*, 3124.
- (153) Hallenbeck, K. K.; Turner, D. M.; Renslo, A. R.; Arkin, M. R. *Curr Top Med Chem* **2017**, *17*, 4.
- (154) Lagoutte, R.; Patouret, R.; Winssinger, N. *Current Opinion in Chemical Biology* **2017**, *39*, 54.
- (155) Adeniyi, A. A.; Muthusamy, R.; Soliman, M. E. *Expert Opin Drug Discov* **2016**, *11*, 79.
- (156) Pan, Z.; Scheerens, H.; Li, S. J.; Schultz, B. E.; Sprengeler, P. A.; Burrill, L. C.; Mendonca, R. V.; Sweeney, M. D.; Scott, K. C. K.; Grothaus, P. G.; Jeffery, D. A.; Spoerke, J. M.; Honigberg, L. A.; Young, P. R.; Dalrymple, S. A.; Palmer, J. T. *ChemMedChem* **2007**, *2*, 58.
- (157) Liu, N.; Hoogendoorn, S.; van de Kar, B.; Kaptein, A.; Barf, T.; Driessen, C.; Filippov, D. V.; van der Marel, G. A.; van der Stelt, M.; Overkleeft, H. S. *J Org Biomol Chem* **2015**, *13*, 5147.
- (158) Li, D.; Ambrogio, L.; Shimamura, T.; Kubo, S.; Takahashi, M.; Chirieac, L. R.; Padera, R. F.; Shapiro, G. I.; Baum, A.; Himmelsbach, F.; Rettig, W. J.; Meyerson, M.; Solca, F.; Greulich, H.; Wong, K. K. *Oncogene* **2008**, *27*, 4702.
- (159) Waterson, A. G.; Petrov, K. G.; Hornberger, K. R.; Hubbard, R. D.; Sammond, D. M.; Smith, S. C.; Dickson, H. D.; Caferro, T. R.; Hinkle, K. W.; Stevens, K. L.; Dickerson, S. H.; Rusnak, D. W.; Spehar, G. M.; Wood, E. R.; Griffin, R. J.; Uehling, D. E. *Bioorg Med Chem Lett* **2009**, *19*, 1332.
- (160) Ponader, S.; Chen, S. S.; Buggy, J. J.; Balakrishnan, K.; Gandhi, V.; Wierda, W. G.; Keating, M. J.; O'Brien, S.; Chiorazzi, N.; Burger, J. A. In *Blood* 2012; Vol. 119, p 1182.
- (161) Bissantz, C.; Kuhn, B.; Stahl, M. *J Med Chem* **2010**, *53*, 5061.
- (162) Krishnan, S.; Miller, R. M.; Tian, B.; Mullins, R. D.; Jacobson, M. P.; Taunton, J. *J Am Chem Soc* **2014**, *136*, 12624.
- (163) Shannon, D. A.; Weerapana, E. *Curr Opin Chem Biol* **2015**, *24*, 18.
- (164) Ph.D., R. A. C. *Enzymes: A Practical Introduction to Structure, Mechanism, and Data Analysis, Second Edition*; John Wiley & Sons Inc.: New York, NY, USA, 2000.
- (165) Strelow, J. M. *SLAS Discov* **2017**, *22*, 3.
- (166) Bauer, R. A. *Drug Discov Today* **2015**, *20*, 1061.
- (167) Zhao, Z.; Bourne, P. E. *Drug Discov Today* **2018**, *23*, 727.
- (168) Wu, S.; Luo Howard, H.; Wang, H.; Zhao, W.; Hu, Q.; Yang, Y. *Biochem Biophys Res Commun* **2016**, *478*, 1268.
- (169) Jost, C.; Nitsche, C.; Scholz, T.; Roux, L.; Klein, C. D. *J Med Chem* **2014**, *57*, 7590.
- (170) Cuesta, A.; Taunton, J. *Annu Rev Biochem* **2019**, *88*, 365.
- (171) Mukherjee, H.; Grimster, N. P. *Curr Opin Chem Biol* **2018**, *44*, 30.
- (172) Moura, A.; Savageau, M. A.; Alves, R. *PLoS One* **2013**, *8*, e77319.
- (173) Engel, J.; Lategahn, J.; Rauh, D. *ACS Med Chem Lett* **2016**, *7*, 2.

- (174) Gerberick, G. F.; Vassallo, J. D.; Foertsch, L. M.; Price, B. B.; Chaney, J. G.; Lepoittevin, J. P. *J Toxicol Sci* **2007**, *97*, 417.
- (175) Aksnes, H.; Drazic, A.; Marie, M.; Arnesen, T. *Trends Biochem Sci* **2016**, *41*, 746.
- (176) Pettinger, J.; Jones, K.; Cheeseman, M. D. *Angew Chem Int Ed Engl* **2017**, *56*, 15200.
- (177) Platzer, G.; Okon, M.; McIntosh, L. P. *J Biomol NMR* **2014**, *60*, 109.
- (178) Harris, T. K.; Turner, G. J. *IUBMB Life* **2002**, *53*, 85.
- (179) Hacker, S. M.; Backus, K. M.; Lazear, M. R.; Forli, S.; Correia, B. E.; Cravatt, B. F. *Nat Chem* **2017**, *9*, 1181.
- (180) Liu, R.; Yue, Z.; Tsai, C. C.; Shen, J. *J Am Chem Soc* **2019**, *141*, 6553.
- (181) Powers, J. C.; Asgian, J. L.; Ekici, O. D.; James, K. E. *Chem Rev* **2002**, *102*, 4639.
- (182) Hunkapiller, M. W.; Smallcombe, S. H.; Witaker, D. R.; Richards, J. H. *J Biol Chem* **1973**, *248*, 8306.
- (183) Grimsley, G. R.; Scholtz, J. M.; Pace, C. N. *Protein Sci* **2009**, *18*, 247.
- (184) Ishikita, H. *FEBS Letters* **2010**, *584*, 3464.
- (185) Isom, D. G.; Castaneda, C. A.; Cannon, B. R.; Garcia-Moreno, B. *Proc Natl Acad Sci U S A* **2011**, *108*, 5260.
- (186) Huang, Y.; Harris, R. C.; Shen, J. *J Chem Inf Model* **2018**, *58*, 1372.
- (187) van Linden, O. P.; Kooistra, A. J.; Leurs, R.; de Esch, I. J.; de Graaf, C. *J Med Chem* **2014**, *57*, 249.
- (188) London, N.; Miller, R. M.; Krishnan, S.; Uchida, K.; Irwin, J. J.; Eidam, O.; Gibold, L.; Cimermancic, P.; Bonnet, R.; Shoichet, B. K.; Taunton, J. *Nat Chem Biol* **2014**, *10*, 1066.
- (189) Dalton, S. E.; Dittus, L.; Thomas, D. A.; Convery, M. A.; Nunes, J.; Bush, J. T.; Evans, J. P.; Werner, T.; Bantscheff, M.; Murphy, J. A.; Campos, S. *J Am Chem Soc* **2018**, *140*, 932.
- (190) Sutherlin, D. P.; Baker, S.; Bisconte, A.; Blaney, P. M.; Brown, A.; Chan, B. K.; Chantry, D.; Castanedo, G.; DePledge, P.; Goldsmith, P.; Goldstein, D. M.; Hancox, T.; Kaur, J.; Knowles, D.; Kondru, R.; Lesnick, J.; Lucas, M. C.; Lewis, C.; Murray, J.; Nadin, A. J.; Nonomiya, J.; Pang, J.; Pegg, N.; Price, S.; Reif, K.; Safina, B. S.; Salphati, L.; Staben, S.; Seward, E. M.; Shuttleworth, S.; Sohal, S.; Sweeney, Z. K.; Ultsch, M.; Waszkowycz, B.; Wei, B. *Bioorg Med Chem Lett* **2012**, *22*, 4296.
- (191) Wymann, M. P.; Bulgarelli-Leva, G.; Zvelebil, M. J.; Pirola, L.; Vanhaesebroeck, B.; Waterfield, M. D.; Panayotou, G. *Mol Cell Biol* **1996**, *16*, 1722.
- (192) Arcaro, A.; Wymann, M. P. *Biochem J* **1993**, *296* (Pt 2), 297.
- (193) Brian, P. W.; Curtis, P. J.; Hemming, H. G.; Norris, G. L. F. *Trans Br Mycol Soc* **1957**, *40*, 365.
- (194) Ward, S.; Sotsios, Y.; Dowden, J.; Bruce, I.; Finan, P. *Chem Biol* **2003**, *10*, 207.
- (195) Knight, Z. A.; Gonzalez, B.; Feldman, M. E.; Zunder, E. R.; Goldenberg, D. D.; Williams, O.; Loewith, R.; Stokoe, D.; Balla, A.; Toth, B.; Balla, T.; Weiss, W. A.; Williams, R. L.; Shokat, K. M. *Cell* **2006**, *125*, 733.

- (196) Gharbi, S.; Zvelebil, M.; Shuttleworth, S.; Hancox, T.; Saghir, N.; Timms, J.; D Waterfield, M. *Exploring the specificity of the PI3K family inhibitor LY294002*, 2007; Vol. 404.
- (197) Yuan, H.; Pupo, M. T.; Blois, J.; Smith, A.; Weissleder, R.; Clardy, J.; Josephson, L. *Bioorg Med Chem Lett* **2009**, *19*, 4223.
- (198) Choi, S.; Connelly, S.; Reixach, N.; Wilson, I. A.; Kelly, J. W. *Nat Chem Biol* **2009**, *6*, 133.
- (199) Berndt, A.; Miller, S.; Williams, O.; Le, D. D.; Houseman, B. T.; Pacold, J. I.; Gorrec, F.; Hon, W. C.; Liu, Y.; Rommel, C.; Gaillard, P.; Ruckle, T.; Schwarz, M. K.; Shokat, K. M.; Shaw, J. P.; Williams, R. L. *Nat Chem Biol* **2010**, *6*, 117.
- (200) Rutaganira, F. U.; Fowler, M. L.; McPhail, J. A.; Gelman, M. A.; Nguyen, K.; Xiong, A.; Dornan, G. L.; Tavshanjian, B.; Glenn, J. S.; Shokat, K. M.; Burke, J. E. *J Med Chem* **2016**, *59*, 1830.
- (201) Jackson, P. A.; Widen, J. C.; Harki, D. A.; Brummond, K. M. *J Med Chem* **2017**, *60*, 839.
- (202) Baker, B. R. *Acc Chem Res* **2002**, *2*, 129.
- (203) Dong, J.; Krasnova, L.; Finn, M. G.; Sharpless, K. B. *Angew Chem Int Ed Engl* **2014**, *53*, 9430.
- (204) Narayanan, A.; Jones, L. H. *Chem Sci* **2015**, *6*, 2650.
- (205) Baranczak, A.; Liu, Y.; Connelly, S.; Du, W. G.; Greiner, E. R.; Genereux, J. C.; Wiseman, R. L.; Eisele, Y. S.; Bradbury, N. C.; Dong, J.; Noodleman, L.; Sharpless, K. B.; Wilson, I. A.; Encalada, S. E.; Kelly, J. W. *J Am Chem Soc* **2015**, *137*, 7404.
- (206) Moellering, R. E.; Cravatt, B. F. *Chem Biol* **2012**, *19*, 11.
- (207) Bunnage, M. E.; Chekler, E. L.; Jones, L. H. *Nat Chem Biol* **2013**, *9*, 195.
- (208) Zhao, Q.; Ouyang, X.; Wan, X.; Gajiwala, K. S.; Kath, J. C.; Jones, L. H.; Burlingame, A. L.; Taunton, J. *J Am Chem Soc* **2017**, *139*, 680.
- (209) Hett, E. C.; Xu, H.; Geoghegan, K. F.; Gopalsamy, A.; Kyne, R. E., Jr.; Menard, C. A.; Narayanan, A.; Parikh, M. D.; Liu, S.; Roberts, L.; Robinson, R. P.; Tones, M. A.; Jones, L. H. *ACS Chem Biol* **2015**, *10*, 1094.
- (210) Jones, L. H. *Angew Chem Int Ed* **2018**, *57*, 9220-9223.
- (211) Gu, C.; Shannon, D. A.; Colby, T.; Wang, Z.; Shabab, M.; Kumari, S.; Villamor, J. G.; McLaughlin, C. J.; Weerapana, E.; Kaiser, M.; Cravatt, B. F.; van der Hoorn, R. A. *Chem Biol* **2013**, *20*, 541.
- (212) Mukherjee, H.; Debreczeni, J.; Breed, J.; Tentarelli, S.; Aquila, B.; Dowling, J. E.; Whitty, A.; Grimster, N. P. *Org Biomol Chem* **2017**, *15*, 9685.
- (213) Cramer, R.; Coffman, D. *J Org Chem* **1961**, *26*, 4164.
- (214) Zhou, H.; Mukherjee, P.; Liu, R.; Evrard, E.; Wang, D.; Humphrey, J. M.; Butler, T. W.; Hoth, L. R.; Sperry, J. B.; Sakata, S. K.; Helal, C. J.; am Ende, C. W. *Org Lett* **2018**, *20*, 812.
- (215) Jones, L. H. *ACS Med Chem Lett* **2018**, *9*, 584.
- (216) Martin-Gago, P.; Olsen, C. A. *Angew Chem Int Ed Engl* **2019**, *58*, 957.
- (217) Fadeyi, O. O.; Hoth, L. R.; Choi, C.; Feng, X.; Gopalsamy, A.; Hett, E. C.; Kyne, R. E., Jr.; Robinson, R. P.; Jones, L. H. *ACS Chem Biol* **2017**, *12*, 2015.

- (218) Mortenson, D. E.; Brighty, G. J.; Plate, L.; Bare, G.; Chen, W.; Li, S.; Wang, H.; Cravatt, B. F.; Forli, S.; Powers, E. T.; Sharpless, K. B.; Wilson, I. A.; Kelly, J. W. *J Am Chem Soc* **2018**, *140*, 200.
- (219) Wang, N.; Yang, B.; Fu, C.; Zhu, H.; Zheng, F.; Kobayashi, T.; Liu, J.; Li, S.; Ma, C.; Wang, P. G.; Wang, Q.; Wang, L. *J Am Chem Soc* **2018**, *140*, 4995.
- (220) Hughes, J. P.; Rees, S.; Kalindjian, S. B.; Philpott, K. L. *Br J Pharmacol* **2011**, *162*, 1239.
- (221) Giordanetto, F.; Jin, C.; Willmore, L.; Feher, M.; Shaw, D. E. *J Med Chem* **2019**, *62*, 3381.
- (222) Erlanson, D. A.; McDowell, R. S.; O'Brien, T. *J Med Chem* **2004**, *47*, 3463.
- (223) Erlanson, D. A.; Fesik, S. W.; Hubbard, R. E.; Jahnke, W.; Jhoti, H. *Nat Rev Drug Discov* **2016**, *15*, 605.
- (224) Resnick, E.; Bradley, A.; Gan, J.; Douangamath, A.; Krojer, T.; Sethi, R.; Geurink, P. P.; Aimon, A.; Amitai, G.; Bellini, D.; Bennett, J.; Fairhead, M.; Fedorov, O.; Gabizon, R.; Gan, J.; Guo, J.; Plotnikov, A.; Reznik, N.; Ruda, G. F.; Diaz-Saez, L.; Straub, V. M.; Szommer, T.; Velupillai, S.; Zaidman, D.; Zhang, Y.; Coker, A. R.; Dowson, C. G.; Barr, H. M.; Wang, C.; Huber, K. V. M.; Brennan, P. E.; Ovaa, H.; von Delft, F.; London, N. *J Am Chem Soc* **2019**, *141*, 8951.
- (225) Lamoree, B.; Hubbard, R. E. *Essays Biochem* **2017**, *61*, 453.
- (226) Baurin, N.; Aboul-Ela, F.; Barril, X.; Davis, B.; Drysdale, M.; Dymock, B.; Finch, H.; Fromont, C.; Richardson, C.; Simmonite, H.; Hubbard, R. E. *J Chem Inf Comput Sci* **2004**, *44*, 2157.
- (227) Keseru, G. M.; Erlanson, D. A.; Ferenczy, G. G.; Hann, M. M.; Murray, C. W.; Pickett, S. D. *J Med Chem* **2016**, *59*, 8189.
- (228) Parker, C. G.; Galmozzi, A.; Wang, Y.; Correia, B. E.; Sasaki, K.; Joslyn, C. M.; Kim, A. S.; Cavallaro, C. L.; Lawrence, R. M.; Johnson, S. R.; Narvaiza, I.; Saez, E.; Cravatt, B. F. *Cell* **2017**, *168*, 527.
- (229) Murale, D. P.; Hong, S. C.; Haque, M. M.; Lee, J. S. *Proteome Sci* **2016**, *15*, 14.
- (230) Smith, E.; Collins, I. *Future Med Chem* **2015**, *7*, 159.
- (231) Cisar, J. S.; Cravatt, B. F. *J Am Chem Soc* **2012**, *134*, 10385.
- (232) Murale, D. P.; Hong, S. C.; Haque, M. M.; Lee, J. S. *Proteome Sci* **2016**, *15*, 14.
- (233) Erlanson, D. A.; Wells, J. A.; Braisted, A. C. *Annu Rev Biophys Biomol Struct* **2004**, *33*, 199.
- (234) Kathman, S. G.; Xu, Z.; Statsyuk, A. V. *J Med Chem* **2014**, *57*, 4969.
- (235) Johansson, H.; Isabella Tsai, Y. C.; Fantom, K.; Chung, C. W.; Kumper, S.; Martino, L.; Thomas, D. A.; Eberl, H. C.; Muelbaier, M.; House, D.; Rittinger, K. *J Am Chem Soc* **2019**, *141*, 2703.
- (236) Liu, Z.; Li, J.; Li, S.; Li, G.; Sharpless, K. B.; Wu, P. *J Am Chem Soc* **2018**, *140*, 2919.
- (237) McPherson, C. G.; Caldwell, N.; Jamieson, C.; Simpson, I.; Watson, A. J. B. *Org Biomol Chem* **2017**, *15*, 3507.
- (238) Chinthakindi, P. K.; Arvidsson, P. I. *Eur J Org Chem* **2018**, *2018*, 3648.

- (239) Leas, D. A.; Dong, Y.; Vennerstrom, J. L.; Stack, D. E. *Org Lett* **2017**, *19*, 2518.
- (240) Davies, A. T.; Curto, J. M.; Bagley, S. W.; Willis, M. C. *Chem Sci* **2017**, *8*, 1233.
- (241) Zhou, H.; Mukherjee, P.; Liu, R.; Evrard, E.; Wang, D.; Humphrey, J. M.; Butler, T. W.; Hoth, L. R.; Sperry, J. B.; Sakata, S. K.; Helal, C. J.; Am Ende, C. W. *Org Lett* **2018**, *20*, 812.
- (242) Veryser, C.; Demaerel, J.; Bieliu Nas, V.; Gilles, P.; De Borggraeve, W. M. *Org Lett* **2017**, *19*, 5244.
- (243) Clohessy, T. A.; Roberts, A.; Manas, E. S.; Patel, V. K.; Anderson, N. A.; Watson, A. J. B. *Org Lett* **2017**, *19*, 6368.
- (244) Genovese, F.; Lazzari, S.; Venturi, E.; Costantino, L.; Blazquez, J.; Ibacache-Quiroga, C.; Costi, M. P.; Tondi, D. *Med Chem Res* **2017**, *26*, 975.
- (245) McCaw, C. J. A.; Spillane, W. J. *J Phys Org Chem* **2006**, *19*, 512.
- (246) Pacholarz, K. J.; Garlish, R. A.; Taylor, R. J.; Barran, P. E. *Chem Soc Rev* **2012**, *41*, 4335.
- (247) Burke, J. E.; Inglis, A. J.; Perisic, O.; Masson, G. R.; McLaughlin, S. H.; Rutaganira, F.; Shokat, K. M.; Williams, R. L. *Science* **2014**, *344*, 1035.
- (248) Baggio, C.; Udompholkul, P.; Gambini, L.; Salem, A. F.; Jossart, J.; Perry, J. J. P.; Pellicchia, M. *J Med Chem* **2019**, *62*, 9188.
- (249) Cheng, H. C. *J Pharm Tox Met* **2001**, *46*, 61.
- (250) Copeland, R. A.; Basavapathruni, A.; Moyer, M.; Scott, M. P. *Anal Biochem* **2011**, *416*, 206.
- (251) Kumar, M.; Lowery, R. G. *SLAS Discov* **2017**, *22*, 915.
- (252) Gehringer, M.; Laufer, S. A. *J Med Chem* **2019**, *62*, 5673.
- (253) Daniel A. Erlanson, S. W. F., Roderick E. Hubbard, Wolfgang Jahnke & Harren Jhoti *Nat. Rev. Drug Discov* **2016**, *15*, 605.
- (254) Scott, D. E.; Coyne, A. G.; Hudson, S. A.; Abell, C. *Biochem* **2012**, *51*, 4990.
- (255) Boyd, S. M.; Turnbull, A. P.; Walse, B. *Comput Mol Sci* **2012**, *2*, 868.
- (256) Pattabiraman, V. R.; Bode, J. W. *Nat* **2011**, *480*, 471.
- (257) Sabatini, M. T.; Boulton, L. T.; Sneddon, H. F.; Sheppard, T. D. *Nat Catal* **2019**, *2*, 10.
- (258) Grant, E. K.; Fallon, D. J.; Eberl, H. C.; Fantom, K. G. M.; Zappacosta, F.; Messenger, C.; Tomkinson, N. C. O.; Bush, J. T. *Angew Chem Int Ed Engl* **2019**, *58*, 17322.
- (259) Liu, P.; Wang, Y.; Li, X. *Acta Pharm Sin B* **2019**, *9*, 871.
- (260) O'Bryan, J. P. *Pharmacol Res* **2019**, *139*, 503.
- (261) Janes, M. R.; Zhang, J.; Li, L. S.; Hansen, R.; Peters, U.; Guo, X.; Chen, Y.; Babbar, A.; Firdaus, S. J.; Darjania, L.; Feng, J.; Chen, J. H.; Li, S.; Li, S.; Long, Y. O.; Thach, C.; Liu, Y.; Zariéh, A.; Ely, T.; Kucharski, J. M.; Kessler, L. V.; Wu, T.; Yu, K.; Wang, Y.; Yao, Y.; Deng, X.; Zarrinkar, P. P.; Brehmer, D.; Dhanak, D.; Lorenzi, M. V.; Hu-Lowe, D.; Patricelli, M. P.; Ren, P.; Liu, Y. *Cell* **2018**, *172*, 578.
- (262) Fell, J. B.; Fischer, J. P.; Baer, B. R.; Ballard, J.; Blake, J. F.; Bouhana, K.; Brandhuber, B. J.; Briere, D. M.; Burgess, L. E.; Burkard, M. R.; Chiang, H.; Chicarelli,

M. J.; Davidson, K.; Gaudino, J. J.; Hallin, J.; Hanson, L.; Hee, K.; Hicken, E. J.; Hinklin, R. J.; Marx, M. A.; Mejia, M. J.; Olson, P.; Savechenkov, P.; Sudhakar, N.; Tang, T. P.; Vigers, G. P.; Zecca, H.; Christensen, J. G. *ACS Med Chem Lett* **2018**, *9*, 1230.

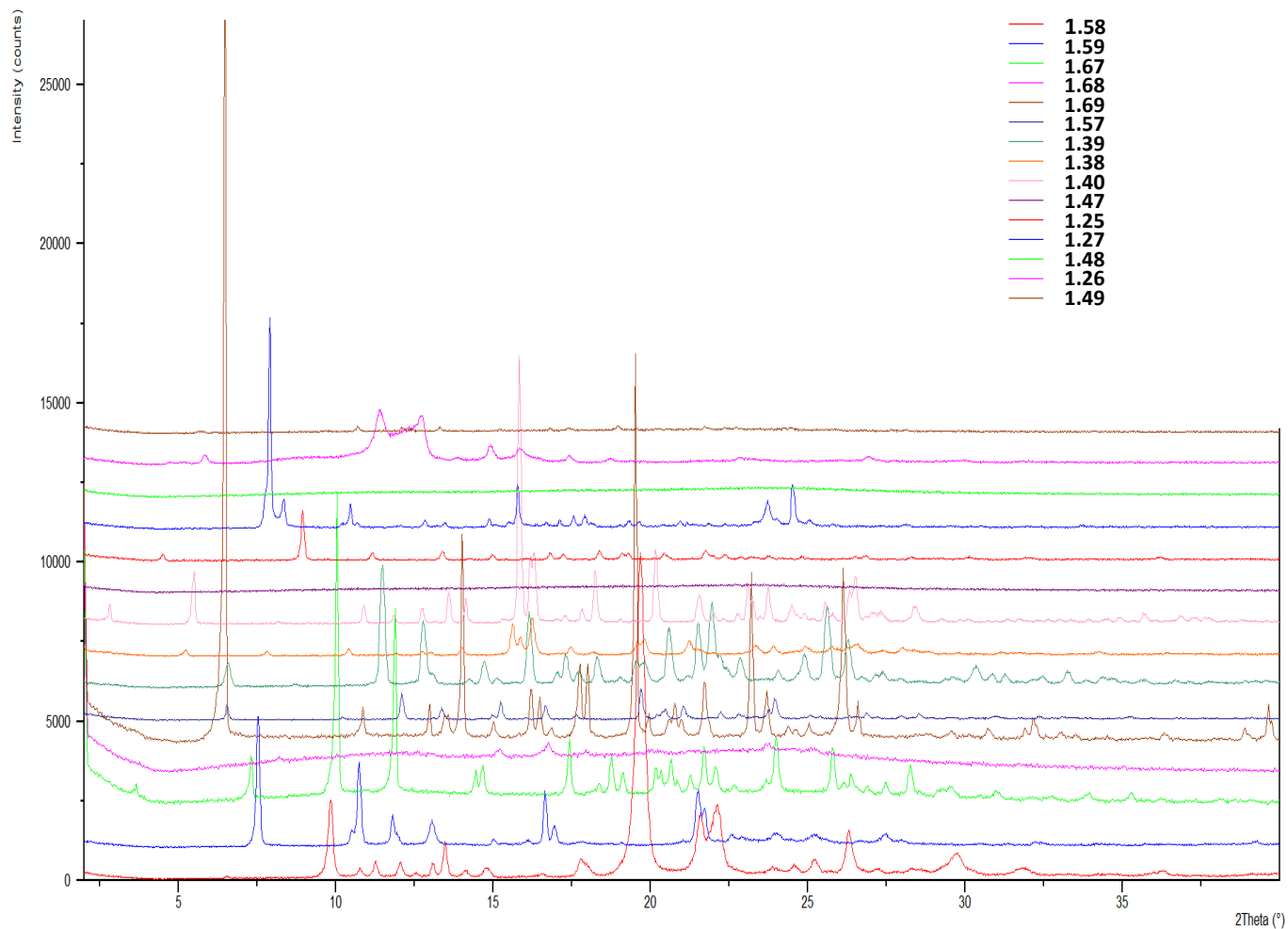
(263) Hansen, R.; Peters, U.; Babbar, A.; Chen, Y.; Feng, J.; Janes, M. R.; Li, L. S.; Ren, P.; Liu, Y.; Zarrinkar, P. P. *Nat Struct Mol Biol* **2018**, *25*, 454.

(264) Dang, C. V.; Reddy, E. P.; Shokat, K. M.; Soucek, L. *Nat Rev Cancer* **2017**, *17*, 502.

(265) Patick, A. K.; Binford, S. L.; Brothers, M. A.; Jackson, R. L.; Ford, C. E.; Diem, M. D.; Maldonado, F.; Dragovich, P. S.; Zhou, R.; Prins, T. J.; Fuhrman, S. A.; Meador, J. W.; Zalman, L. S.; Matthews, D. A.; Worland, S. T. *Antimicrob Agents Chemother* **1999**, *43*, 2444.

3 APPENDICES

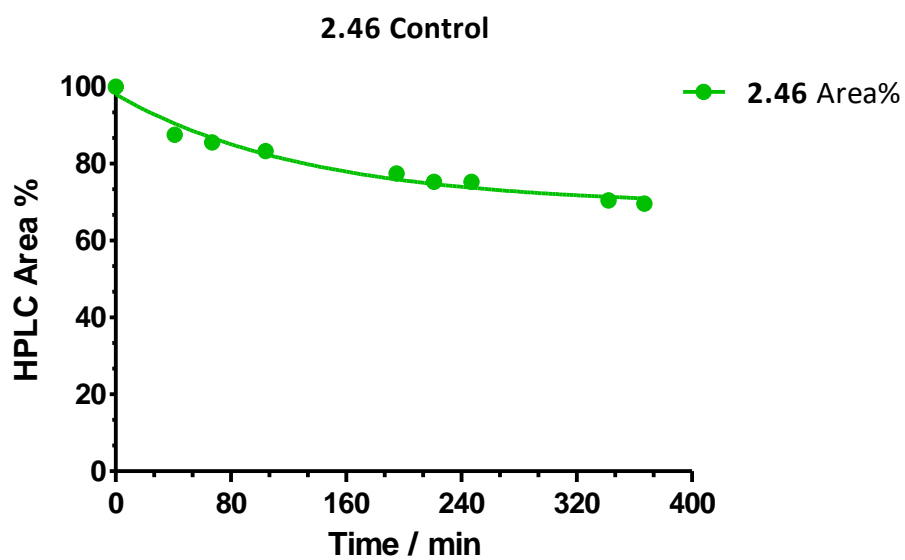
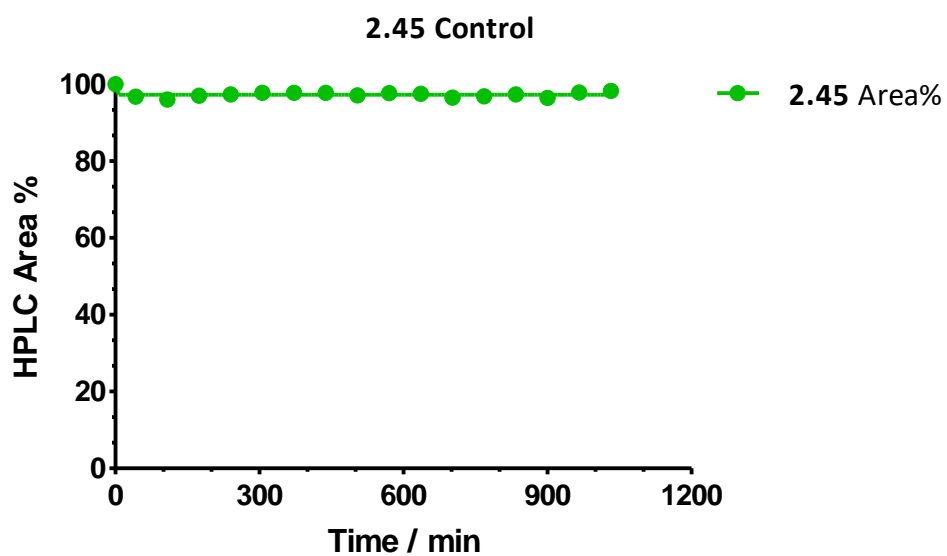
3.1 XRPD analysis



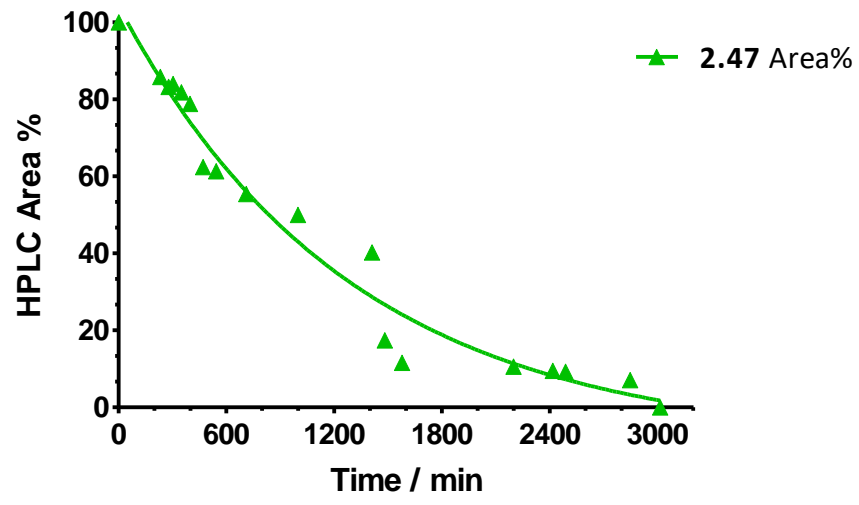
3.2 Lipid kinase screen of 2.45

PI4KIII β	7.9
PI3K γ	5.5
PI3K δ	4.9
PI3K β	4.8
PI3K α	4.4
SPHK1	4.9
DAG	4.9
PIP4K2A	4.9
CHKB	4.9
SPHK2	4.9
Choline kinase α	4.9
Diacylglycerol kinase γ	4.9
Dag kinase ζ	4.9

3.3 HPLC reference control plots



2.47 Control



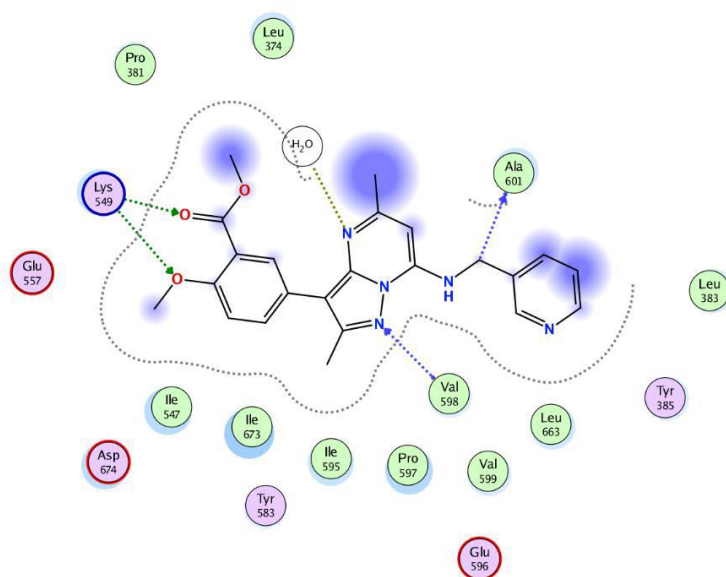
3.4 Crystallography data

All crystallographic data was obtained by Don O Somers who resides in the Structural and Biophysical Sciences at GSK (Stevenage).

Compound 2.23

1.78Å Human PI4KIIIβ (291-801 Isoform 2 (del 416-503) R409Q, R412Q) in complex.

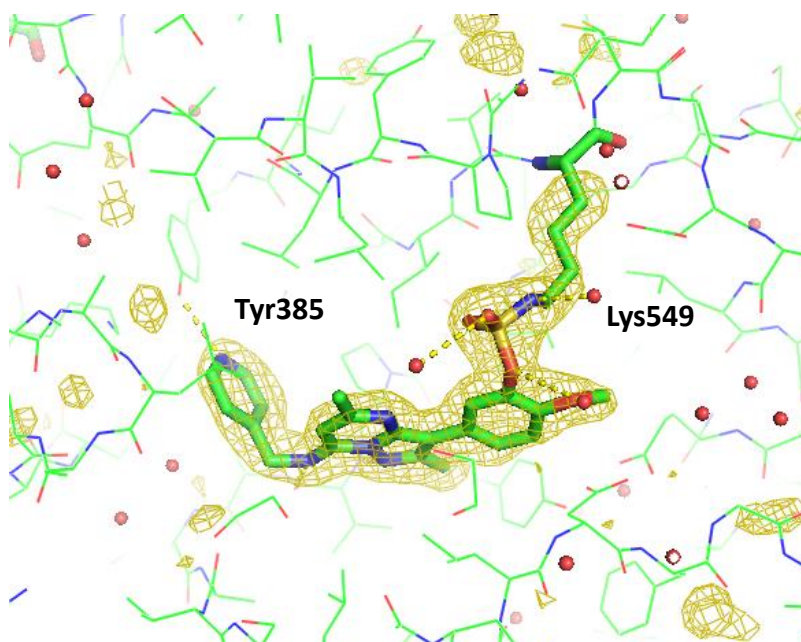
Beamline	Diamond Light Source ID30A-1	Detector	Pilatus-6M	Date Collected	2017-10-20
Resolution	1.780Å	Space Group	P 21 21 21	Record Date	2017-12-15
R	0.2208700	R-free	0.2639200	Structure Quality	A
A	54.482Å	B	67.754Å	C	106.740Å
Alpha	90.00°	Beta	90.00°	Gamma	90.00°



Compound 2.45

1.60Å human PI4KIIIβ (291-801 isoform 2 (del416-503) R409Q, R412Q) in complex covalently bound.

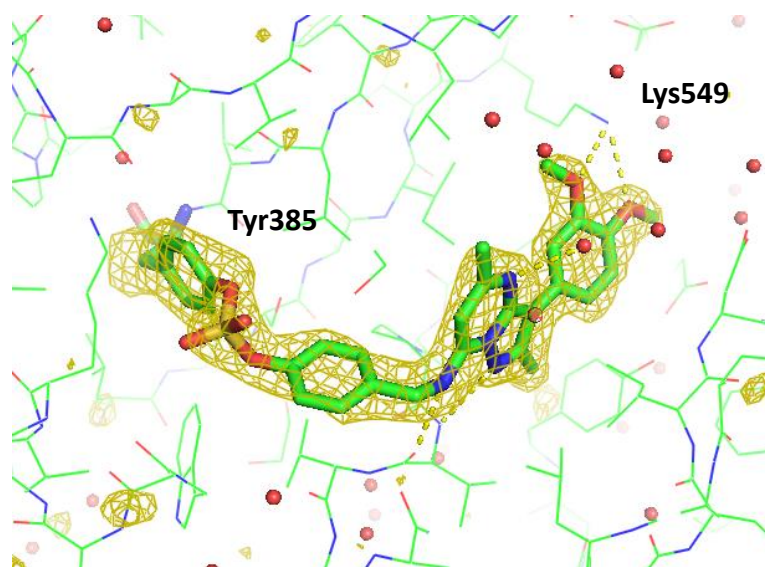
Beamline	Diamond Light Source ID30A-1	Detector	Pilatus-6M	Date Collected	2018-07-09
Resolution	1.600 Å	Space Group	P 21 21 21	Record Date	2018-07-24
R	0.2166200	R-free	0.2298900	Structure Quality	A
A	59.219 Å	B	67.545 Å	C	106.925 Å
Alpha	90.00°	Beta	90.00°	Gamma	90.00°



Compound 2.76

1.77Å human PI4KIIIβ (291-801 isoform 2 (del416-503) R409Q, R412Q) in complex covalently bound.

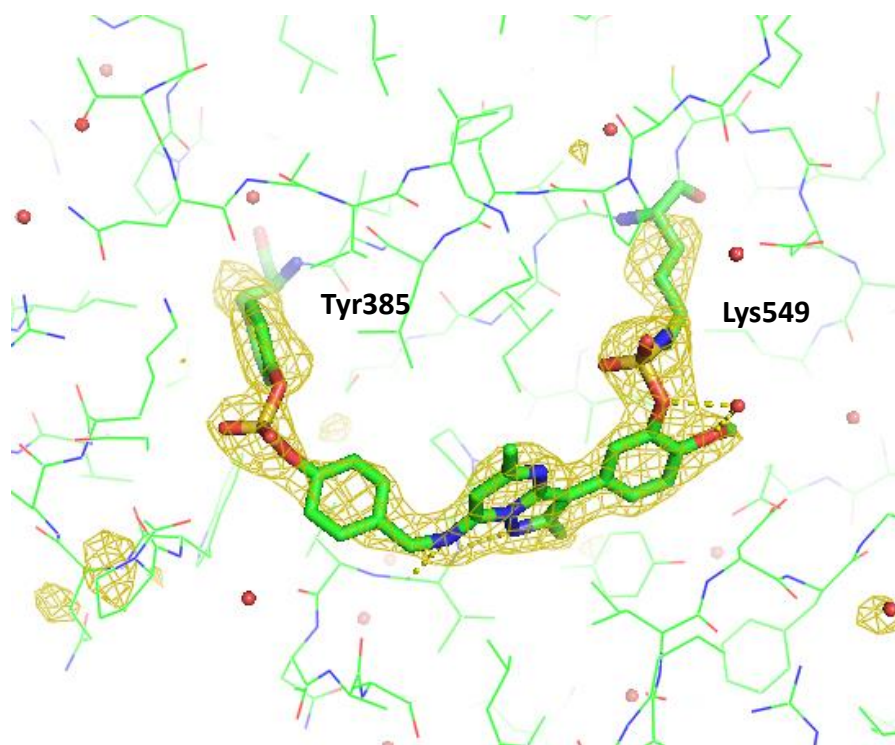
Beamline	Diamond Light Source ID30A-1	Detector	Pilatus-6M	Date Collected	2018-08-29
Resolution	1.770 Å	Space Group	P 21 21 21	Record Date	2018-09-08
R	0.2119300	R-free	0.2497200	Structure Quality	A
A	58.216Å	B	67.950 Å	C	107.166 Å
Alpha	90.00°	Beta	90.00°	Gamma	90.00°



Compound **2.83**

2.09Å human PI4KIIIβ (291-801 isoform 2 (del416-503) R409Q, R412Q) in complex covalently bound.

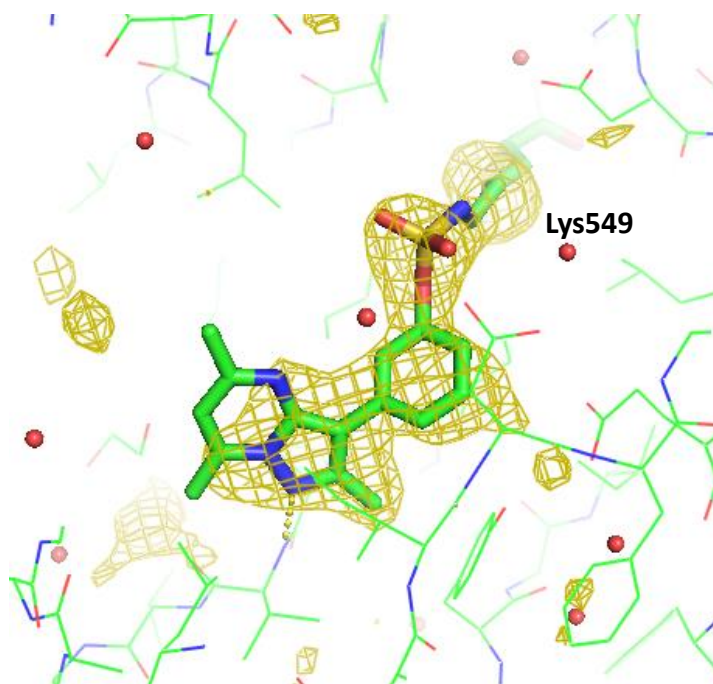
Beamline	Diamond Light Source I04	Detector	Pilatus-6M	Date Collected	2018-10-11
Resolution	2.090Å	Space Group	P 21 21 21	Record Date	2018-10-22
R	0.2119800	R-free	0.2658400	Structure Quality	A
A	58.862Å	B	67.857Å	C	107.070Å
Alpha	90.00°	Beta	90.00°	Gamma	90.00°



Compound **2.90**

1.67Å human PI4KIIIβ (291-801 isoform 2 (del416-503) R409Q, R412Q) in complex covalently bound.

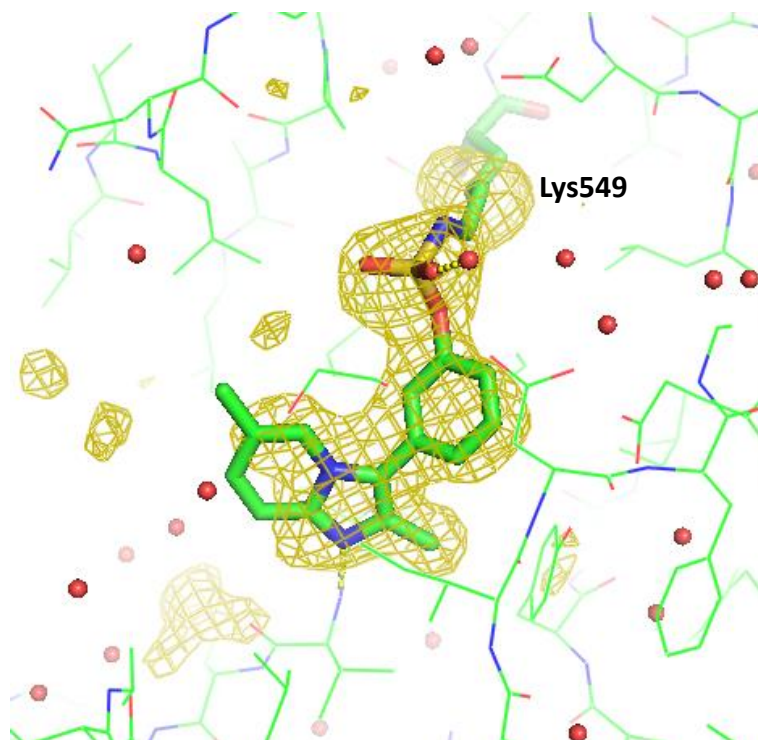
Beamline	Diamond Light Source I04	Detector	Eiger 16M	Date Collected	2019-05-20
Resolution	1.670Å	Space Group	P 21 21 21	Record Date	2019-06-11
R	0.1884600	R-free	0.2161100	Structure Quality	A
A	58.040Å	B	68.090Å	C	107.290Å
Alpha	90.00°	Beta	90.00°	Gamma	90.00°



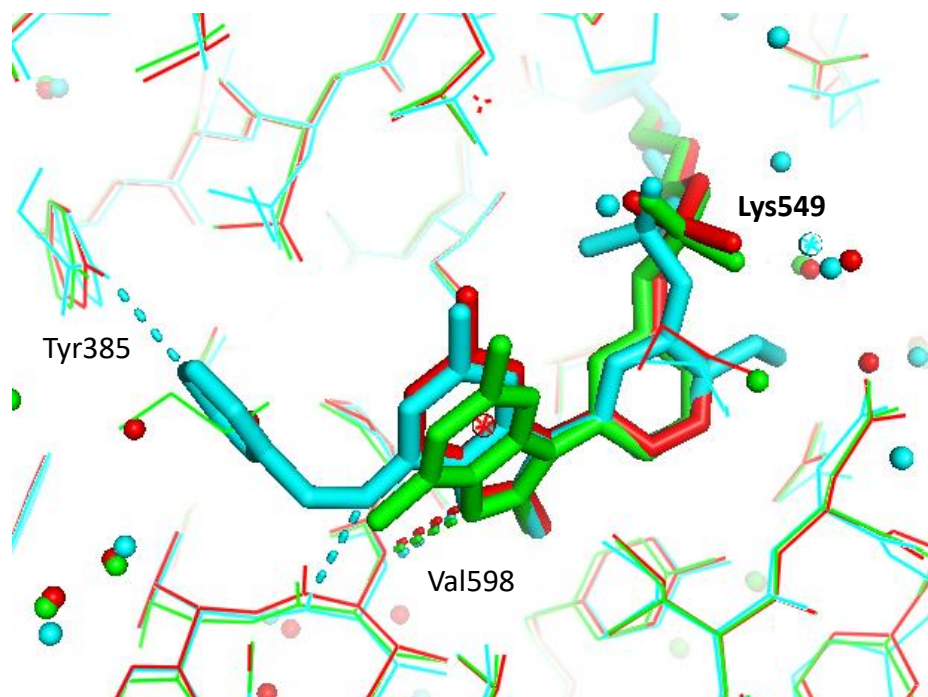
Compound **2.95**

1.67Å human PI4KIIIβ (291-801 isoform 2 (del416-503) R409Q, R412Q) in complex covalently bound.

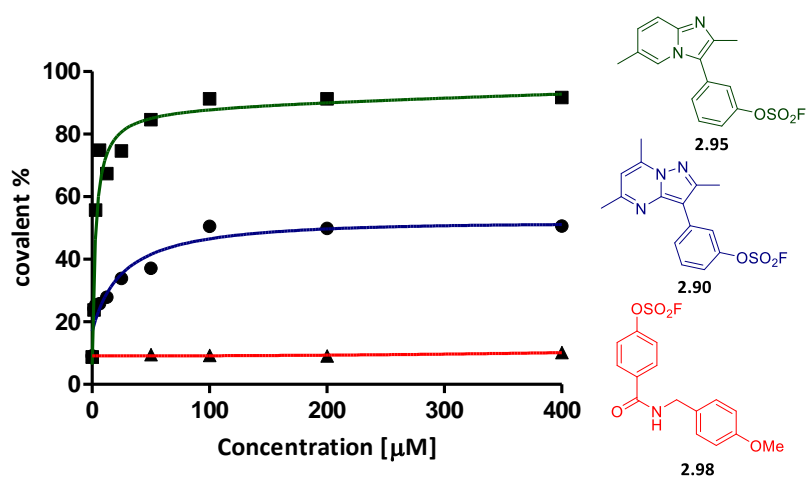
Beamline	Diamond Light Source I04	Detector	Eiger 16M	Date Collected	2019-05-20
Resolution	1.670Å	Space Group	P 21 21 21	Record Date	2019-06-11
R	0.1884600	R-free	0.2161100	Structure Quality	B
A	58.040Å	B	68.090Å	C	107.290Å
Alpha	90.00°	Beta	90.00°	Gamma	90.00°



X-ray overlay of covalent inhibitors **2.45**, **2.90** & **2.95** bound to Lys549.



3.5 Fragment mass spectrometry control compound 2.98



Covalent labelling of PI4KIIIβ detected with fragments **2.90** and **2.95**. No covalent modification observed for **2.98**.